

AD723960

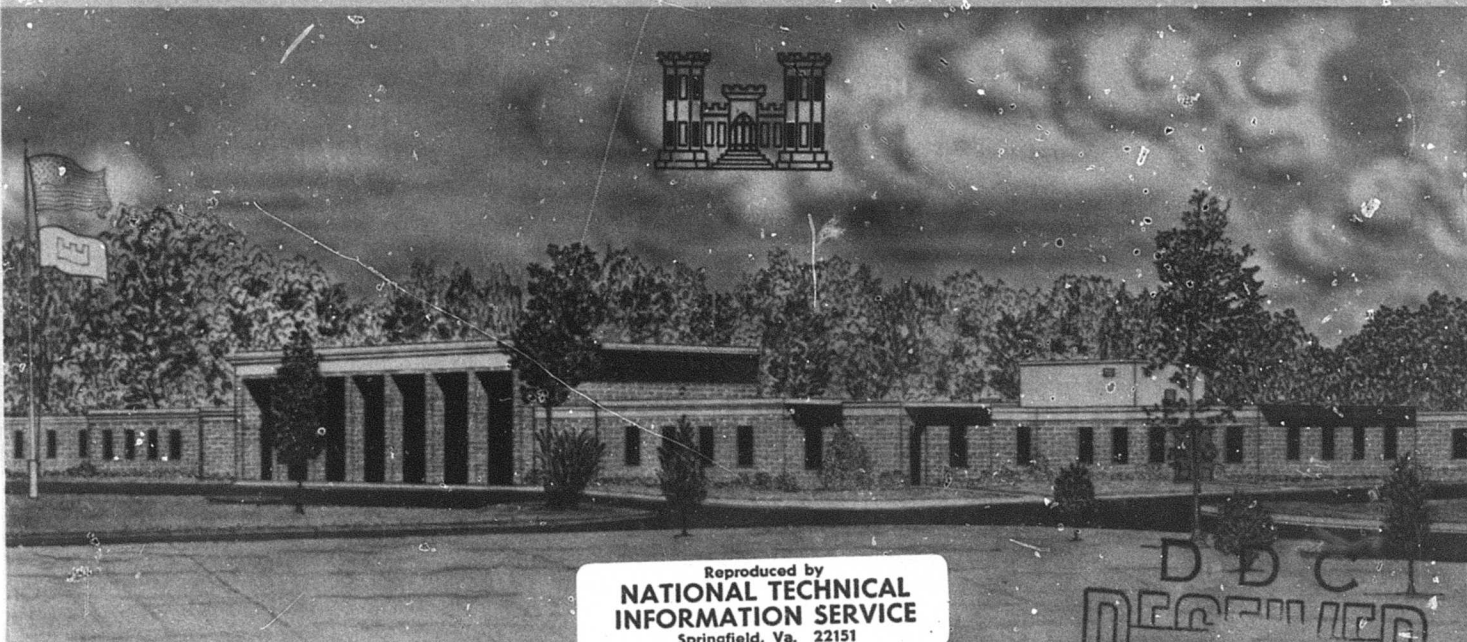


MISCELLANEOUS PAPER N-71-3

# DYNAMIC TESTS OF A MODEL FLEXIBLE-ARCH-TYPE PROTECTIVE SHELTER

by

T. E. Kennedy



Reproduced by  
**NATIONAL TECHNICAL  
INFORMATION SERVICE**  
Springfield, Va. 22151

April 1971

D B C  
**RECORDED**  
JUN 1 1971  
**RECEIVED**  
C

Sponsored by **Office, Chief of Engineers, U. S. Army**

Conducted by **U. S. Army Engineer Waterways Experiment Station, Vicksburg, Mississippi**

Unclassified

Security Classification

**DOCUMENT CONTROL DATA - R & D**

*(Security classification of title, body of abstract and indexing annotation must be entered when the overall report is classified)*

1. ORIGINATING ACTIVITY (Corporate author) U. S. Army Engineer Waterways Experiment Station Vicksburg, Mississippi		2a. REPORT SECURITY CLASSIFICATION Unclassified	
		2b. GROUP	
3. REPORT TITLE DYNAMIC TESTS OF A MODEL FLEXIBLE-ARCH-TYPE PROTECTIVE SHELTER			
4. DESCRIPTIVE NOTES (Type of report and inclusive dates) Final report			
5. AUTHOR(S) (First name, middle initial, last name) Thomas E. Kennedy			
6. REPORT DATE April 1971	7a. TOTAL NO. OF PAGES 173	7b. NO. OF REFS 9	
8a. CONTRACT OR GRANT NO. a. PROJECT NO. 4A022601A880-03		8b. ORIGINATOR'S REPORT NUMBER(S) Miscellaneous Paper N-71-3	
c.		8c. OTHER REPORT NO(S) (Any other numbers that may be assigned this report)	
d.			
9. DISTRIBUTION STATEMENT Approved for public release; distribution unlimited			
11. SUPPLEMENTARY NOTES		12. SPONSORING MILITARY ACTIVITY Office, Chief of Engineers, U. S. Army Washington, D. C.	
13. ABSTRACT The general objective of this study was to determine the dynamic response of a buried model flexible-arch troop shelter to simulated nuclear blast overpressures. To accomplish this, a model structure was constructed using a geometric scaling ratio of 1 to 4.5. The structure was buried in dense, dry sand with the depth of cover over the crown equal to one-fourth of the arch diameter and tested in the Waterways Experiment Station Large Blast Load Generator. A series of five tests was conducted at overpressures ranging from 37 to 177 psi with the model being excavated and rebuilt after each test. Strain, acceleration, and deflection were measured at various points on the structure; measurements were also made of the pressure inside the structure, stress and acceleration in the free field, and overpressure at the soil surface. Visible damage consisted of arch deformation, footing deflection, and fracture of the end truss bulkhead connector at the higher overpressures. All transient measurements in general were recorded successfully. The results of this study show that the model structure as designed can withstand almost twice the design overpressure of 100 psi for large duration times (100 to 200 msec). Redesign of the truss connector can be accomplished as detailed in Appendix D so that no fracture occurs in this area. The instrumentation employed is described in detail in Appendix A. Raw and computed data are contained in Appendixes B and C, respectively.			

DD FORM 1473 1 NOV 66

REPLACES DD FORM 1473, 1 JAN 64, WHICH IS OBSOLETE FOR ARMY USE.

173

Unclassified

Security Classification

14. KEY WORDS	LINK A		LINK B		LINK C	
	ROLE	WT	ROLE	WT	ROLE	WT
Dynamic tests Explosion effects Model structures Shelters Subsurface structures						



MISCELLANEOUS PAPER N-71-3

# DYNAMIC TESTS OF A MODEL FLEXIBLE-ARCH-TYPE PROTECTIVE SHELTER

by

T. E. Kennedy



April 1971

Sponsored by Office, Chief of Engineers, U. S. Army  
Project 4A022601A880-03

Conducted by U. S. Army Engineer Waterways Experiment Station, Vicksburg, Mississippi

ARMY-MRC VICKSBURG, MISS.

APPROVED FOR PUBLIC RELEASE; DISTRIBUTION UNLIMITED



THE CONTENTS OF THIS REPORT ARE NOT TO BE  
USED FOR ADVERTISING, PUBLICATION, OR  
PROMOTIONAL PURPOSES. CITATION OF TRADE  
NAMES DOES NOT CONSTITUTE AN OFFICIAL EN-  
DORSEMENT OR APPROVAL OF THE USE OF SUCH  
COMMERCIAL PRODUCTS.

## ABSTRACT

The general objective of this study was to determine the dynamic response of a buried model flexible-arch troop shelter to simulated nuclear blast overpressures. To accomplish this, a model structure was constructed using a geometric scaling ratio of 1 to 4.5. The structure was buried in dense, dry sand with the depth of cover over the crown equal to one-fourth of the arch diameter and tested in the Waterways Experiment Station Large Blast Load Generator. A series of five tests was conducted at overpressures ranging from 37 to 177 psi with the model being excavated and rebuilt after each test. Strain, acceleration, and deflection were measured at various points on the structure; measurements were also made of the pressure inside the structure, stress and acceleration in the free field, and overpressure at the soil surface.

Visible damage consisted of arch deformation, footing deflection, and fracture of the end truss bulkhead connector at the higher overpressures. All transient measurements in general were recorded successfully. The results of this study show that the model structure as designed can withstand almost twice the design overpressure of 100 psi for large duration times (100 to 200 msec). Redesign of the truss connector can be accomplished as detailed in Appendix D so that no fracture occurs in this area.

The instrumentation employed is described in detail in Appendix A. Raw and computed data are contained in Appendixes B and C, respectively.

## PREFACE

This study was conducted at the U. S. Army Engineer Waterways Experiment Station (WES) for the Office, Chief of Engineers, Department of the Army, as a part of Task O3, "Military Engineering Applications of Nuclear Weapons Effects Research," Project 4A022601A880-03. It was accomplished during the period August 1965 through October 1967 under the general supervision of Mr. G. L. Arbuthnot, Jr., Chief of the Nuclear Weapons Effects Division, and under the direct supervision of Mr. W. J. Flathau, Chief, Protective Structures Branch (PSB). This report was prepared by Mr. T. E. Kennedy of PSB. Mr. G. L. Carre assisted during all phases of the fabrication and testing, and Mrs. C. M. Lloyd assisted with all data reduction.

COL John R. Oswalt, Jr., CE, COL Levi A. Brown, CE, and COL Ernest D. Peixotto, CE, were Directors of WES during the conduct of this study and preparation of this report. Technical Directors were Messrs. J. B. Tiffany and F. R. Brown.

## CONTENTS

ABSTRACT-----	4
PREFACE-----	5
NOTATION-----	10
CONVERSION FACTORS, BRITISH TO METRIC UNITS OF MEASUREMENT-----	12
CHAPTER 1 INTRODUCTION-----	13
1.1 Background-----	13
1.2 Objectives-----	15
1.3 Scope-----	15
1.4 Scaling Considerations-----	15
CHAPTER 2 PROCEDURE-----	19
2.1 Structure-----	19
2.1.1 General Description-----	19
2.1.2 Arch Ribs-----	20
2.1.3 Wooden Elements-----	20
2.1.4 Bulkhead and Truss-----	20
2.2 Test Configuration-----	20
2.2.1 Test Device-----	20
2.2.2 Test Layout-----	21
2.2.3 Specimen Construction-----	21
2.3 Soil Properties-----	22
CHAPTER 3 RESULTS-----	34
3.1 Loading Input-----	34
3.1.1 Surface Airblast-----	34
3.1.2 Free Field-----	35
3.2 Visual Damage Survey-----	35
3.2.1 General Gross Motion and Damage-----	35
3.2.2 Component Damage-----	36
CHAPTER 4 DISCUSSION OF RESULTS-----	51
4.1 Structural Loading-----	51
4.1.1 Free Field-----	51
4.1.2 Radial Interface Loading-----	52
4.2 Structure Motion-----	53
4.3 Structural Response-----	54
4.4 Interior Environment-----	56
CHAPTER 5 CONCLUSIONS AND RECOMMENDATIONS-----	79
5.1 Conclusions-----	79
5.2 Recommendations-----	79
APPENDIX A INSTRUMENTATION DETAILS AND TABULATED RESULTS-----	81
APPENDIX B RAW DATA-----	101

APPENDIX C COMPUTED DATA-----	129
APPENDIX D BULKHEAD-TRUSS CONNECTOR REDESIGN-----	157
REFERENCES-----	165

TABLES

1.1 Model and Prototype Resistance and Response Parameters-----	16
2.1 Preshot Soil Densities-----	24
3.1 Surface Airblast Overpressure Parameters-----	38
4.1 Ratio of Radial Load to Peak Transient Radial Load-----	57
4.2 Tabulated Thrust Data-----	58
4.3 Tabulated Moment Data-----	59
A.1 Oscillograph System Frequency Response-----	85
A.2 Airblast Results-----	86
A.3 Soil Stress Results-----	87
A.4 Acceleration Results-----	88
A.5 Deflection Results-----	89
A.6 Strain Gage Results-----	90

FIGURES

1.1 Field shelter in place with entrance-----	17
1.2 Exploded view of the field shelter and entrance complex-----	18
2.1 Steps in structure assembly-----	25
2.2 Test geometry and location in the IBLG-----	27
2.3 Plate-bearing test results at footing level-----	28
2.4 Grain-size distribution curve for the test sand-----	29
2.5 Relation between angle of internal friction and density for the test sand-----	30
2.6 One-dimensional static confined compression test data for the test sand-----	31
2.7 Stress-strain curves for the test sand; density 99.7 pcf-----	32
2.8 Velocity data for the test sand; density 99.7 pcf-----	33
3.1 Composite surface airblast overpressure curves-----	39
3.2 Initial impulse data-----	40
3.3 Typical airblast data-----	41
3.4 Depression in the sand surface caused by the gross motion of the structure during Shot 4-----	42
3.5 Postshot crown curvature-----	43
3.6 Postshot damage to crown timber-----	44
3.7 Postshot view of the damaged footings showing the punching damage-----	45
3.8 Section views of the damage shown in Figure 3.7 to the footings at the section shown (Section AA)-----	46
3.9 Sand spall of the interior floor surface during Shot 4-----	47
3.10 Dislocation of Gage 51VA caused by spalling of the interior floor during Shot 5-----	48
3.11 Shear damage to connector bolts, main photographs showing the post-pilot-test damage-----	49
3.12 Damage to the redesigned bulkhead beam-truss connector-----	50
4.1 Soil stress wave velocity-----	60

4.2	Idealized and typical free-field soil stress data-----	61
4.3	Radial load distribution-----	62
4.4	Permanent deformation of Rib 6 after Shots 3, 4, and 5----	63
4.5	Angle of point of maximum outward deflection-----	64
4.6	Level survey, postshot crown deflection with respect to the footings-----	65
4.7	Level survey data for footings-----	66
4.8-4.10	Footing motion of the north footing center during Shots 3 through 5-----	67
4.11	Peak acceleration of footing-----	70
4.12	Peak velocity of footing-----	70
4.13	Typical motion data at footing center; Shot 5, Gage 53VA--	71
4.14	Rib idealization-----	72
4.15	Idealized thrust and moment histories-----	73
4.16	Typical elastic and plastic thrust and moment data-----	74
4.17	Peak transient thrust-----	75
4.18	Peak interior pressure versus footing deflection-----	76
4.19	Acceleration- and velocity-time histories of the interior floor, Shot 4 (Gage 51VA)-----	77
4.20	Peak motions of the interior floor (Gage 51VA)-----	78
A.1	General view of the recording and conditioning equipment--	94
A.2	Instrumentation diagrams for Shots 1 to 5-----	95
A.3	Transducers used during the test series-----	96
A.4	Footing and crown deflection rig, Preshot 1-----	97
A.5	Fully instrumented structure prior to placing timber lagging, Preshot 3-----	98
A.6	Numbering convention-----	99
A.7	Free-field and motion gage locations-----	100
B.1-B.5	Shot 1, oscillograph record from Recorders 1 through 5----	102
B.6-B.10	Shot 2, oscillograph record from Recorders 1 through 5----	107
B.11-B.16	Shot 3, oscillograph record from Recorders 1 through 6----	112
B.17-B.22	Shot 4, oscillograph record from Recorders 1 through 6----	118
B.23-B.26	Shot 5, oscillograph record from Recorders 1 through 4----	124
C.1-C.5	Velocity data, Shots 1 through 5-----	130
C.6-C.10	Displacement data, Shots 1 through 5-----	135
C.11	Thrust data, Shot 1-----	140
C.12	Moment data, Shot 1-----	141
C.13	Thrust data, Shot 2-----	142
C.14	Moment data, Shot 2-----	143
C.15	Thrust data, Shot 3-----	144
C.16	Moment data, Shot 3-----	146
C.17	Thrust data, Shot 4-----	148
C.18	Moment data, Shot 4-----	150
C.19	Thrust data, Shot 5-----	152
C.20	Moment data, Shot 5-----	153
C.21-C.23	Footing motion components, Shots 3 through 5-----	154
D.1	Assumed loading on the prototype and on the model truss---	160
D.2	Detail of the modifications made to the structure column- truss connection-----	161

D.3	Detail of the modifications made in the prototype truss connector design-----	162
D.4	Detail of the modifications made in the prototype column connector design-----	163
D.5	Plate detail for prototype column connector modification-----	164

## NOTATION

A	Area, in <sup>2</sup>
D <sub>r</sub>	Relative density of the test sand
E	Modulus of elasticity, psi
g	Gravitation constant, 32.2 ft/sec <sup>2</sup>
I	Moment of inertia, in <sup>4</sup> or in <sup>4</sup> /in
L	Length, inches
L <sub>f</sub>	Footing length, inches
M <sub>P</sub>	Peak transient moment, in-lb/in
M <sub>R</sub>	Peak reflected moment, in-lb/in
M <sub>ss</sub>	Steady-state moment, in-lb/in
N <sub>P</sub>	Peak transient thrust, lb/in
N <sub>R</sub>	Peak reflected thrust, lb/in
N <sub>ss</sub>	Steady-state thrust, lb/in
P <sub>I</sub>	Incident peak, psi
P <sub>IN</sub>	Interior pressure, psi
P <sub>R</sub>	Reflected peak, psi
P <sub>so</sub>	Surface overpressure peak, psi
R	Arch radius, inches
R <sub>s</sub>	Arch rib spacing center to center, inches
S	Section modulus of timber lagging per unit width, in <sup>3</sup> /in
t <sub>p</sub>	Time of peak, msec
t <sub>r</sub>	Rise time to peak, msec
t <sub>R</sub>	Time of reflected peak, msec
w	Footing width, inches
w'	Width of arch rib system per unit area of arch, in/in <sup>2</sup>
X	Velocity, in/sec
X	Acceleration, g's
δ <sub>d</sub>	Dimensionless footing deflection
δ <sub>f</sub>	Footing deflection, inches
θ	Angle up from footing, degrees
σ <sub>b</sub>	Flexural stress at proportional limit in timber, psi

$\sigma_{ULT}$  Ultimate plate bearing stress, psi  
 $\sigma_y$  Yield stress, psi

CONVERSION FACTORS, BRITISH TO METRIC UNITS OF MEASUREMENT

British units of measurement used in this report can be converted to metric units as follows.

Multiply	By	To Obtain
inches	25.4	millimeters
feet	0.3048	meters
square inches	645.16	square millimeters
cubic yards	0.7645549	cubic meters
megatons	0.9071847	teragrams
kip	4.448222	kilonewtons
pounds per inch	175.1268	newtons per meter
pounds per foot	14.59390	newtons per meter
pounds per square inch	6.894757	kilonewtons per square meter
kip per square inch	6.894757	meganewtons per square meter
kip per square foot	4.788026	kilonewtons per square meter
pounds per cubic foot	16.01846	kilograms per cubic meter
microinches per inch	0.001	microns per millimeter
inch-pounds per inch	4.448222	newton-meters per meter

## CHAPTER 1

### INTRODUCTION

#### 1.1 BACKGROUND

The development of strategic and tactical nuclear weapons and efficient delivery systems has exposed the field Army to all the hazards of nuclear warfare. No longer is the nuclear weapon a rarity in arsenals of the major powers of the world, but it now has a wide range of yield and is a relatively inexpensive form of explosive. Currently, the envisioned military usage of these weapons ranges from barrier formation caused by cratering action to destruction of bridges and other individual structures to megalopolis annihilation.

If a modern military establishment is to withstand an attack by such weapons, the various units (functions) of such an establishment must survive the effects of these weapons. This means that each military unit should have some degree of protection, the level of protection varying with the value of the individual unit. Reduced vulnerability of a military unit can be achieved either by hardening the unit or by duplicating it; obviously, there is a trade off between the two techniques. As the importance of the functional unit increases, generally, the cost per unit also increases, so that the cost of duplication becomes greater and the value of economical hardening increases. The requirements of providing a high degree of hardening for the individual soldier are minimal, whereas an important command center would require a high degree of hardening.

In order to provide a field-shelter concept to furnish a relatively hard cover for field use, a contract was awarded to N. M. Newmark (NMN), Consulting Engineering Services, Urbana, Illinois, by the U. S. Army Engineer Waterways Experiment Station (WES), Vicksburg, Mississippi, in December 1957 to develop an economical 51-man protective troop shelter for field use. The concept was to provide protection against the effects of a megaton<sup>1</sup> nuclear weapon at a 100-psi air overpressure level. In addition, the

---

<sup>1</sup> A table of factors for converting British units of measurement to metric units is presented on page 12.

shelter had to be of such design that construction could be completed within one week by a 51-man platoon. Results of this work were published in Reference 1. Based on considerations of economy, hardness level, radiation protection, and ease of construction, an underground flexible structure to be placed in soil above the ground water table was selected.

The prototype shelter is 16 by 48 feet in plan and is to be supplied in 12-foot-long, air-droppable modular kits. The shelter and entrance complexes are shown in Figures 1.1 and 1.2. The shelter consists of 8-foot-radius steel arch ribs, which support timber blocks. These ribs are made of rolled or forged quarter-circle, split, structural tees with the stem of the tee turned out. The rib sections are welded to bearing plates which are bolted to a crown or ridge timber and to a composite heavy timber and steel channel footing at the base. The timber blocks forming the roof are supported by the flanges of the tees. The end rib is made of an angle section that frames and supports the top of the end bulkhead. The forces at the base of the bulkhead are resisted by a welded steel truss reacting against the footings of the structure. Vertical wide-flange beams extend from the truss to the arch end rib. The bulkhead wall is formed by placing timber blocks horizontally between the webs of the vertical beams; the blocks are held in place by angle sections welded to the webs. Ingress and egress are provided by means of separate entrance kits which can be used at either or both ends. The entrance complex also provides space for ventilation equipment, a power generator, and fuel storage.

The mechanism of load transfer to a buried structure, sometimes referred to as soil arching, is not fully understood. Because of this uncertainty, it is necessary to overdesign such structures--a procedure which usually produces an uneconomical structure that may not necessarily be safe. A full-scale nuclear field test is the ideal method of design verification; however, because of the moratorium on atmospheric nuclear testing, it was decided to conduct a series of design verification tests on a model of the shelter in the WES Large Blast Load Generator (LBIG). Consequently, the contract with NMN was extended to encompass the design of a scale model of the field shelter and to propose a test program to verify structural adequacy of the prototype (Reference 2).

## 1.2 OBJECTIVES

The basic objective of the study reported herein was to determine, in a general manner, the response characteristics of a model of the flexible-arch troop shelter when subjected to the design overpressure of 100 psi and to determine the ultimate load-carrying capability of the structure. Specific objectives were (1) to determine areas of weakness in the design and to modify the design to overcome these weaknesses and (2) to determine footing response and extrados loading.

## 1.3 SCOPE

A model structure was constructed, and a series of tests was conducted using overpressures below, up to, and exceeding the design overpressure. Including the pilot test reported in Reference 3, six tests were conducted at overpressures ranging from 37 to 177 psi. All tests were conducted dynamically in dense dry sand with the crown of the structure buried one-fourth the diameter of the arch below the soil surface. Measurements were made of surface air overpressure, structural strain, accelerations, deflection, and free-field response in the vicinity of the structure.

## 1.4 SCALING CONSIDERATIONS

The scaling of the model is outlined in detail in Reference 2 and will be briefly discussed in the following. The model was constructed from the same materials as the prototype, and the linear dimensions were changed by a factor of  $1/4.5$ . Using this scaling, the soil stresses at these shallow depths due to the applied loads are assumed the same in both the model and prototype; consequently, the applied loads are assumed to be the same. The scaled differences in dead-load stresses were ignored since these stresses are small compared to the applied dynamic loads. Whenever minor deviations from geometrical scaling were required, the areas or moments of inertia were scaled, e.g., for axial or shear-loaded members the areas were scaled as  $(1/4.5)^2$ , and for members loaded in flexure the section modulus was scaled by  $(1/4.5)^3$ . Some values of response parameters are given in Table 1.1 for the model and prototype.

TABLE 1.1 MODEL AND PROTOTYPE RESISTANCE AND RESPONSE PARAMETERS

Symbols used are defined in the Notation which precedes the text.

Response Mode	Relation	Prototype Value	Model Value
Rib compression mode resistance	$\frac{\sigma_y A}{RR_s}$	124 psi	152 psi
Rib buckling mode resistance	$\frac{3EI}{R^3 R_s}$	26 psi	34 psi
Timber lagging flexural resistance	$\frac{8\sigma_b S}{L^2}$	260 psi	266 psi
Compression mode period (no soil)	$2\pi(R) \left( \frac{w'}{EA_g} \right)^{1/2}$	2.9 msec	0.677 msec
Flexural mode period (no soil)	$1.28\pi \left( \frac{w'}{EI_g} \right)^{1/2}$	139 msec	29.8 msec

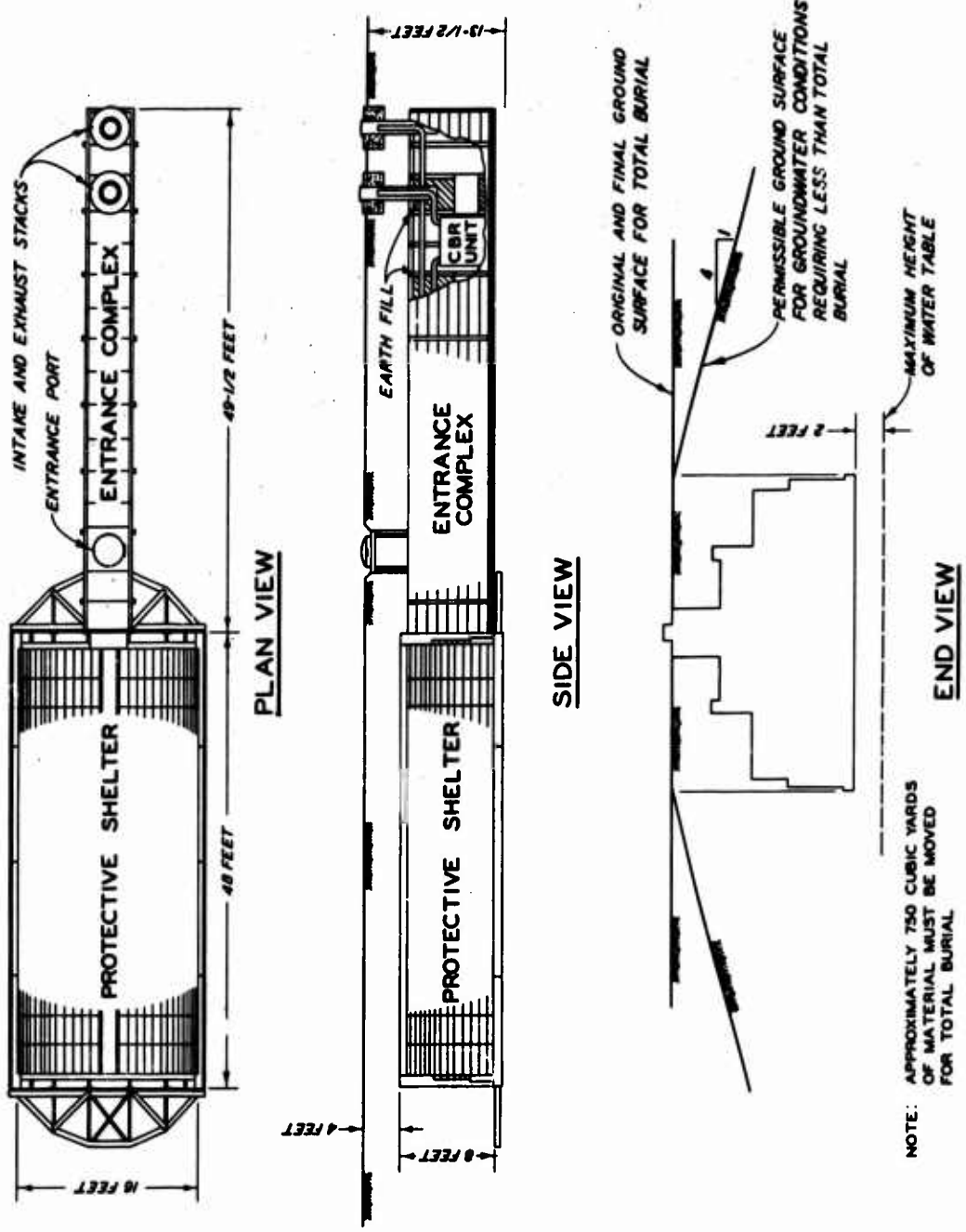


Figure 1.1 Field shelter in place with entrance.

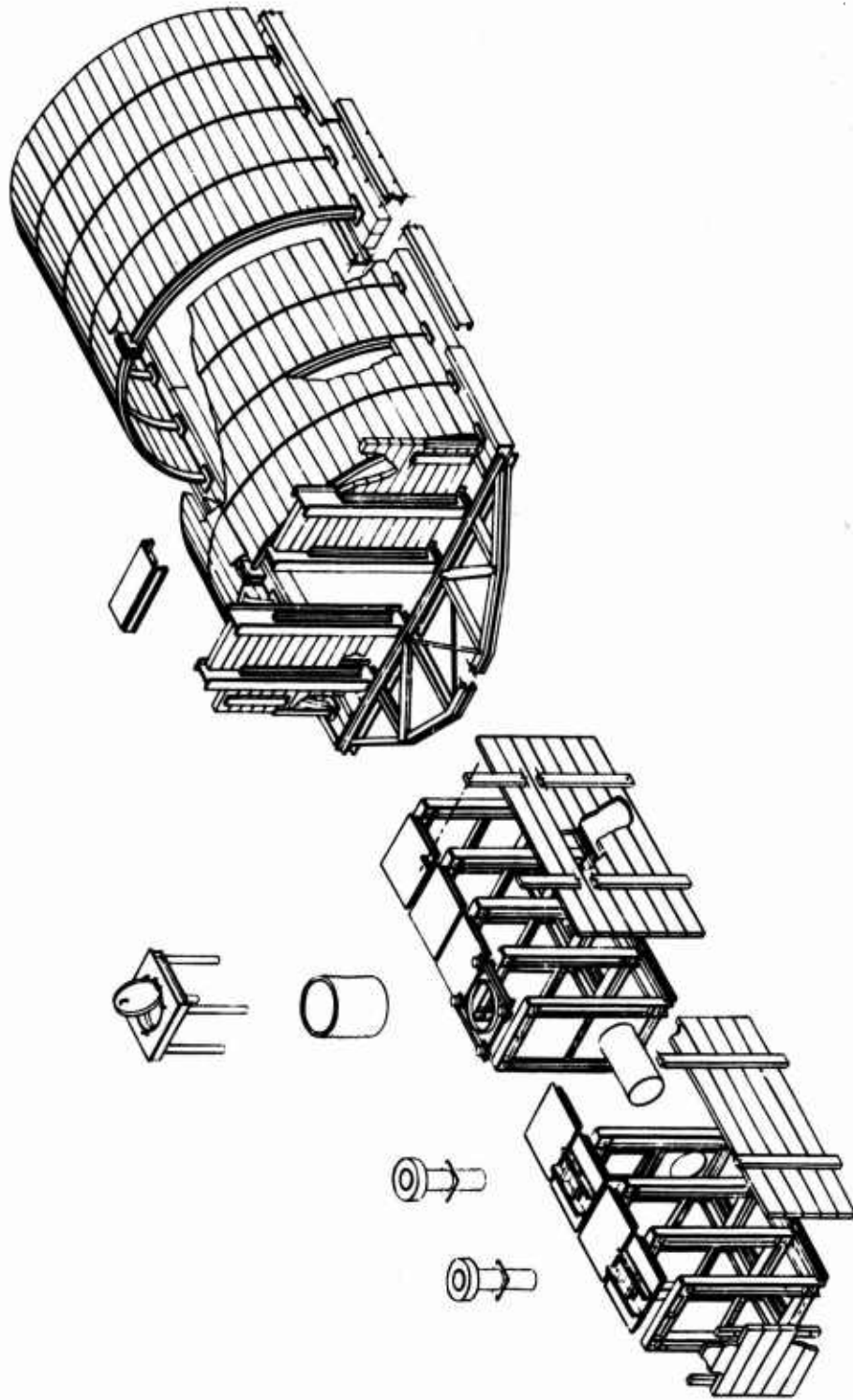


Figure 1.2 Exploded view of the field shelter and entrance complex.

## CHAPTER 2

### PROCEDURE

Five<sup>1</sup> tests (Shots 1 to 5) were conducted during the test series. With the exception of Shot 1, the model was excavated after each test. Shot 2 was a repeat loading of the Shot 1 configuration. On excavation after each shot, all damaged components and all fasteners (nuts, bolts, etc.) were replaced.

#### 2.1 STRUCTURE

2.1.1 General Description. The design of both the prototype and the model is described in detail in References 1 and 2, the model (hereafter called the structure) being a scale (1/4.5) version of the prototype. The physical properties of the steel, wood, etc., used in construction of the structure are given in Reference 3. The structure is a free-end arch composed of steel inverted-tee ribs spanned by timber elements. The footings are made of timber held together by steel channel elements. The ends of the structure are closed by means of bulkheads composed of four steel I-beam uprights filled between with timber elements. Reaction at the base of the I-beams is taken by a steel end truss reacting on the footing ends.

Assembly of the structure, and in like manner the prototype, is initiated by assembling and placing the two footings (Figure 2.1a). Each footing is assembled by bolting steel channels on both sides of timber sills. The sill timber joints do not coincide with the channel joints (Figure 2.1a). Next in the assembly process, the arch crown timber is placed, ribs are raised, and end trusses are bolted in position (Figure 2.1b). To complete the steel construction, the bulkhead beams are raised and bolted (Figure 2.1d). The wooden blocks forming the roof are placed next, and, finally, the wooden block bulkheads are positioned. Figure 2.1e

---

<sup>1</sup> The pilot test was reported in Reference 3 and is not considered to be part of this series. However, the data obtained from the pilot test are included whenever data plots are shown since they are pertinent.

shows an end view of the structure bulkhead, and Figure 2.1f shows the model with a section of the arch roof removed.

2.1.2 Arch Ribs. The arch ribs were fabricated from 6 by 1-7/8 junior beams, each beam being ripped down its length and then trimmed to form a 1.09-inch-deep tee section. All dimensions were held to  $\pm 0.005$  inch. To form the required arch, the tee angle sections were cold rolled using special roller adapters to prevent distortion of the stems and outstanding angle legs. Bearing plates were welded to the structural tee to complete the rib fabrication.

2.1.3 Wooden Elements. All wooden elements were made of clear coastal-region Douglas fir. Besides the footings, the other wooden elements were the crown timber running the length of the arch crown, and the roof and bulkhead blocks. The roof blocks were slightly tapered to conform with the curvature of the roof. The bulkhead blocks were of various sizes to conform to the beam spacing. Two short blocks were required because of the rib joint at the crown.

2.1.4 Bulkhead and Truss. The bulkheads consist of four main vertical beams and two small columns, one at each footing. These beams bolt to a truss at their base, which, in turn, reacts against the ends of both footings. There are four bolts at the base of each beam connecting the beam and the truss. The beams and truss are shown in Figures 2.1c and 2.1d. The spaces between the beams are filled with the bulkhead blocks (described in Section 2.1.3) which are held in place by a pair of angles welded to the centers of the beams.

## 2.2 TEST CONFIGURATION

2.2.1 Test Device. The tests reported herein were conducted in the LBIG, a device that will simulate the blast effects of a nuclear device. It is used primarily for testing semihard underground protective structures and can produce airblast overpressures to 500 psi on a 23-foot-diameter by 10-foot-deep soil specimen. Basically, the LBIG consists of four major components (1) Central Firing Station (CFS), (2) test chamber, (3) firing tube assembly, and (4) platen and rail-lift mechanism.

The CFS is a massive concrete structure, reinforced in three

directions with prestressed steel rods and cables. It is essentially a rectangular block with an opening through it and serves as a reaction structure for the test chamber.

The test chamber which contained the structure is formed by stacking three large steel rings, one on top of the other, on a movable platen. After soil, structure, and instrumentation placement is completed, the ring containing the firing tubes and the chamber bonnet or lid are set in place. This assembly is rolled into the CFS, and the platen is lowered to the floor, after which the top ring is raised to rest firmly against the ceiling of the CFS. The test is then conducted by detonating the explosive charges placed previously in the firing tubes. Primacord (pentaerythritol tetranitrate) is used as the explosive charge. The firing tube assembly consists of 15 cylindrical steel tubes, perforated with numerous round holes to permit the escape of the gases generated by the detonation of the explosive. A rigid grid of baffle plates supported below the firing tube assembly provides support for the assembly and serves to smooth out the blast wave that is generated.

A detailed description of the test device and its supporting equipment is given in Reference 4, and a detailed evaluation of the free-field response is given in Reference 5.

2.2.2 Test Layout. All tests were conducted in the LBLG with the test chamber filled with sand to a height of 10 feet. The surface of the sand specimen was covered with an 8-mil plastic membrane material which was in turn covered by a 2-inch sand layer to prevent burning. The plastic membrane was also used to seal the structure to prevent sand from filtering into the structure interior. The location of the structure in the test chamber is shown in Figure 2.2. The depth of crown cover was  $11-1/32$  inches, which corresponds to a depth of one-fourth the diameter of the structure. The total depth to the lower surface of the footing was  $35-5/32$  inches.

2.2.3 Specimen Construction. Two methods of sand placement were used during the construction of each test configuration. Below the level of the structure footings, the sand was placed in 6-inch lifts with each being vibrated. After the structure was assembled in the LBLG and the free-field instrumentation was placed, a sprinkling technique was used to build the

remainder of the sand specimen to avoid any risk of damage to the extensive instrumentation. During this process, the sand is dropped through a series of nozzles and a screen with a drop height of approximately 30 inches. A vibrator is used on the side of the sand hopper to promote sand flow through the nozzles. A detailed description of this placement method can be found in Reference 6.

Soil tests were conducted to determine the in situ physical properties of the sand surrounding the structure prior to each test. It was determined that the uniformity using the placement techniques described above was good, with a slightly lower density resulting from vibration than from sprinkling. The density data are tabulated in Table 2.1. Static plate-bearing tests were conducted at footing level to obtain load-carrying data at this level. These data are shown in Figure 2.3.

### 2.3 SOIL PROPERTIES

The sand used as the backfill during these tests was obtained from a natural deposit along the Big Black River in Warren County near Yokena, Mississippi, and is locally called Reid-Bedford model sand. This sand is a clean, uniform, fine sand (classified as SP according to the Unified Soil Classification System) with particles that are partly subangular and partly subrounded. The grain-size distribution is shown in Figure 2.4. The effective grain size ( $D_{10}$ ) is 0.16 mm, and the uniformity coefficient is 1.15. The specific gravity of the solids is 2.65. The minimum and maximum densities are 86.0 and 105.3 pcf, respectively, which correspond to void ratios of 0.924 and 0.570. The relation between the angle of internal friction and relative density is shown in Figure 2.5. This relation was obtained from a series of stress-controlled, consolidated-drained, direct-shear tests at several initial relative densities under normal pressures of 1, 3, and 6 kips/ft<sup>2</sup>. One-dimensional static confined compression curves are shown in Figure 2.6.

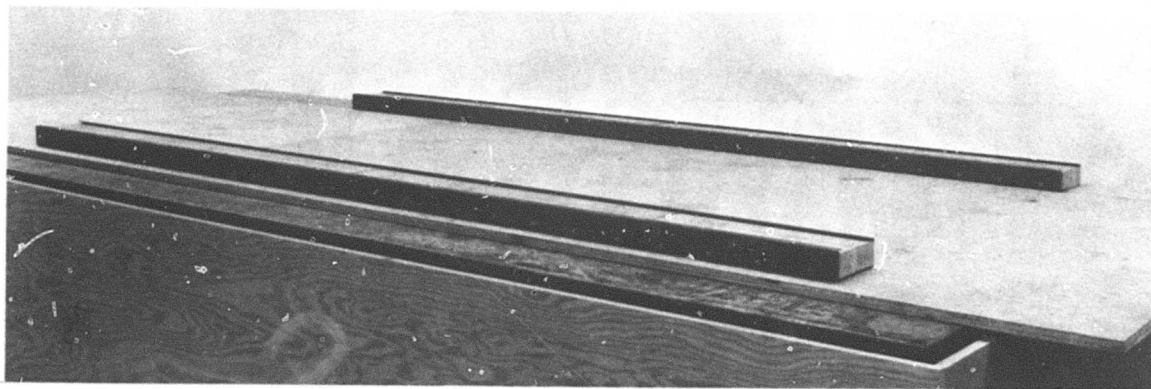
A series of tests was conducted on this sand by United Research Services, Inc. (Reference 7), to determine its dynamic characteristics. A test device which had relatively rigid confining boundaries was used to obtain the one-dimensional stress characteristics of the sand. Quasi-static

(loading rate too slow to produce wave phenomenon) and dynamic (based on wave propagation) stress-strain results are shown in Figure 2.7. Stress wave propagation velocity and peak particle velocity data are shown in Figure 2.8.

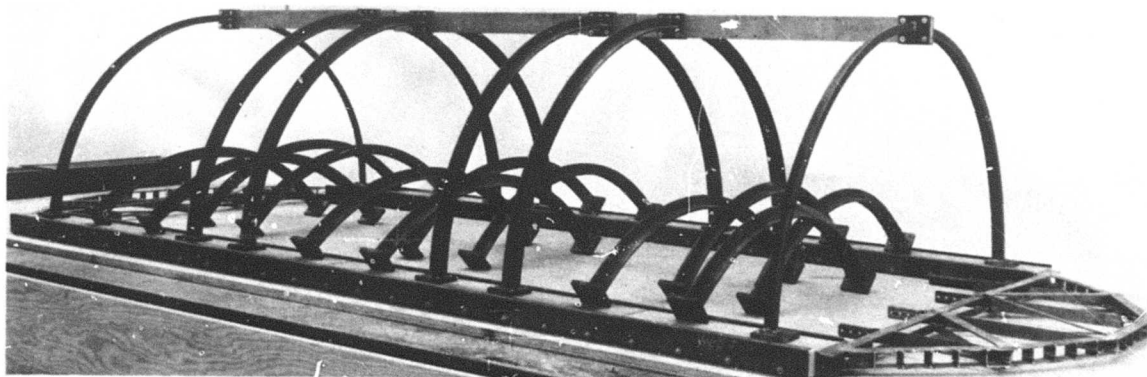
TABLE 2.1 PRESHOT SOIL DENSITIES

Shot 2 was a repeat loading of the Shot 1 configuration; therefore, the structure was not excavated and soil densities were not determined.

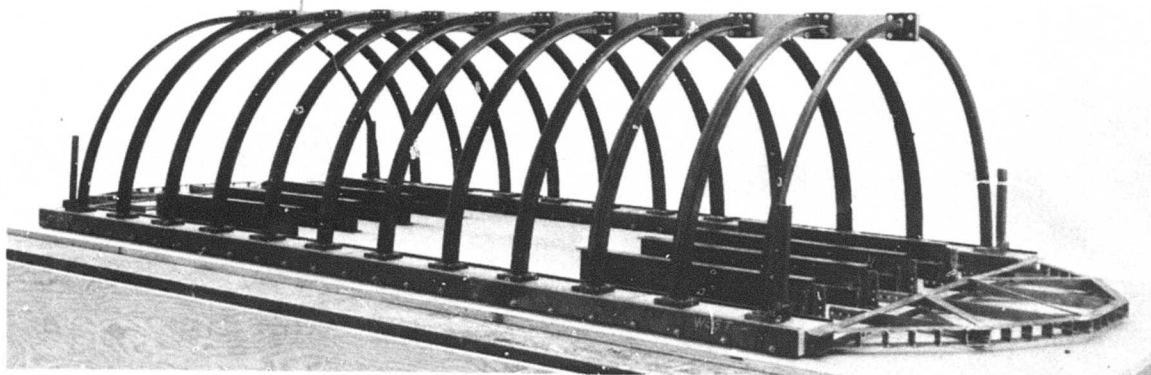
Elevation with Respect to Footing Level	Radius	Direction	Unit Weight
feet	feet		pcf
Preshot 1:			
-3.0	6.50	NE	100.4
	6.50	SE	100.5
	6.50	SW	100.1
	6.50	NW	99.5
		Average	100.1
0.0 (footing level)	8.00	N	100.8
	8.00	E	101.0
	8.00	S	101.0
	8.00	W	100.4
		Average	100.8
+2.8	9.80	N	101.3
	9.80	E	100.8
	9.80	S	102.4
	9.80	W	102.6
		Average	101.8
Preshot 3:			
0.0 (footing level)	8.00	N	99.4
	8.00	E	100.0
	8.00	S	100.5
	8.00	W	99.6
		Average	99.9
Preshot 4:			
0.0 (footing level)	8.00	N	100.3
	8.00	E	102.6
	8.00	S	100.1
	8.00	W	101.2
		Average	101.0
+2.8	10.00	N	102.5
	9.00	N	100.7
	9.00	S	102.5
	10.00	S	100.3
		Average	101.5
Preshot 5:			
0.0 (footing level)	8.00	N	101.0
	8.00	E	100.3
	8.00	S	100.8
	8.00	W	99.4
		Average	100.4



a. Structure footings assembled and in position.

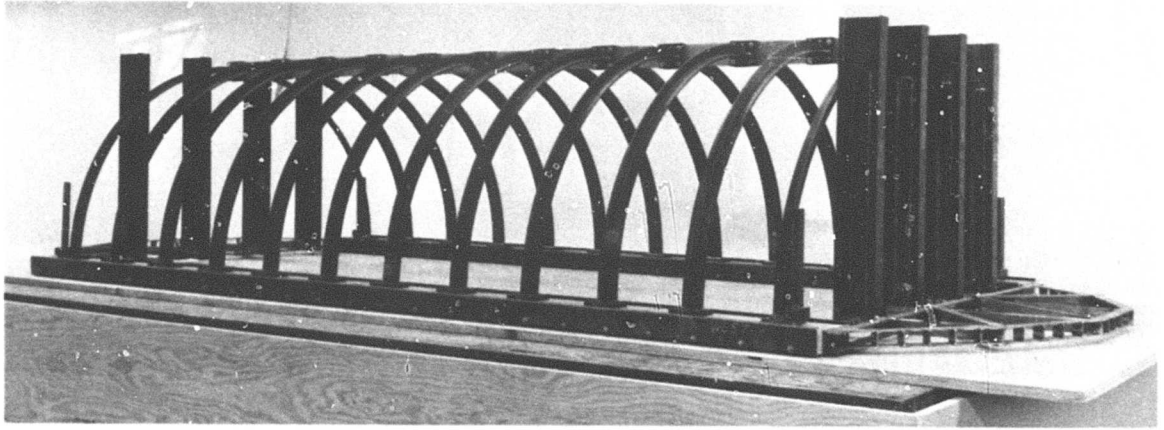


b. Structure with crown timber and six ribs in position.

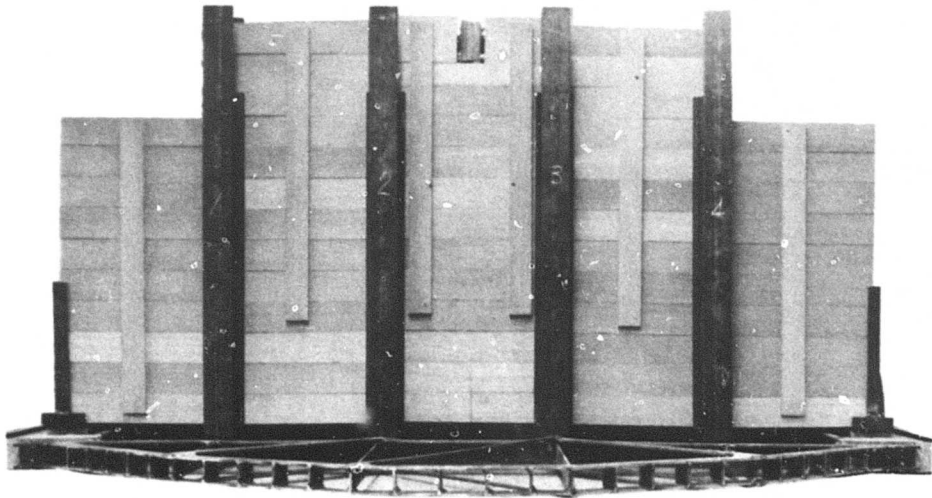


c. Structure with ribs raised and bulkhead edge support channels.

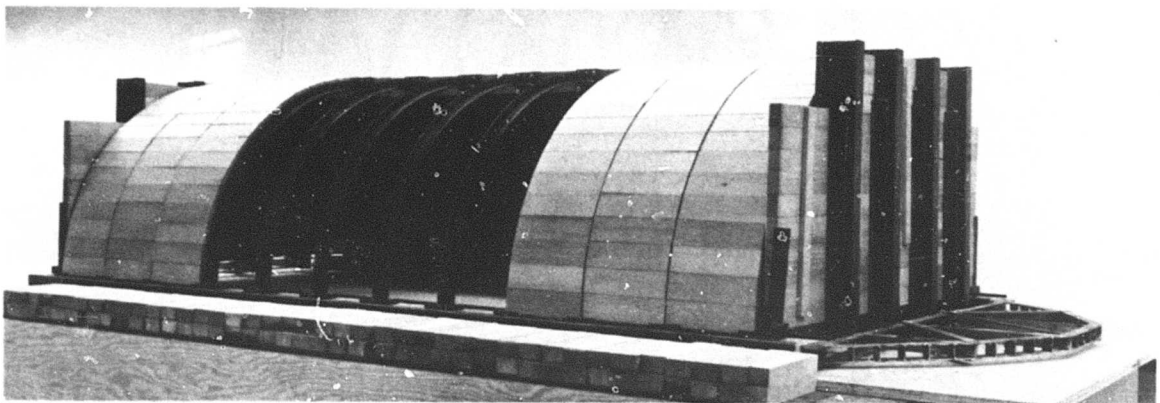
Figure 2.1 Steps in structure assembly (Sheet 1 of 2).



d. Structure with all steel structural elements assembled.



e. Assembled bulkhead.



f. General view of structure with a portion of the roof lagging removed.

Figure 2.1 (Sheet 2 of 2).

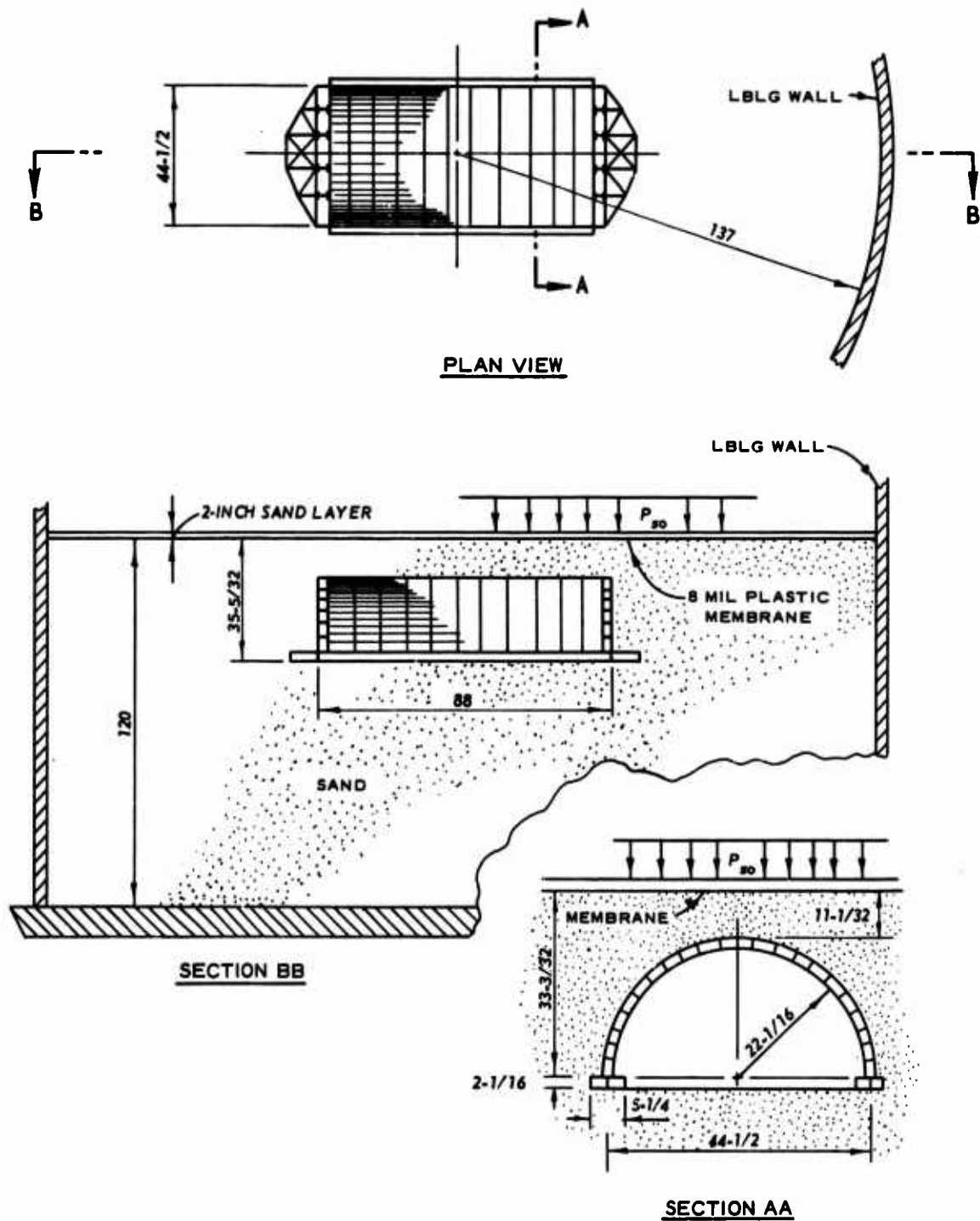


Figure 2.2 Test geometry and location in the LBLG. Dimensions are in inches.

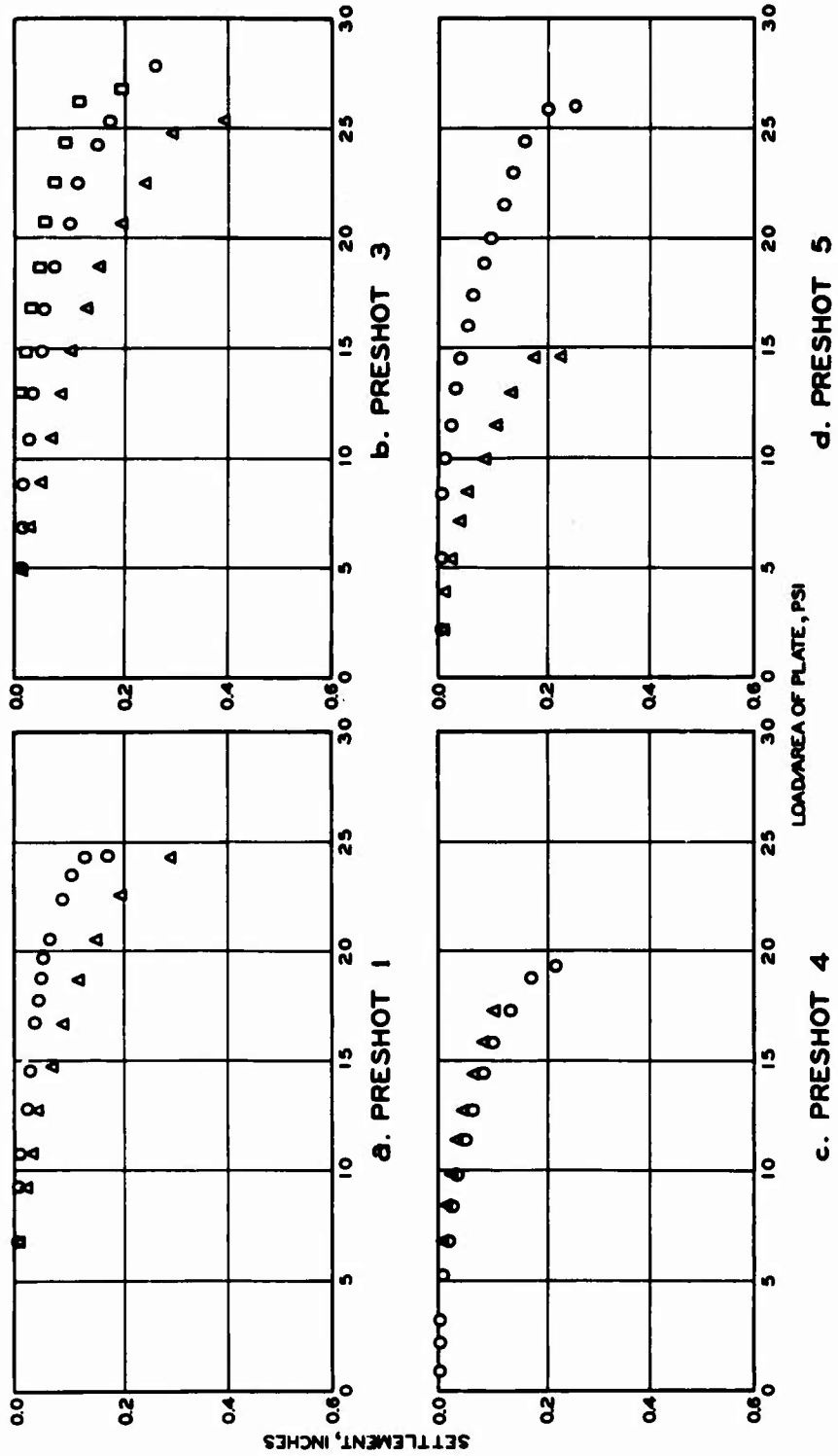


Figure 2.3 Plate-bearing test results at footing level. Shot 2 was a repeat loading of the Shot 1 configuration, and plate-bearing tests were not conducted.



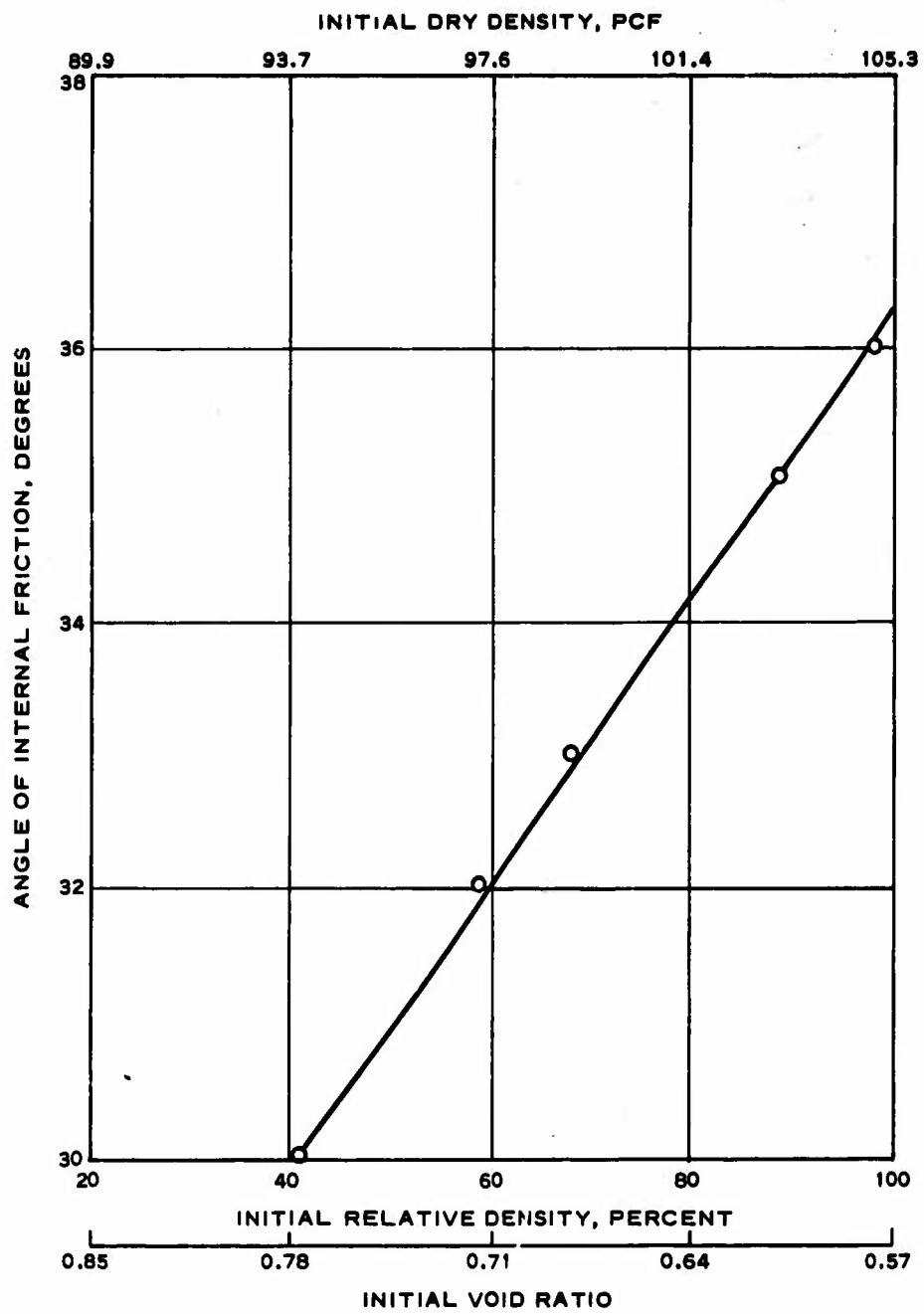
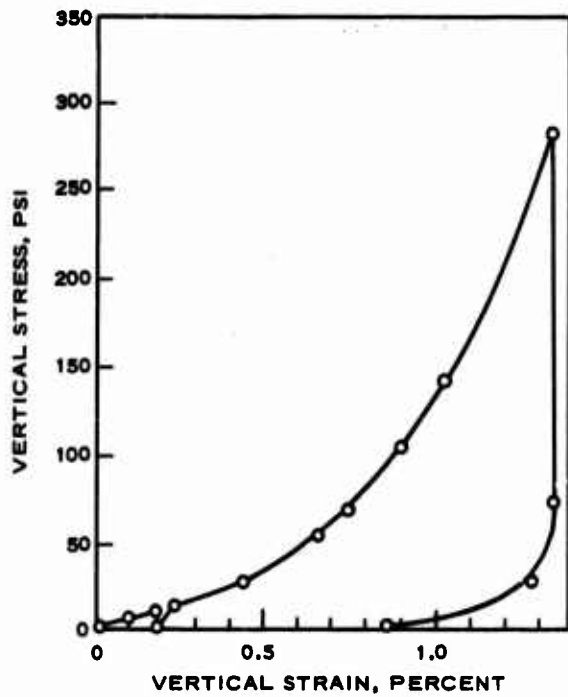
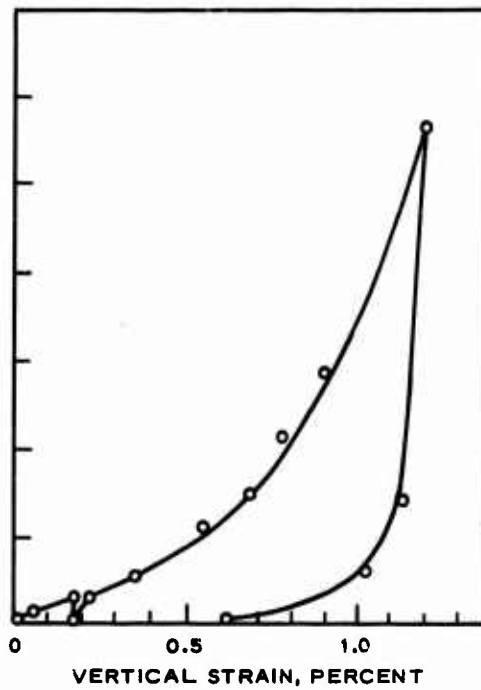


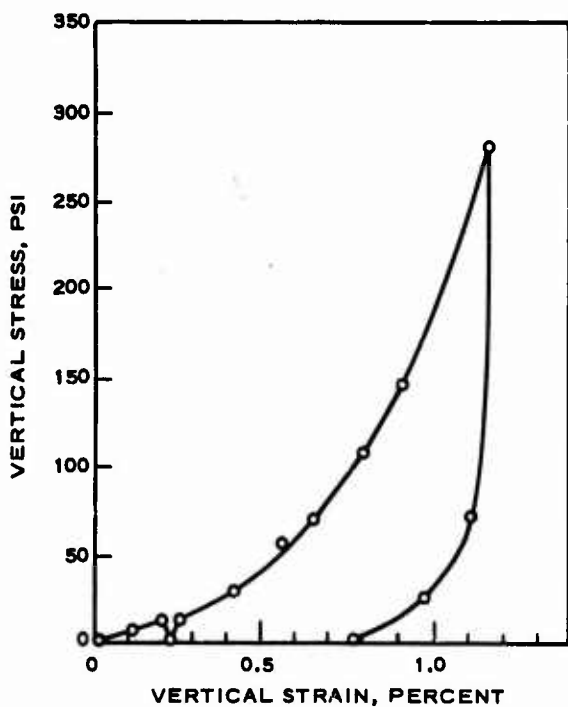
Figure 2.5 Relation between angle of internal friction and density for the test sand.



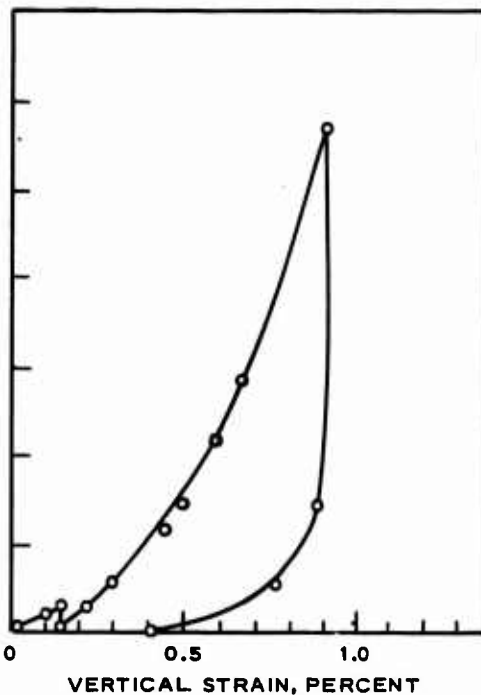
a. 96.7-PCF INITIAL DRY DENSITY  
( $D_r = 55\%$ )



b. 99.6-PCF INITIAL DRY DENSITY  
( $D_r = 70\%$ )



c. 100.8-PCF INITIAL DRY DENSITY  
( $D_r = 77\%$ )



d. 103.0-PCF INITIAL DRY DENSITY  
( $D_r = 90\%$ )

Figure 2.6 One-dimensional static confined compression test data for the test sand.

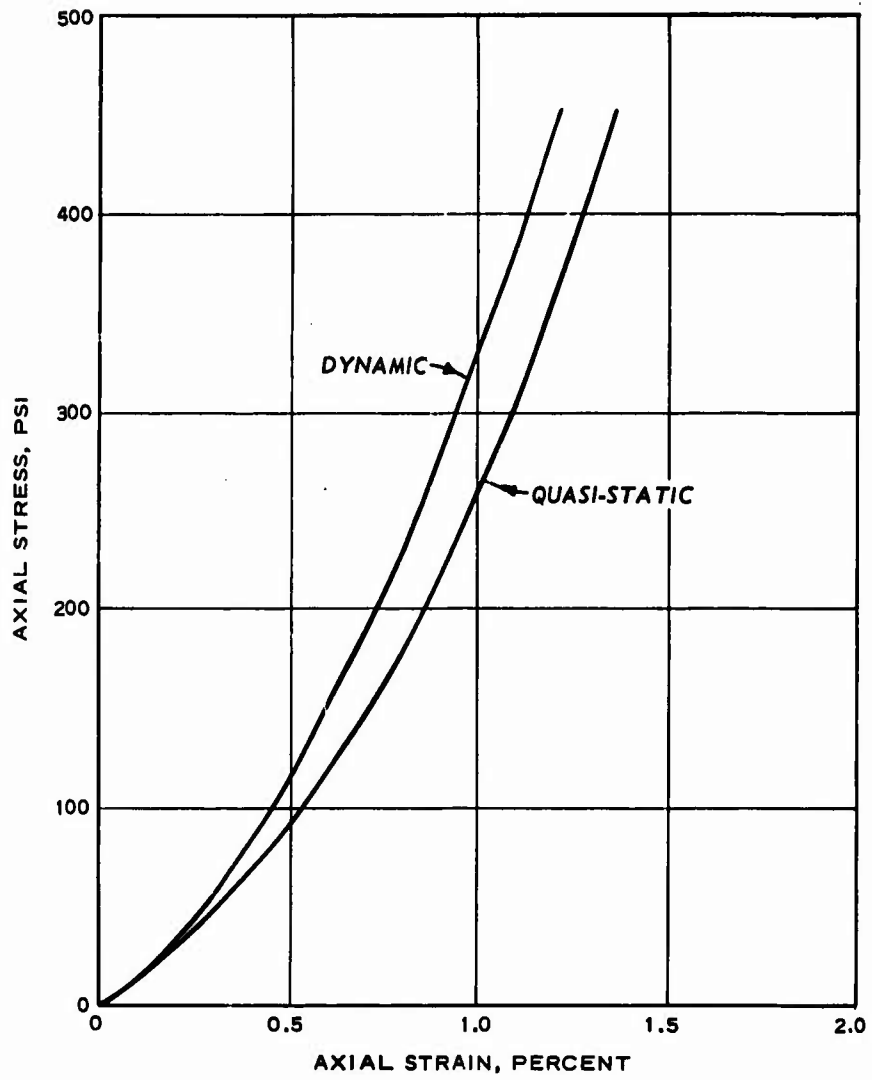


Figure 2.7 Stress-strain curves for the test sand; density 99.7 pcf.

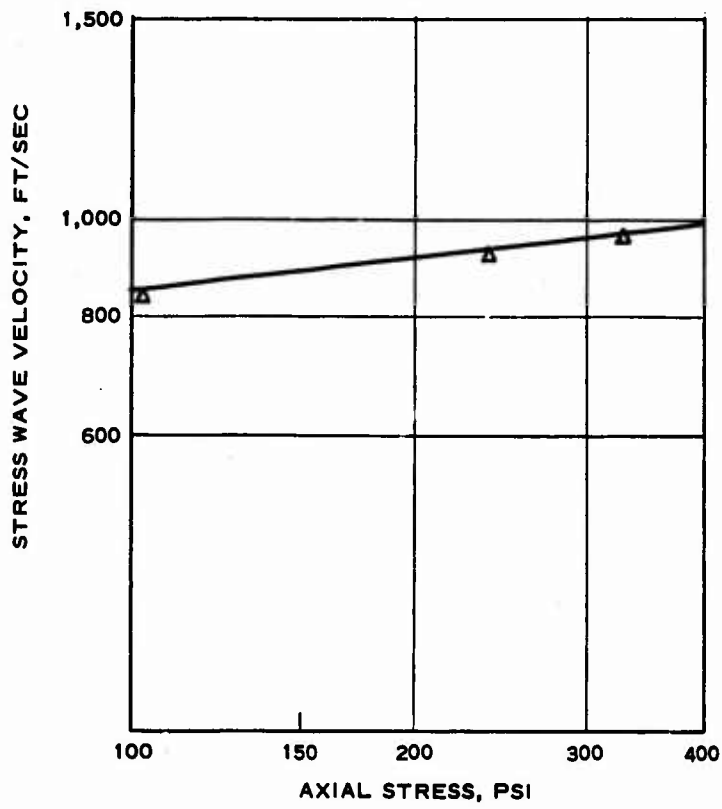
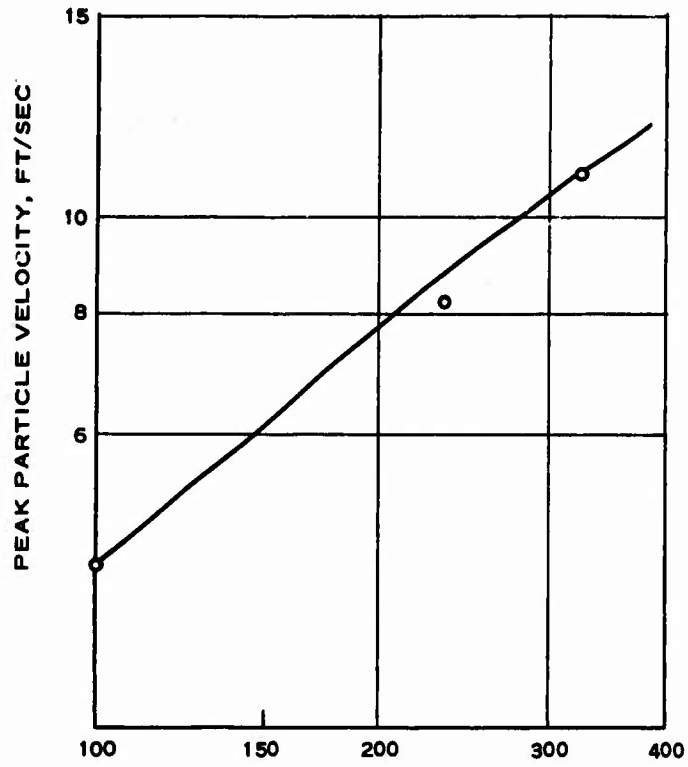


Figure 2.8 Velocity data for the test sand; density 99.7 pcf.

## CHAPTER 3

### RESULTS

The data results of this study are presented in tabular form in Appendix A, Appendix B contains time histories of the test records, and Appendix C contains computed data based on the raw data. Typical records are presented throughout the main text of this report whenever their inclusion is believed of value to the reader.

#### 3.1 LOADING INPUT

3.1.1 Surface Airblast. Typical of the surface airblast overpressure ( $P_{so}$ ) histories is the presence of a number of small shocks during approximately the first 10 msec of response. These shocks are due to reflections occurring within the baffle and firing tubes and are a result of the pressure-generation geometry. The action of the soil is such that it tends to smooth out the airblast wave as it is transferred into and propagates through the soil. This being true, the presence of the high-frequency spikes in the airblast wave has little effect on subsurface structures; consequently, a relatively smooth pressure signature was determined for each shot in the test series by dividing the overpressure histories into a number of time increments, selecting a mean pressure value for each time increment, being careful to preserve impulse, and constructing a smooth curve using the mean values. Based on the individual smoothed curves, a composite surface airblast overpressure history was constructed for each shot by averaging all the individual smoothed peak pressures to arrive at a peak surface airblast overpressure. Using this peak value, all of the smoothed curves were normalized and averaged together to give the composite surface airblast overpressure curves shown in Figure 3.1. The composite peak pressures are close (within 10 percent) to those predicted, based on total weight of explosive used, and show a difference of not more than 10 percent in the values averaged to obtain the normalizing peak overpressure.

Certain of the recorded data were judged invalid, and these data were not considered in the construction of the composite curves. If an individual smoothed peak pressure was appreciably (50 percent) higher or lower

than predicted based on explosive weight it was eliminated. For example, in the case of Shot 4 only record BP(6965) was used since both SP1 and SP2 indicated pressures even lower than Shot 3. During the period of Shot 4 almost all of the airblast transducers were diverted from the Blast Load Generator Facility for use on a high-priority field test. The record for Gage BP(6965) does not appear to have been reliable much past peak as can be seen when comparing the impulse curves for the various shots (Figure 3.2). This figure shows the impulse for Shot 4 was less than that for Shot 3 which was a lower energy shot. The impulse data indicate that with the exception of Shot 4, the impulse increased as expected.

A portion of the tape playback for Gage SP1, Shot 3, is shown in Figure 3.3 along with the condensed composite record for Shot 3. The only sets of pressure records indicating duration were obtained for Shots 3 and 4. Generally, the high temperature at the soil surface causes the pressure gages to begin drifting after about 400 msec, and eventually to register a negative pressure. On Shot 3 this did not occur and some confidence can be attached to the duration observed. A duration was observed in Shot 4 without negative pressure registration, but the poor impulse correlation raises some doubt as to the validity of this duration time. Tabulated in Table 3.1 are the surface airblast overpressure parameters as measured for each shot.

3.1.2 Free Field. Free-field stress and acceleration data were taken during the test series. Shots 3 and 4 were extensively instrumented while Shots 1, 2, and 5 were lightly instrumented. These data are tabulated in Tables A.3 and A.4, respectively.

## 3.2 VISUAL DAMAGE SURVEY

3.2.1 General Gross Motion and Damage. Shots 4 and 5 were the only tests in which the gross motion of the structure was sufficient to create a noticeable depression of the sand surface in the vicinity immediately above the structure (Figure 3.4). It became evident during excavation of the structure that the depression was caused by the vertical deformation of the steel ribs and downward deflection of the footings. While considerable displacement and deformation of the structure were noted after

Shot 3, no definite depression was observed. Shown in Figure 3.5 is a sequence of photographs showing the structure crown curvature after Shots 3, 4, and 5.

3.2.2 Component Damage. In every shot, the crown timber suffered damage. It appears to have been twisted and to have acted like a buffer absorbing some of the thrust forces. At the lower overpressures ( $P_{so} < 85$  psi), the crown timber split slightly. However, at the higher overpressures, extensive splitting due to twist and crushing occurred (Figure 3.6). No damage was done to the timber lagging until Shot 5. During this shot the rib deformation was extensive enough to allow the lagging to bear on the footing and to take some of the thrust loading in compression. This caused some visible compressive damage to the lagging; however, the damage was slight and was structurally insignificant.

The footings were damaged extensively at the high overpressures, but were only slightly damaged at overpressures below 120 psi. They generally were bent inward and downward in the central region after each shot. This inward deformation can be seen in Figure 3.7 which shows the damage to the three sets of footings from Shots 3 to 5. Parts of the footings for Shot 3 were misplaced and are shown as black dummy sections in the figure. Generally, the damage was greater with increasing overpressure as can be clearly seen in Figure 3.8, a photograph of a section cut through the footing below Rib 9. Also shown in this figure is the deformation of the footing caused by the timber lagging as it was forced into the supporting footing during Shot 5.

Some attempt was made to determine if a significant amount of spalling and motion of the sand floor occurred during Shots 4 and 5. In these shots a tape strip was placed vertically at about the center of the east side of the structure floor to try to measure the extent the sand surface moved upward. Figure 3.9 shows the sand distribution obtained. This record indicates that the interior floor moved up about 1.45 inches and the sand particles were thrown to a height of about 5.40 inches above the original floor level. The tape for Shot 5 did not yield favorable results. However, the interior floor accelerometer, 51VA, was thrown up and displaced from its preshot location below a sandbag (Figure 3.10). This

accelerometer was not displaced during Shot 4, which indicated, as expected, that the floor was disturbed to a greater degree during Shot 5.

The only serious damage at low overpressure occurred at the connecting bolts between the bulkhead beams and the end trusses. Damage was first noticed here during the pilot test (Figure 3.11), and was initially attributed to insufficient bolt area causing high shearing stresses to occur. Consequently, the bolt sizes for future shots were increased slightly to provide additional shear area. During Shots 1 and 2, the same damage occurred (see inset, Figure 3.11). After closer examination, it was decided that the end truss extending out into the free field acted like a paddle, tending to rotate as the structure moved downward. This rotation occurred about the inner bolt and sheared the bolts off starting with the outer one as shown in the inset of Figure 3.11. A redesign of the connection was made using a pin connector which allows rotation. The redesign used the original shear area of the four bolts as the area of the pin and is detailed in Appendix D. Testing was continued using the modified connectors during Shots 3, 4, and 5. During Shot 3, excessive rotation caused cracks to appear in the tongue between the bulkhead beams and the end truss (Figure 3.12a). Possibly, this distress was due to fatigue since this component had been tested three times previously at lower overpressures. Prior to Shot 4, the end truss tongues were replaced and rotation cracks appeared. Again the tongues were replaced and during Shot 5 complete failure occurred (Figure 3.12b). The fact that complete failure did not occur during Shot 4 seems to indicate that the Shot 3 distress was due in part to fatigue.

TABLE 3.1 SURFACE AIRBLAST OVERPRESSURE PARAMETERS

Shot	Peak Pressure	Duration	Rise Time
	psi	msec	msec
Pilot	85	--	1.0
1	37	--	1.6
2	67	--	1.0
3	117	956	0.5
4	143	950	0.4
5	177	--	0.5

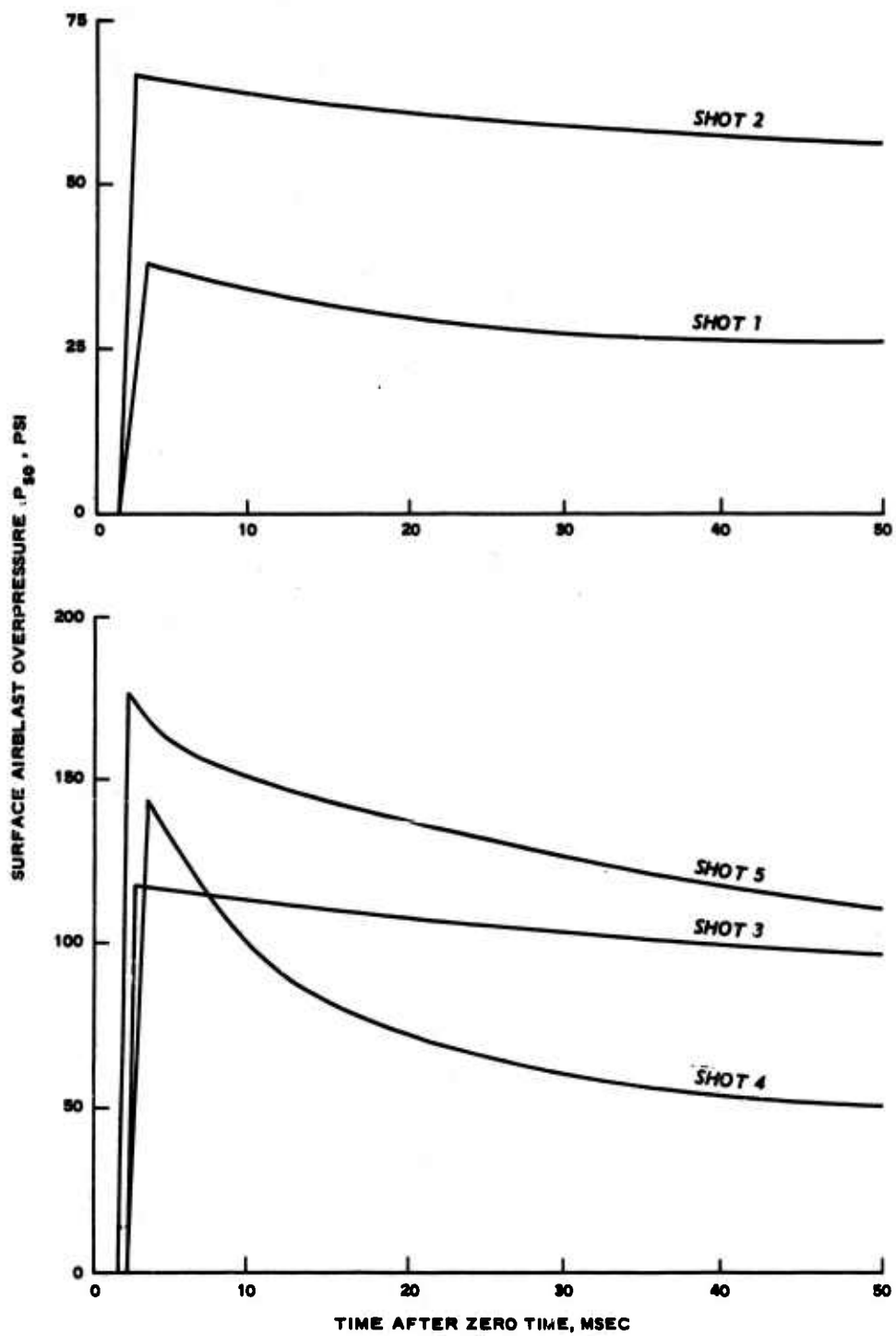


Figure 3.1 Composite surface airblast overpressure curves.

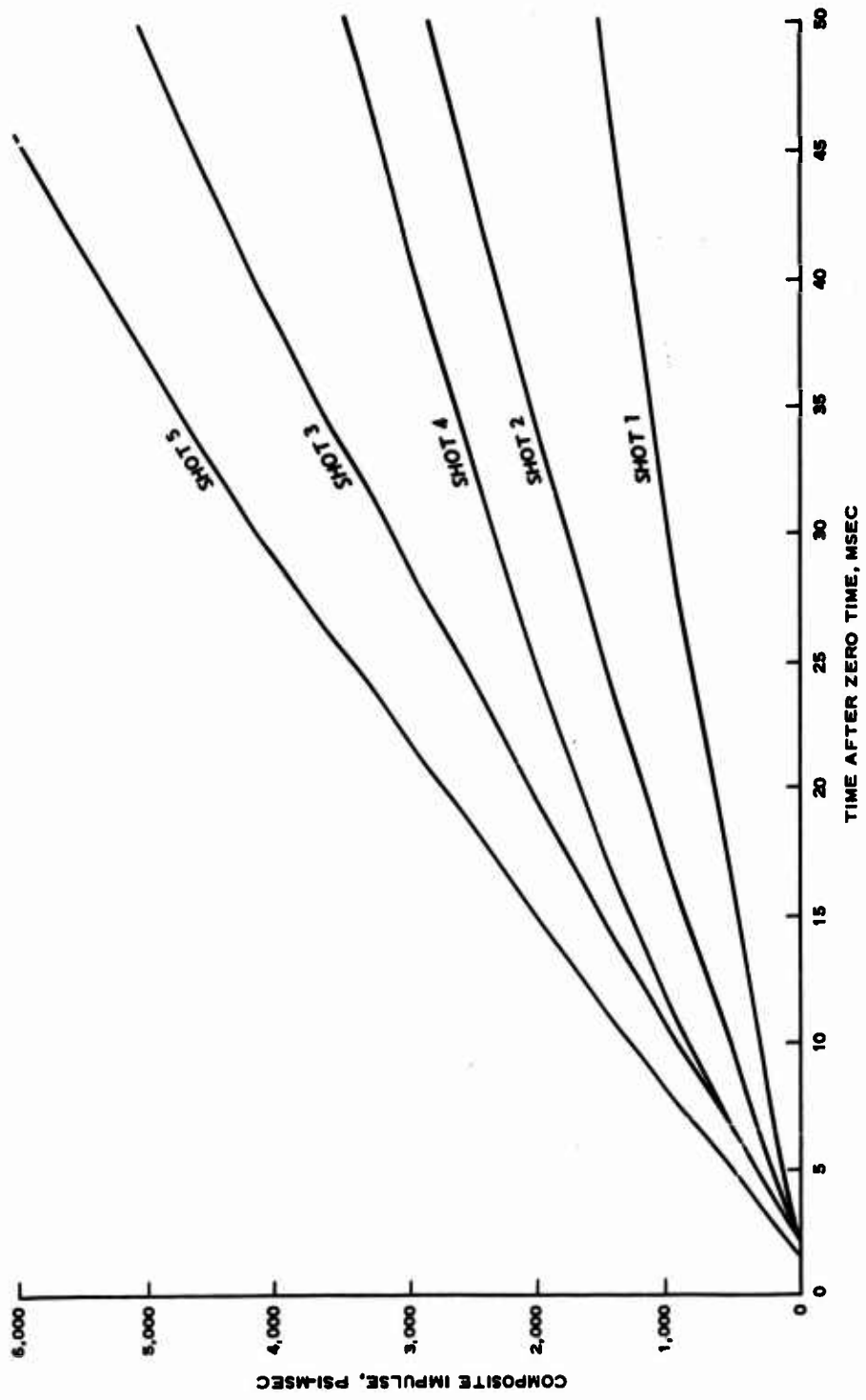


Figure 3.2 Initial impulse data.

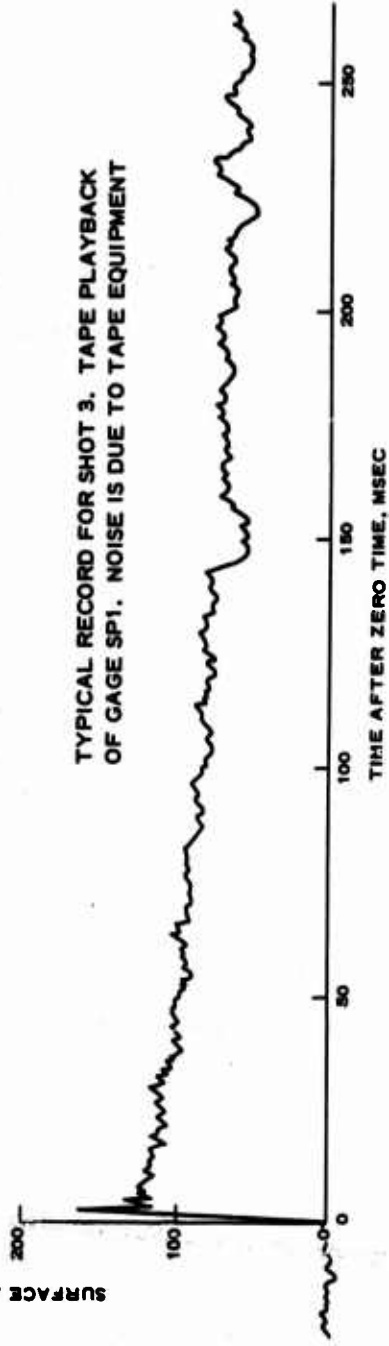
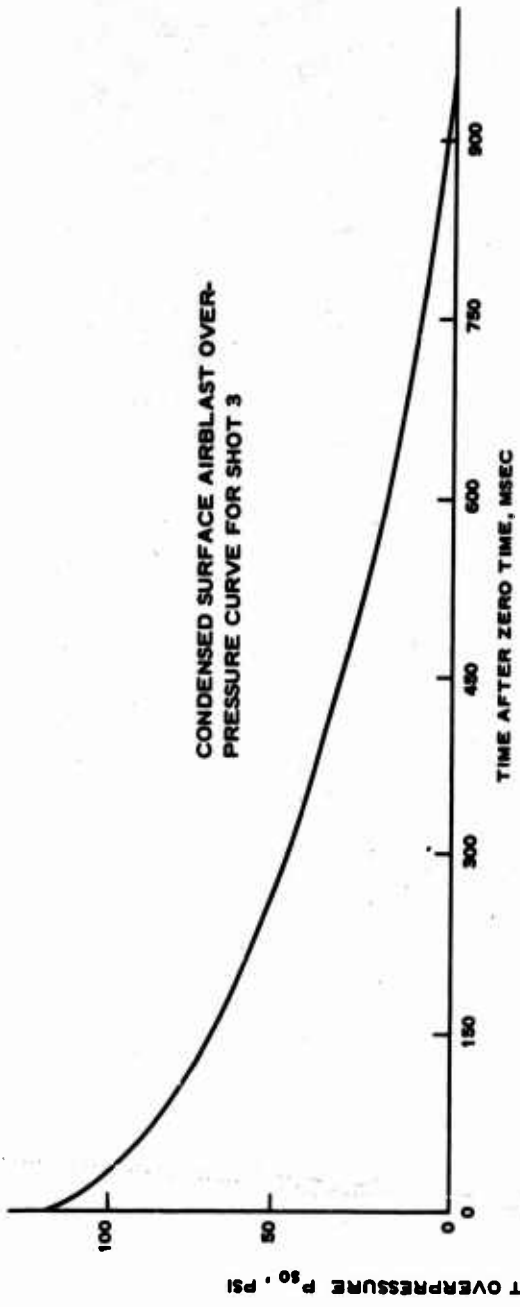


Figure 3.3 Typical airblast data.

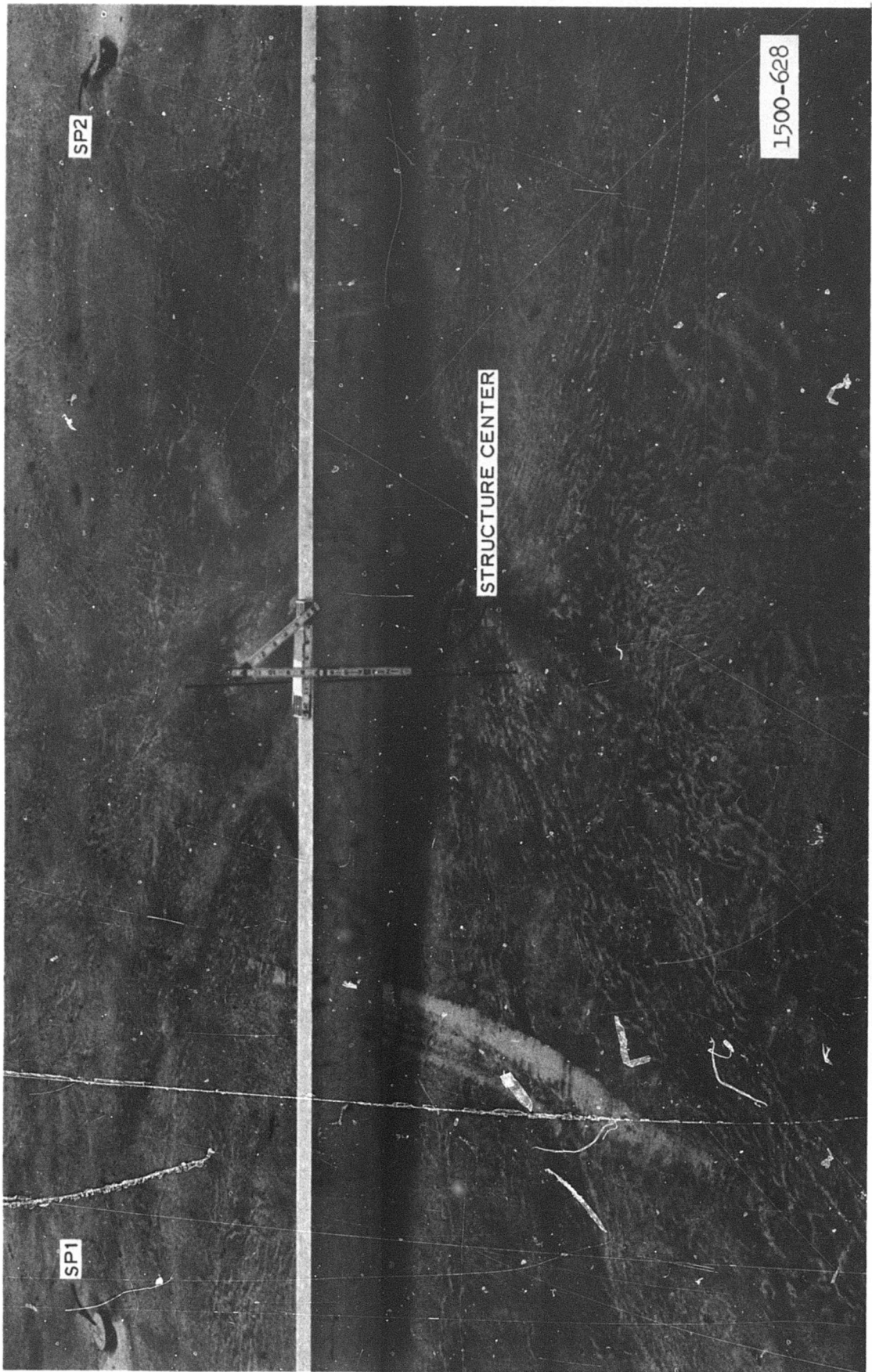
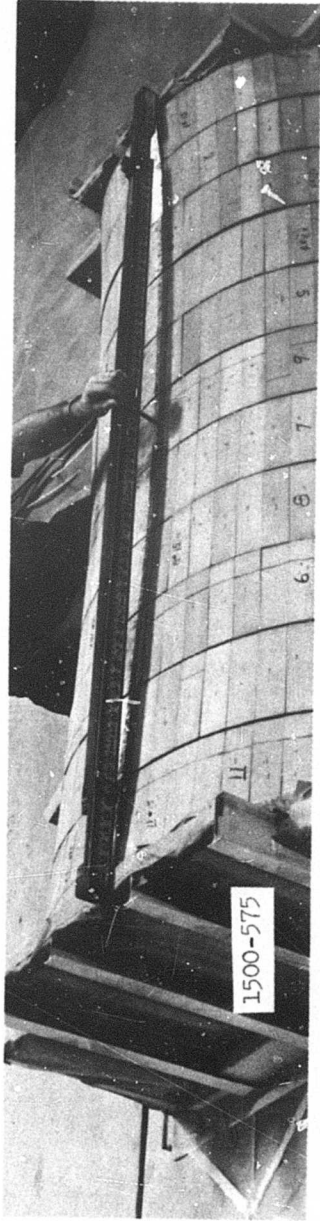
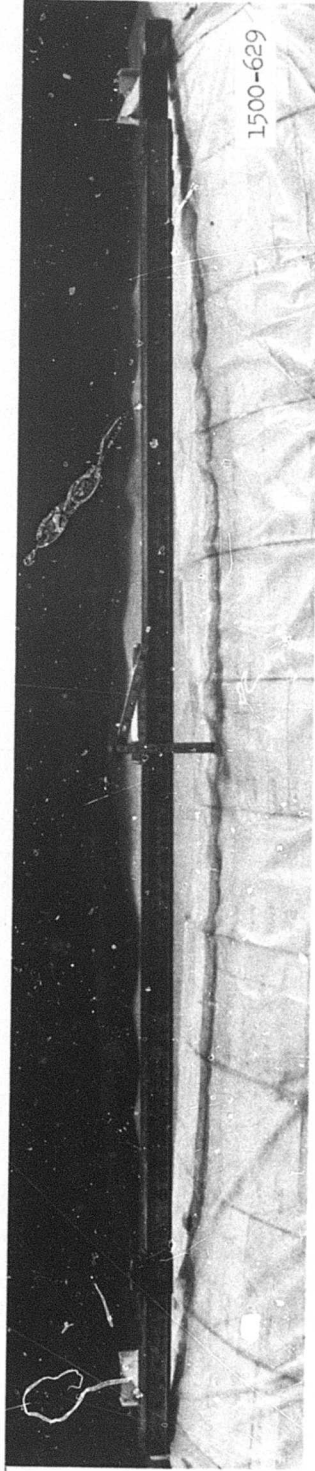


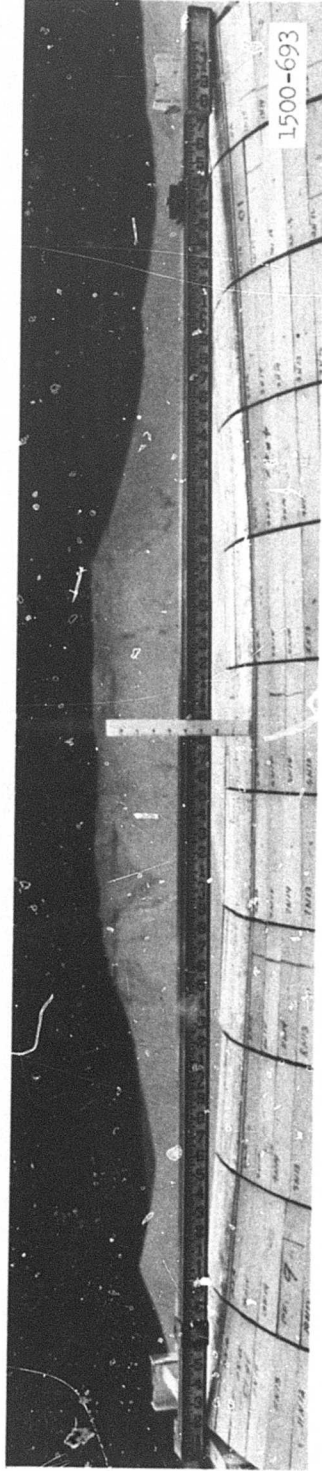
Figure 3.4 Depression in the sand surface caused by the gross motion of the structure during Shot 4. Note the presence of airblast Gage SP1 in the upper left-hand corner.



a. Postshot 3.

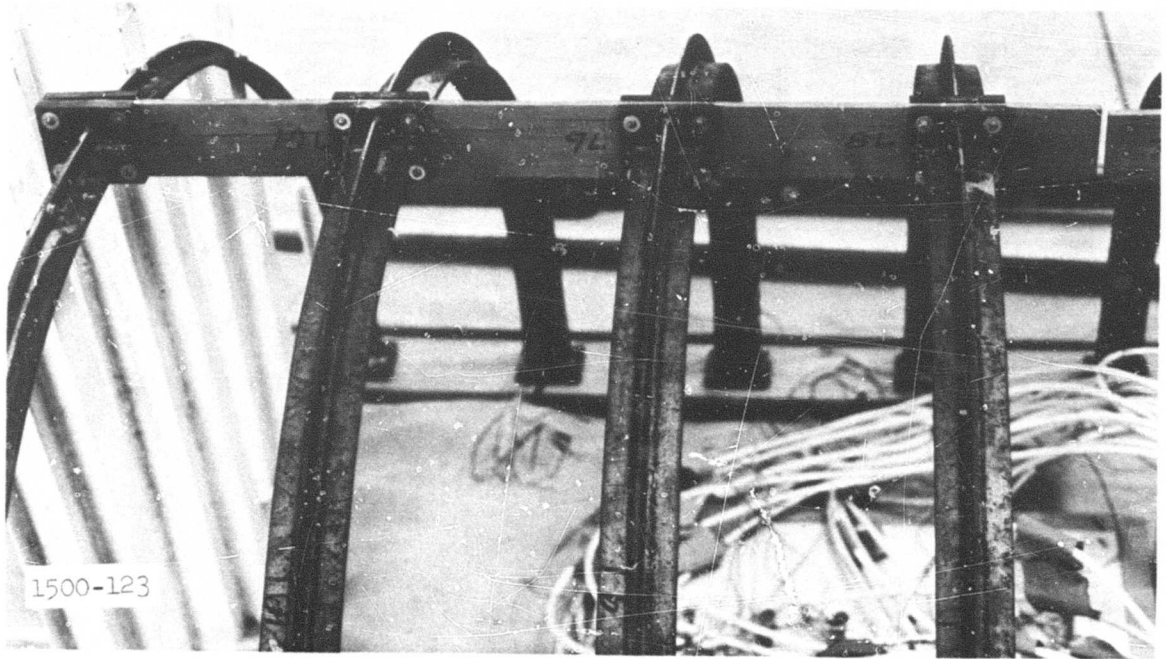


b. Postshot 4.

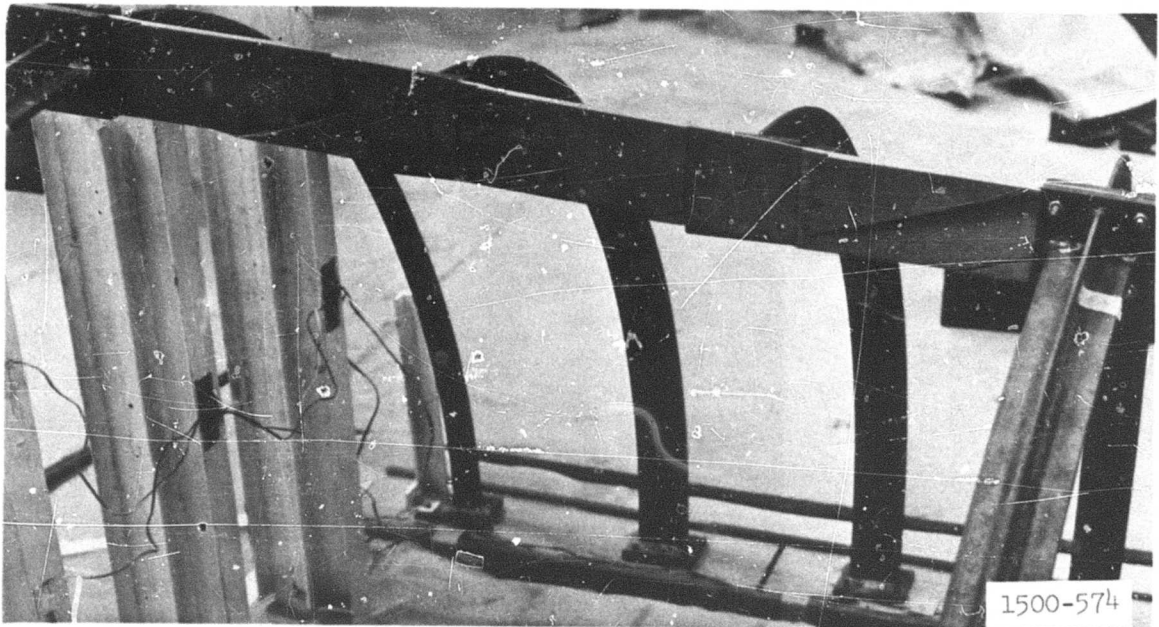


c. Postshot 5.

Figure 3.5 Postshot crown curvature.

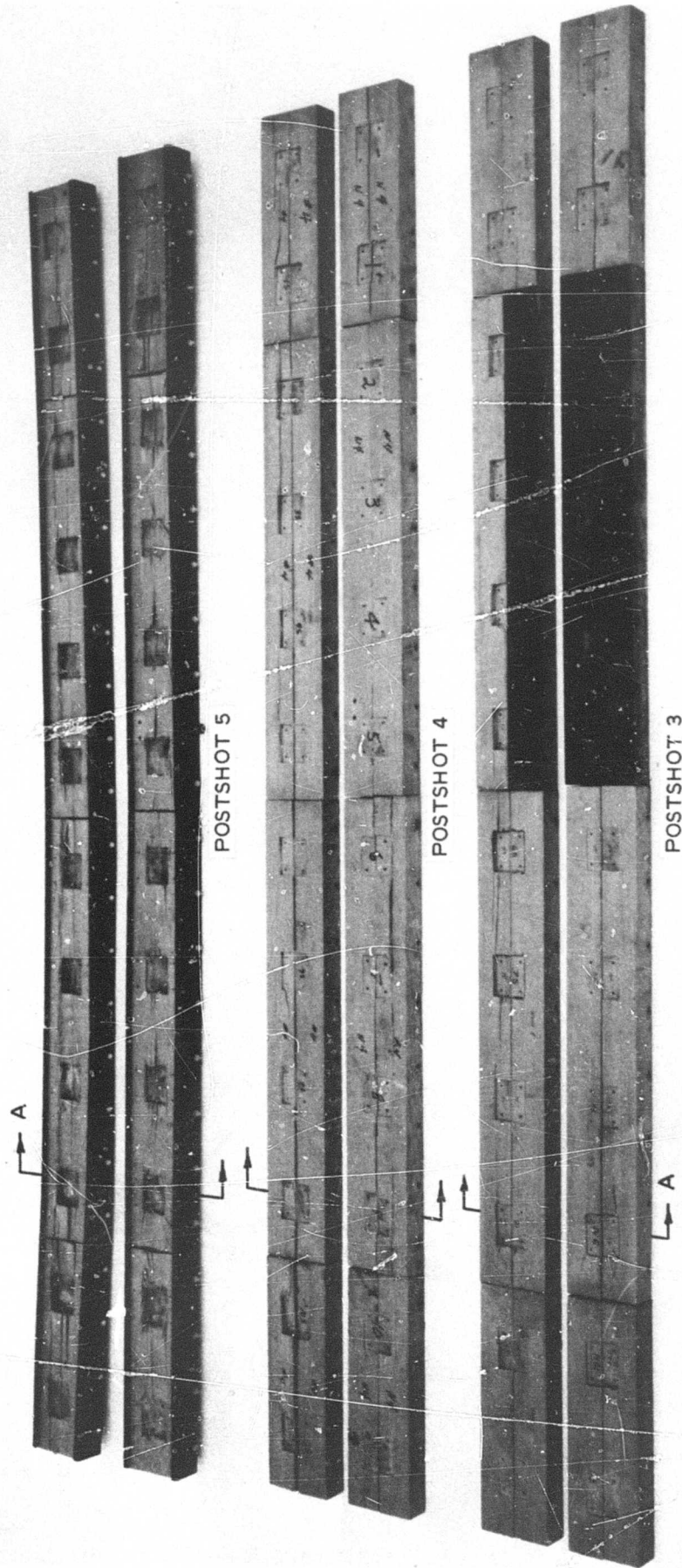


a. Pilot test.



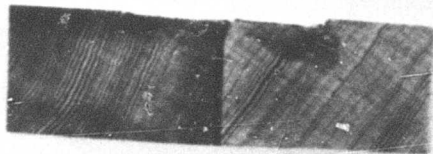
b. Shot 3.

Figure 3.6 Postshot damage to crown timber.

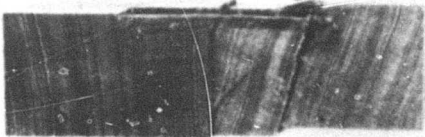
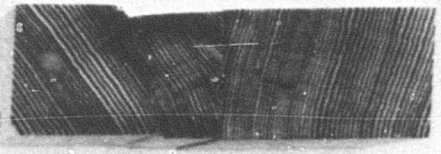


1500-746

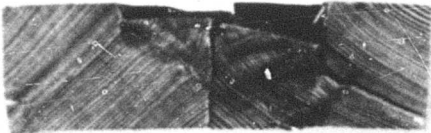
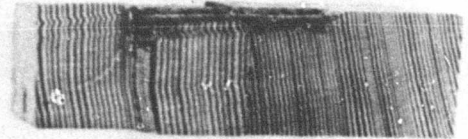
Figure 3.7 Postshot view of the damaged footings showing the punching damage. Note also the inward bow of the Shot 5 footings.



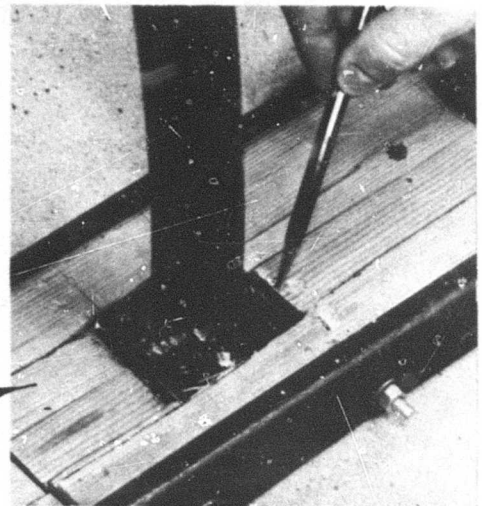
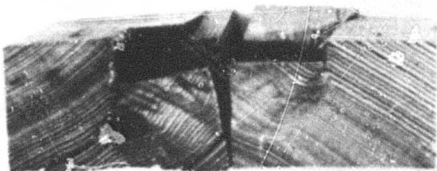
POSTSHOT 3



POSTSHOT 4



POSTSHOT 5



RIB SHOWN IN PLACE  
POSTSHOT 5

1500-749

Figure 3.8 Section views of the damage shown in Figure 3.7 to the footings at the section shown (Section AA).

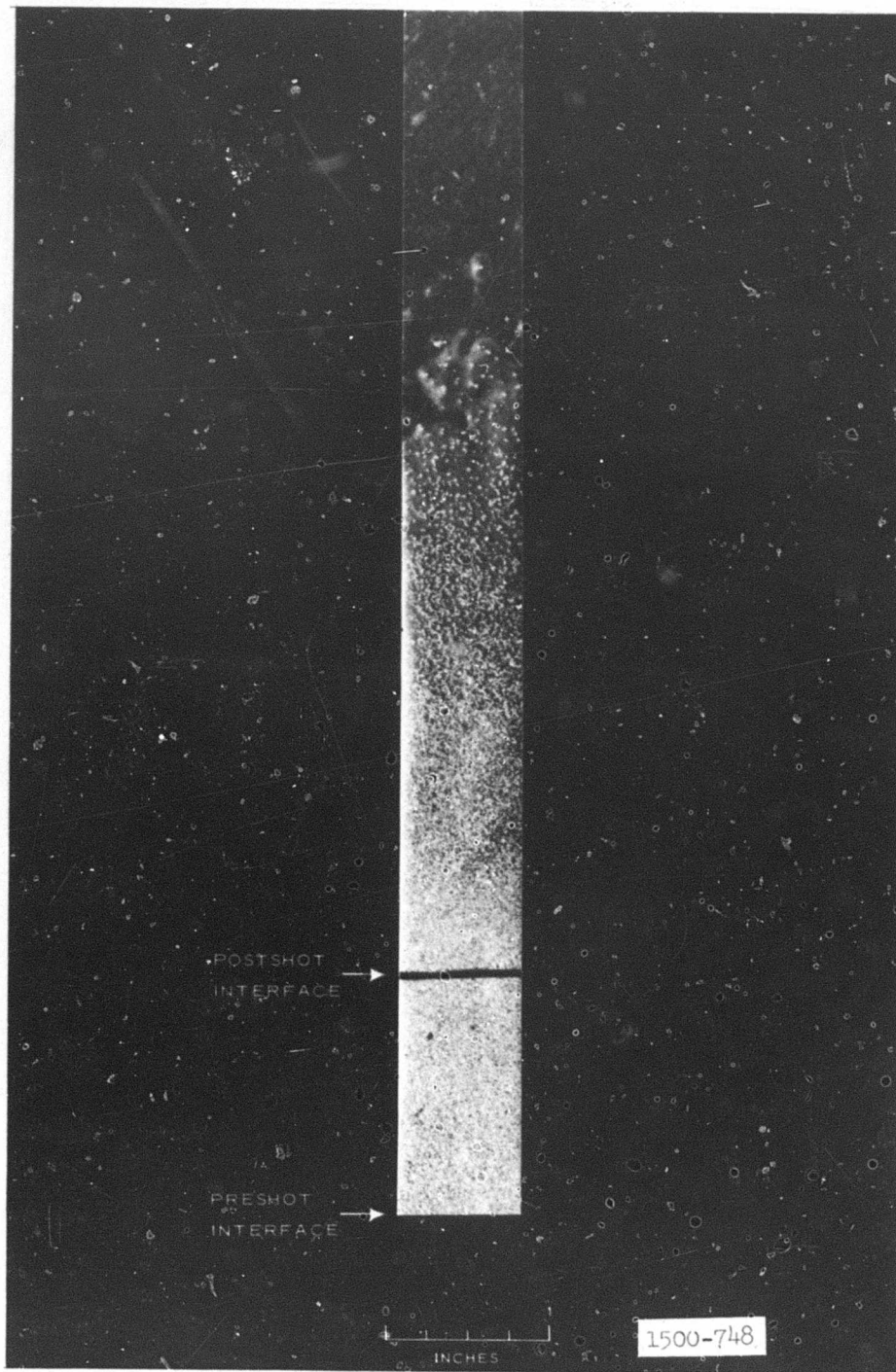


Figure 3.9 Sand spall of the interior floor surface during Shot 4.

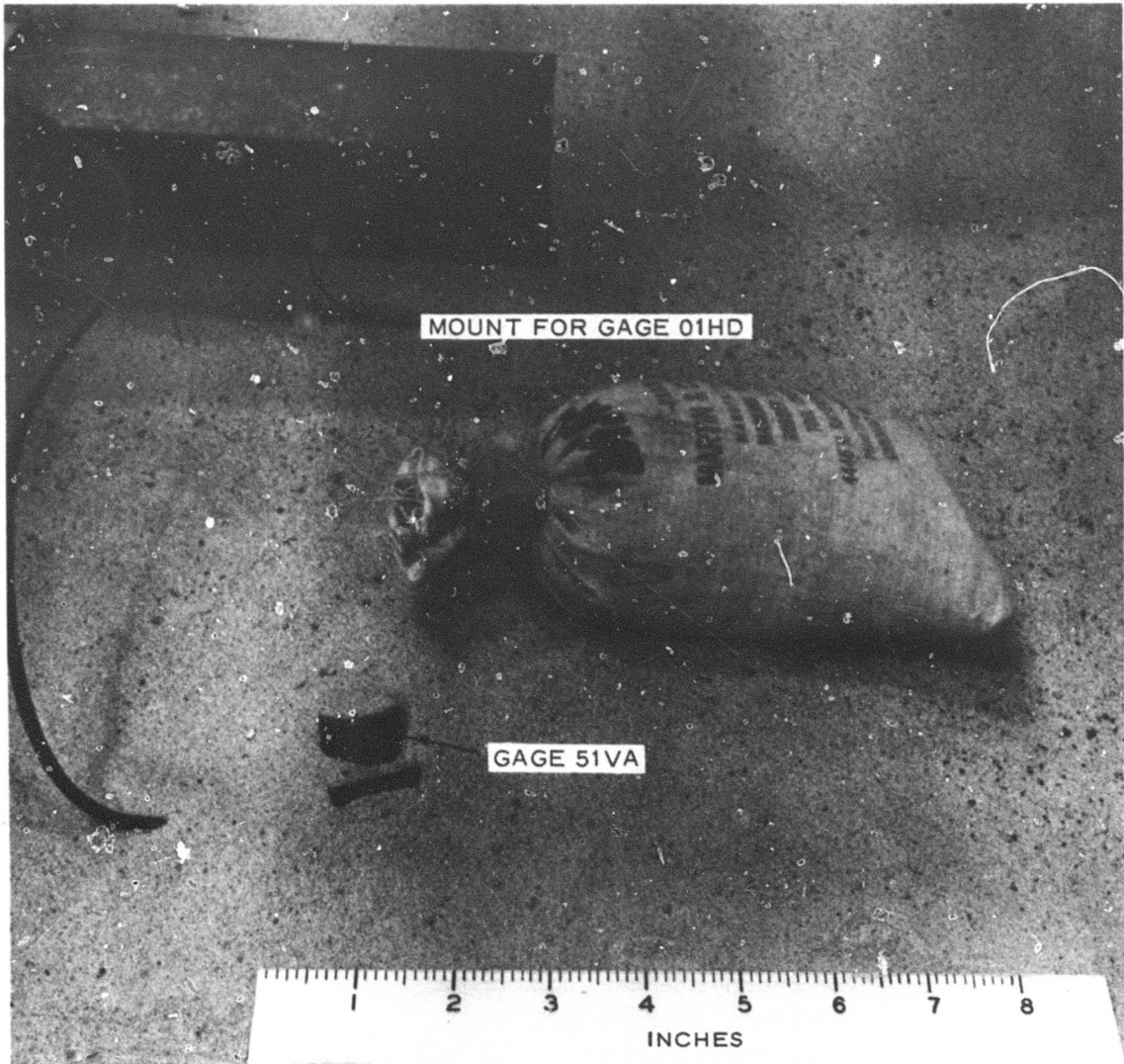


Figure 3.10 Dislocation of Gage 51VA caused by spalling of the interior floor during Shot 5.

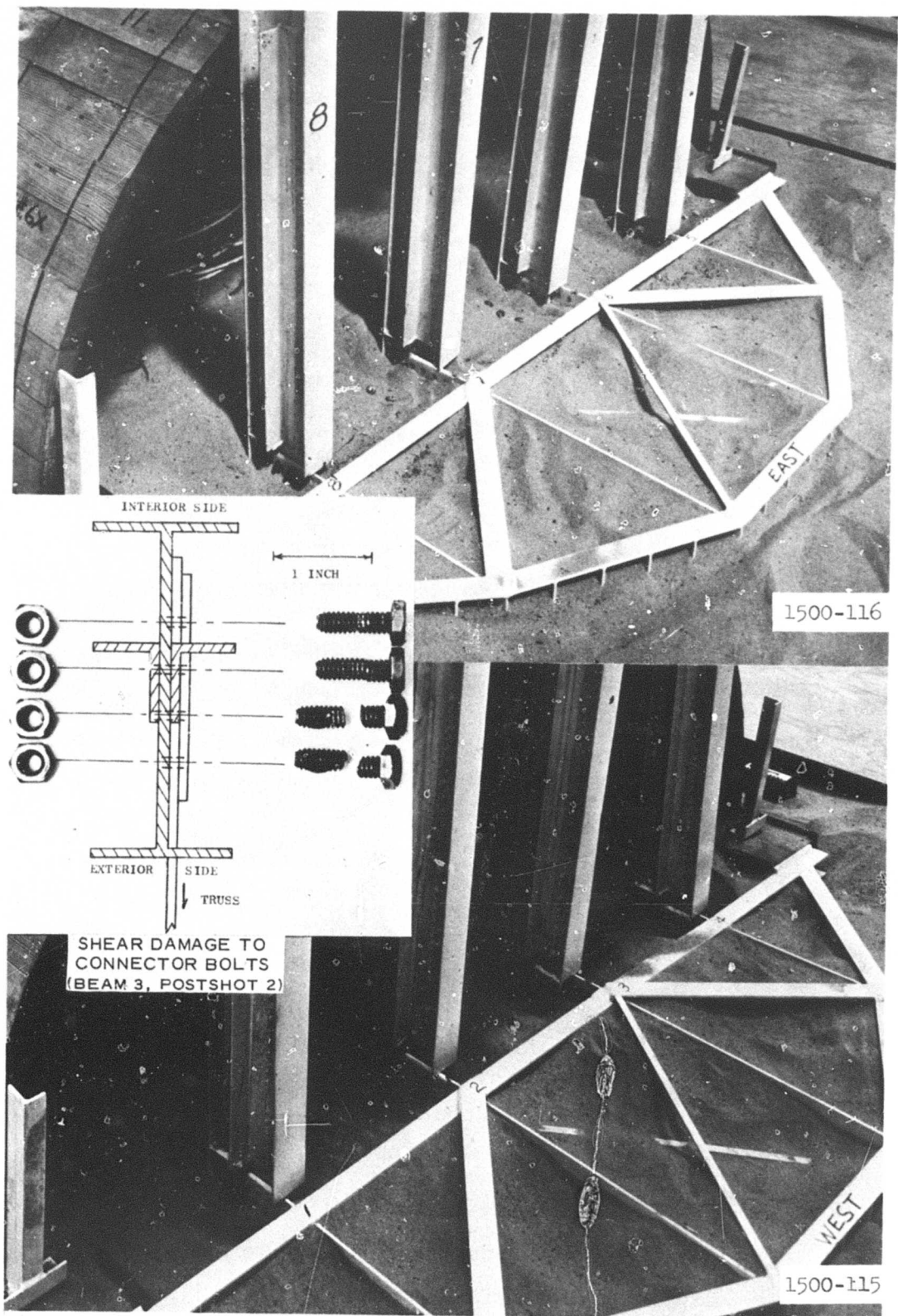
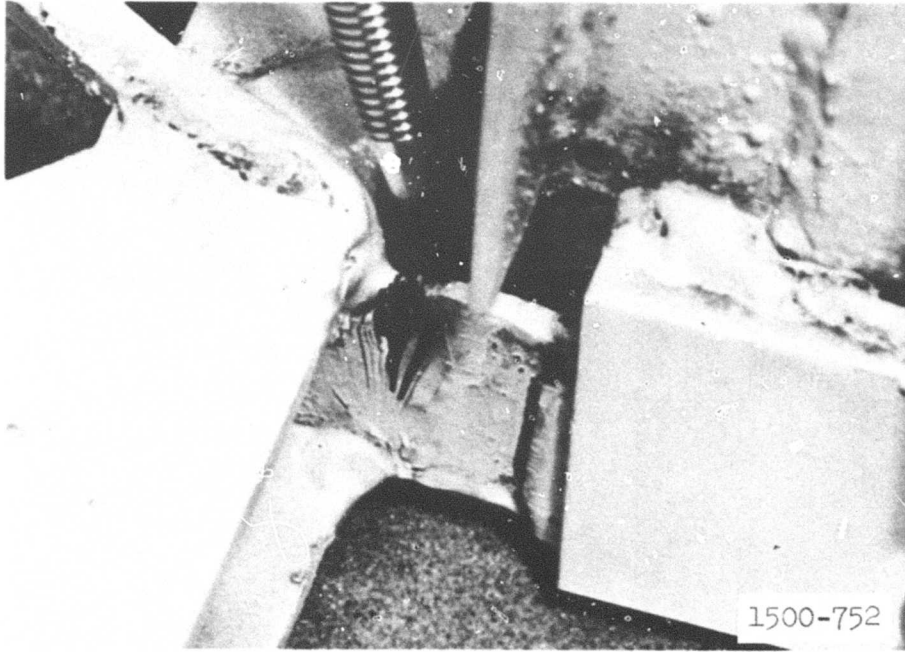
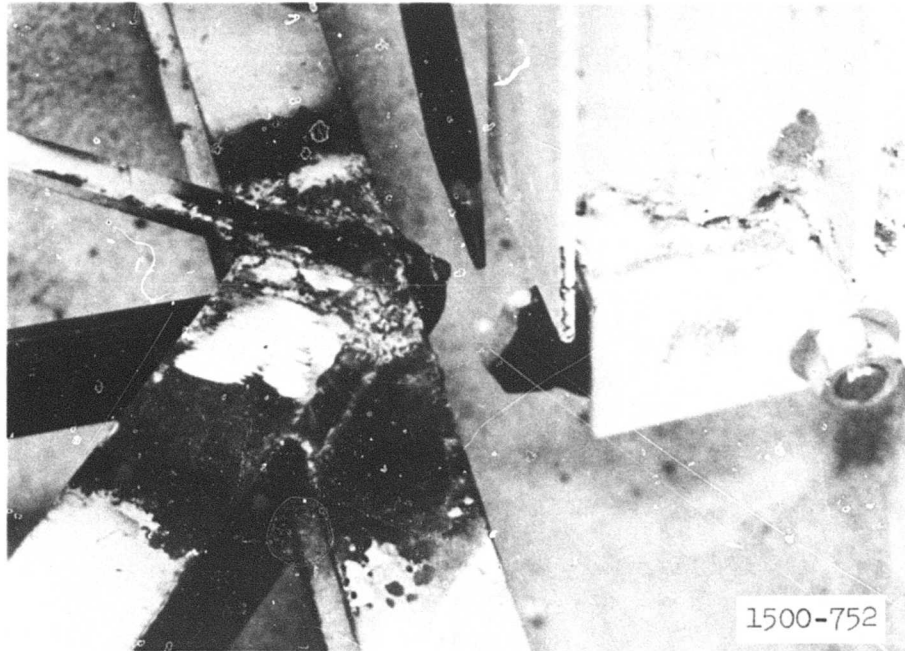


Figure 3.11 Shear damage to connector bolts, main photographs showing the post-pilot-test damage.



a. Postshot 3. Shear damage to the Beam 2 connector tongue.



b. Postshot 5. Shear damage to the Beam 2 connector tongue.

Figure 3.12 Damage to the redesigned bulkhead beam-truss connector.

## CHAPTER 4

### DISCUSSION OF RESULTS

#### 4.1 STRUCTURAL LOADING

4.1.1 Free Field. The test results and past experience in the LBLG show that the surface overpressure level generally does not affect the initial shape of the soil stress wave or the shape of the acceleration pulse for overpressures in the range of interest. Soil stress peaks are affected by overpressure as is stress wave velocity. Figure 4.1 shows the velocity of the stress wave across the structure as a function of overpressure and also shows the engulfment time. As shown, the velocity increases with overpressure up to about 100 psi and then becomes fairly constant at about 875 ft/sec. The data from Shot 2 indicate that the velocity through the previously loaded material was significantly higher than through a virgin specimen at the same overpressure. The presence of the structure does not seem to have a significant effect on the surrounding stress field. However, the limited quantity of data taken and the uncertainty involved in making soil stress measurements under dynamic conditions make this conclusion rather uncertain.

Based on the test data, the ratio of the horizontal to vertical soil stress is about 0.52 and the ratio of the incident soil stress to that reflected off the LBLG bottom about 0.62. The reflection arrives at the footing level around 17 msec after zero time and is traveling at a higher velocity than the incident stress wave, since it is passing through a prestressed medium. It is no longer a shock, but has a relatively long rise time (2 or 3 msec), and since it is acting mainly on the underside of the structure, hence affecting mainly the footing area, its influence on arch response is not as great as that of the incident loading. Assuming that there is little attenuation of the stress wave as it passes through the first few feet of soil, the incident soil stress acting on the structure is essentially the same as the surface airblast overpressure. Figure 4.2 shows an ideal soil stress shape based on the above discussion and a typical record from Shot 3.

The quality and quantity of the free-field motion data are such that

no meaningful analysis can be made. The peaks are tabulated in Table A.4 and the integrated velocity and displacement data presented in Appendix C.

4.1.2 Radial Interface Loading. The load on the arch in the radial direction was measured with strain gages attached to the inside surface of six of the arch blocks. After calibrating these blocks with a single point loading, they were then placed at various locations at one arch section near the center. Because the exact pressure distribution on these blocks is unknown, there is no way to correlate between the calibrated load and the exact load except in a qualitative manner. To do this, it was assumed that the load distribution on the blocks under dynamic loading was the same during each shot and was the same on each block.

Because of the reflected soil stress wave, there was a reflected peak in the interface loading as well as the incident load level. The incident load is considered to be the significant load. In order to compare the radial load distribution from shot to shot and at various times, all data from a shot were normalized by dividing by the peak value of the transient load measured during a shot. These data are tabulated in Table 4.1 and shown in Figure 4.3. The data generally fall in two sets, one being the two low-pressure shots and the other being the three higher-pressure shots. The low-pressure shots show that the load was somewhat uniformly distributed around the structure except at the footings where the horizontal freedom of the footing at even the low pressures allowed load relief. At the higher pressures, the greater relative inward deflection of the crown caused greater load relief than did the outward deflection of the area 30 degrees above the footing. The relative deflection causing this load relief was observed in the permanently deflected shape of the ribs observed after each shot. Figure 4.4 shows the permanent deformation of Rib 6 measured with the footing ends positioned postshot in their preshot location. The deflected shape generally corresponds to the shape of the load distribution shown in Figure 4.3. In order to determine the general location of the point of greatest outward deflection, each rib was examined after the three high-pressure shots. These results are shown in Figure 4.5 and show that the location of this point is between 25 and 30 degrees with some variance along the arch length. These data indicate that the presence of the

bulkhead did affect to some extent the radial distribution of load on the arch, but probably not in a significant manner. Further evidence of the influence of the bulkheads is shown in Figure 4.6 where it can be observed that the crown deflection was generally less at the bulkheads than in the central area.

#### 4.2 STRUCTURE MOTION

Level survey measurements were made to determine the total movement of the structure after Shots 3, 4, 5, and the pilot test shot. No measurements of this type were made for Shot 2 since it was a repeat loading of the Shot 1 configuration. Figure 4.7a shows the raw footing survey data and Figure 4.7b a plot of dimensionless deflection where

$$\delta_d = \frac{(\delta_f)(\sigma_{ULT})}{(w)(P_{so})} \quad \text{where} \quad \begin{array}{l} 10 \text{ psi} < \sigma_{ULT} < 30 \text{ psi} \\ 100 \text{ psi} < P_{so} < 200 \text{ psi} \\ w = 5.25 \text{ inches} \end{array} \quad (4.1)$$

In this expression,  $\delta_f$  is the measured deflection in inches,  $P_{so}$  is the airblast overpressure in pounds per square inch,  $w$  is the footing width in inches, and  $\sigma_{ULT}$  is the ultimate static plate-bearing pressure in pounds per square inch taken from Figure 2.3 and assumed to be 27, 20, 23, and 23 psi for Shots 3, 4, and 5 and the pilot test, respectively. A polynomial fit to the deflection data produces the following expression for deflection:

$$\delta_d = (1.79 \times 10^{-2}) + (1.67 \times 10^{-3})L_f \quad 0 < L_f < 44 \text{ inches} \quad (4.2)$$

where  $L_f$  is the distance along the footing from one end in inches.

In Figure 4.6 the surveyed crown deflection relative to the footing deflection is shown with the average of the north and south footing deflections at a location being assumed as the footing deflection. Both the footing and the crown deflection data show more scatter at the west end, especially in the case of Shot 4. This is thought to be due to the

presence of the free-field instrumentation cables which generally were run out the west end of the structure to the free-field gages. The difference in relative crown deflection between Shots 4 and 5, and between Shot 3 and the pilot test indicates that there was little rib deformation at the lower pressure with most of the motion being rigid-body motion, whereas at the higher pressures rib deformation became a major factor in total crown deflection. The rib strain data as well as the data in Figures 4.4 and 4.5 support this supposition.

The measured time-deflection histories of the footings near the vertical centerline of the structure for Shots 3, 4, and 5 are shown in Figures 4.8, 4.9, and 4.10, respectively. These data were calculated using the deflection gage data from the rig shown in Figure A.4. The deflection components are shown in Appendix C. These data show that there was an initial displacement radially outward corresponding to the arrival of the loading at the crown region of the structure. This was followed by a downward deflection as engulfment occurred during which time the outward motion reversed to become an inward displacement. Final downward displacement occurred in a jerky fashion because of the arrival of the reflected stress wave. The final position of the footing as measured agrees with those data in Figure 4.7 and agrees with observed final shape of the footings as shown in Figure 3.7, i.e. bowed inward.

Acceleration measurements were made at the center of the footing and at one end of the footing to determine what differences in motion occurred at these locations, i.e. to determine what influence the bulkheads had in altering the footing acceleration. The peak accelerations and velocities resulting at these two locations as a function of overpressure are shown in Figures 4.11 and 4.12, respectively. In both cases, the quantities measured at the end of the footing were lower in magnitude than those at the center locations. A typical acceleration record and the velocity- and displacement-time histories resulting from single and double integration of these data are shown in Figure 4.13.

#### 4.3 STRUCTURAL RESPONSE

Whenever a structural element undergoes a combination of thrust and

moment, an interaction of these two quantities occurs which tends to either move the section nearer to or away from its ultimate load-carrying ability. In the case of the arch being considered, the element being loaded was a tee-section rib having dimensions as shown in Figure 4.14a. The steel had a stress-strain curve as shown in Figure 4.14b. The test results indicate that the ribs exceeded their elastic limit during some of the tests. To simplify the analysis of these data, an elastic-plastic idealization (Figure 4.14b) was made. Yield stress at 0.1 percent offset was 59,930 psi and yield strain was 0.23 percent. Based on this idealization of the stress-strain curve, the rib strain data were converted into moment and thrust. Moments producing compression in the outer fibers are considered positive and thrusts producing fiber compression are considered positive. All moment- and thrust-time histories are shown in Appendix C.

The general shape of the strain data, hence the moment and thrust data, followed the free-field stress wave shape. Thus, there was an initial or transient peak in the data, generally occurring about 5 to 10 msec after detonation, and a reflected peak occurring 15 to 20 msec after detonation. The thrust and moment data are tabulated in Tables 4.2 and 4.3 and the quantities tabulated are defined in Figure 4.15. The shape of these data also reflect the interface loading as described in Section 4.1. Figure 4.16 shows typical data for a section remaining elastic and for a section that has strains exceeding the elastic limit.

The peak transient thrust data are plotted in Figure 4.17 and show considerable scatter. However, data analysis indicates that the thrust throughout the arch ring is generally uniform with a slight tendency for the thrust to increase as the arch crown is approached. Regression analysis of these data gives the following equation for the peak transient thrust in the arch section in terms of peak overpressure  $P_{so}$  and angle above the footing  $\theta$ .

$$N_p = (26.2 + 11.1P_{so} + 1.98\theta) \text{ lb/in} \quad (4.3)$$

$$0 < \theta < 75 \text{ degrees}$$

$$30 < P_{so} < 200 \text{ psi}$$

The lines shown in Figure 4.17 are based on this equation.

The moment data show appreciable scatter. During the first two shots it appears that the loading was not great enough to fully flex the structure; hence, even the sign of the data exhibited scatter. As the load increased, the moments up to 45 degrees were generally negative, which corresponds to the permanent deflection measurements. Because of the scatter in these data, no detailed data analysis was attempted.

#### 4.4 INTERIOR ENVIRONMENT

Two quantities were measured inside the structure, interior pressure and floor acceleration. The peak pressure appears to be directly related to the decrease in interior volume caused by the punching of the footings since no breach occurred which would allow the airblast overpressure to enter the inside of the structure. Peak pressure versus footing punch from the survey data is shown in Figure 4.18 where the footing data are those extrapolated to the Rib 5 location on the north and south footings. Using the equation given, assuming the straight line fit of these data and the normalized data in Figure 4.7b as expressed by Equation 4.2, the interior pressure can be presented as

$$P_{IN} = \left[ \frac{3.58(w)(P_{SO})}{100(\sigma_{ULT})} (1.79 + 0.167L_x) - 3.11 \right] \text{ psi} \quad (4.4)$$

The acceleration measured on the interior floor was characterized by two sharp spikes (Figure 4.19). The first and largest spike was caused by engulfment and punching of the footings and the second spike by the reflection off the base of the LBLG. Double integration of the data gave poor results as far as displacement was concerned, but gave reasonable velocity data. These data are shown as time histories in Appendix C and the peak data are shown in Figure 4.20.

TABLE 4.1 RATIO OF RADIAL LOAD TO PEAK TRANSIENT RADIAL LOAD

NR - not recovered.

Angle Above Footing	Load Ratio at				
	Incident Peak	10 msec	20 msec	30 msec	40 msec
degrees					
Shot 1:					
8	Insignificantly small				
24	0.91	0.79	0.71	0.21	0.23
45	0.95	0.74	0.90	0.82	0.74
45	0.99	0.80	0.98	0.84	0.75
67	0.67	0.49	0.59	0.28	0.15
83	1.00	0.81	0.98	0.87	0.71
Shot 2:					
8	0.25	0.13	0.20	0.06	0.03
24	0.91	0.81	0.72	0.22	0.06
45	0.93	0.82	0.93	0.56	0.44
45	1.00	0.91	0.96	0.62	0.50
67	0.75	0.66	0.82	0.56	0.54
83	0.81	0.79	0.85	0.60	0.66
Shot 3:					
8	0.36	0.34	0.17	0.03	0.09
24	1.00	1.00	0.83	0.46	0.46
45	NR	NR	NR	NR	NR
45	0.65	0.61	0.51	0.30	0.33
67	NR	NR	NR	NR	NR
83	0.52	0.51	0.43	0.32	0.34
Shot 4:					
8	0.36	0.34	0.25	-0.08	-0.02
24	1.00	0.89	1.28	0.49	0.44
45	0.51	0.41	0.59	0.26	0.28
45	0.75	0.68	0.70	0.19	0.23
67	0.61	0.55	0.69	0.39	0.42
83	0.60	0.56	0.57	0.32	0.33
Shot 5:					
8	0.23	0.21	0.25	0.09	0.16
24	0.86	0.86	0.69	0.27	0.41
45	1.00	0.96	0.91	0.31	0.51
45	NR	NR	NR	NR	NR
67	0.52	0.46	0.54	0.22	0.31
83	0.60	0.60	0.46	0.15	0.23

TABLE 4.2 TABULATED THRUST DATA

Symbols used are defined in the Notation which precedes the text and are illustrated in Figure 4.15.

Gage Pair	$\theta$	$t_r$	$t_p$	$t_R$	$N_p$	$N_R$	$N_{ss}$
	degrees	msec	msec	msec	lb/in	lb/in	lb/in
Shot 1:							
11NE-12NE	0	10.1	14	22	545	580	216
13SE-14SE	0	10.4	16	20	350	640	120
41NE-42NE	0	11.0	14	22	528	513	170
51NE-52NE	0	9.7	13	22	570	530	217
53SE-54SE	0	9.2	12	20	564	651	228
63SE-64SE	0	21.0	21	21	1,160	1,160	440
81NE-82NE	0	10.0	14	22	528	547	152
101NE-102NE	0	8.3	13	22	535	632	239
115NE-116NE	60	11.2	15	22	581	700	296
613NE-614NE	60	11.3	13	21	705	794	--
15NE-16NE	10	8.8	12	22	644	661	271
Shot 2:							
11NE-12NE	0	3.7	6.4	18	731	779	--
51NE-52NE	0	8.1	10	19	894	898	264
53SE-54SE	0	7.4	10	19	831	978	350
53SE-64SE	0	6.7	10	19	825	1,002	267
81NE-82NE	0	6.8	10	19	706	769	230
83SE-84SE	0	6.8	10	19	740	996	278
101NE-102NE	0	7.4	11	18	800	924	303
15NE-16NE	10	7.7	10	20	1,010	1,103	443
65NE-66NE	10	6.7	10	19	1,007	1,087	--
67NE-68NE	20	7.1	10	19	978	1,102	--
87NE-88NE	60	6.6	10	20	948	1,186	384
Shot 3:							
11NE-12NE	0	5.0	7.0	18	1,530	1,400	657
21NE-22NE	0	10	10	18	1,070	1,140	560
515SE-516SE	0	7.5	9.0	17	2,050	1,260	50
71NE-72NE	0	10	10	17	1,230	1,070	190
81NE-82NE	0	9.0	9.0	17	1,470	1,290	760
101NE-102NE	0	5.8	8	18	1,450	1,460	800
33NE-34NE	10	7.6	9.0	18	1,150	1,210	830
53NE-54NE	10	7.7	9.0	17	1,260	1,260	--
23NE-24NE	20	6.8	9.0	17	1,180	1,190	340
35NE-36NE	20	8.0	9.0	17	1,360	1,400	--
43NE-44NE	20	6.8	9.0	17	1,390	1,270	550
55NE-56NE	20	8.0	9.0	17	1,480	1,520	--
57NE-58NE	30	a	a	a	a	a	3,230
15NE-16NE	60	7.0	9.0	18	1,710	2,140	1,100
45NE-46NE	60	8.0	10	17	1,800	1,900	750
59NE-510NE	60	9.0	10	17	1,620	1,790	700
511NE-512NE	60	8.0	9.0	17	1,690	1,920	620
Shot 4:							
11NE-12NE	0	7.0	7.0	17	970	970	255
21NE-22NE	0	7.0	7.0	17	1,550	1,410	645
41NE-42NE	0	5.0	7.0	17	1,360	950	165
51NE-52NE	0	7.0	10	17	1,340	1,120	190
61NE-62NE	0	3.0	5.0	a	2,040	b	--
91NE-92NE	0	7.2	9.0	16	526	450	--
101NE-102NE	0	7.5	10	a	990	a	--
517NE-518NE	20	10	10	17	1,130	1,030	380
53NE-54NE	30	a	a	a	a	a	3,210
515SE-516SE	30	7.2	10	18	1,850	2,400	1,860
83NE-84NE	30	8.0	11	19	2,040	2,320	2,000
103NE-104NE	30	b	b	15	b	3,200	3,230
105NE-106NE	45	7.2	10	18	1,560	2,100	1,760
513NE-514NE	45	a	a	19	a	3,200	3,240
57NE-58NE	60	2.6	6.0	11	1,000	1,090	--
87NE-88NE	60	7.2	10	18	1,500	1,710	43
89NE-810NE	75	3.4	6.0	18	1,510	1,820	--
Shot 5:							
21NE-22NE	0	1.7	5.0	17	2,060	1,560	560
31NE-32NE	0	3.0	8.0	17	990	910	410
53NE-54NE	30	4.0	10	17	2,600	2,680	2,080
55NE-56NE	60	9.2	11	17	2,040	2,640	910

a Indeterminate.

b Steady rise up to  $N_R$ .

TABLE 4.3 TABULATED MOMENT DATA

Symbols used are defined in the Notation which precedes the text and are illustrated in Figure 4.15.

Gage Pair	$\theta$	$t_r$	$t_p$	$t_R$	$M_p$	$M_R$	$M_{ss}$
	degrees	msec	msec	msec	in-lb/in	in-lb/in	in-lb/in
Shot 1:							
11NE-12NE	0	6.4	9.0	20	+40.7	+22.9	+4.2
13SE-14SE	0	2.8	6.0	23	-137	-4.3	-33.0
41NE-42NE	0	6.3	9.0	22	+92.5	+88.7	-3.8
51NE-52NE	0	2.7	6.0	24	-72.4	+50.5	-28.4
53SE-54SE	0	2.8	6.0	18	-87.3	-66.3	-61.5
63SE-64SE	0	13.5	16.0	29	-80.5	-88.0	-27.0
81NE-82NE	0	5.7	8.0	23	+104	+89.9	-9.4
101NE-102NE	0	2.8	5.0	18	-28.5	-15.8	-0.7
15NE-16NE	10	14	18	24	-167	-162	-136
115NE-116NE	60	9.2	15	21	+104	+136	+23.1
613NE-614NE	60	7.5	13	21	-41.7	-43.2	--
Shot 2:							
11NE-12NE	0	6.2	11	19	+69.7	+96.2	--
51NE-52NE	0	6.2	8.0	18	+61.6	+65.1	-73.4
53SE-54SE	0	2.3	5.0	19	-96.2	-99.7	-96.4
63SE-64SE	0	5.9	7.0	17	+116	+34.0	-5.0
81NE-82NE	0	5.1	7.0	18	+100	+47.8	-58.0
83SE-84SE	0	7.5	8.0	17	+119	+73.0	-67.0
101NE-102NE	0	a	a	19	a	-140	-89.0
15NE-16NE	10	6.5	9.0	b	-123	b	-92.5
65NE-66NE	10	8.1	11	20	-266	-311	--
67NE-68NE	20	b	b	25	b	-600	-754
87NE-88NE	60	b	b	b	b	b	-126
Shot 3:							
11NE-12NE	0	b	b	b	b	b	-199
21NE-22NE	0	10	10	b	237	b	61
515SE-516SE	0	2.5	4.0	15	-135	-123	-38
71NE-72NE	0	8.0	10	b	-42	b	-82
81NE-82NE	0	5.0	5.0	b	-140	b	-63
101NE-102NE	0	1.0	3.0	14	-149	-2	-40
33NE-34NE	10	1.5	3.0	15	-247	-62	-95
53NE-54NE	10	1.5	3.0	18	-168	-282	--
23NE-24NE	20	2.0	3.0	17	-177	-468	--
35NE-36NE	20	0.8	3.0	16	-200	-270	--
43NE-44NE	20	1.0	3.0	19	-220	-402	-440
55NE-56NE	20	1.2	3.0	17	-176	-468	--
57NE-58NE	30	4.2	5.0	b	-102	b	0
15NE-16NE	60	b	24	24	b	-174	-217
45NE-46NE	60	55	8.0	21	-189	-227	-222
59NE-510NE	60	6.7	9.0	20	-154	-175	-162
511NE-512NE	60	a	a	20	a	-206	-142
Shot 4:							
11NF-12NE	0	5.0	5.0	32	-90	-74	-130
21NE-22NE	0	5.0	5.0	34	-122	-79	-3.0
41NE-42NE	0	5.5	7.0	33	-176	14	29
51NE-52NE	0	4.0	7.0	33	-126	-26	3.0
61NE-62NE	0	6.4	9.0	b	-89	b	--
91NE-92NE	0	2.9	5.0	b	-309	-184	--
101NE-102NE	0	6.6	9.0	b	4	a	--
517NE-518NE	20	4.0	4.0	17	-135	81	42
53NE-54NE	30	2.7	5.0	17	-112	-45	4.0
515SE-516SE	30	a	a	16	a	-540	-630
83NE-84NE	30	a	a	15	a	-568	-614
103NE-104NE	30	5.0	5.0	18	-70	-42	0
105NE-106NE	45	b	b	b	b	b	-538
513SE-514SE	45	5.0	5.0	18	-105	-2.0	0
57NE-58NE	60	3.0	5.0	12	-25	-69	--
87NE-88NE	60	6.0	9.0	33	-66	-86	-109
89NE-810NE	75	0.5	3.0	14	94	25	--
Shot 5:							
21NE-22NE:	0	a	a	17	a	186	251
31NE-32NE	0	3.0	8.0	17	-142	-47	73
53NE-54NE	30	2.6	9.0	15	-441	-490	-607
55NE-56NE	60	b	a	19	b	-44	-82

<sup>a</sup> Steady rise up to  $M_R$ .  
<sup>b</sup> Indeterminate.

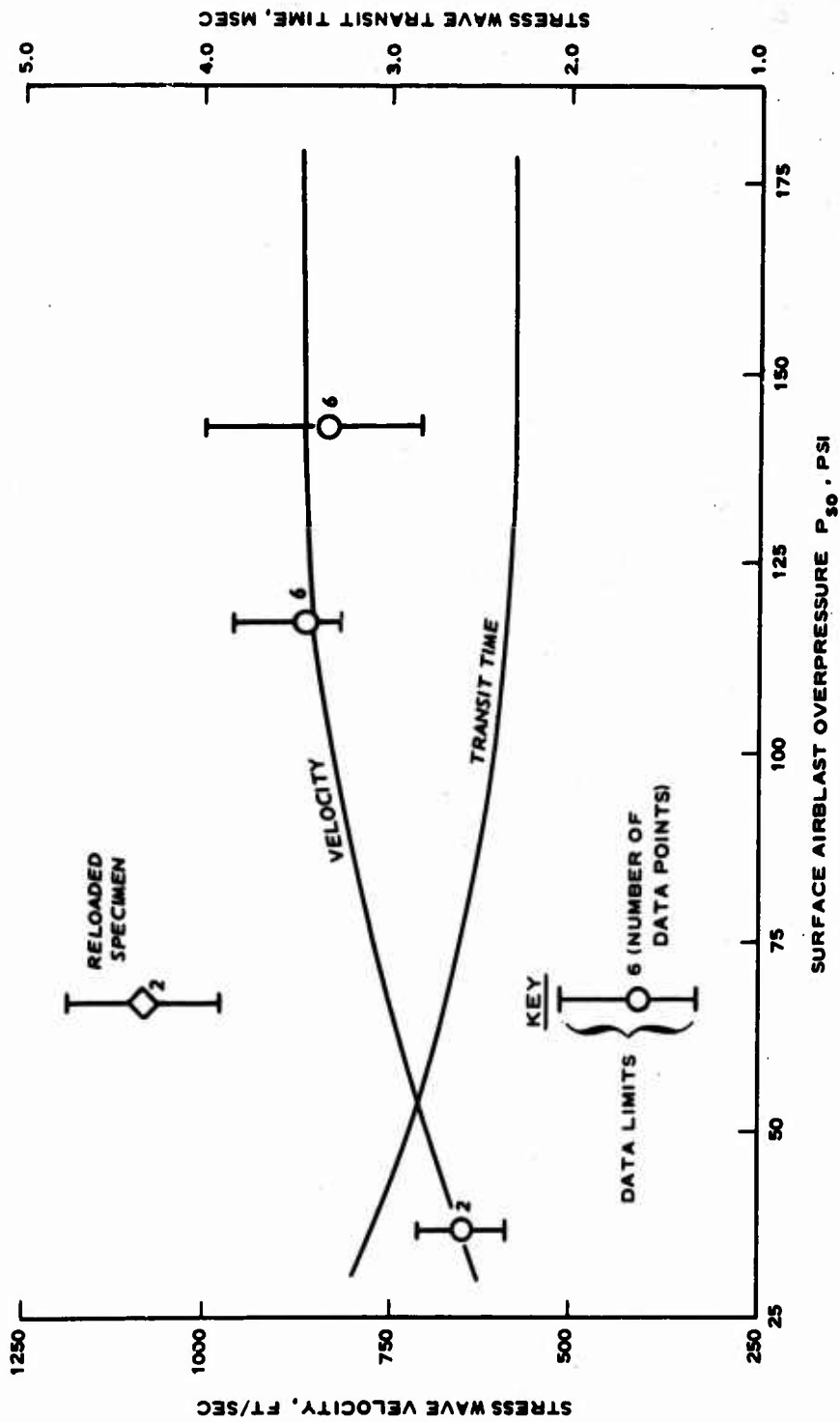
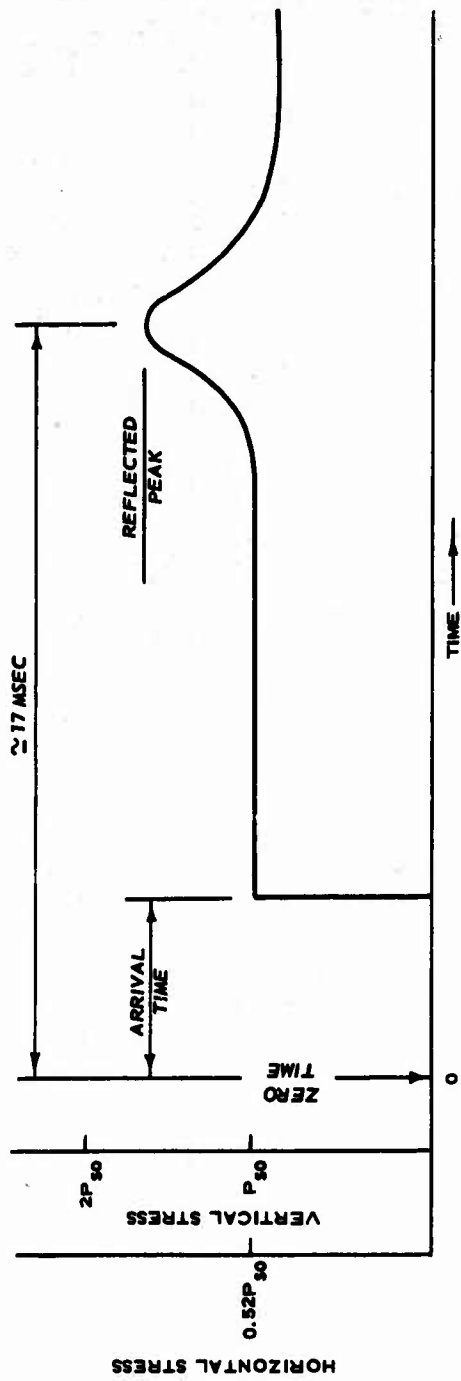
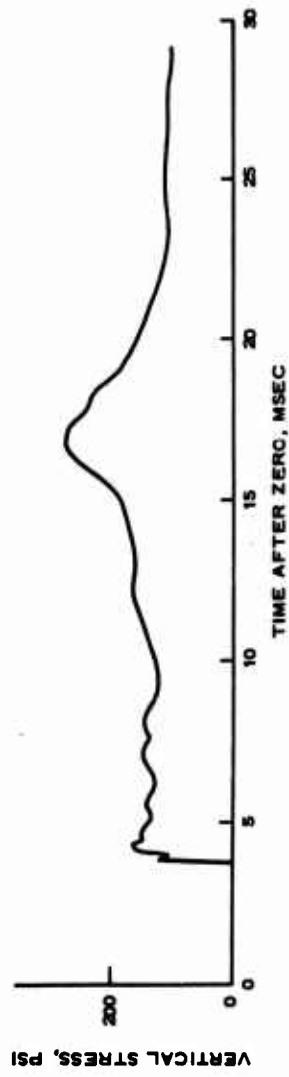


Figure 4.1 Soil stress wave velocity.



a. IDEALIZED FREE-FIELD STRESS TIME HISTORY



b. TYPICAL FREE-FIELD STRESS TIME HISTORY, SHOT 3 GAGE SS4

Figure 4.2 Idealized and typical free-field soil stress data.

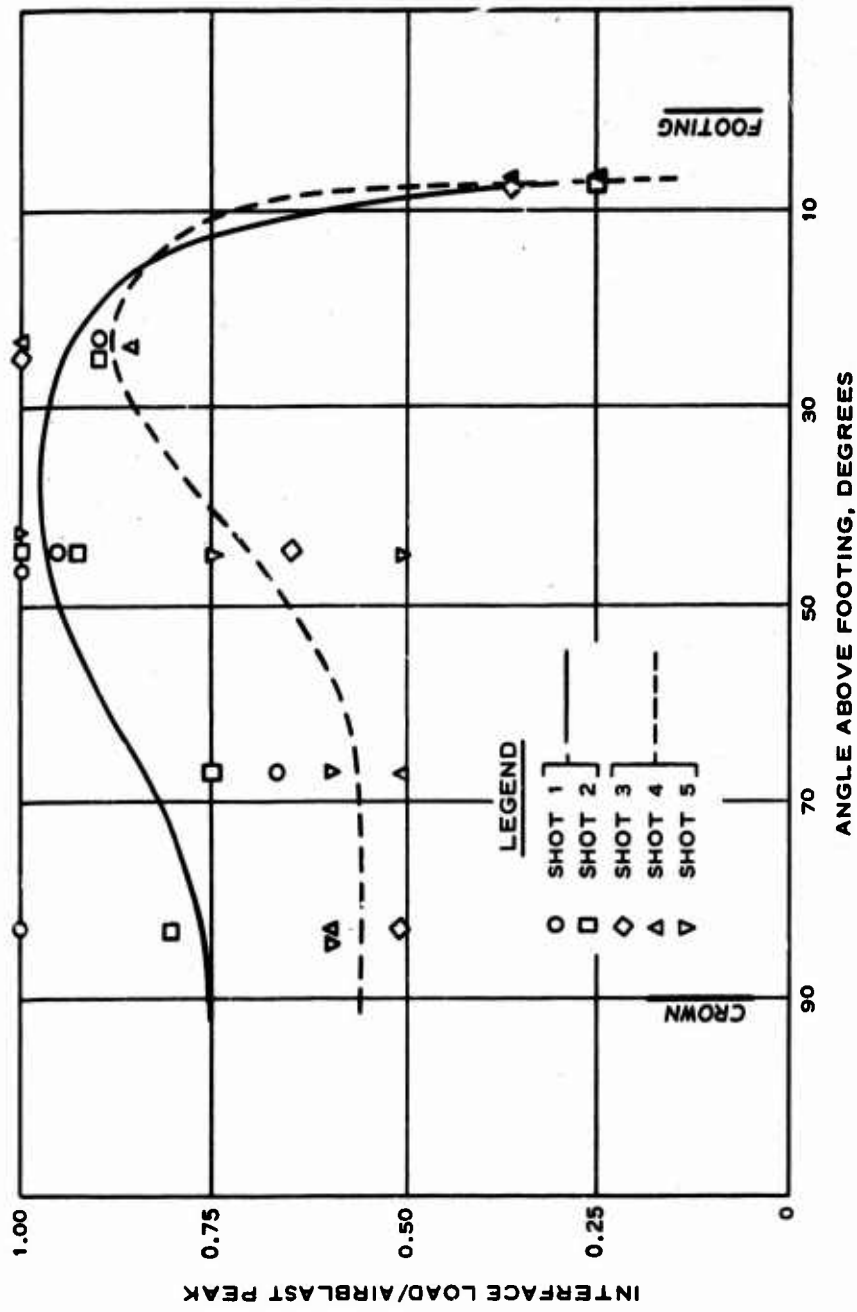


Figure 4.3 Radial load distribution.



Figure 4.4 Permanent deformation of Rib 6 after Shots 3, 4, and 5.

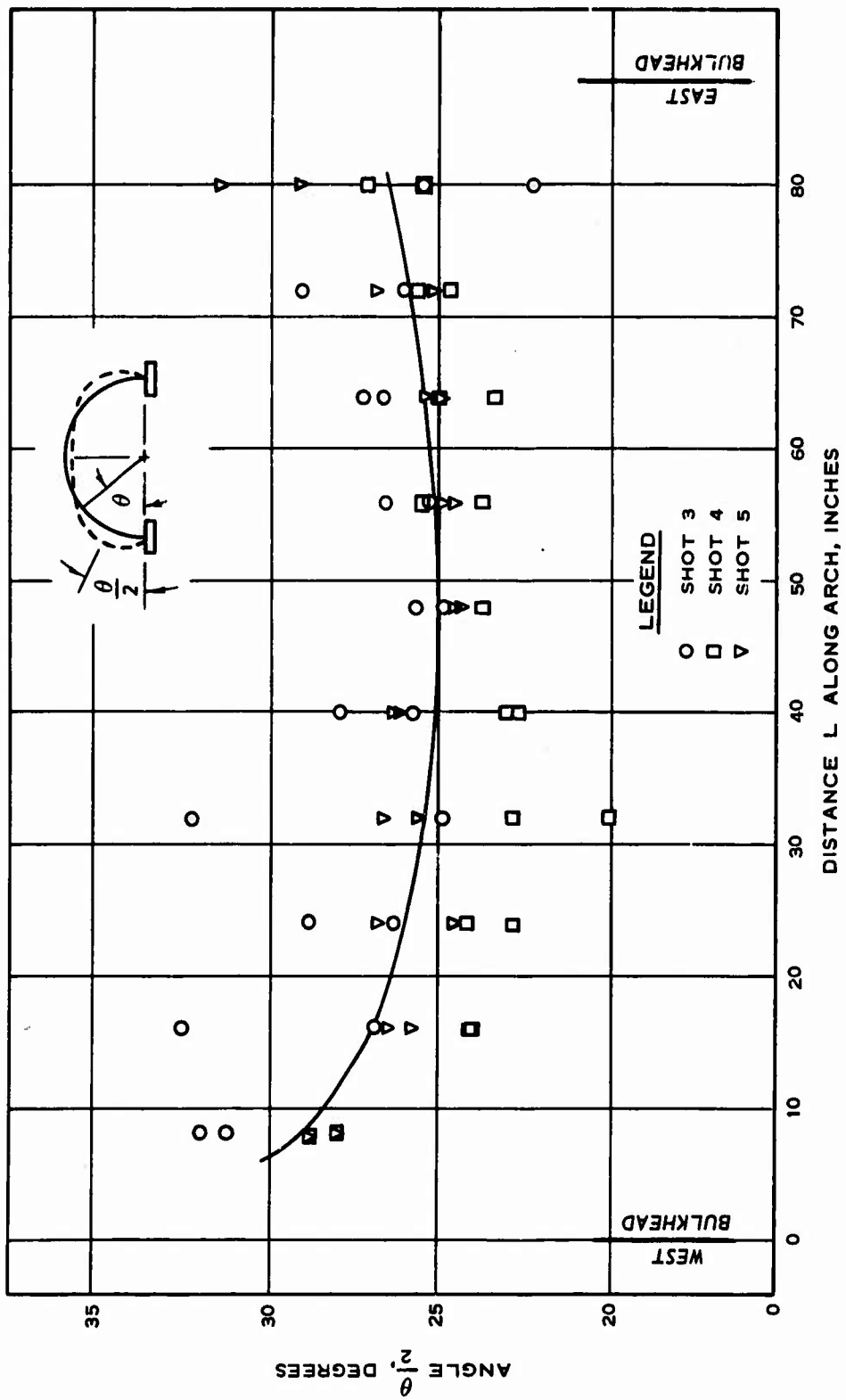


Figure 4.5 Angle of point of maximum outward deflection.

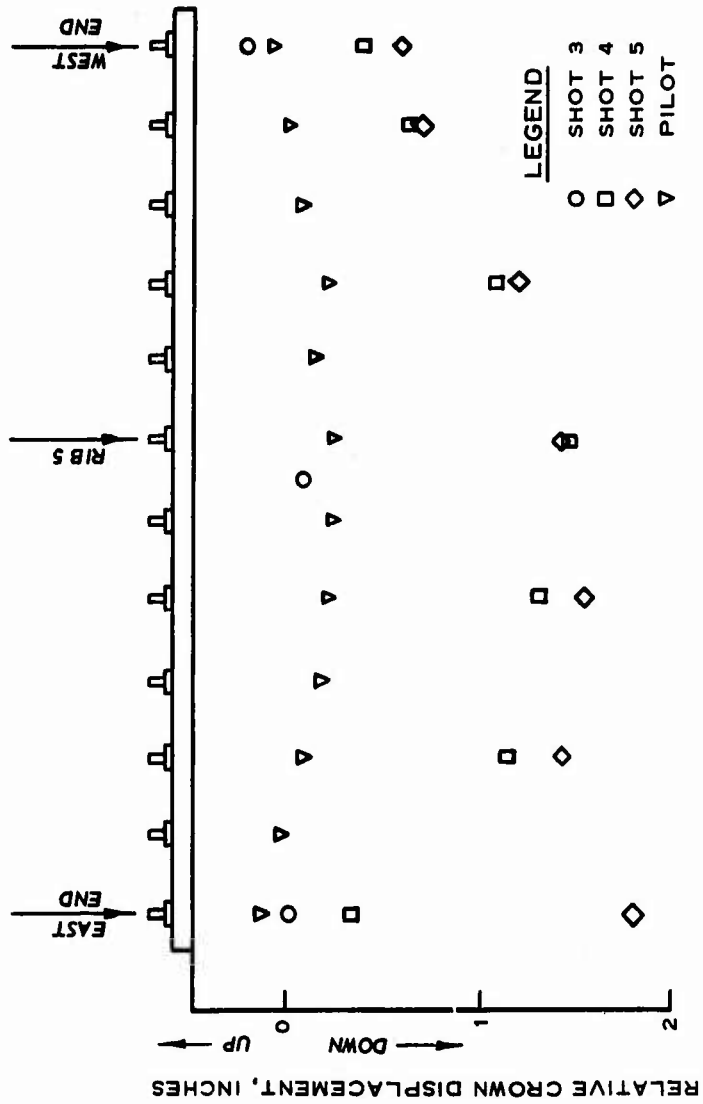
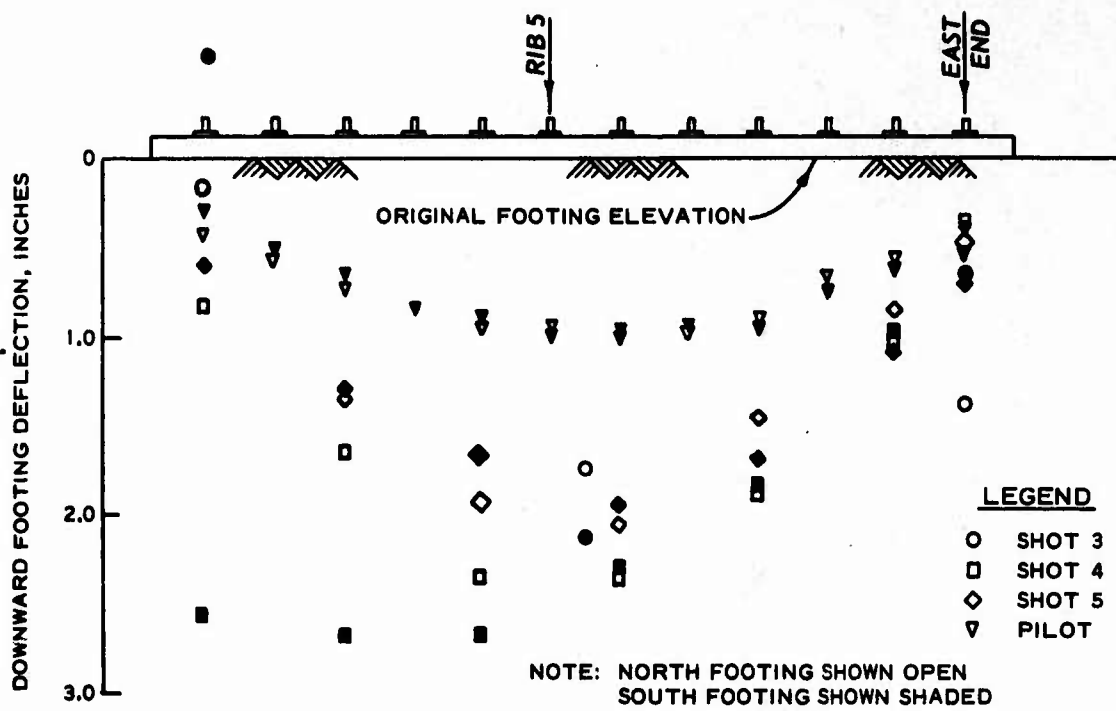
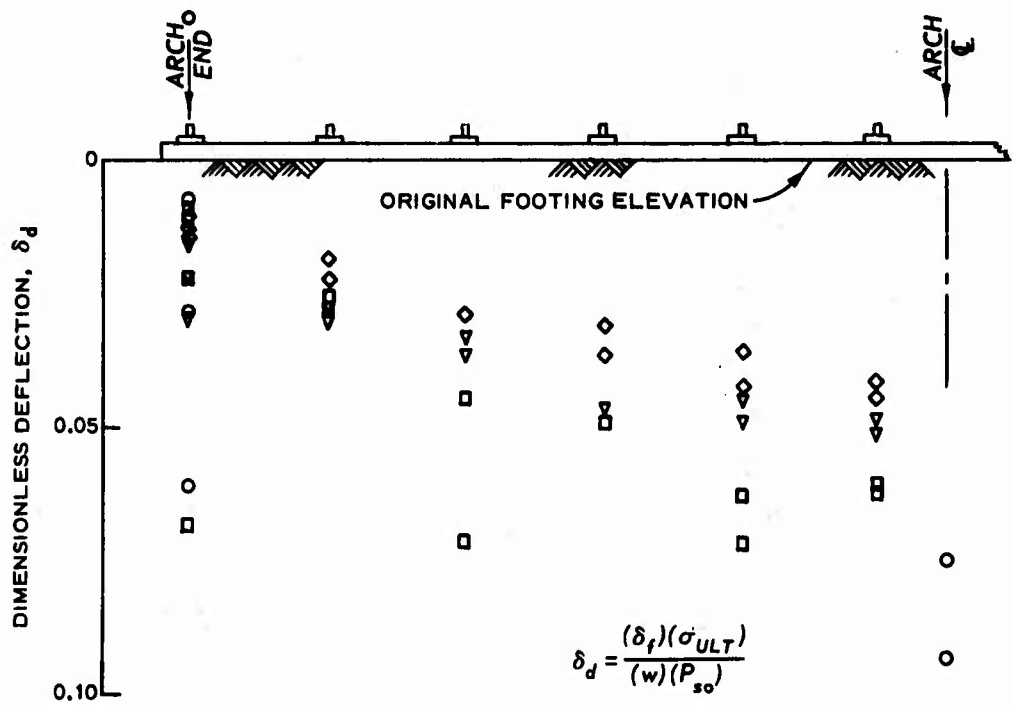


Figure 4.6 Level survey, postshot crown deflection with respect to the footings.

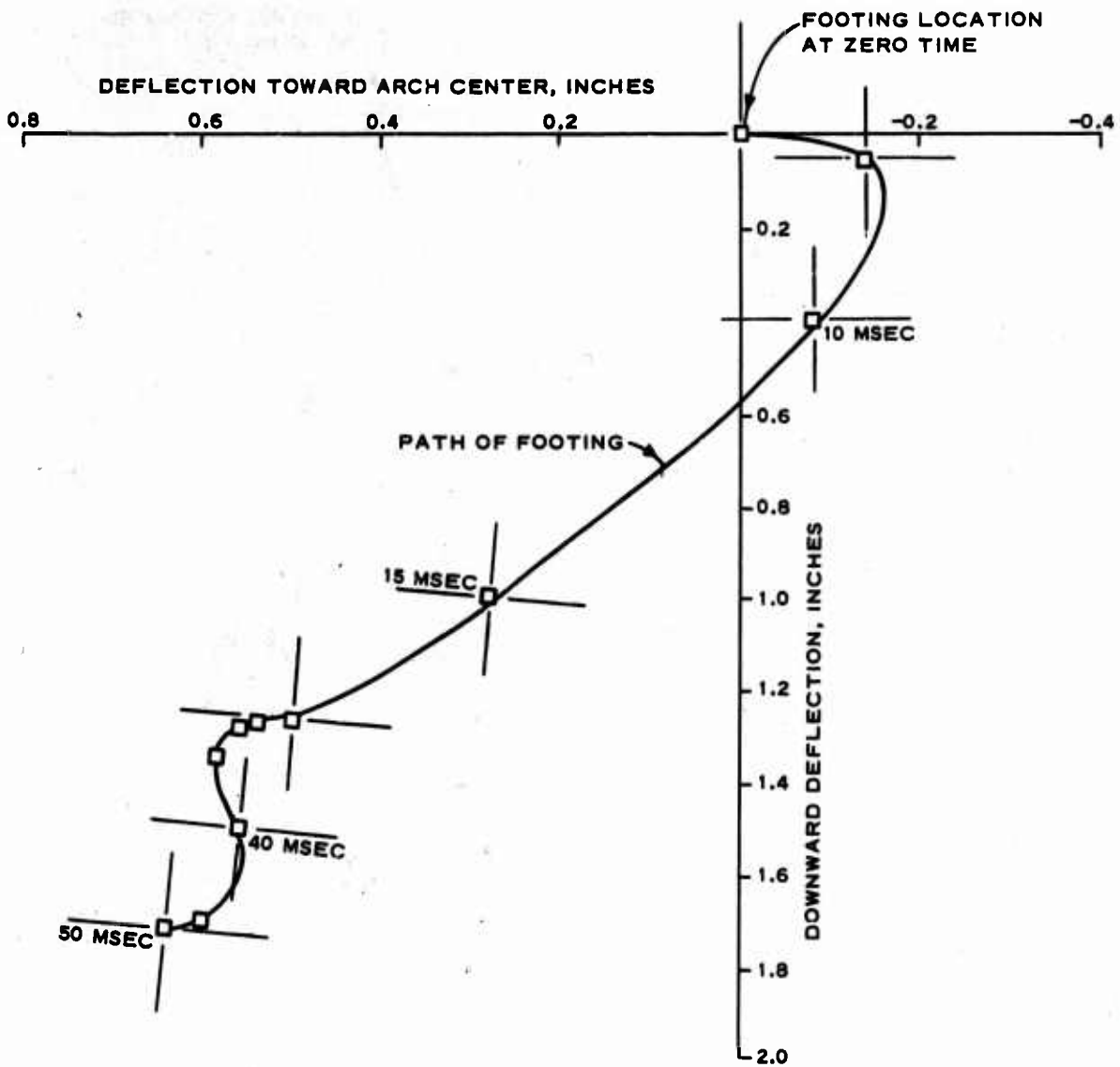


a. RAW DATA



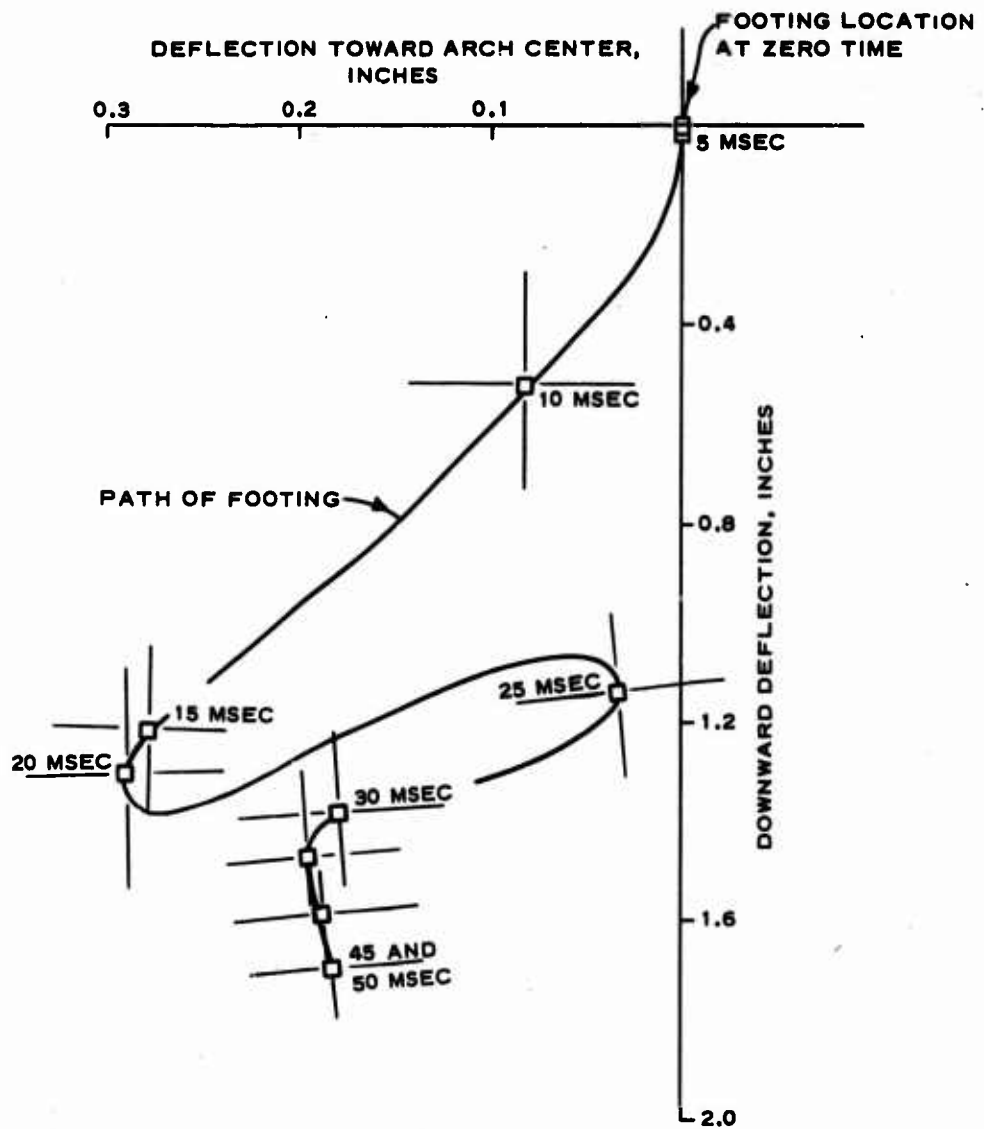
b. NORMALIZED DATA

Figure 4.7 Level survey data for footings.



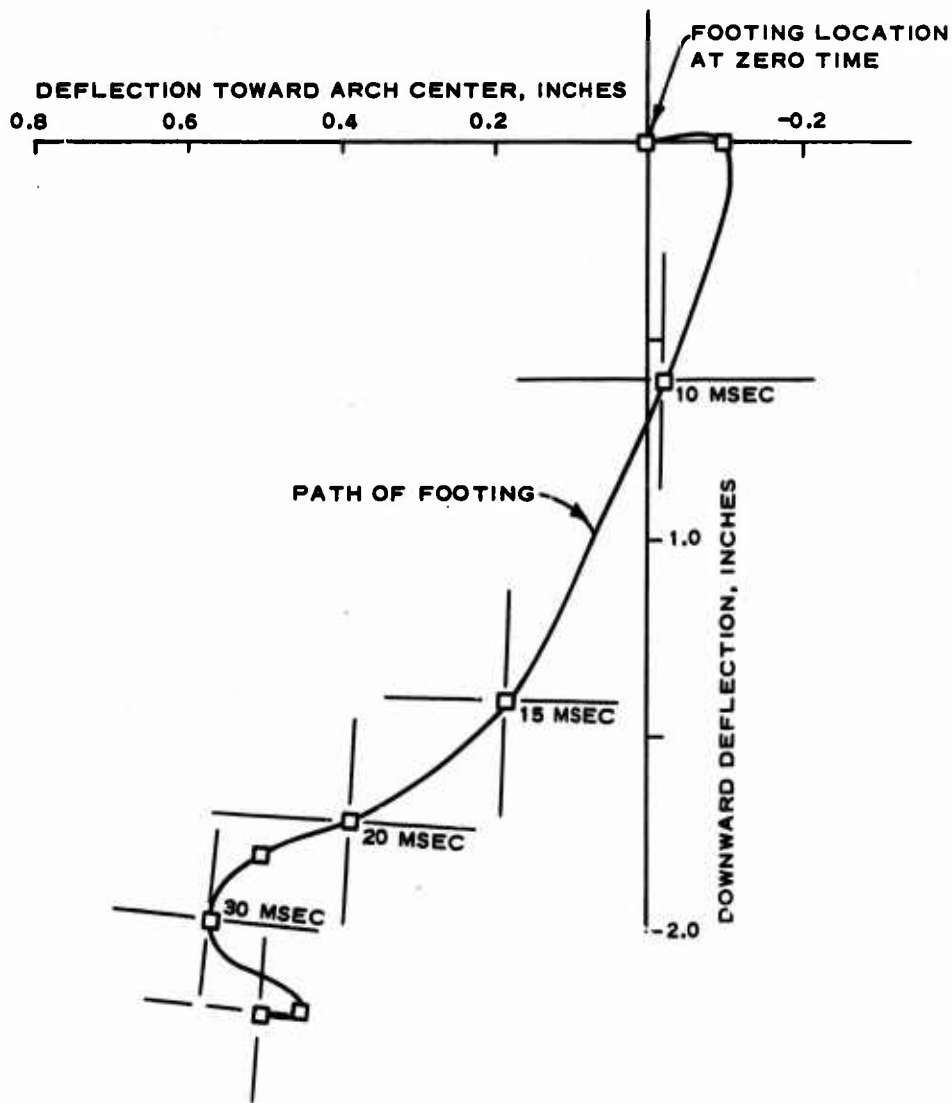
NOTE: EACH SQUARE REPRESENTS A 5-MSEC INTERVAL. THE ANGLE OF THE LINES WITH THE SQUARE REPRESENTS THE ANGLE OF THE FOOTING AT THAT TIME.

Figure 4.8 Footing motion of the north footing center during Shot 3.



NOTE: EACH SQUARE REPRESENTS A 5-MSEC INTERVAL. THE ANGLE OF THE LINES WITH THE SQUARE REPRESENTS THE ANGLE OF THE FOOTING AT THAT TIME.

Figure 4.9 Footing motion of the north footing center during Shot 4.



NOTE: EACH SQUARE REPRESENTS A 5-MSEC INTERVAL. THE ANGLE OF THE LINES WITH THE SQUARE REPRESENTS THE ANGLE OF THE FOOTING AT THAT TIME.

Figure 4.10 Footing motion of the north footing center during Shot 5.

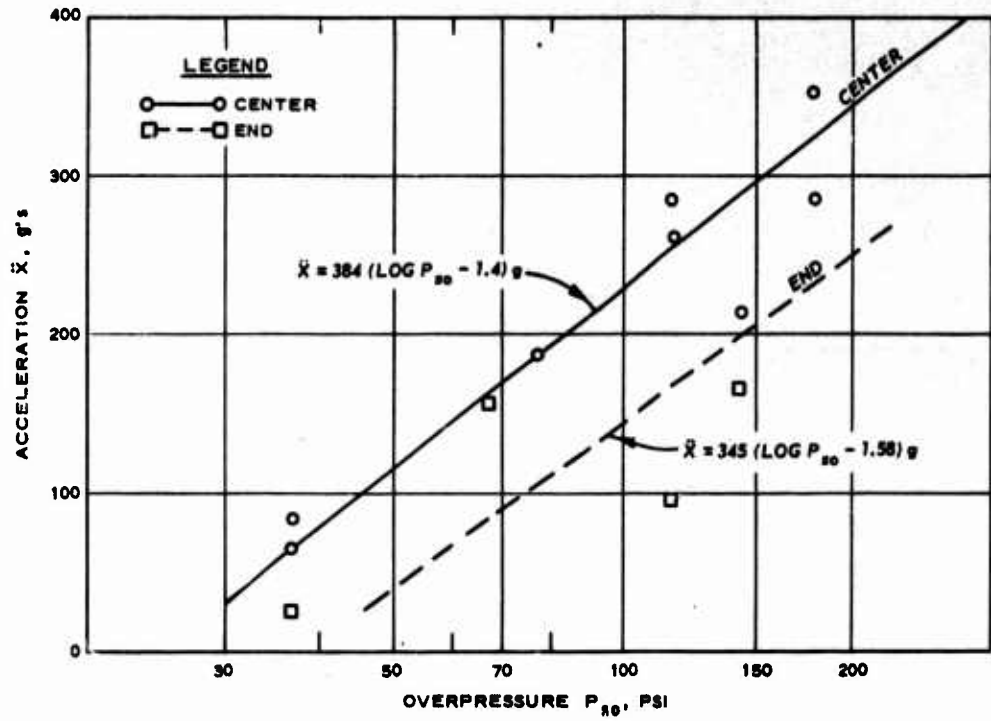


Figure 4.11 Peak acceleration of footing.

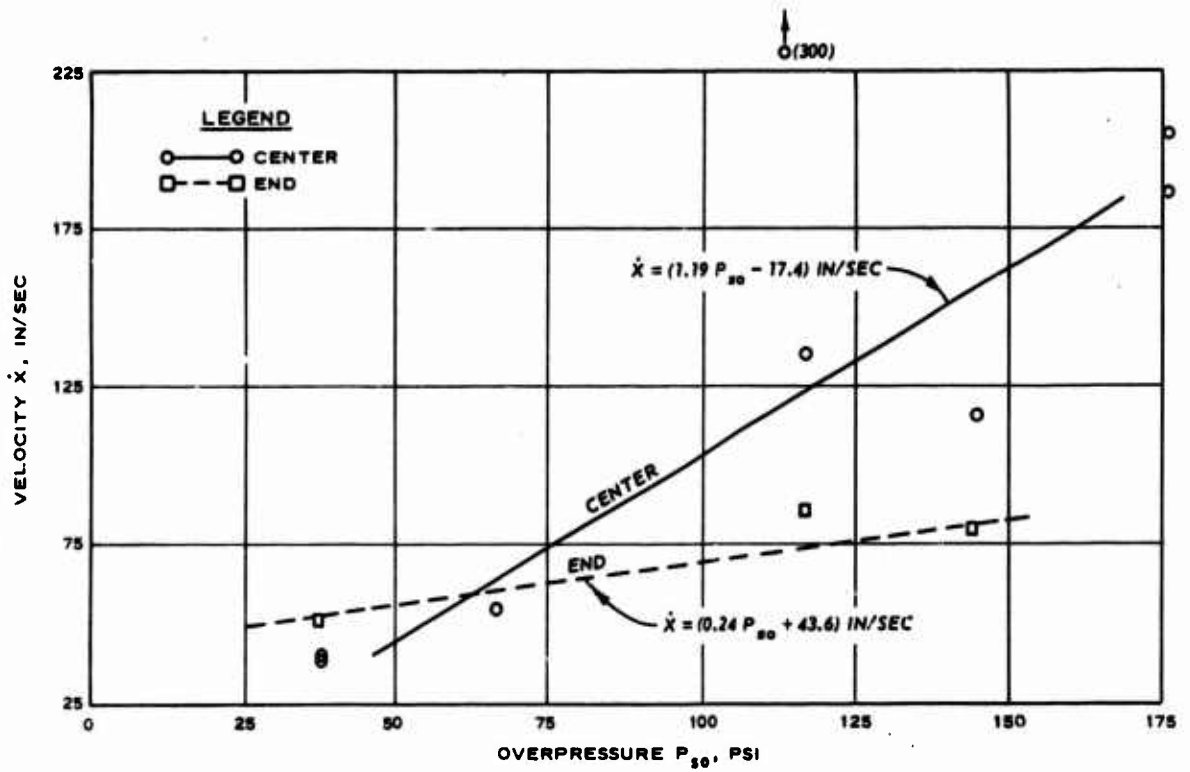


Figure 4.12 Peak velocity of footing.

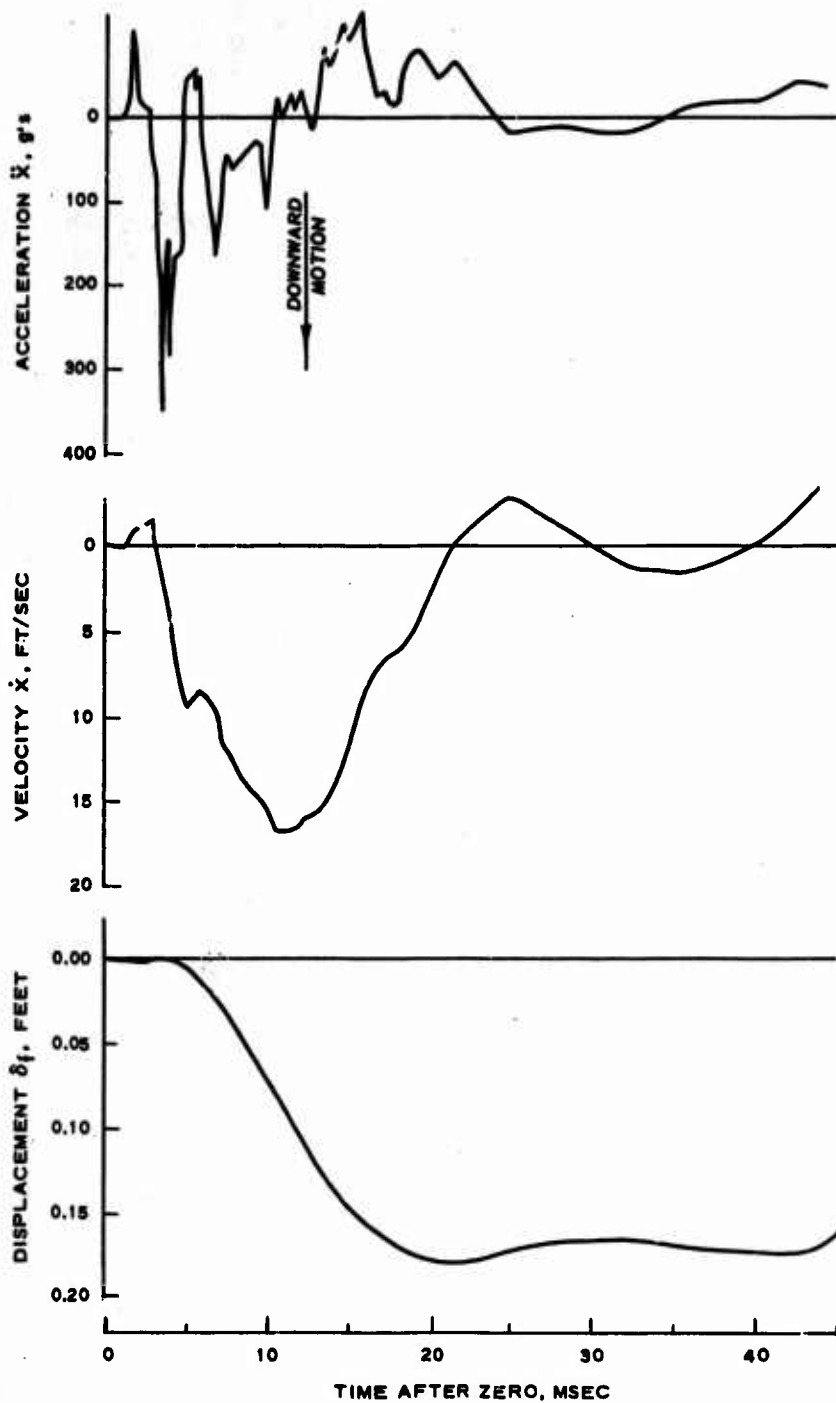
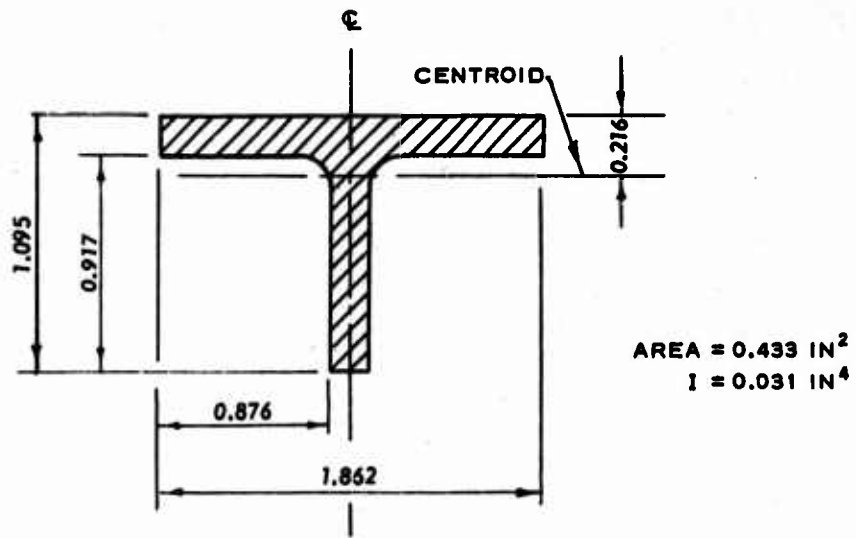
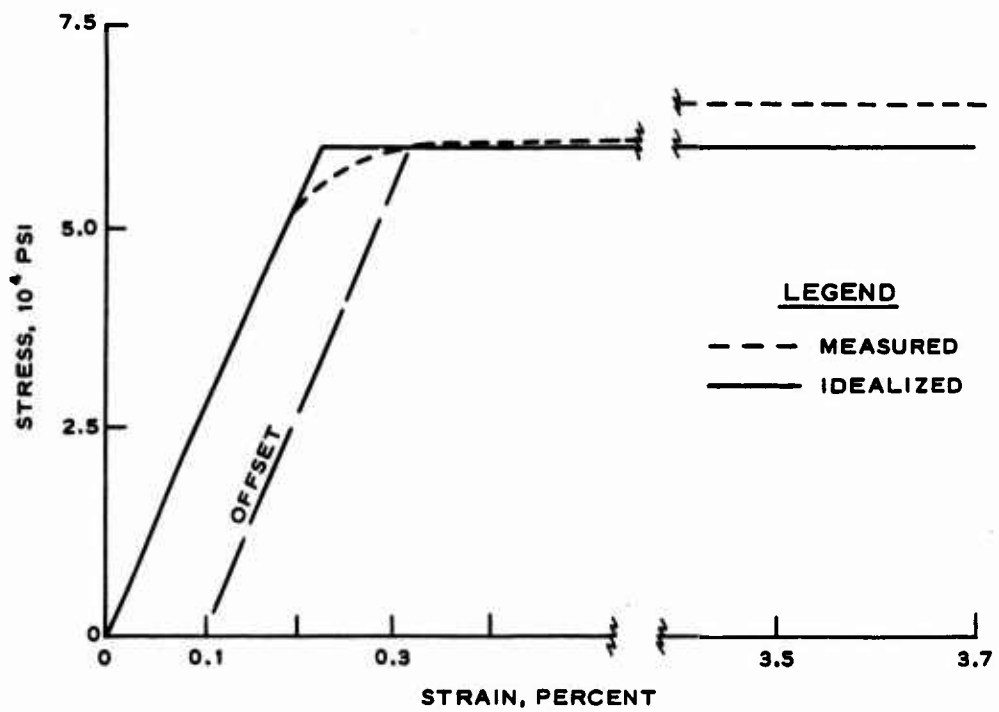


Figure 4.13 Typical motion data at footing center; Shot 5, Gage 53VA.

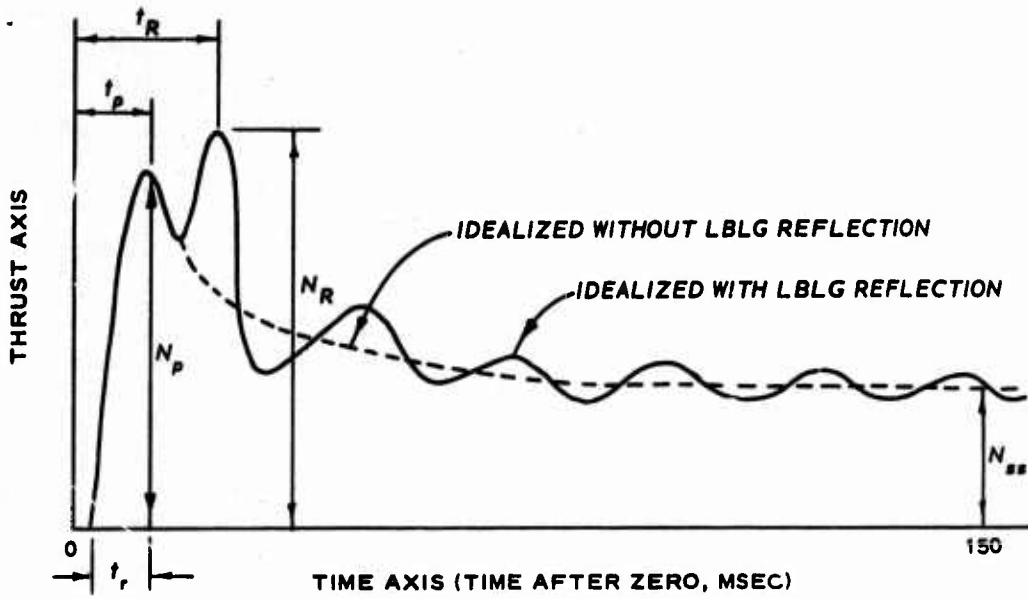


a. Physical dimensions (in inches) of a typical rib section.

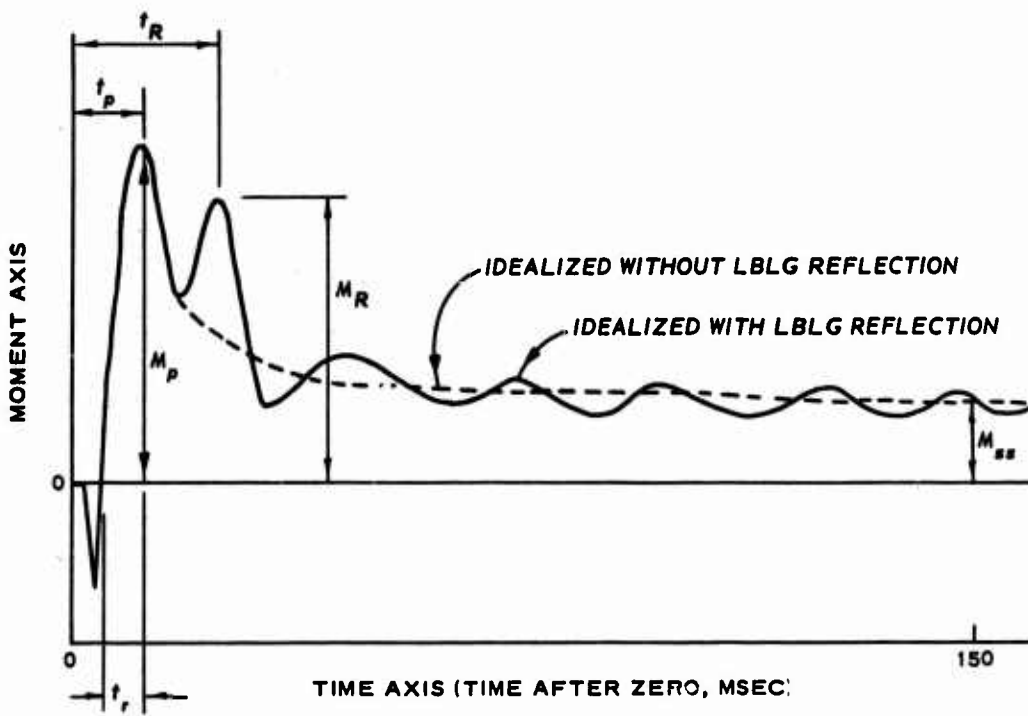


b. Stress-strain curve of steel.

Figure 4.14 Rib idealization.

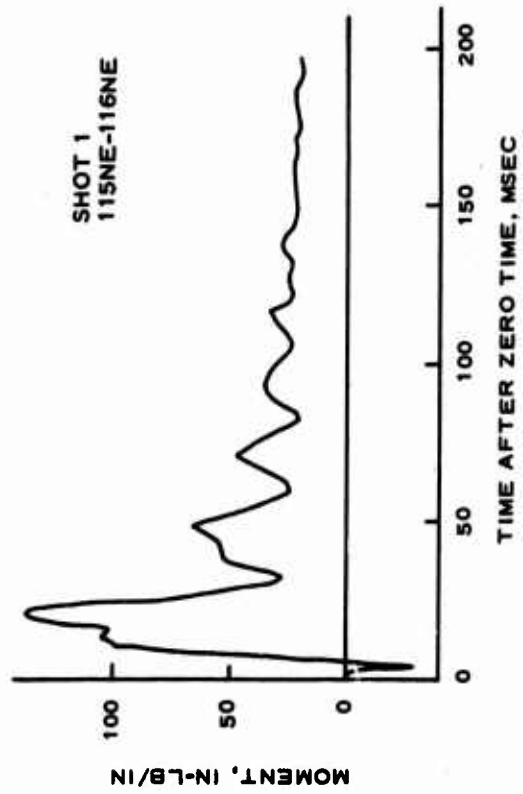
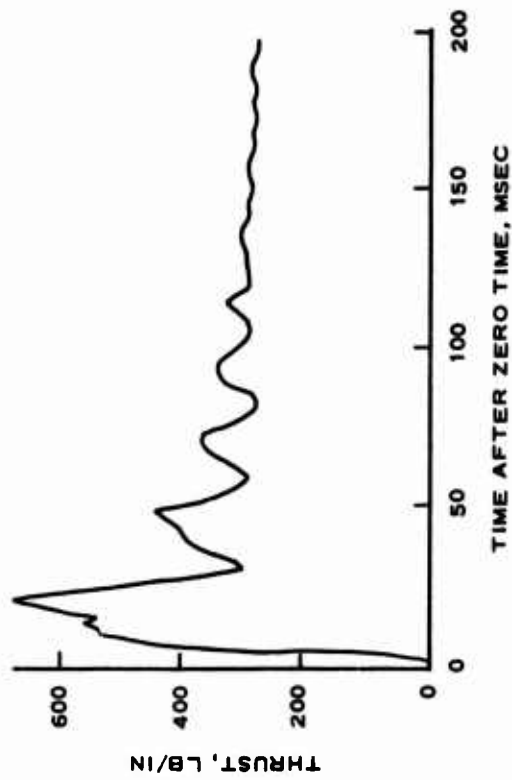


a. Thrust.

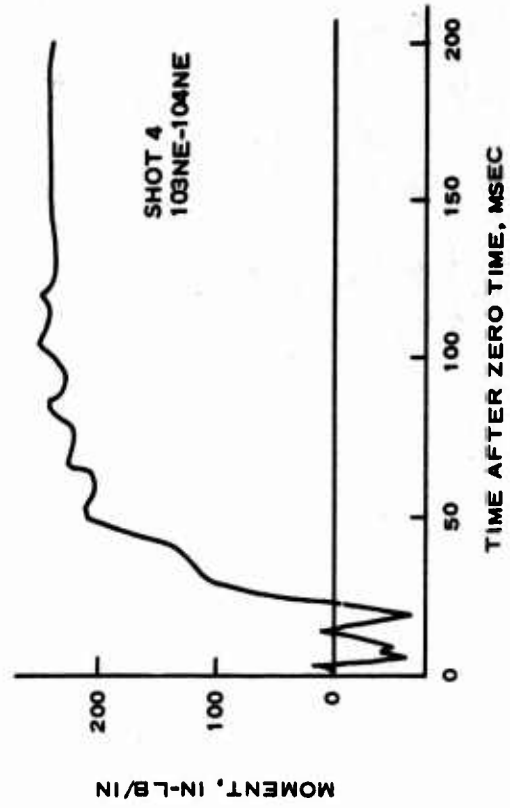
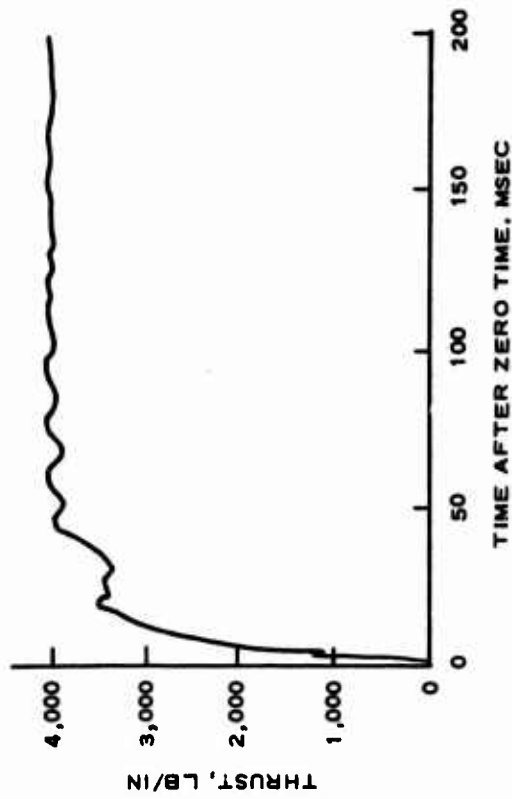


b. Moment.

Figure 4.15 Idealized thrust and moment histories.



a. ELASTIC SECTION



b. PLASTIC SECTION

Figure 4.16 Typical elastic and plastic thrust and moment data.

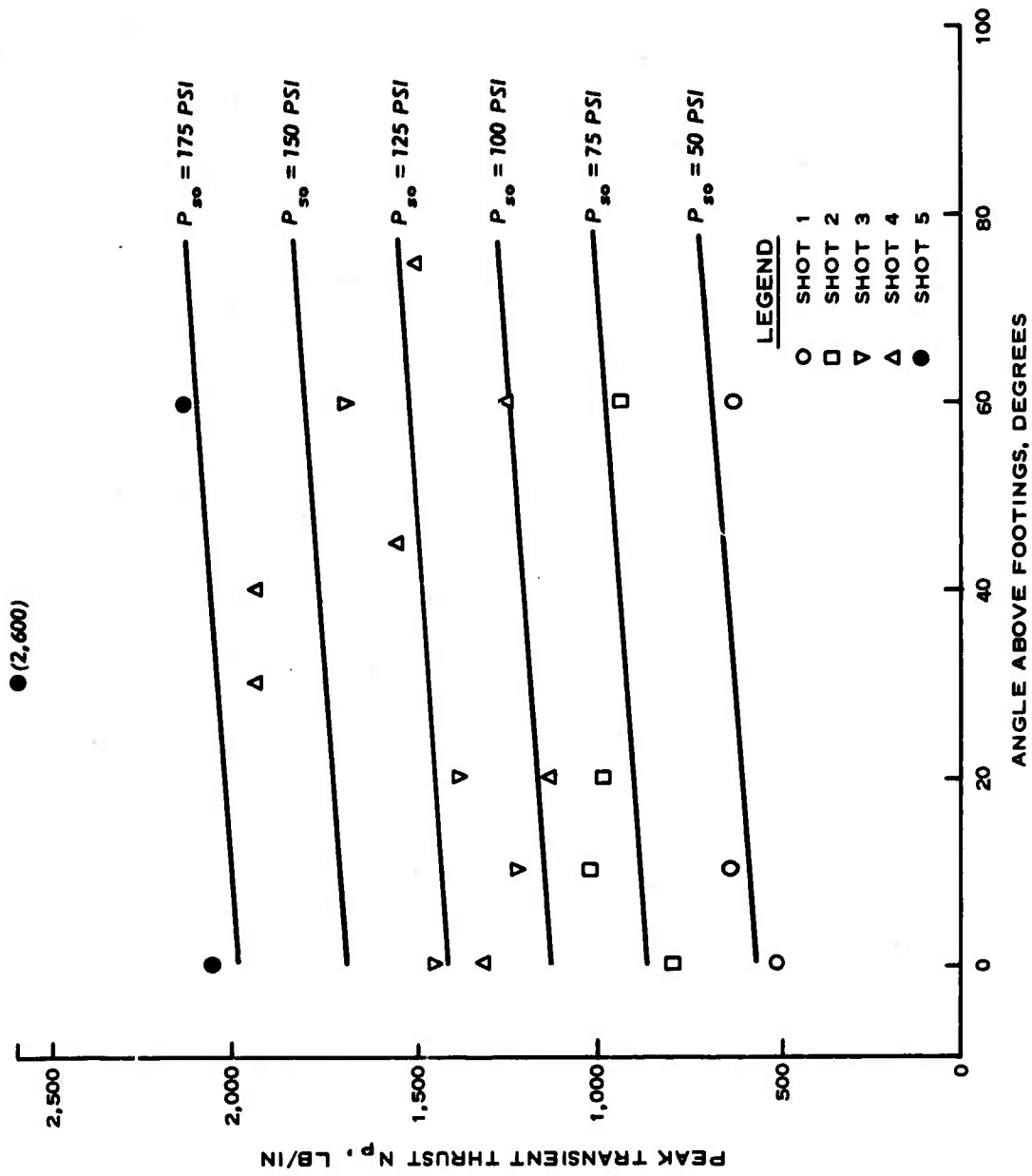


Figure 4.17 Peak transient thrust.

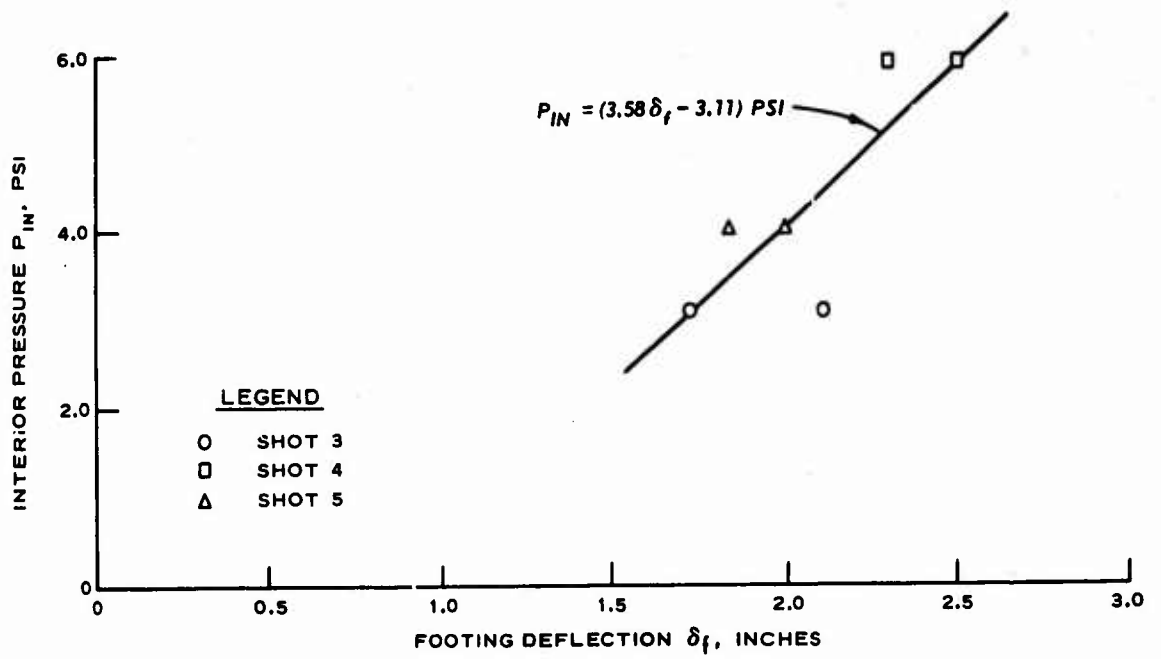


Figure 4.18 Peak interior pressure versus footing deflection.

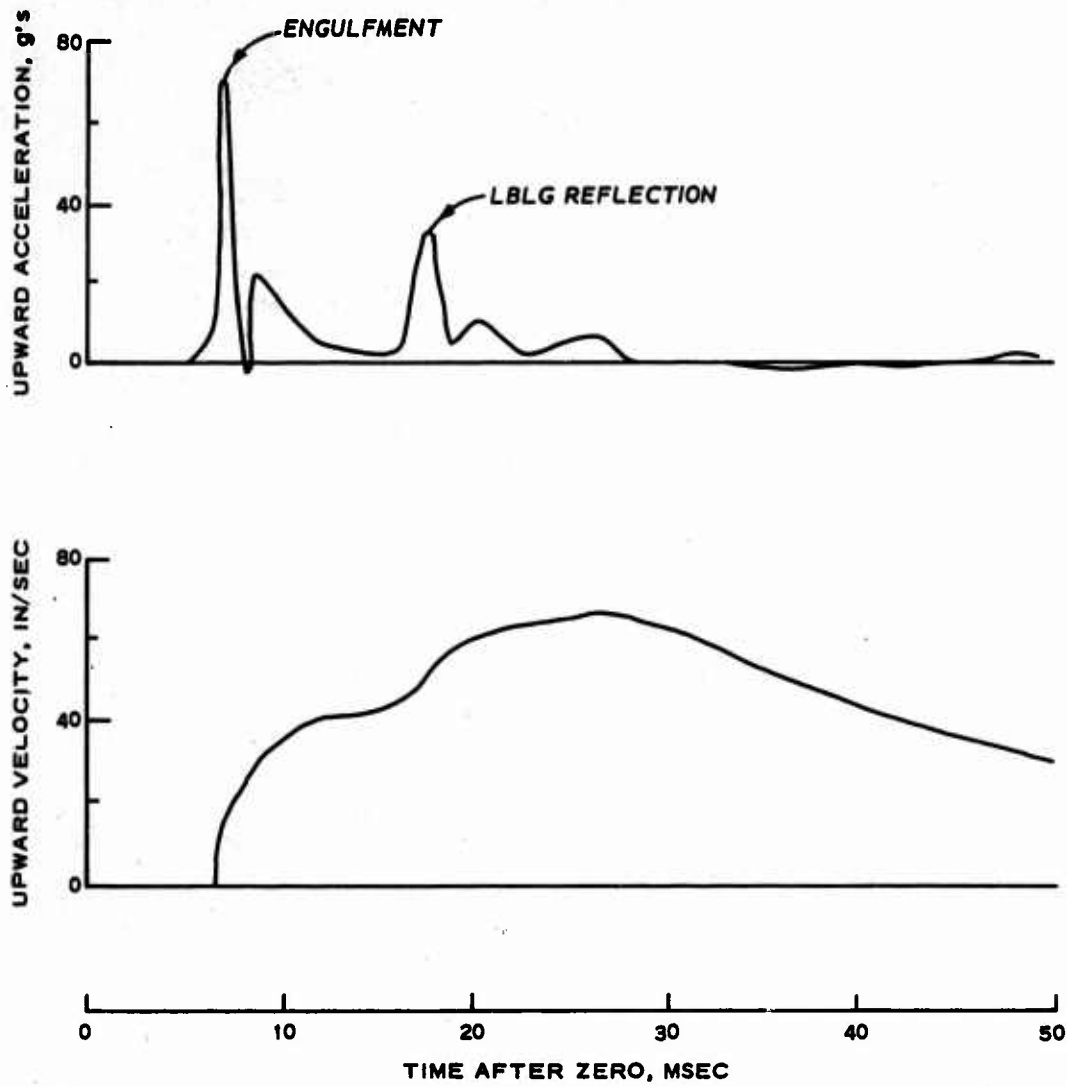


Figure 4.19 Acceleration- and velocity-time histories of the interior floor, Shot 4 (Gage 51VA).

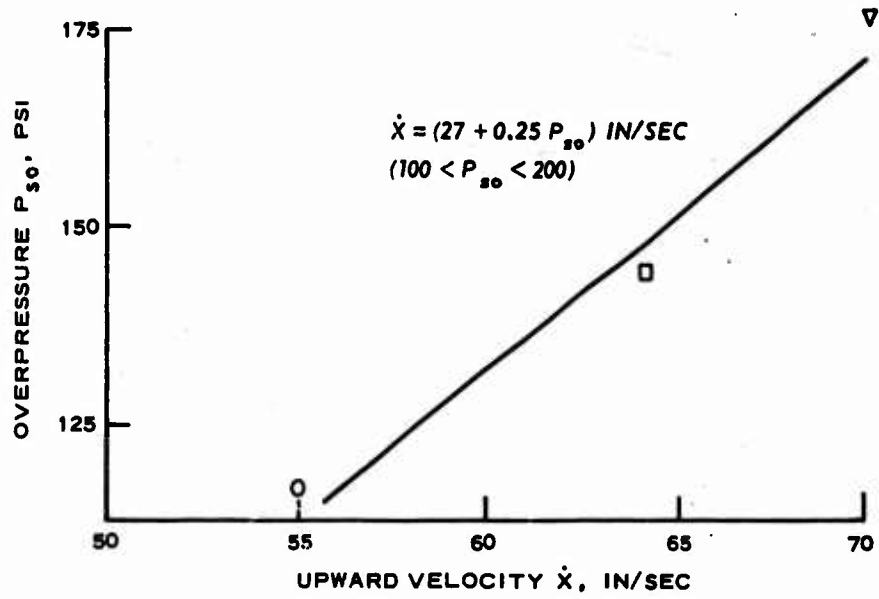
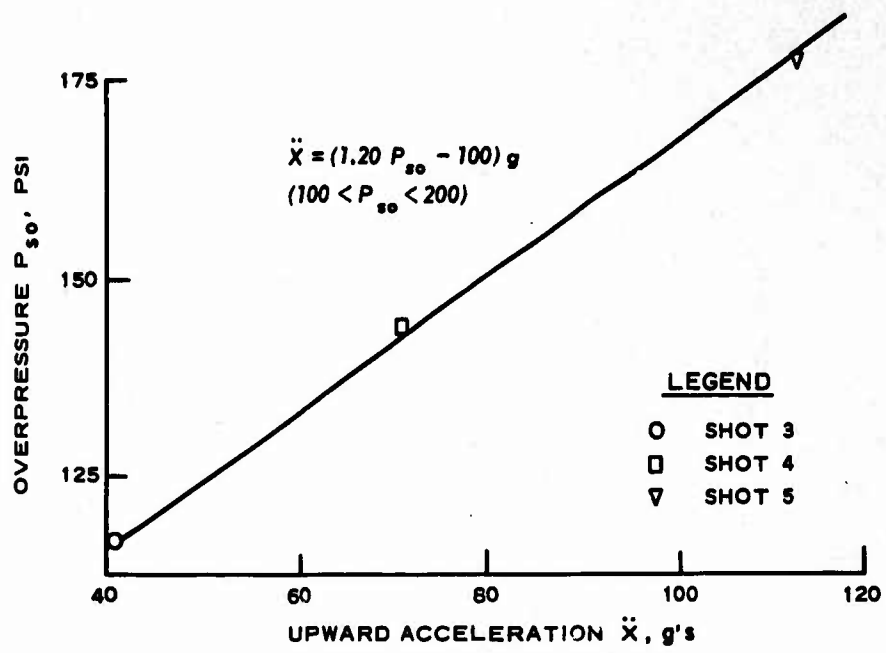


Figure 4.20 Peak motions of the interior floor (Gage 51VA).

## CHAPTER 5

### CONCLUSIONS AND RECOMMENDATIONS

#### 5.1 CONCLUSIONS

The structure as tested easily withstood the design overpressure of 100 psi with little damage, and in subsequent testing withstood almost twice the design overpressure. Since the reflected stress wave from the bottom of the test chamber tends to stop the motion of the structure, it is concluded that the relative displacements experienced in the laboratory are somewhat less than those which would be experienced in the field, whereas the stress levels in the structure are higher in the laboratory tests due to the reflected stress wave.

It is concluded that the revised truss as outlined in Appendix D is workable and an improvement over the original design. The bulkhead design appears to be more than adequate, probably a bit more overdesigned than the arch itself.

Limited spalling tests indicate that dust inhalation could be a problem in the prototype, and some means of dust prevention such as oiling the interior floor should be considered.

It is believed that with a minimum redesign the overpressure resistance of the structure can be increased to near 200 psi for a 1-Mt weapon. However, because the earth cover provides minimum protection from radiation effects at 100 psi, the depth of cover would have to be increased to provide protection at this overpressure level with the lower yield weapons producing the critical radiation levels.

#### 5.2 RECOMMENDATIONS

Based on the laboratory findings, it is recommended that the bulkhead truss connection be redesigned as outlined in Appendix D. This redesign will eliminate problems occurring as a result of truss rotation. With regard to the truss itself, it is recommended that a cheaper configuration be designed. It is possible to use a pair of the arch ribs laid flat and connected to the bulkhead column bases by rods.

It is recommended that spikes be used to fasten the ribs to the

footings rather than lag screws, since the only purpose served by these connectors is to position and to resist a small amount of shear. The spikes are cheaper and faster to use. It also appears possible to decrease the thickness of the wooden arch blocks, and it is recommended that this be considered.

If it is assumed that the hardness of the structure exceeds the original 100-psi design as the tests indicate, then it is recommended that the earth cover over the structure be increased to provide additional radiation protection. Exactly how much protection is required will depend upon the mission of the protected personnel.

Because of the large amount of settlement that will be associated with the response of this structure, any lines, wires, pipes, etc., will have to be designed for this relative motion between the components and the structure. It is recommended that flexible couplings be used with these components.

The entranceway described in Reference 1 is complex and quite expensive. It is recommended that, for general use, an entranceway be fabricated of concrete pipe cattle pass with a steel vertical shaft and blast-proof door of the type shown in Reference 1. With this entranceway, the use of corrugated-steel pipe to form a ventilation duct at either end of the structure with a blast-activated blast valve is recommended. It is further recommended that an emergency exit be provided that is constructed of corrugated-steel pipe and filled with sandbags and has a concealed surface exit.

The test series reported herein was conducted in dense, dry sand in a plane-wave device. It is recommended that (1) tests be conducted in soils other than dry sand in the same device, and (2) a field test of a larger model be conducted in sand to determine the severity of the laboratory environment as opposed to the field. It is also recommended that limited instrumentation be used with these tests, with emphasis being put on the footing response and the interior environment, as a means of correlating the laboratory and field results. By extrapolating these data to the prototype, to other soil types, and to modified construction, a structural analysis can be developed based on a discrete approximation to the structure.

**APPENDIX A**  
**INSTRUMENTATION DETAILS**  
**AND TABULATED RESULTS**

The Large Blast Load Generator facility is ideally suited for conducting heavily instrumented tests on structures of the type tested in this study. An ultimate capability of nearly 100 data channels (Figure A.1) means that large quantities of information can be obtained from a single test. With tests requiring approximately 100 data channels such as are reported herein, no single system of instrumentation can be used, and care must be exercised to see that frequencies of systems are compatible with what is being measured. Diagrams of the test instrumentation hookup are shown in Figure A.2. Magnetic tape was used for primary data recording and was backed up with recording oscillograph equipment. Since only about 50 channels of tape were available, it was not possible to use tape in all cases. Consequently, some data were recorded only on oscillograph recorders.

The system used was composed essentially of three parts: transducers, amplifiers, and recorders. All strain gages used on the steel elements were manufactured by the Budd Company and were foil-type high-elongation gages with a resistance of 120 ohms. Strain in the wooden components was measured with 1- by 1/8-inch high-elongation foil-type gages manufactured by the Budd Company. Deflections were measured using 6-inch-range LVDT-type transducers manufactured by Crescent Instruments. Piezoelectric accelerometers from Columbia Instruments and strain-gage-type accelerometers from Consolidated Electrodynamics Corporation (CEC) were used to measure acceleration. Soil pressure was measured using W-type transducers (Shots 1 and 2) developed at the Waterways Experiment Station (Reference 8) and using Road Research Cells (RRC) (Shots 3, 4, and 5) from the Road Research Laboratories (Reference 9). Overpressure at the soil surface was monitored using Norwood blast-pressure transducers, and air pressure in the structure was monitored using a CEC pressure transducer. Figure A.3 is a photograph of all the transducers used.

Various amplifiers were used to condition the signals prior to recording. Three carrier systems manufactured by CEC were used, the 1-118 with a 3-kcps response, the 1-127 with a 20-kcps response, and the System D with a 3-kcps response. Dana 2000-DC amplifiers and Alinco Model SAM 1 amplifiers were also used. In use with the piezoelectric transducers were Kistler Model 65656 charge amplifiers. Final recording of the data was

done using CEC-type 5-119 galvanometer oscillographs at paper speeds of 160 in/sec and Sangamo Model 472RB and Ampex Model ES-100 magnetic-tape recorders.

The frequency response of the total system varied, depending on the recording equipment. In the case of the magnetic-tape data channels, the frequency limitation was the transducer response since the tape equipment had a 20-kcps capability. In the case of the oscillograph-data channels, the frequency response limitations were caused by the type of galvanometer used in the system. Table A.1 is a tabulation of the maximum frequency response of each recorder used.

The LBLG has the advantage of providing a fixed reference to which all motion measurements can be referenced. To take advantage of this, a 6-inch-square steel column was welded to the center of the floor of the LBLG and extended upward to the level of the structure footings. It was necessary to measure three vertical components of deflection to determine the rigid body motion of the footing since it had three degrees of freedom. Consequently, a rig mounting three deflection gages was designed and rigidly attached to the steel column. The deflection gages were attached to the footing by means of rollers, pin joints, and a rocking beam as shown in Figure A.4. The crown deflection in Shots 1, 2, and 3 was tied into this reference column. During Shots 3 and 4, a steel angle rod was extended toward the east bulkhead and a deflection gage (OLHD) was mounted on this rod to measure the base deflection of Bulkhead Beam 2. This gage and mounting rod can be seen in Figure A.5. This figure shows the instrumentation in place prior to sand placement for Shot 3.

Figures A.6 and A.7 show the gage locations used and the numbering system used with the ribs and bulkhead beams throughout the test series. Tables A.2 through A.6 give a detailed tabulation of various peaks, times of arrival, etc., considered to be of greatest importance. Appendix B contains the raw records from which Tables A.2 through A.6 were made.

The gage designations in Tables A.2 through A.6 indicate the type of measurement and the gage location.

For the air pressure and soil stress gages (Tables A.2 and A.3), the first two letters indicate the type of measurement, as follows:

SS - soil stress.

SP - surface airblast pressure.

IP - interior air pressure.

The final number is a location number which, for the soil stress gages, is odd for a horizontal gage and even for a vertical gage.

Gage designations for accelerometers and deflection gages (Tables A.4 and A.5) are four characters, indicating:

1. The rib nearest to or upon which the gage is placed (see Figure A.6). Omitted for free-field gages.
2. Location.
3. V - vertical, H - horizontal.
4. A - acceleration, or D - deflection.

Gage designations for strain gages (Table A.6) are also four characters, indicating:

1. The rib or column nearest to or on which the gage is placed (see Figure A.6).
2. Location. In general, even for extrados and odd for intrados.
3. N - north, S - south, E - interior, or W - exterior.
4. E - arch strain, B - timber block strain, C - bulkhead column strain.

TABLE A.1 OSCILLOGRAPH SYSTEM FREQUENCY RESPONSE

Recorder No.	Maximum Response, cps			
	Shots 1 and 2	Shot 3	Shot 4	Shot 5
1	1,000	1,000	1,000	1,000
2	1,000	1,000	1,000	1,000
3	2,500	2,500	2,500	1,000
4	600	1,000	1,000	1,000
5	600	1,000	1,000	--
6	--	2,500	2,500	--

TABLE A.2 AIRBLAST RESULTS

NR - No interpretable record.

Shot	Gage No.	Spike Peak	Averaged Peak	100-msec <sup>a</sup> Level
		psi	psi	psi
1	SP1	54	39	22
1	SP2	38	34	19
1	BP1(7362)	109	37	23
1	BP2(7369)	70	39	21
2	SP1	81	45	24
2	SP2	82	64	53
2	BP1(7362)	123	70	57
2	BP2(7369)	103	64	49
3	SP1	132	117	76
3	SP2	243	117	79
3	SP3	117	106	56
3	BP1(7367)	153	113	78
3	IP1	3.1	3.1	3.1
4	SP1	144	107	77
4	SP2	66	35	32
4	SP3	NR	NR	NR
4	BP1(6965)	178	143	126
4	BP2(8622)	NR	NR	NR
4	IP1	5.9	5.9	4.9
5	SP1	330	287	0
5	SP2	183	170	67
5	SP3	230	180	71
5	BP1(7363)	265	205	108
5	BP2(8551)	NR	NR	NR
5	IP1	4.0	4.0	3.2

<sup>a</sup> 100 msec after zero time.

TABLE A.3 SOIL STRESS RESULTS

NR - No interpretable record.

Shot No.	Gage No.	Incident Peak, P <sub>I</sub>	P <sub>I</sub>	First Reflected Peak, P <sub>R</sub>	P <sub>R</sub>	100-msec <sup>a</sup> Level
			Arrival Time		Arrival Time	
		psi	msec	psi	msec	psi
1	SS2 <sup>b</sup>	34	5.6	NR	NR	38
1	SS3 <sup>c</sup>	NR	NR	154	20.0	77
1	SS4 <sup>d</sup>	78	4.9	98	19.0	37
2	SS2 <sup>b</sup>	NR	2.6	NR	NR	NR
2	SS3 <sup>c</sup>	84	4.3	149	17.4	107
2	SS4 <sup>d</sup>	128	4.3	212	17.4	94
3	SS1	90	3.5	157	17.1	55
3	SS2	216	3.7	482	17.5	194
3	SS3	79	3.8	140	17.2	72
3	SS4	145	3.9	259	17.1	109
3	SS5	NR	3.8	NR	NR	NR
3	SS6	174	4.0	294	16.9	119
3	SS7	57	1.5	59	17.7	23
3	SS8	96	1.7	134	17.9	70
3	SS9	48	1.7	66	14.5	24
3	SS10	159	1.6	181	17.6	113
3	SS12	121	1.7	176	18.2	120
3	SS13	51	3.6	94	17.1	52
3	SS14	106	3.5	220	16.8	78
3	SS15	58	2.2	62	17.9	46
3	SS16	184	2.2	296	17.0	147
4	SS1	31	NR	62	NR	29
4	SS2	NR	NR	NR	NR	68
4	SS3	22	NR	55	NR	26
4	SS4	43	NR	88	NR	29
4	SS5	18	NR	61	NR	35
4	SS6	57	NR	98	NR	45
4	SS7	41	NR	74	NR	42
4	SS8	65	NR	90	NR	49
4	SS9	33	NR	52	NR	19
4	SS10	54	NR	71	NR	40
4	SS11	23	NR	45	NR	24
4	SS12	101	NR	181	NR	101
4	SS13	NR	NR	NR	NR	NR
4	SS14	38	NR	96	NR	35
4	SS15	28	NR	43	NR	19
4	SS16	44	NR	84	NR	42

<sup>a</sup> 100 msec after zero time.

<sup>b</sup> Gage located 24 inches south of center of the south footing level with the crown. Measured vertical pressure.

<sup>c</sup> Gage located 24 inches north of center of the north footing level with the footing. Measured vertical pressure.

<sup>d</sup> Gage located 24 inches north of center of the north footing level with the crown. Measured vertical pressure.

TABLE A.4 ACCELERATION RESULTS

NR - No interpretable record. Initial peak, largest first peak; second peak, largest peak in direction opposite initial peak. Peak velocity corrected during integration such that velocity is zero before 100 msec. Peak displacement, displacement based on the corrected velocity.

Shot	Gage No.	Initial Peak	Second Peak	Peak Velocity	Peak Displacement
		g's	g's	in/sec	inches
1	52VA	84 Down	13 Up	39 Down	0.93 Down
1	53VA	68 Down	22 Up	36 Down	0.51 Down
1	54VA	27 Down	11 Up	24 Down	0.54 Down
2	52VA	189 Down	55 Up	53 Down	0.29 Down
2	53VA	168 Down	26 Up	NR	NR
2	54VA	159 Down	55 Up	28 Down	0.14 Down
3	51VA	41 Up	5 Down	55 Up	1.75 Up
3	52VA	262 Down	111 Up	136 Down	2.28 Down
3	53VA	286 Down	287 Up	300 Down	11.20 Down
3	54VA	99 Down	182 Up	88 Down	2.19 Down
3	1HA	224 <sup>a</sup>	132	16 <sup>a</sup>	0.04 <sup>a</sup>
3	2HA	175 <sup>a</sup>	100	6.5 <sup>a</sup>	0.02 <sup>a</sup>
3	3VA	1,864 Down	784 Up	85 Down	0.23 Down
3	4VA	NR	NR	NR	NR
4	51VA	71 Up	5.7 Down	64 Up	2.11 Up
4	52VA	213 Down	132 Up	117 Down	1.26 Down
4	53VA	NR	NR	NR	NR
4	54VA	167 Down	76 Up	79 Down	0.88 Down
4	55CA	NR	NR	NR	NR
4	3VA	NR	NR	NR	NR
4	4VA	697 Down	378 Up	33 Down	NR
5	51VA	113 Up	28 Down	70 Up	1.69 Up
5	52VA	287 Down	134 Up	189 Down	1.85 Down
5	53VA	353 Down	121 Up	206 Down	2.15 Down
5	54VA	NR	NR	NR	NR
5	55CA	467 Up	264 Down	60 Down	1.12 Down
5	3VA	669 Down	474 Up	36 Down	0.15 Down
5	4VA	NR	NR	NR	NR

<sup>a</sup> Toward the structure.

TABLE A.5 DEFLECTION RESULTS

Shot	Gage No.	Initial Peak	Rise Time to Peak	Reflected Peak	Time <sup>a</sup> of Reflected Peak	100-msec <sup>a</sup> Level
		inches	msec	inches	msec	inches
1	51HD	0.06 Out	11	0.08 In	26	0.07 In
1	52HD	0.02 Out	11	0.02 In	26	0.02 In
1	53VD	0.42 Out	17	0.42 Out	b	0.43 Out
1	54CD	0.67 In	14	0.67 In	b	0.66 In
2	51HD	0.16 Out	11	0.09 In	26	0.06 Out
2	52HD	0.04 Out	11	0.02 In	26	0.05 Out
2	53VD	0.65 Out	24	0.65 Out	b	0.59 Out
2	54CD	c	c	c	c	c
3	51HD	0.16 Out	2	0.11 In	22	0.11 In
3	52HD	0.20 Out <sup>d</sup>	2	0.22 In	22	0.24 In
3	53VD	0.48 Out <sup>d</sup>	20	d	b	0.89 Out
3	54CD	0.66 In <sup>c</sup>	c	c	c	c
3	01HD	0.44 In <sup>d</sup>	16	0.44 In <sup>d</sup>	18	0.32 In
4	51HD	0.12 Out	2	0.37 In	38	0.27 In
4	52HD	0.11 Out	2	0.36 In	38	0.24 In
4	53VD	0.71 Out	12	b	b	1.12 Out
4	01HD	0.15 In <sup>d</sup>	16	b	b	0.14 In
5	51HD	0.16 Out	2	0.14 In	b	0.07 In
5	52HD	0.11 Out	2	0.21 In	b	0.20 In
5	53VD	1.52 Out <sup>d</sup>	60	d	b	1.52 Out

<sup>a</sup> Time after zero time.

<sup>b</sup> No single reflection time evident.

<sup>c</sup> Gage bottomed.

<sup>d</sup> Steady rise to peak.

TABLE A.6 STRAIN GAGE RESULTS

C - Compression, T - Tension, NR - No interpretable record.

Shot No.	Gage No.	Location	Initial Rise <sup>a</sup>		Reflected Peak	Time <sup>a</sup> of Reflected Peak		Location	Initial Peak	Rise Time to Peak	Reflected Peak	Time of Reflected Peak	100-msec Level
			degrees	μin/in		msec	msec						
1	11NE	0	303C	10	343C	22	120C	NR	NR	NR	NR	NR	NR
1	12NE	0	645C	7	533C	20	168C	534C	11	594C	21	279C	NR
1	13SE	0	406C	4	426C	20	148C	206C	1	202C	24	NR	NR
1	14SE	0	985T	2	364C	20	250T	1,080C	5	1,070C	22	143C	74C
1	15NE	10	724C	10	740C	23	472C	NR	NR	NR	NR	NR	NR
1	16NE	10	837T	10	950T	18	894T	NR	NR	NR	NR	NR	NR
1	19NE	20	NR	NR	NR	NR	NR	1,997C <sup>b</sup>	6	1,630C <sup>b</sup>	21	593C	NR
1	110NE	20	NR	NR	NR	NR	NR	NR	NR	NR	NR	NR	NR
1	113NE	30	NR	NR	NR	NR	NR	NR	NR	NR	NR	NR	NR
1	114NE	30	2,630C <sup>b</sup>	13	3,370C <sup>b</sup>	27	3,790C <sup>b</sup>	NR	NR	NR	NR	NR	NR
1	115NE	60	173C	10	194C	23	147C	341C	9	437C	24	108C	NR
1	116NE	60	1,210C	9	1,550C	21	398C	388C	7	435C	22	168C	NR
1	117SE	60	453C	8	NR	NR	217C	229C	12	300C	24	161C	NR
1	118SE	60	NR	NR	NR	NR	NR	147C	5	290C	21	113C	NR
1	31NE	0	NR	NR	NR	NR	NR	NR	NR	NR	NR	NR	NR
1	32NE	0	238C	11	206C	22	299C	NR	NR	NR	NR	702C <sup>b</sup>	NR
1	41NE	0	205C	10	391C	21	120C	NR	NR	NR	NR	NR	NR
1	42NE	0	996C	6	1,040C	22	136C	335C <sup>b</sup>	6	446C	21	171C	NR
1	51NE	0	357C	5	364C	13	188C	466C <sup>b</sup>	3	770C <sup>b</sup>	23	455C <sup>b</sup>	10T <sup>c</sup>
1	52NE	0	426C	3	718C	24	117C	10T <sup>c</sup>	NR	10T <sup>c</sup>	21	10T <sup>c</sup>	NR
1	53SE	0	470C	5	549C	21	282C	390T	11	310T	22	94T	NR
1	54SE	0	509T	2	209T	18	346T	519T	14	521T	27	261T	NR
1	55SE	89	192C	4	168C	21	126C	317T	11	341T	27	237T	NR
1	56SE	89	NR	NR	NR	NR	NR	524T	10	566T	27	402T	NR
1	61NE	0	NR	NR	NR	NR	NR	573T	11	580T	21	348T	NR
1	62NE	0	NR	NR	NR	NR	NR	253T	7	359T	22	194T	NR
1	63SE	0	875C	12	NR	NR	366C	378C	8	483C	22	365C	NR
1	64SE	0	60C	3	204C	21	72C	190T	8	293T	23	179T	NR
1	65NE	10	1,360C	7	1,210C	20	236C <sup>b</sup>	380C	8	480C	22	260C	NR
1	66NE	10	NR	NR	NR	NR	1,070C <sup>b</sup>	NR	NR	NR	NR	NR	NR
1	67NE	20	NR	NR	NR	NR	870T <sup>b</sup>	447C	2	345C	16	24C <sup>b</sup>	NR
1	68NE	20	NR	NR	NR	NR	NR	998C	8	1,280C	20	108C	NR
1	69SE	20	NR	NR	NR	NR	NR	574C	2	475C	18	119C	NR
1	610SE	20	NR	NR	NR	NR	NR	NR	NR	NR	NR	NR	NR
1	611NE	30	843C <sup>b</sup>	12	942C <sup>b</sup>	23	724C <sup>b</sup>	845C	6	827C	18	457C	NR

(Continued)

<sup>a</sup> Time after zero time.  
<sup>b</sup> Questionable result.  
<sup>c</sup> Inches above the truss-bulkhead beam connecting bolt center.

TABLE A.6 (CONTINUED)

Shot No.	Gage No.	Location	Initial Peak	Rise Time to Peak	Reflected Peak	Time of Reflected Peak	100-msec Level	Shot No.	Gage No.	Location	Initial Peak	Rise Time to Peak	Reflected Peak	Time of Reflected Peak	100-msec Level
2	16NE	10	357T	5	243T	19	515T	2	83SE	0	27C	5	639C	19	356C
2	19NE	20	1,014C	5	894C	19	1,220C	2	94SE	0	1,850C	3	1,100C	17	256T
2	110NE	20	NR	NR	NR	NR	NR	2	85NE	20	1,130C	10	1,340C	20	1,230C
2	113NE	30	1,090C	8	1,270C	19	1,150C	2	86NE	20	NR	NR	NR	NR	NR
2	114NE	30	NR	NR	NR	NR	NR	2	87NE	60	685C	7	857C	20	537C
2	115NE	60	571C	7	687C	19	504C	2	88NE	60	441C	3	403C	19	671T
2	116NE	60	796C	3	816C	20	NR	2	101NE	0	634C	7	866C	20	433C
2	117SE	60	571C	8	729C	19	532C	2	102NE	0	370T	2	520T	20	458T
2	118SE	60	NR	NR	NR	NR	NR	2	103SE	0	413C	5	698C	19	413C
2	31NE	0	NR	NR	NR	NR	NR	2	104SE	0	991C	3	913C	16	NR
2	32NE	0	NR	NR	NR	NR	NR	2	105NE	20	1,040C	7	1,340C	19	783C
2	41NE	0	336C	3	383C	20	269C	2	106NE	20	NR	NR	NR	NR	NR
2	42NE	0	NR	NR	NR	NR	NR	2	107NE	60	540C	5	679C	19	398C
2	51NE	0	490C	2	469C	19	323C	2	108NE	60	NR	NR	NR	NR	NR
2	52NE	0	852C	5	1,030C	18	398T	2	51NB	8	1,34T	8	268T	17	48T
2	53SE	0	558C	3	818C	19	391C	2	52NB	24	598T	8	472T	20	105C
2	54SE	0	333C	5	9T	17	582T	2	53NB	45	790T	8	778T	19	271T
2	55SE	89	257C	4	170C	19	213T	2	54NB	67	607T	8	660T	19	456T
2	56SE	89	NR	NR	NR	NR	NR	2	55NB	83	663T	7	719T	18	497T
2	61NE	0	NR	NR	NR	NR	NR	2	56SB	45	900T	8	873T	18	343T
2	62NE	0	1,260C	6	1,170C	19	0	2	21EC	7 <sup>c</sup>	371T	3	540T	19	287T
2	63SE	0	361C	4	647C	20	222C	2	224C	7 <sup>c</sup>	520C	6	672C	20	396C
2	64SE	0	1,370C	4	825C	18	180C	2	23EC	14,5 <sup>c</sup>	166T	2	252T	20	231T
2	65NE	10	1,160C	8	1,270C	20	649C	2	244C	14,5 <sup>c</sup>	504C	7	628C	20	395C
2	66NE	10	1,440T	6	1,760T	20	NR	3	11NE	0	1,130C	6	1,160C <sup>b</sup>	18	784C <sup>b</sup>
2	67NE	20	1,460C	9	1,750C	20	1,500C	3	12NE	0	1,170C	3	100T <sup>b</sup>	18	1,250T
2	68NE	20	2,760T	9	3,860T	21	620T	3	15NE	60	1,340C	8	1,740C	13	1,240C
2	69SE	20	1,220C	7	1,580C	20	1,750C	3	16NE	60	1,020C	2	0	18	1,320T
2	610SE	20	NR	NR	NR	NR	NR	3	17SE	0	1,170C	4	928C	17	538C
2	611NE	30	1,140C	6	1,430C	19	1,700C	3	18SE	0	602T <sup>b</sup>	3	NR	NR	NR
2	612NE	30	NR	NR	NR	NR	NR	3	21NE	0	253C <sup>b</sup>	5	327C <sup>b</sup>	17	285C <sup>b</sup>
2	613NE	60	759C	8	941C	20	581C	3	22NE	0	2,870C	8	d	17	929C
2	614NE	60	NR	NR	NR	NR	NR	3	23SE	20	900C	6	1,110C	17	1,110C
2	81NE	0	311C	8	436C	20	311C	3	24SE	20	NR	NR	NR	NR	NR
2	82NE	0	1,210C	3	872C	19	284T	3							

(Continued)  
 b Questionable result.  
 c Inches above the truss-bulkhead beam connecting bolt center.  
 d No reflection apparent.

TABLE A.6 (CONTINUE)

Shot No.	Gage No.	Location	Initial Peak	Rise Time to Peak	Reflected Peak	Time of Reflected Peak	100-msec Level	Shot No.	Gage No.	Location	Initial Peak	Rise Time to Peak	Reflected Peak	Time of Reflected Peak	100-msec Level
3	31NE	0	NR	NR	NR	NR	NR	3	72WE	0	670C	1	1,060C	17	350T
3	32WE	0	NR	NR	NR	NR	NR	3	81NE	0	1,150C	6	718C	18	495C
3	33WE	10	800C	1	799C	16	492C	3	82NE	0	840C	4	1,400C	17	50T
3	34NE	10	1,560C	2	700C	17	1,290T	3	91NE	0	375C	4	1,98C	18	310C
3	35NE	20	1,180C	6	1,280C	16	1,110C	3	92NE	0	NR	NR	NR	NR	NR
3	36NE	20	1,500T	1	970T	18	2,910T	3	101NE	0	820C	6	835C	18	456C
3	37NE	30	1,620C	7	2,200C	18	2,300C	3	102NE	0	1,240C	4	1,150C	18	970C
3	38NE	30	NR	NR	NR	NR	NR	3	51NB	8	854T	4	680T	18	102T
3	39NE	60	1,210C	6	1,370C	18	768C	3	52NB	24	1,530T	7	1,510T	18	438T
3	30NE	60	NR	NR	NR	NR	NR	3	53NB	45	NR	NR	NR	NR	NR
3	31SE	0	1,220C	6	867C	17	199C	3	54NB	67	NR	NR	NR	NR	NR
3	32SE	0	NR	NR	NR	NR	NR	3	55NB	83	995T	9	d	d	634T
3	41NE	0	NR	NR	NR	NR	NR	3	56SB	45	1,340T	9	1,190T	18	533T
3	42NE	0	NR	NR	NR	NR	1,170C	3	21EC	7 <sup>c</sup>	689T	5	943T	18	509T
3	43NE	20	1,330C	6	1,560C	17	1,560C	3	22WC	7 <sup>c</sup>	758C	5	1,050C	18	469C
3	44NE	20	1,550T	1	d	d	4,150T	3	23EC	14,5 <sup>c</sup>	626T	5	923T	18	446T
3	45NE	60	1,470C	8	1,470C	18	1,010C	3	24WC	14,5 <sup>c</sup>	870C	5	1,410C	18	990C
3	46NE	60	1,570C	3	250C	18	1,710T	4	11NE	0	780C	3	451C	17	472C
3	51NE	0	400C	2	420C	18	308C	4	12WE	0	1,130C	6	1,690C	19	708C
3	52NE	0	1,800C	4	NR	NR	NR	4	21NE	0	1,130C	4	863 <sup>c</sup>	19	454C
3	53NE	10	1,450C	6	1,450C	18	922C	4	22NE	0	1,520C	11	e	e	280C
3	54NE	10	860C	3	1,300T	18	15,500T	4	41NE	0	1,180C	5	480C	18	88T
3	55NE	20	1,560C	6	1,960C	18	2,150C	4	42NE	0	1,060C	5	1,300C	20	345C
3	56NE	20	1,550T	4	2,700T	18	NR	4	51NE	0	1,040C	4	677C	17	190C
3	57NE	30	1,950C	8	2,540C	18	4,980C	4	52NE	0	1,350C	5	e	e	270C
3	58NE	30	2,950C	10	5,200C	28	10,870C	4	53NE	30	1,190C	6	1,690C	18	2,650C
3	59NE	60	1,360C	8	1,460C	18	790C	4	54NE	30	2,480C	4	e	e	5,570C
3	510NE	60	778C	1	20C	18	704T	4	55NE	45	1,220C	3	1,370C	18	1,440C
3	511SE	60	1,370C	8	1,610C	18	768C	4	56NE	45	NR	NR	NR	NR	NR
3	512SE	60	835C	3	70T	18	487T	4	57NE	60	703C	3	1,490C	17	NR
3	513SE	20	3,010C	10	3,440C	16	4,040C	4	58NE	60	504C	3	168C	17	1,850C
3	514SE	20	4,720T	4	NR	NR	NR	4	59NE	75	1,200C	3	1,200C	18	194T
3	515SE	0	1,260C	6	930C	18	156C	4	510NE	75	NR	NR	NR	NR	NR
3	516SE	0	1,400C	4	539C	18	0	4	511SE	60	1,210C	7	1,520C	19	774C
3	71NE	0	1,390C	6	646C	17	495C	4	512SE	60	813C	2	529T	22	150T

(Continued)

<sup>c</sup> Inches above the truss-bulkhead beam connecting bolt center.  
<sup>d</sup> No reflection apparent.  
<sup>e</sup> No discernible peak.

TABLE A.6 (CONCLUDED)

Shot No.	Gage No.	Location	Initial Peak	Rise Time to Peak	Reflected Peak	Time of Reflected Peak	100-msec Level	Shot No.	Gage No.	Location	Initial Peak	Rise Time to Peak	Reflected Peak	Time of Reflected Peak	100-msec Level
4	513SE	45	NR	NR	NR	NR	NR	4	52NB	24	915T	8	1,330T	18	348T
4	514SE	45	1,810T	9	e	19	6,120T	4	53NB	45	855T	8	1,040T	18	315T
4	515SE	30	2,200C	9	4,060C	e	7,420C	4	54NB	67	810T	8	830T	18	311T
4	516SE	30	3,180T	10	e	e	23,500T	4	55NB	83	982T	8	892T	19	449T
4	517NE	20	914C	3	637C	18	332C	4	56SB	45	1,380T	8	1,480T	18	647T
4	518NE	20	1,670C	9	e	e	618C	4	21EC	7 <sup>c</sup>	843T	5	1,100T	18	748T
4	61NE	0	807C	4	690C	17	154C	4	22WC	7 <sup>c</sup>	842C	6	924C	18	408C
4	62NE	0	628C	2	NR	NR	NR	4	23EC	14.5 <sup>c</sup>	818T	6	1,020T	18	780T
4	81NE	0	737C	9	853C	18	446C	4	24WC	14.5 <sup>c</sup>	950C	6	1,200C	18	502C
4	82NE	0	NR	NR	NR	NR	NR	5	11WE	0	690C	f	NR	NR	NR
4	83NE	30	2,330C	7	4,880C	20	5,320C	5	12WE	0	NR	f	NR	NR	NR
4	84NE	30	e	e	e	e	11,200T	5	21WE	0	1,050C	f	612C	17	237T
4	85NE	45	1,930C	7	1,330C	19	1,380C	5	22WE	0	3,490C	f	3,530C	19	2,660C
4	86NE	45	NR	NR	NR	NR	644C	5	31WE	0	950C	f	665C	17	0
4	87NE	60	1,120C	7	1,210C	18	NR	5	32WE	0	583T	f	1,060C	24	1,300C
4	88NE	60	994C	3	994C	18	488T	5	51WE	0	1,190C	f	903T	24	553T
4	89NE	75	830C	3	597C	18	913T	5	52WE	0	NR	f	NR	NR	NR
4	810NE	75	NR	NR	NR	NR	NR	5	53WE	30	6,570C	f	9,530C	18	10,700C
4	811SE	0	NR	NR	NR	NR	NR	5	54WE	30	2,300T	f	4,230T	18	19,300T
4	812SE	0	e	e	887C	14	400T	5	55WE	60	1,240C	f	1,720C	18	698C
4	91NE	0	541C	1	713C	18	418C	5	56WE	60	1,600C	f	1,390C	18	760C
4	92NE	0	2,652C	1	NR	NR	NR	5	51NR	8	663T	3	920T	17	322T
4	101NE	0	585C	5	857C	19	741C	5	52NR	24	1,300T	8	1,440T	17	356T
4	102NE	0	1,430C	2	NR	NR	NR	5	53NB	45	1,370T	8	1,610T	18	438T
4	103NE	30	1,750C	7	2,290C	19	2,120C	5	54NB	67	1,220T	9	1,320T	19	544T
4	104NE	30	2,300C	12	2,790C	20	4,570C	5	55NB	83	1,380T	8	1,560T	17	267T
4	105NE	45	1,240C	6	1,790C	19	2,330C	5	56SB	45	NR	NR	NR	NR	NR
4	106NE	45	797C	8	2,290C	30	3,790C								
4	107NE	60	938C	7	1,240C	19	1,280C								
4	108NE	60	NR	NR	NR	NR	NR								
4	109NE	75	NR	NR	NR	NR	NR								
4	1010NE	75	248C	2	320C	19	744T								
4	1011SE	0	1,250C	7	1,120C	19	785C								
4	1012SE	0	NR	NR	NR	NR	NR								
4	51NB	8	559T	8	476T	17	103T								

c Inches above the truss-bulkhead beam connecting bolt center.  
e No reflection apparent.  
f Because of difficulties experienced and explained in the text it was impossible to determine these data for Shot No. 5.

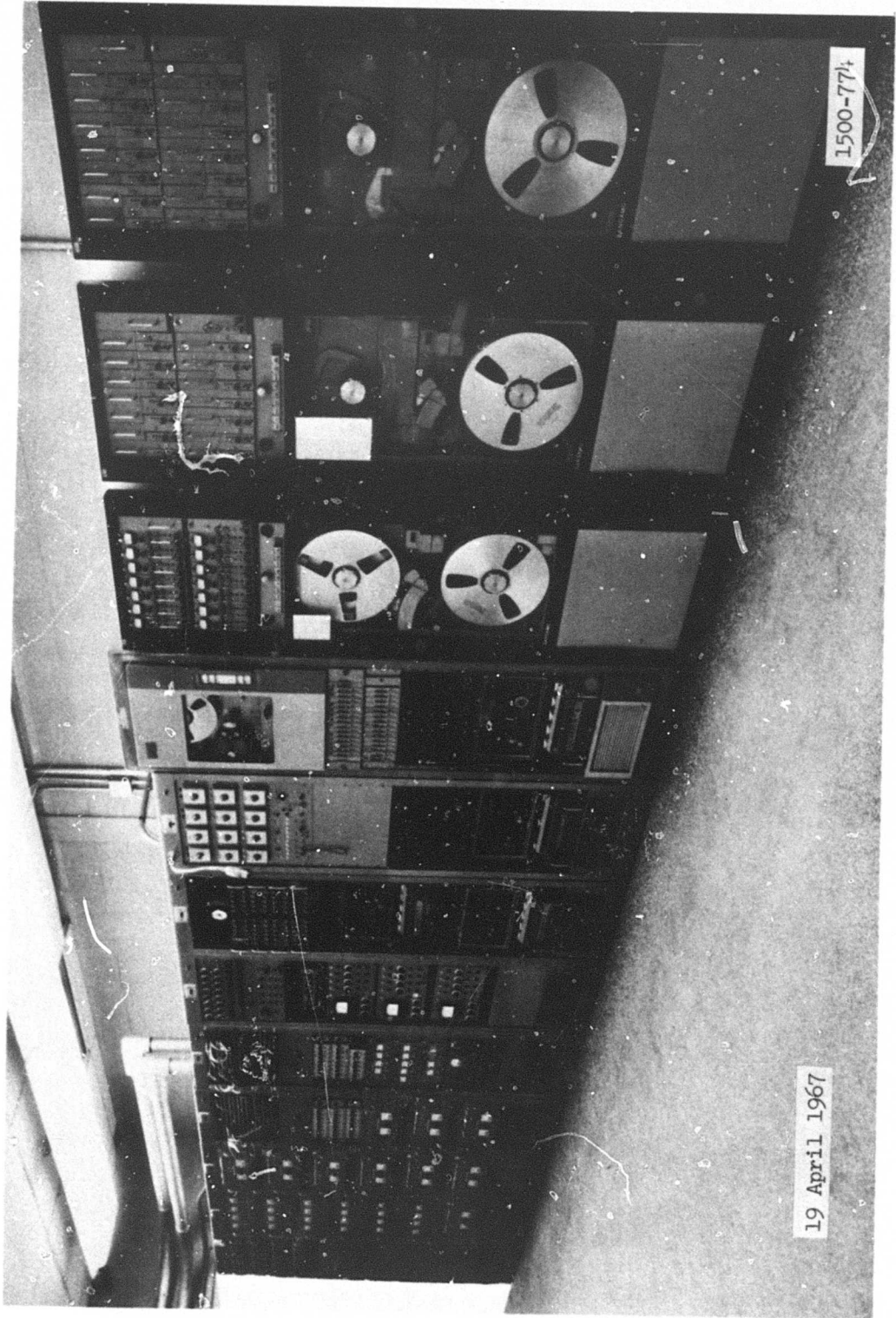
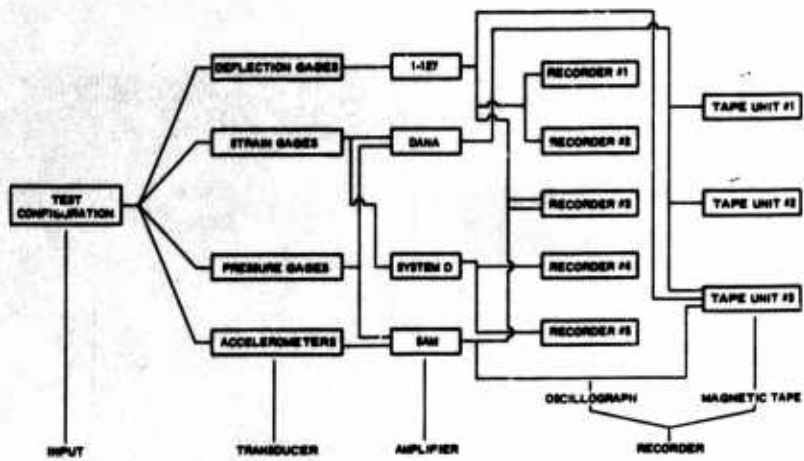
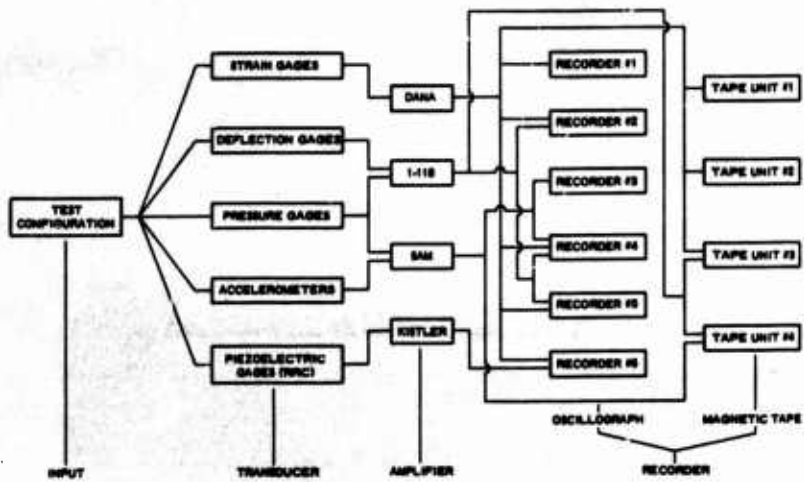


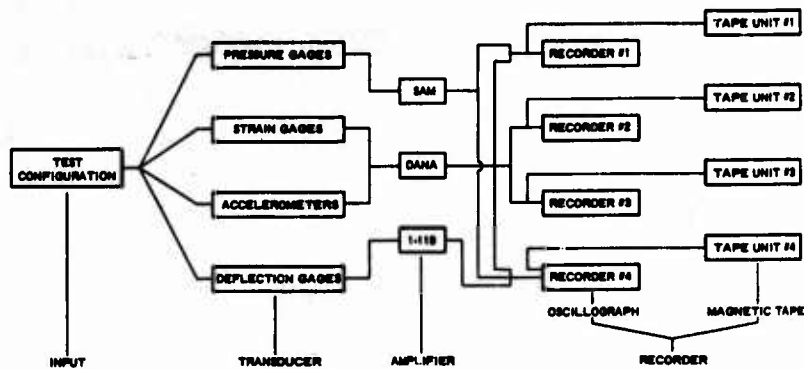
Figure A.1 General view of the recording and conditioning equipment.



a. SHOTS 1 AND 2



b. SHOTS 3 AND 4



c. SHOT 5

Figure A.2 Instrumentation diagrams for Shots 1 to 5.

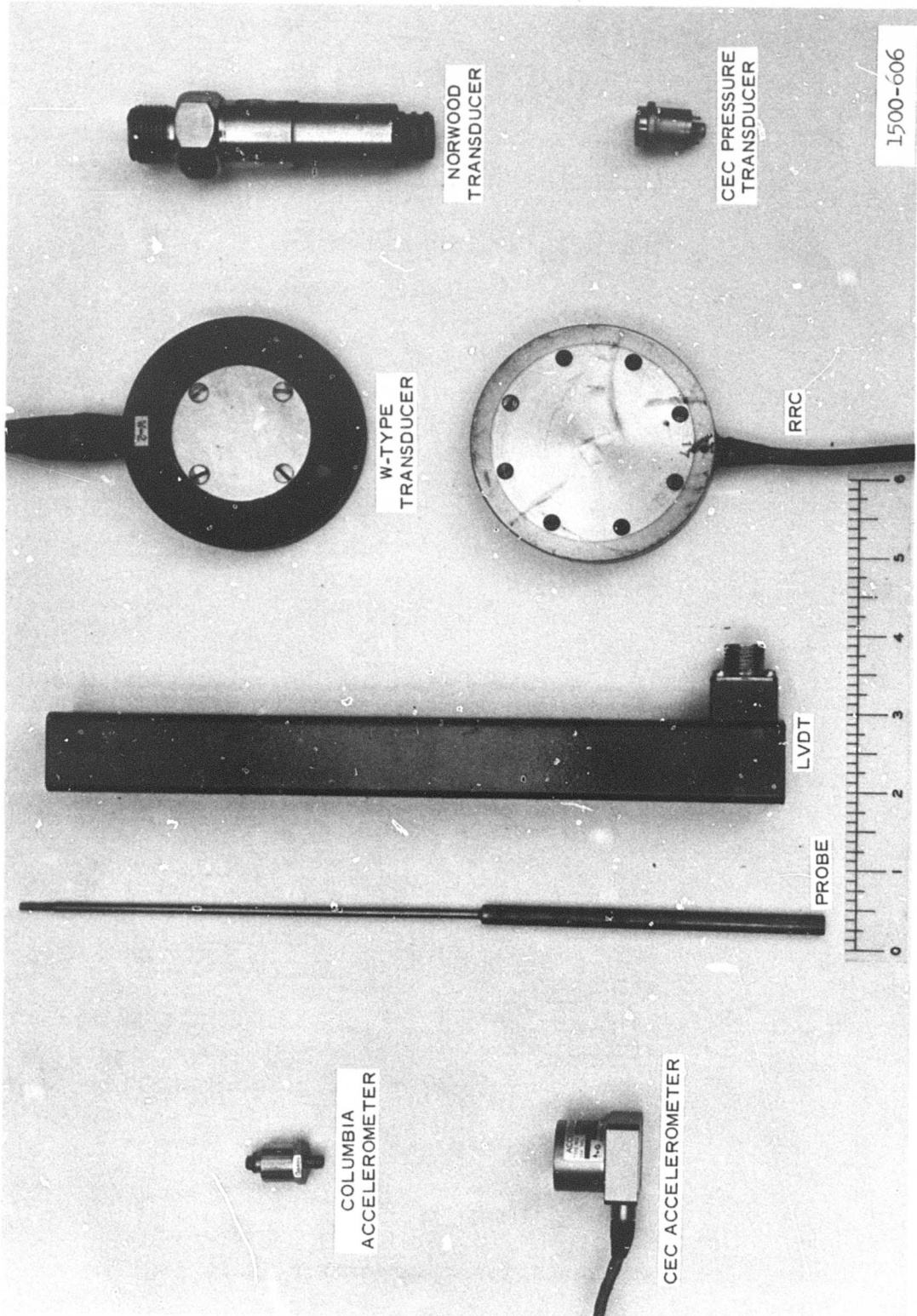
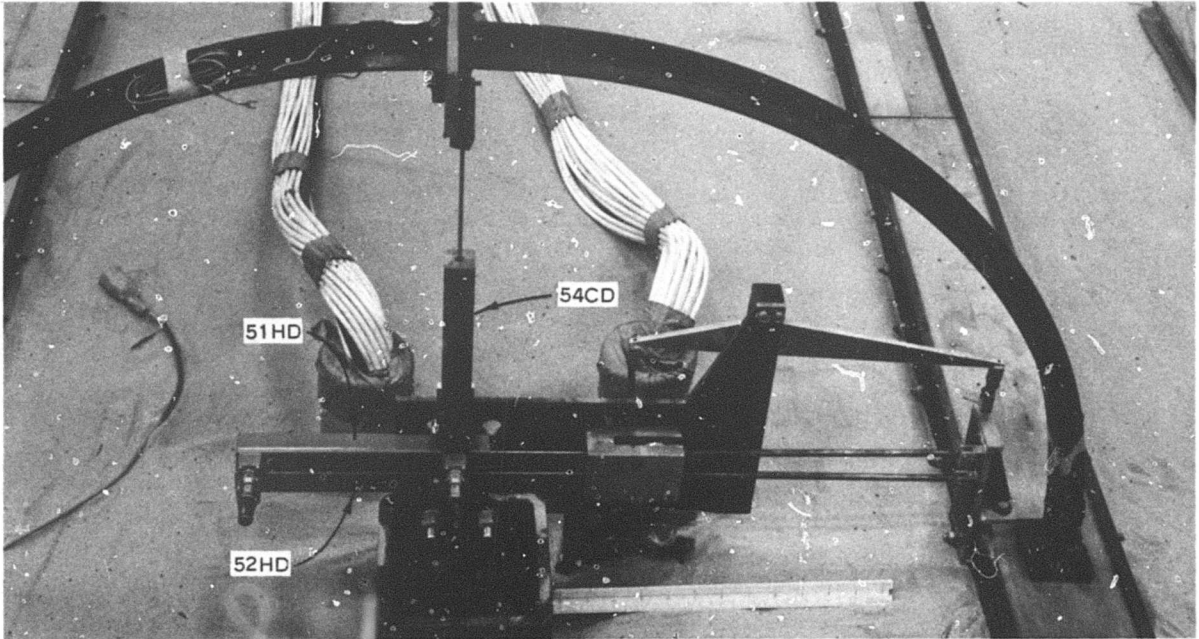
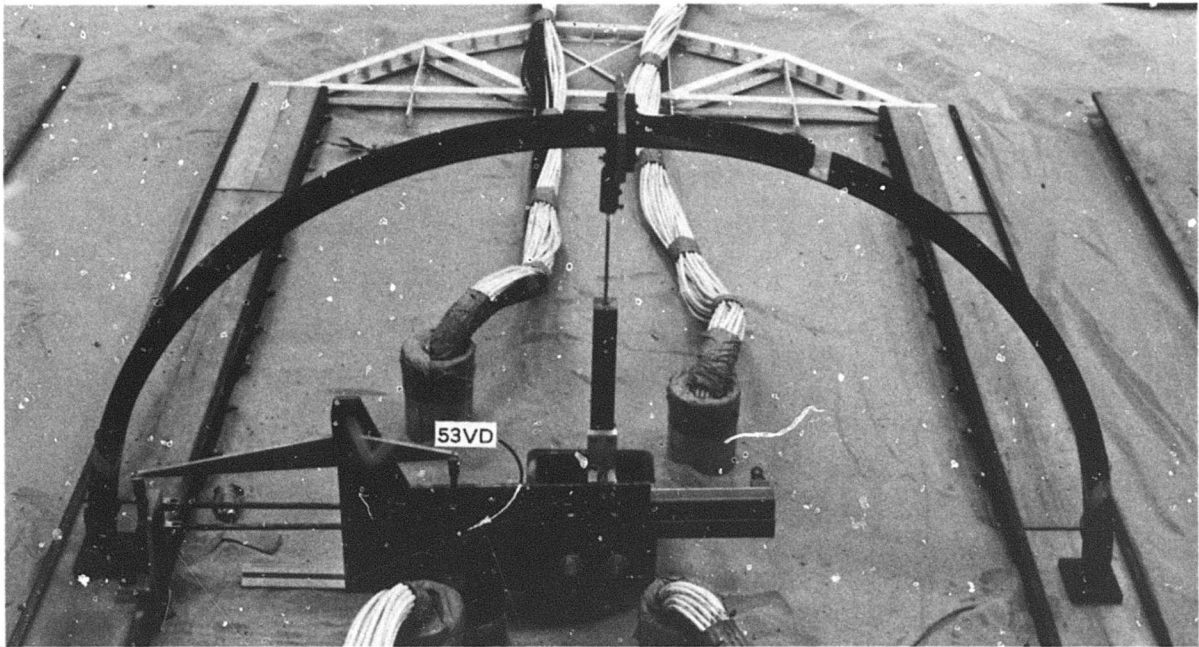


Figure A.3 Transducers used during the test series.



a. East side.



b. West side.

Figure A.4 Footing and crown deflection rig, Preshot 1.

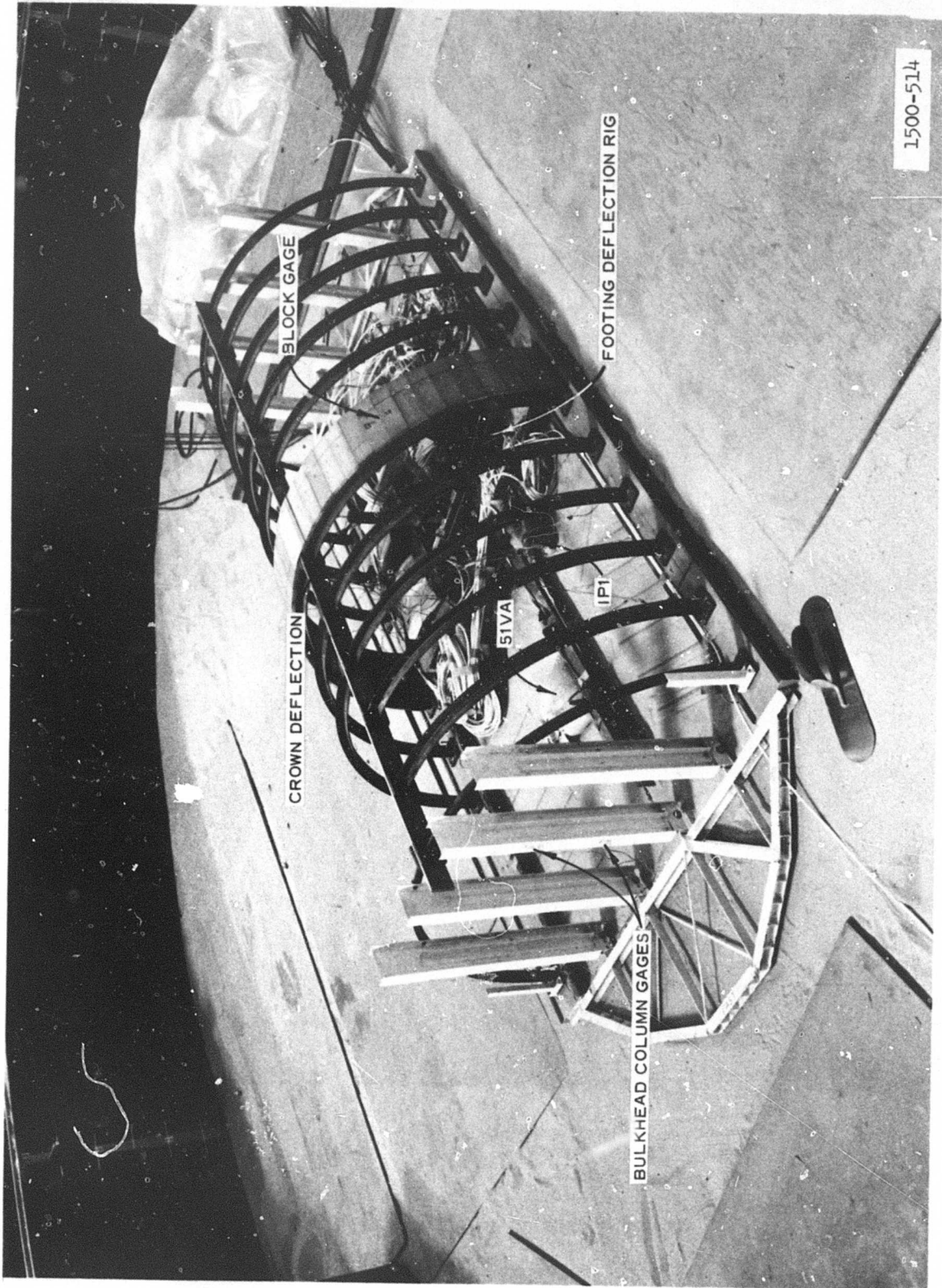
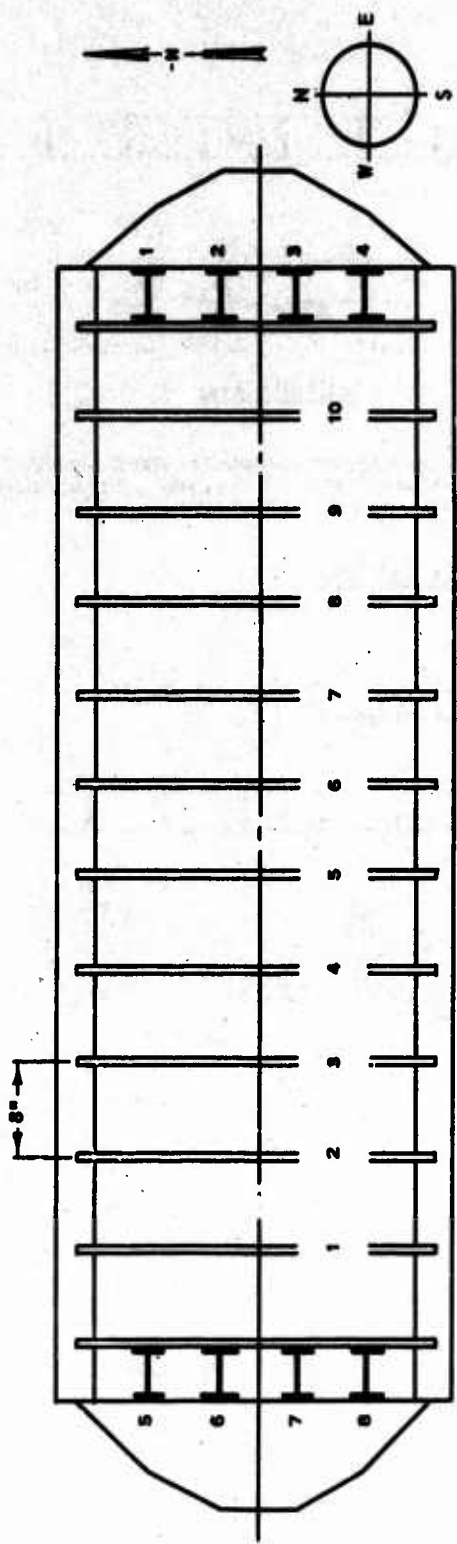


Figure A.5 Fully instrumented structure prior to placing timber lagging, Preshot 3.



RIB AND BEAM NUMBER LOCATIONS

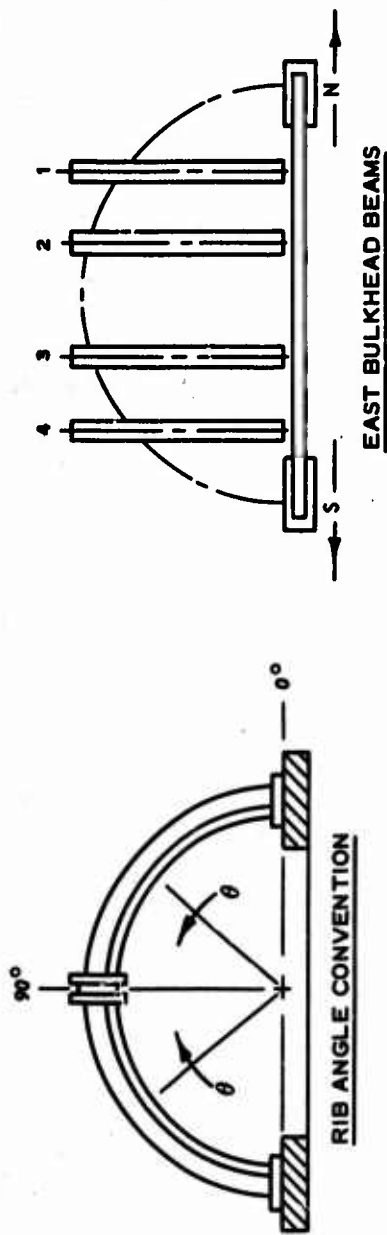
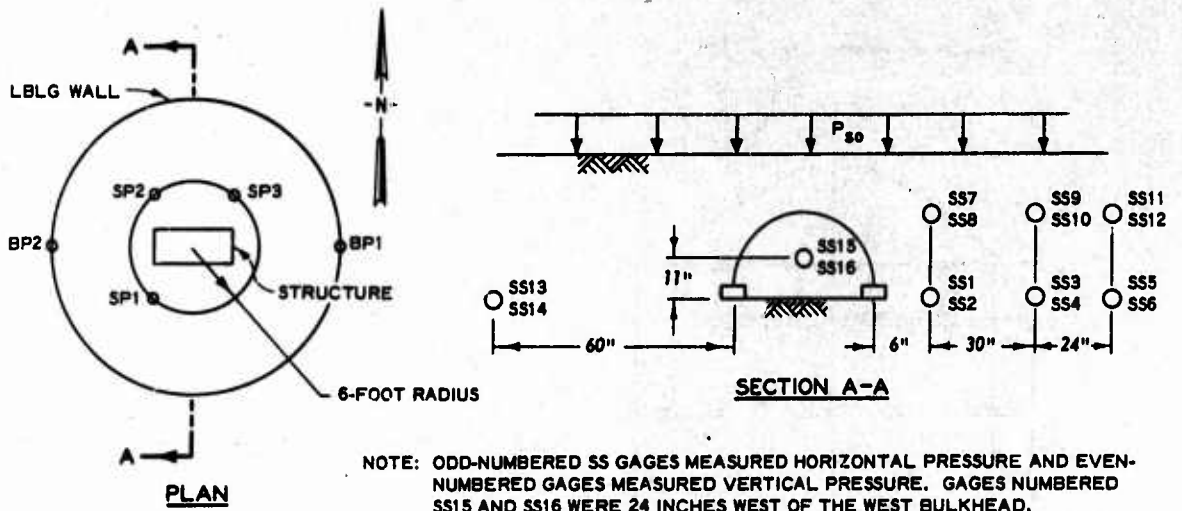
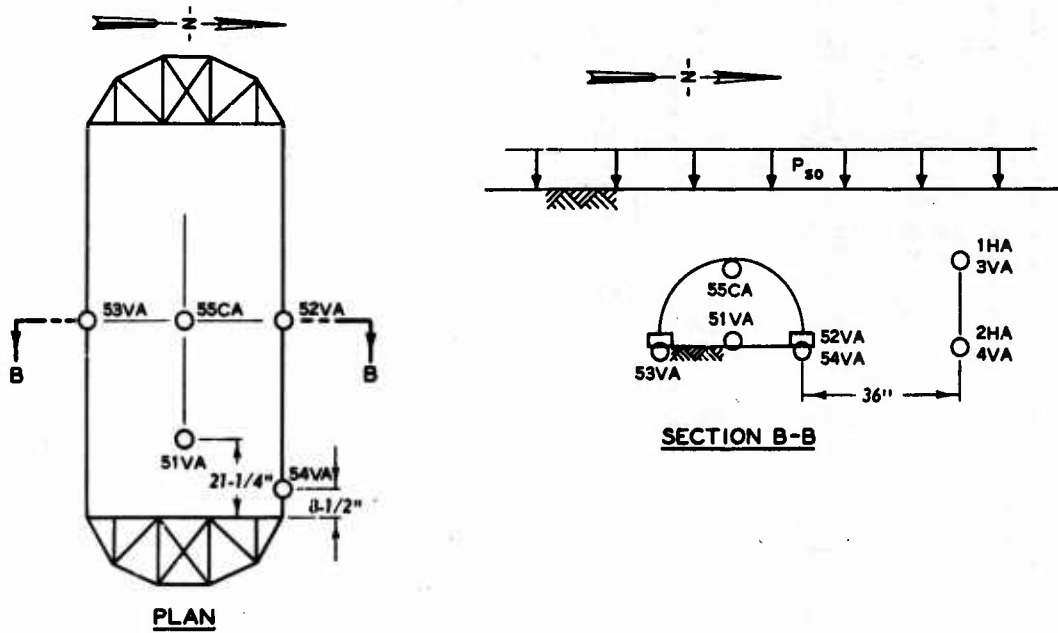


Figure A.6 Numbering convention.



**PRESSURE GAGE LOCATIONS**



**ACCELEROMETER LOCATIONS**

Figure A.7 Free-field and motion gage locations.

**APPENDIX B**

**RAW DATA**

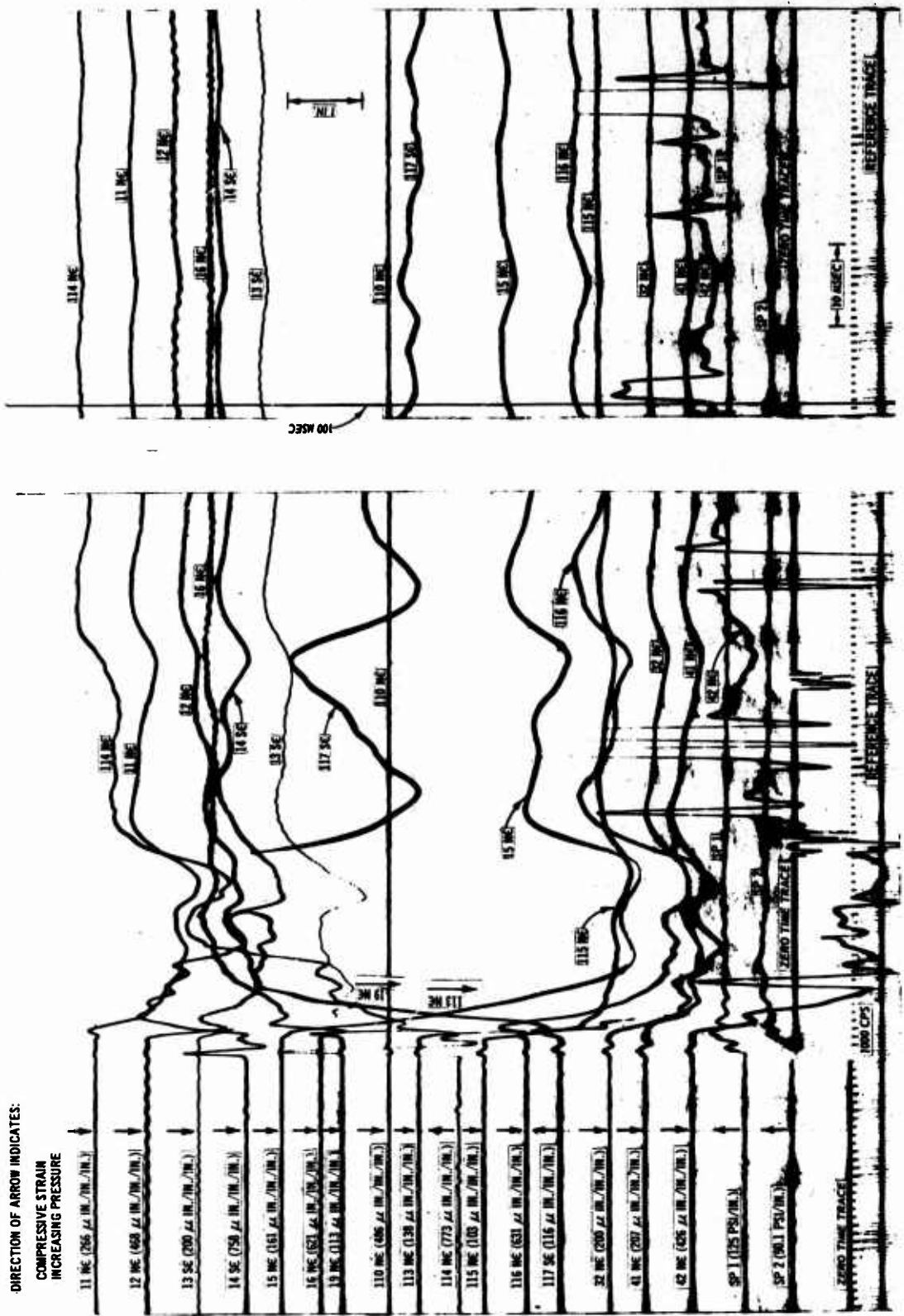


Figure B.1 Shot 1, oscillograph record from Recorder 1.

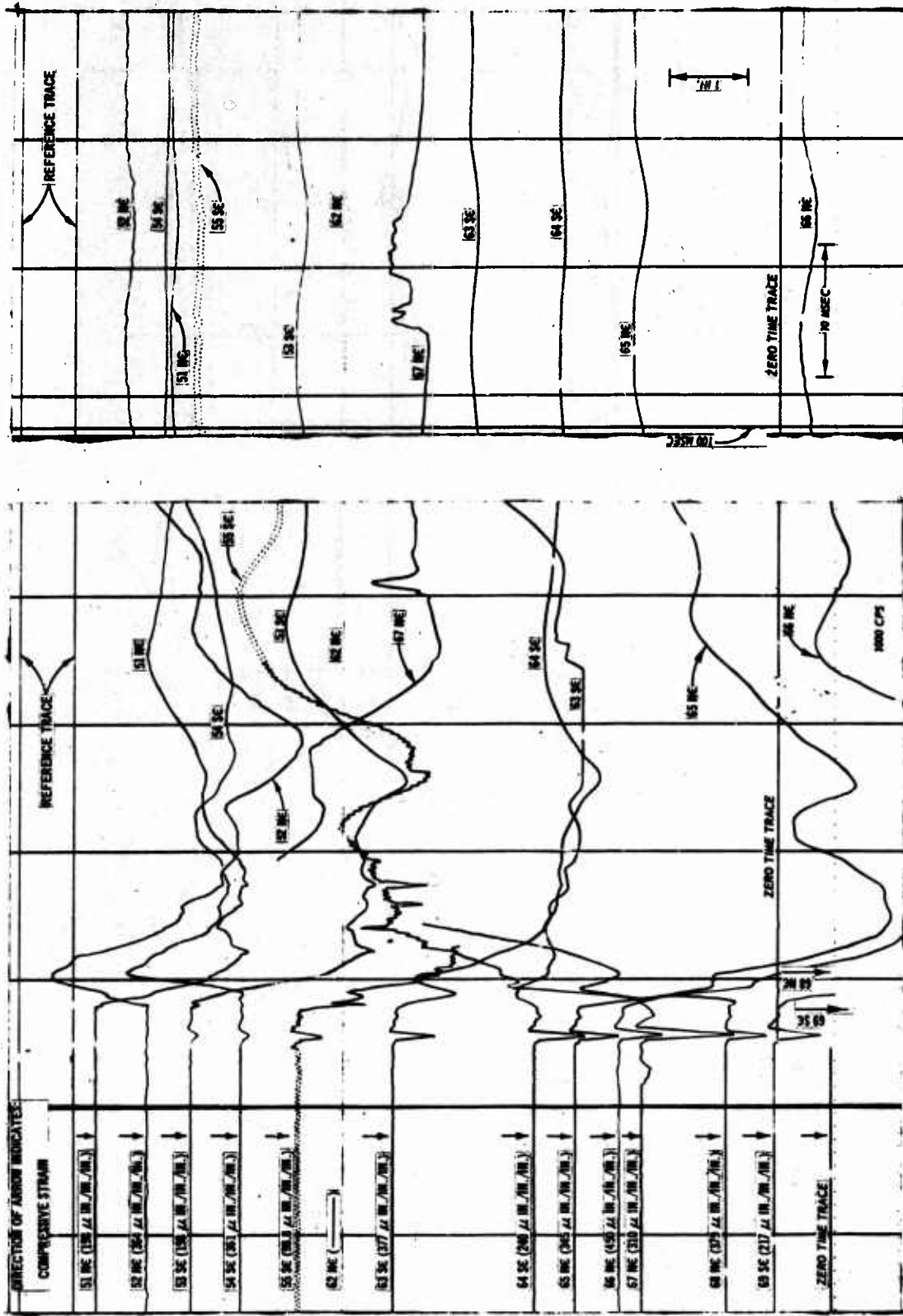


Figure B.2 Shot 1, oscillograph record from Recorder 2.

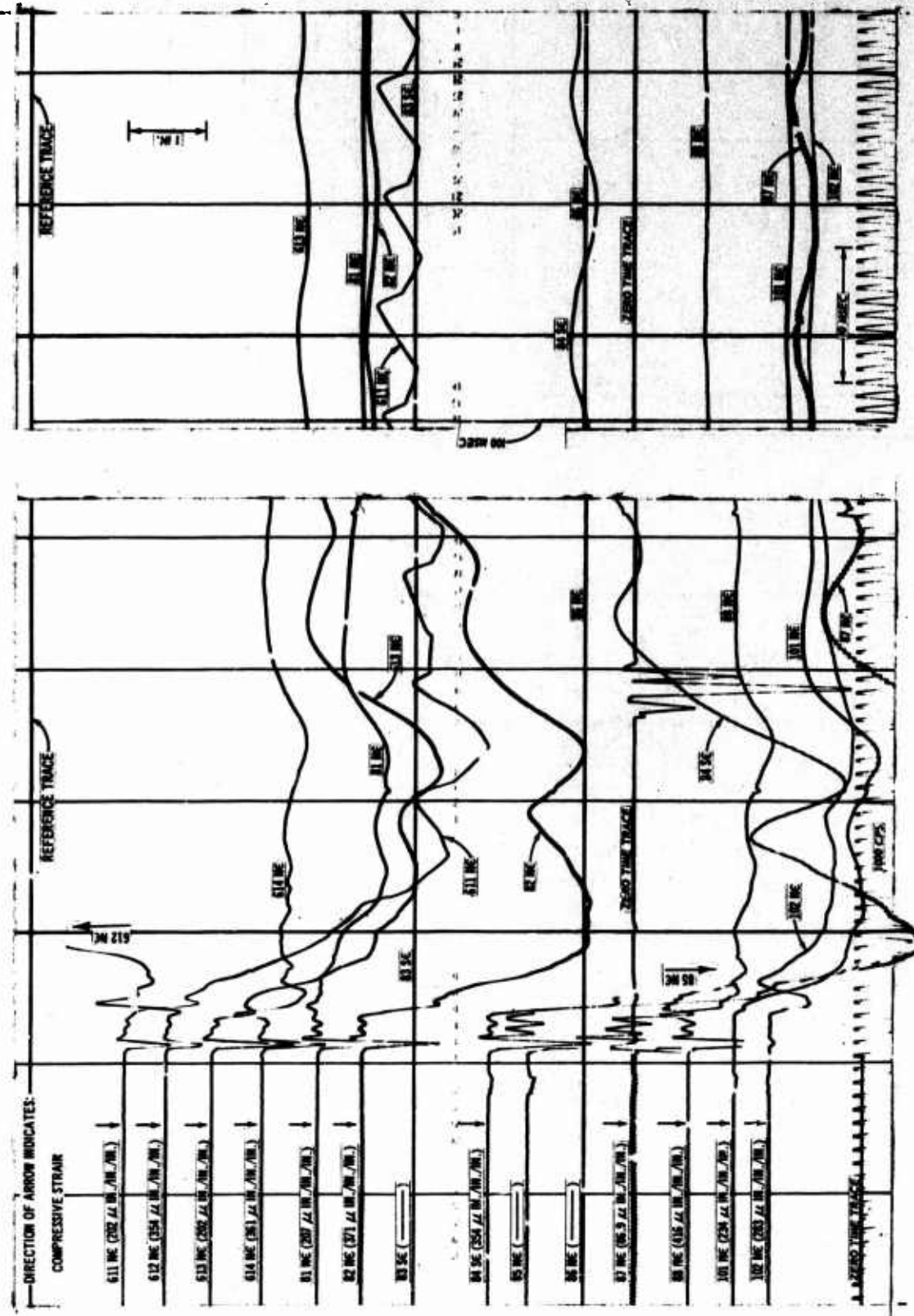


Figure B.3 Shot 1, oscillograph record from Recorder 3.

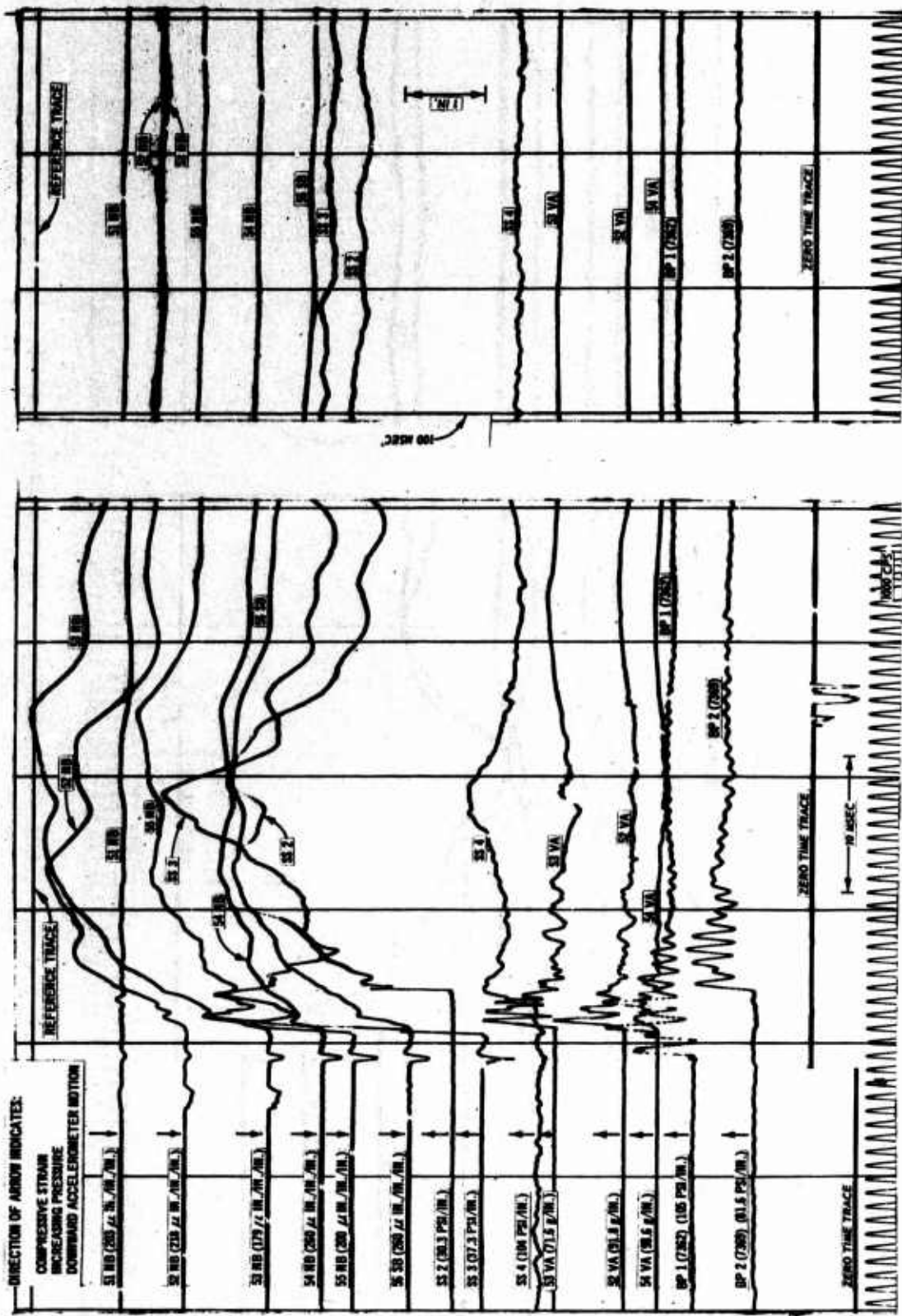


Figure B.4 Shot 1, oscillograph record from Recorder 4.

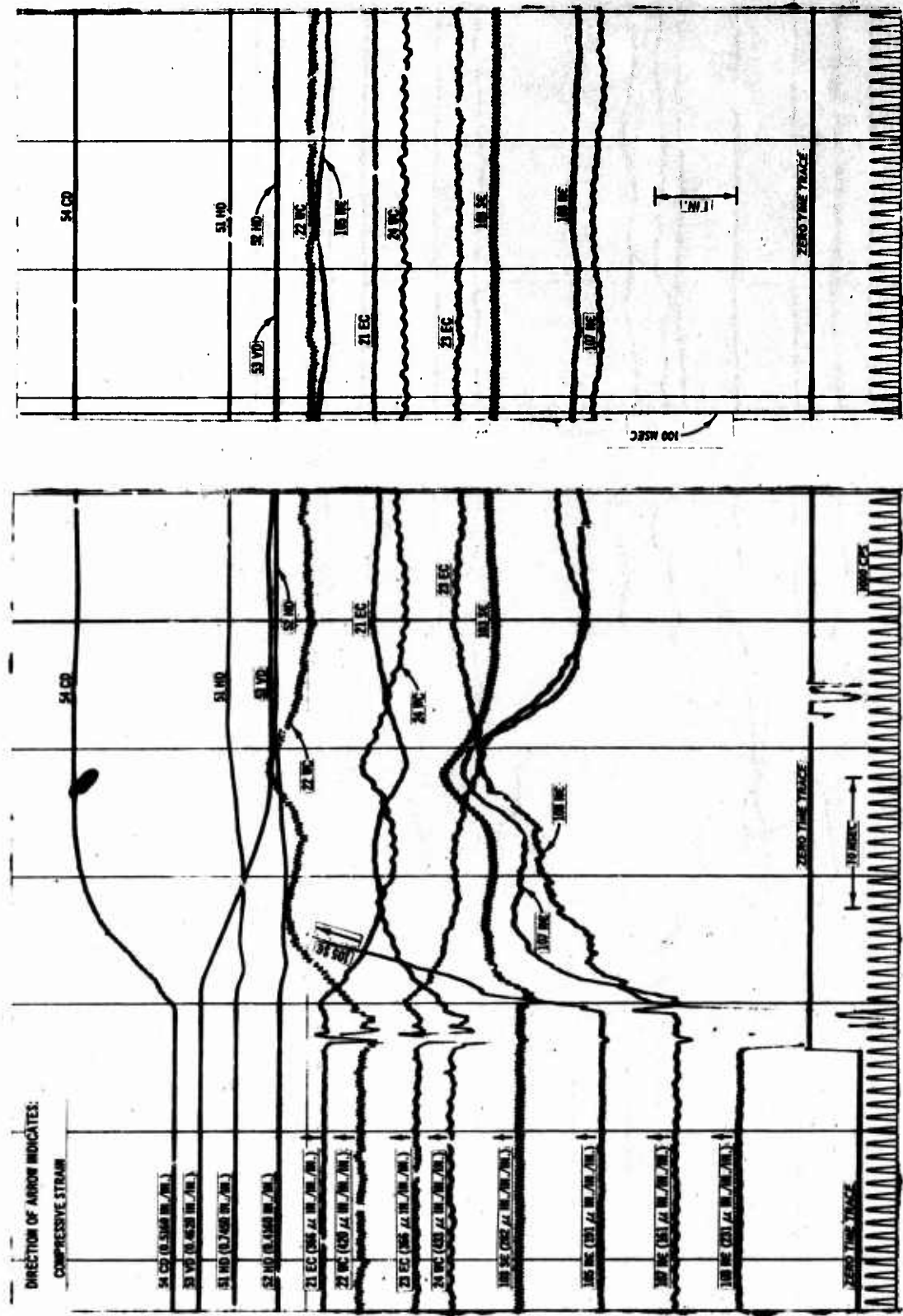


Figure B.5 Shot 1, oscillograph record from Recorder 5.

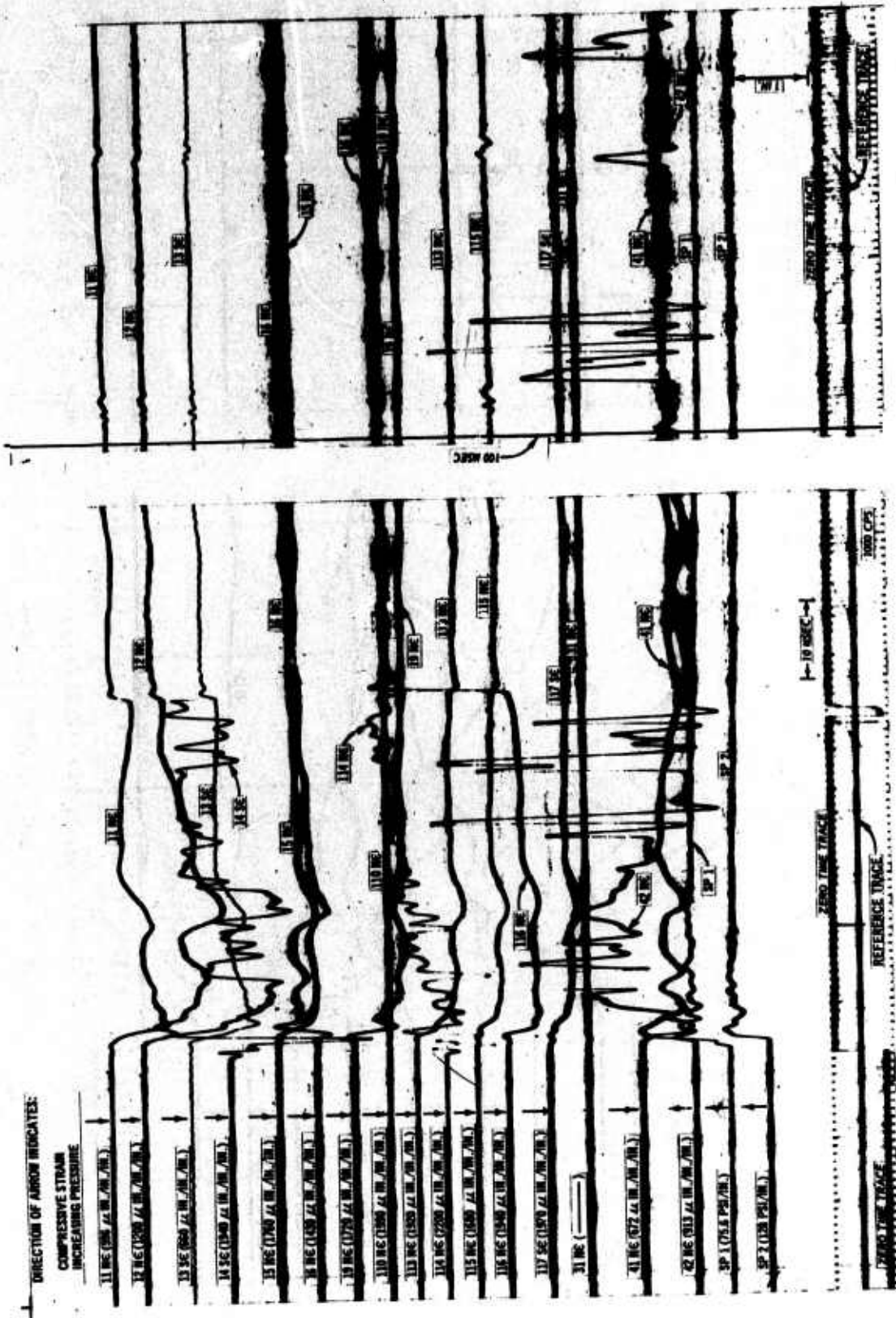


Figure B.6 Shot 2, oscillograph record from Recorder 1.

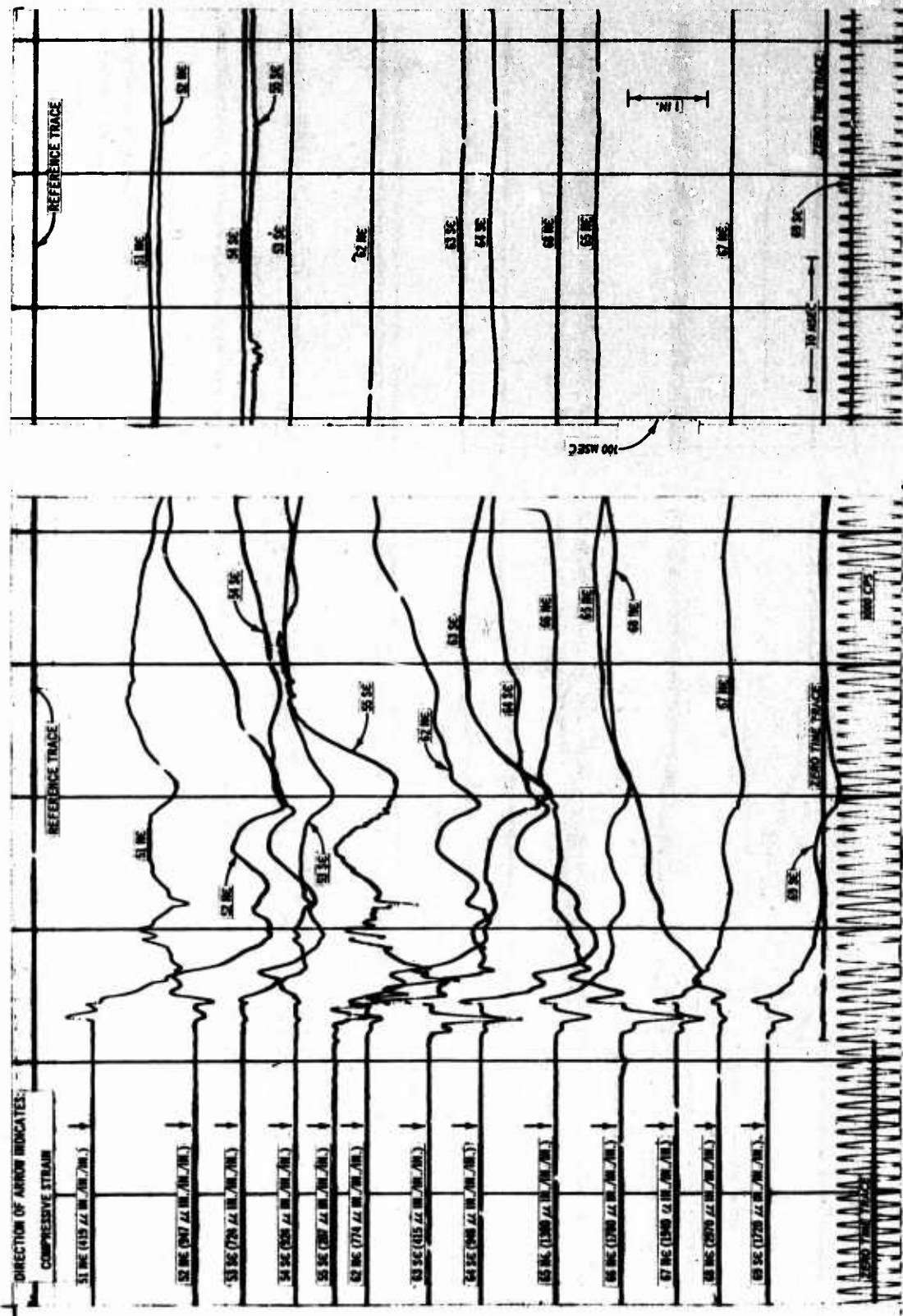


Figure B.7 Shot 2, oscillograph record from Recorder 2.

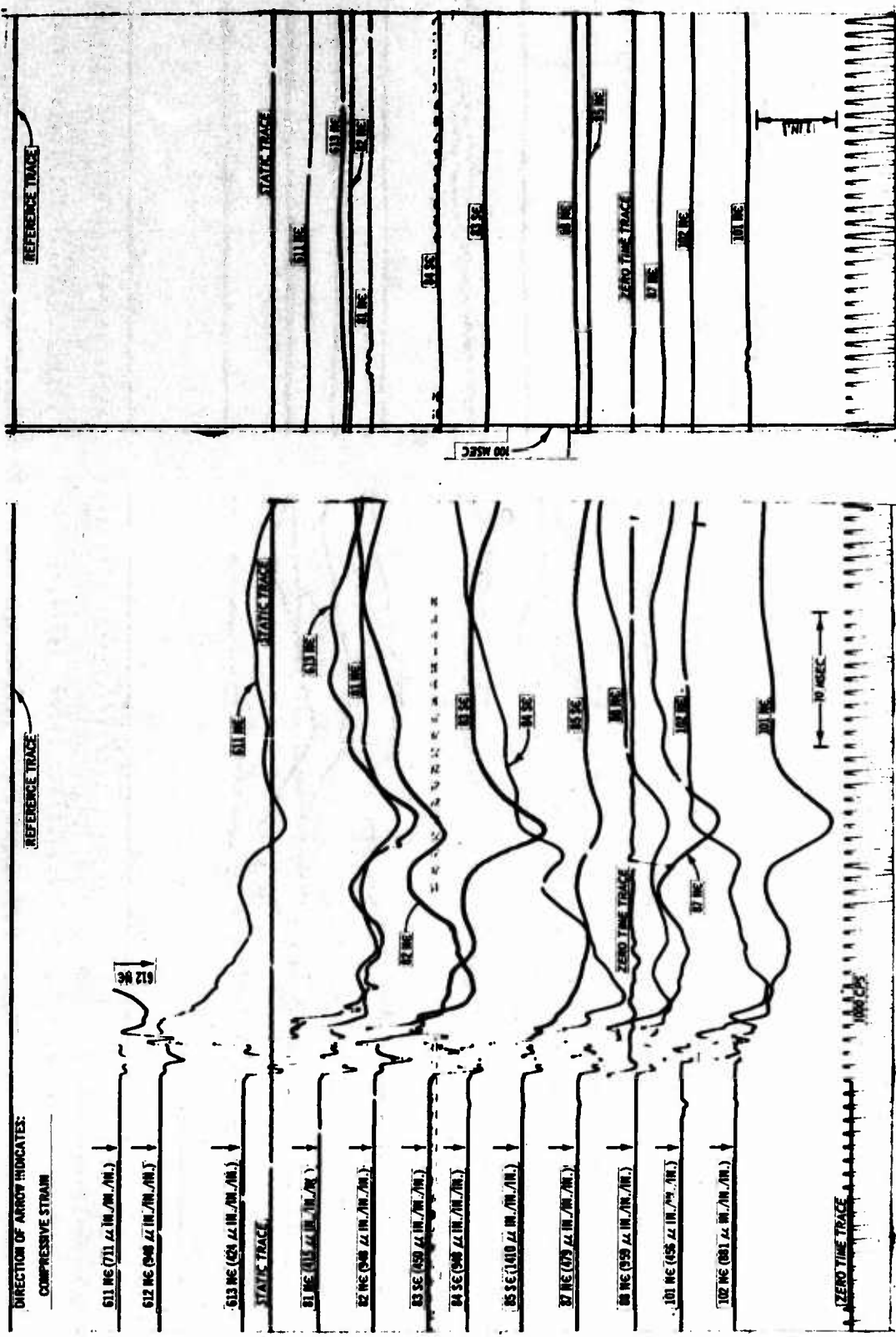


Figure B.8 Shot 2, oscillograph record from Recorder 3.

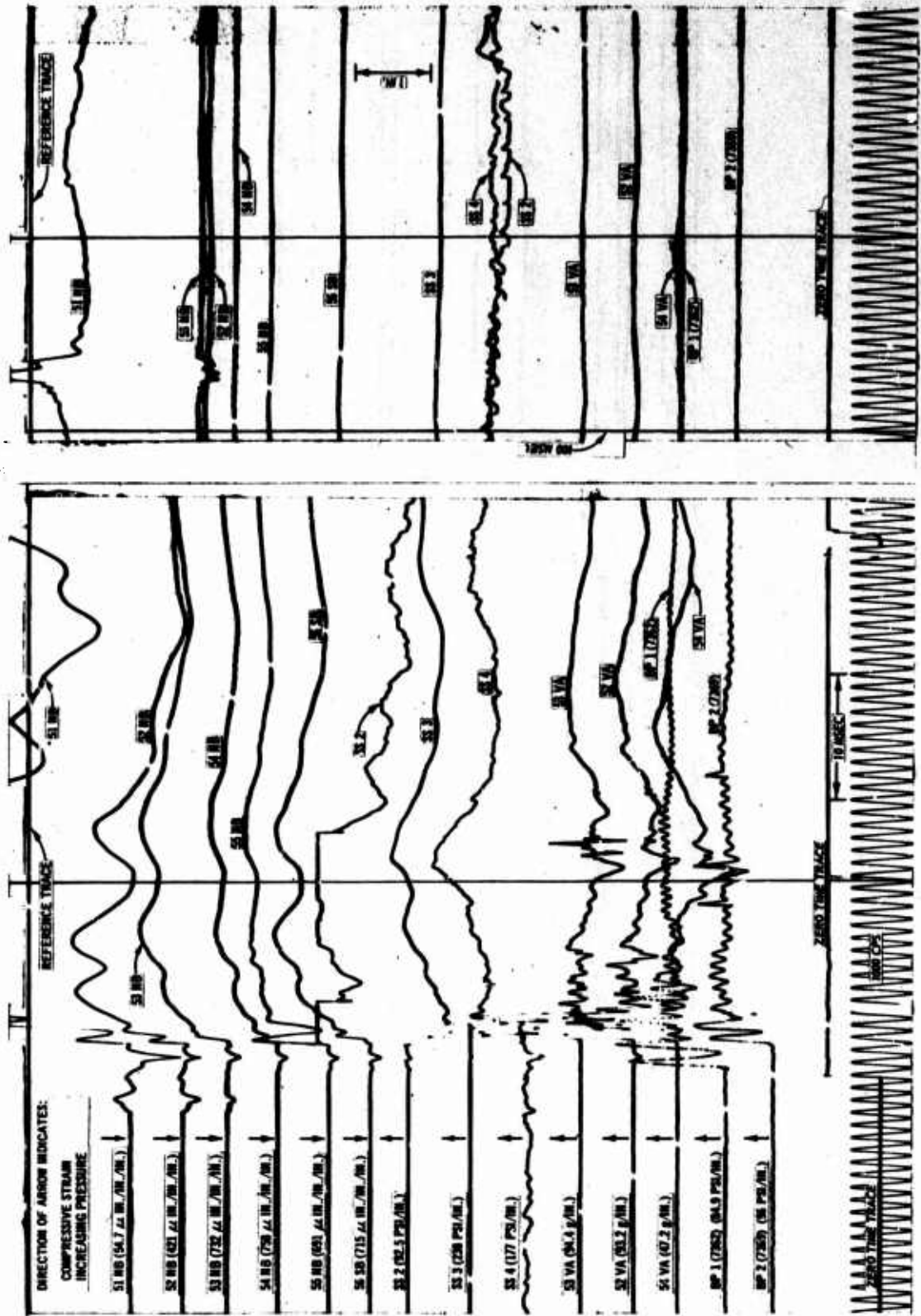


Figure B.9 Shot 2, oscillograph record from Recorder 4.

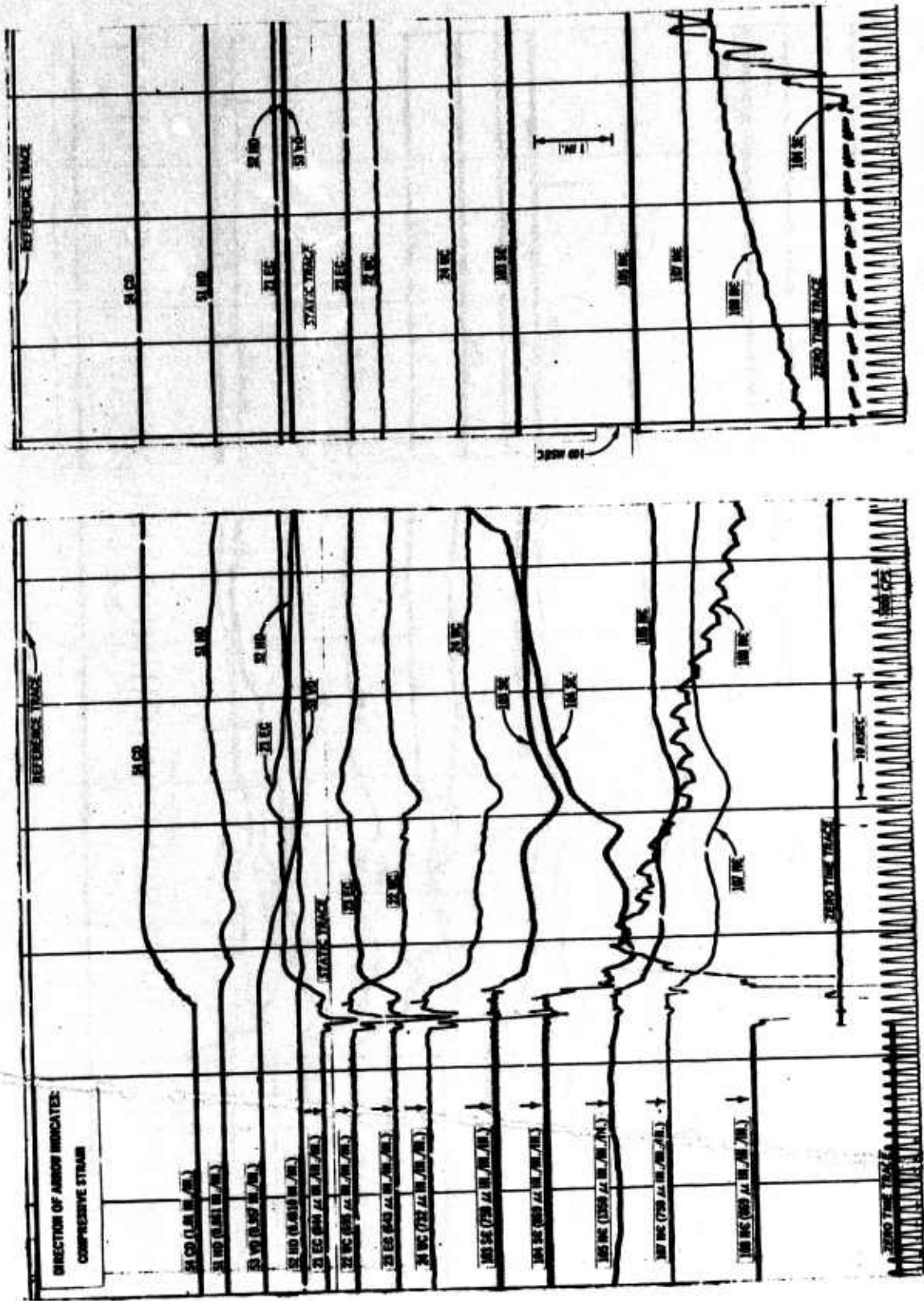


Figure B.10 Shot 2, oscillograph record from Recorder 5.

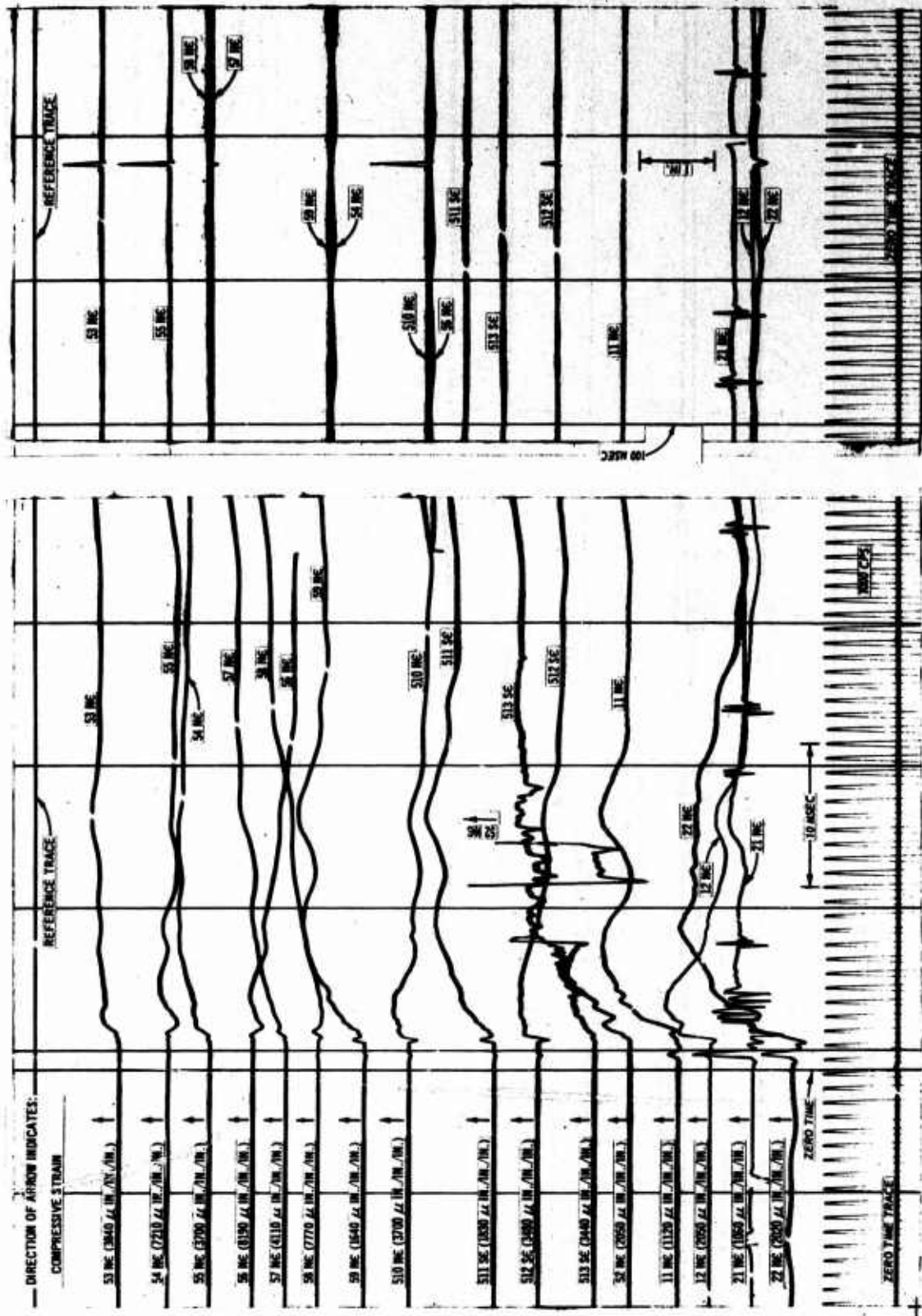


Figure B.11 Shot 3, oscillograph record from Recorder 1.

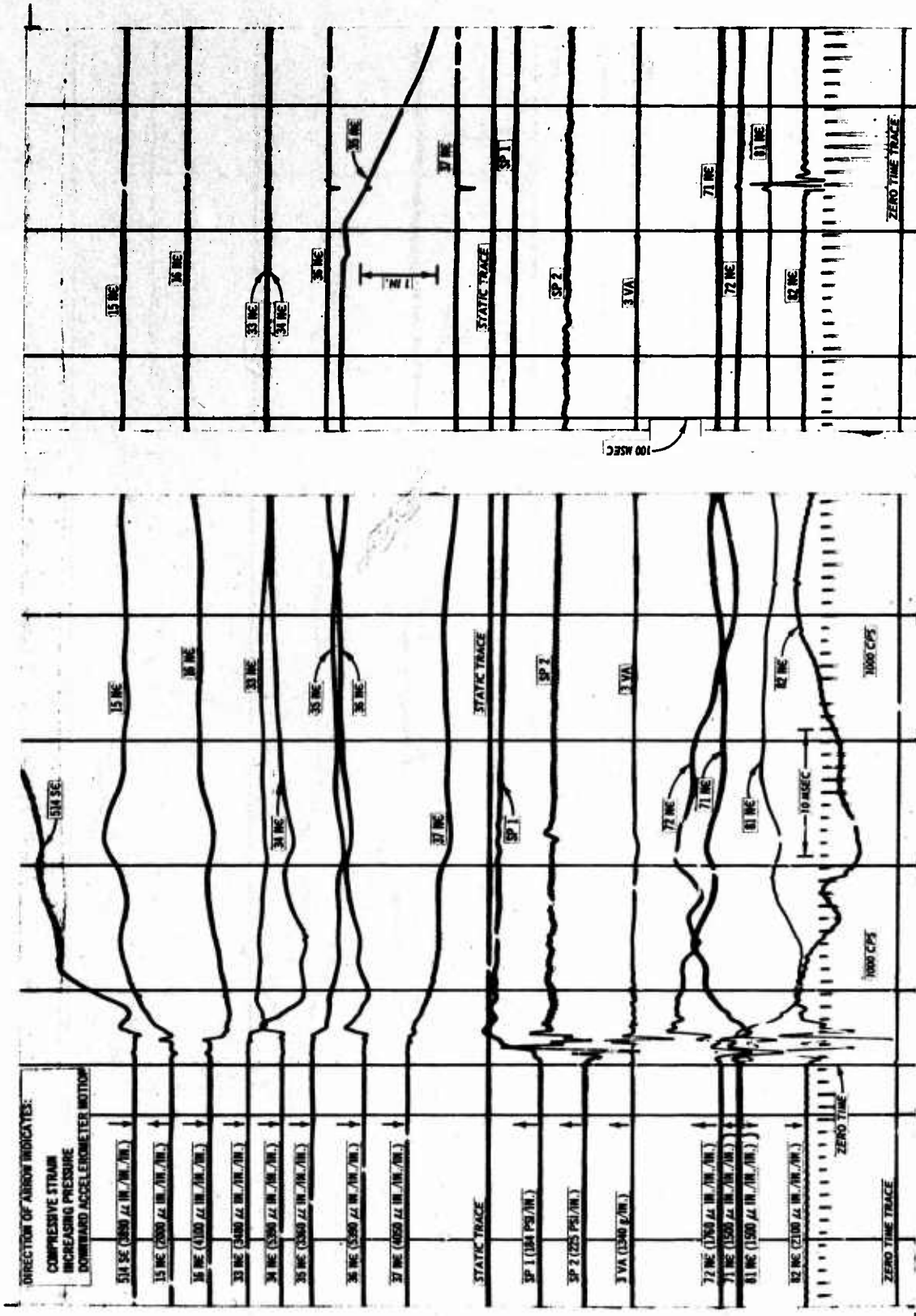


Figure B.12 Shot 3, oscillograph record from Recorder 2.

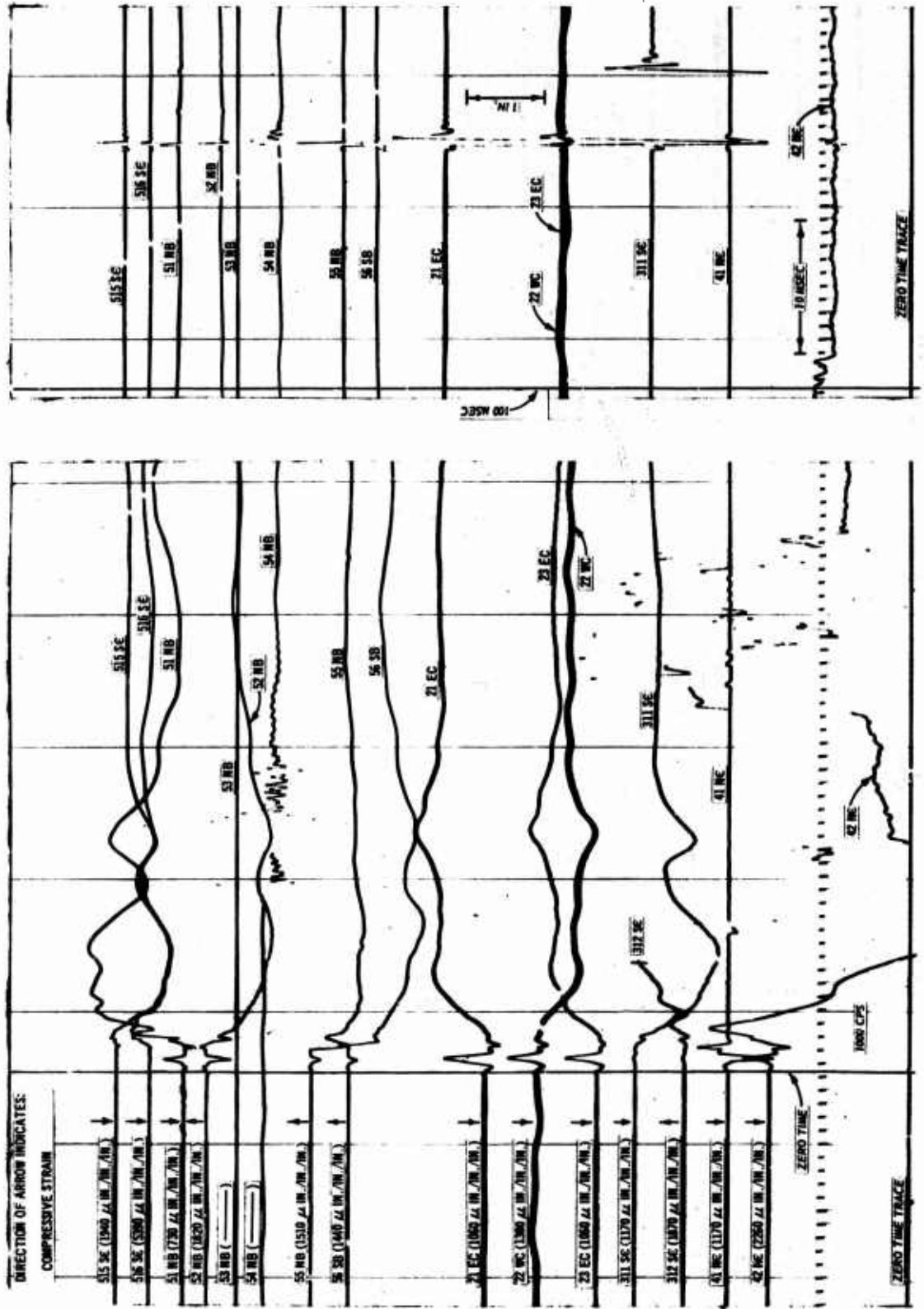


Figure B.13 Shot 3, oscillograph record from Recorder 3.

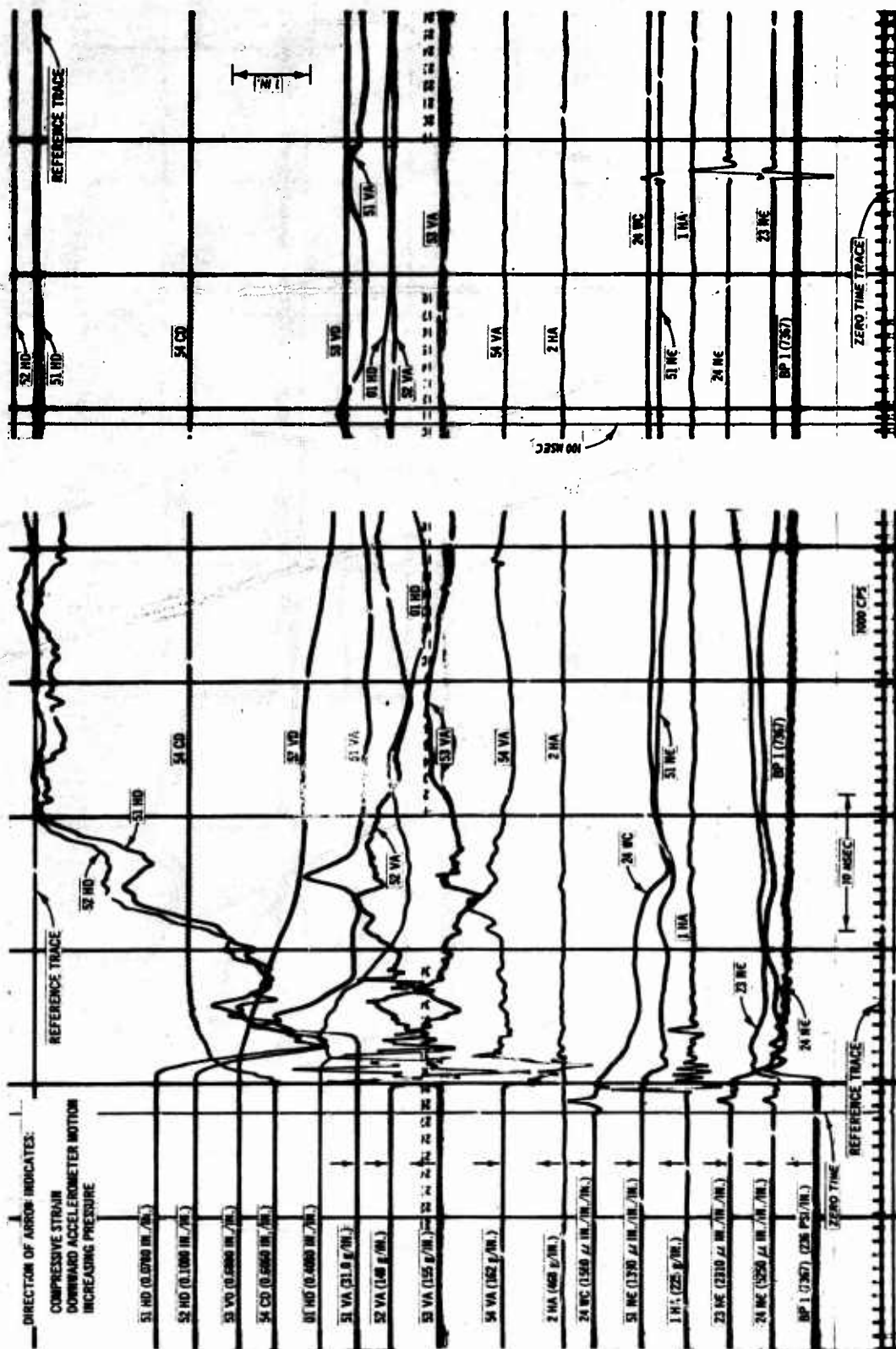


Figure B.14 Shot 3, oscillograph record from Recorder 4.

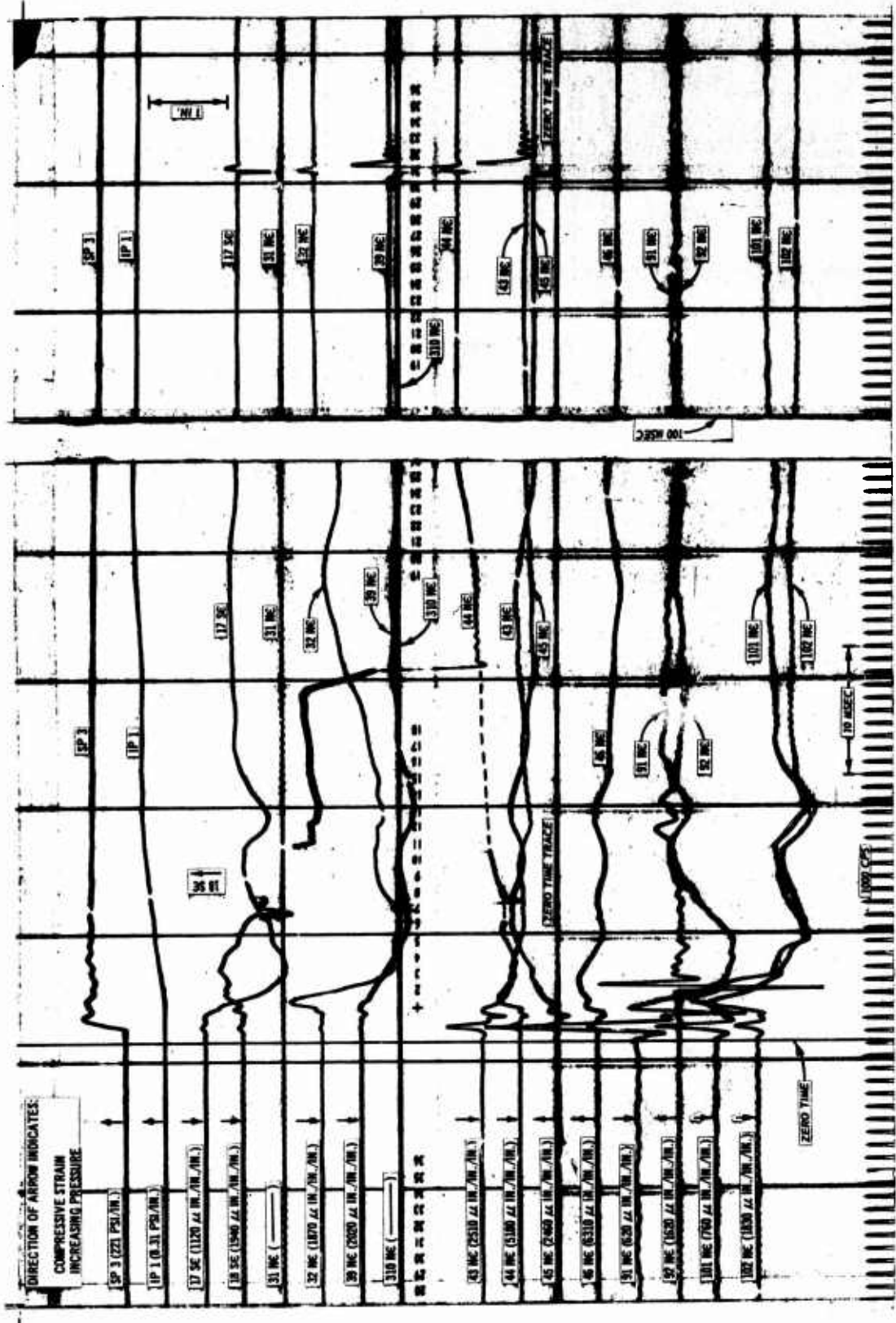


Figure B.15 Shot 3, oscillograph record from Recorder 5.

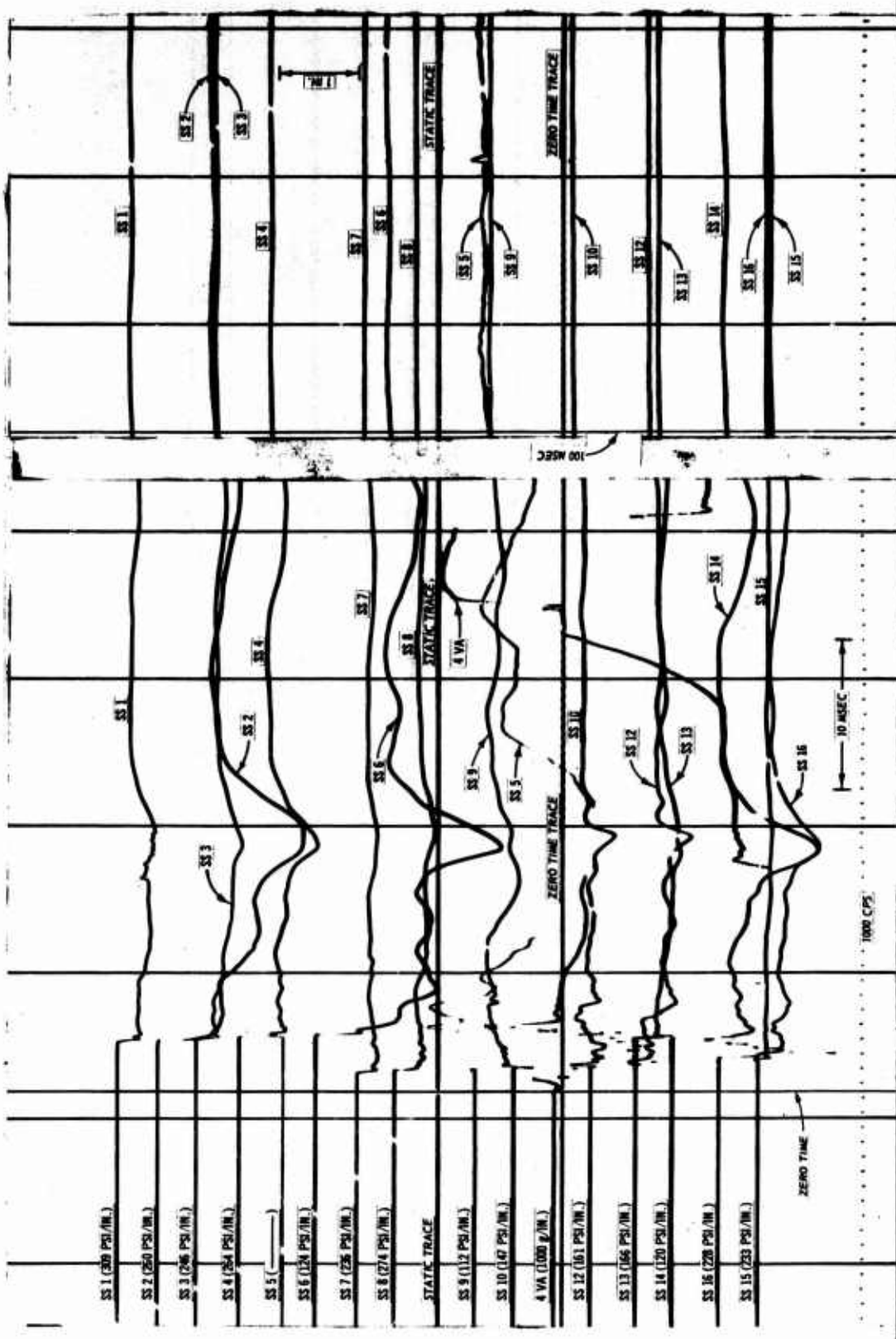


Figure B.16 Shot 3, oscillograph record from Recorder 6.

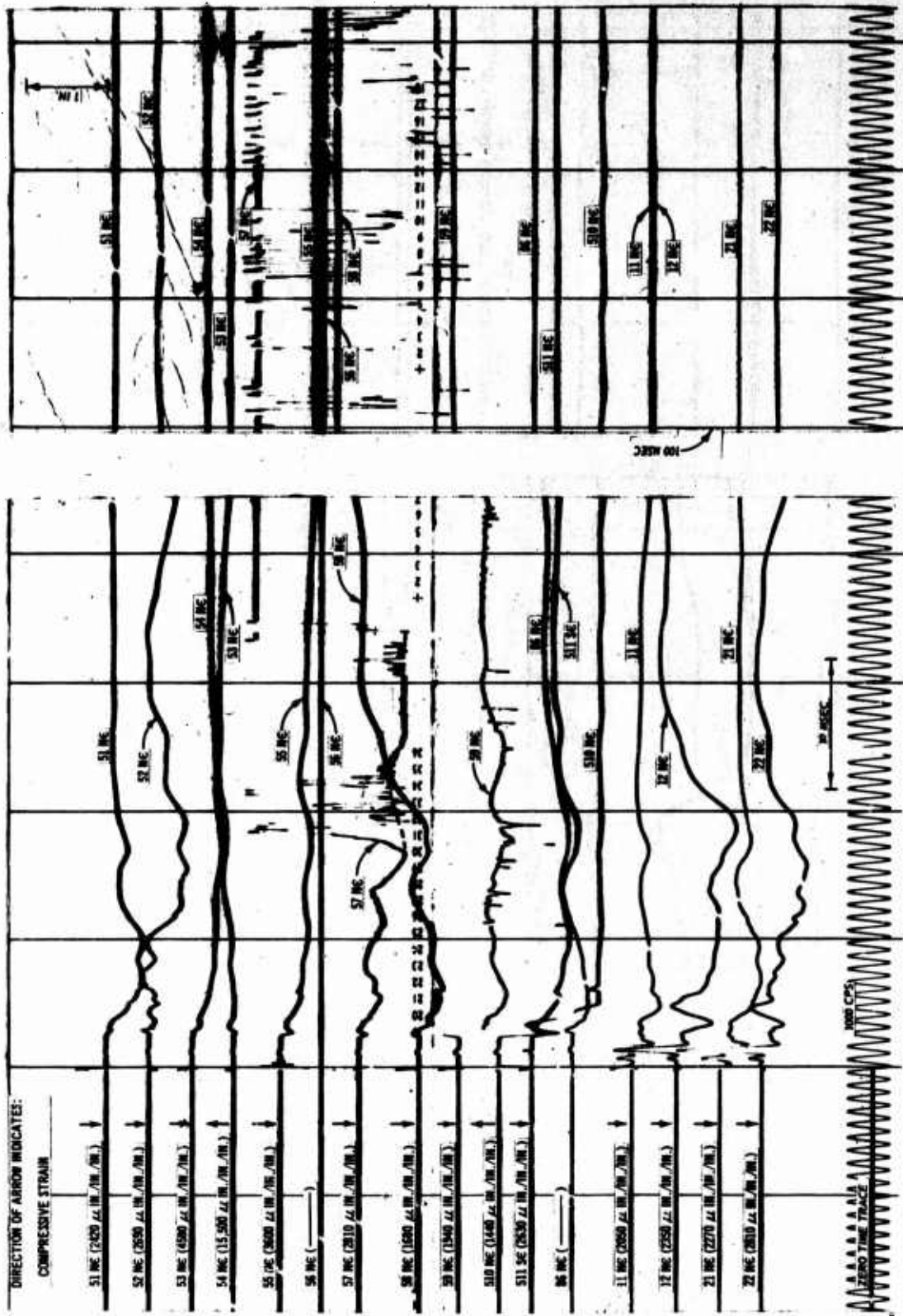


Figure B.17 Shot 4, oscillograph record from Recorder 1.

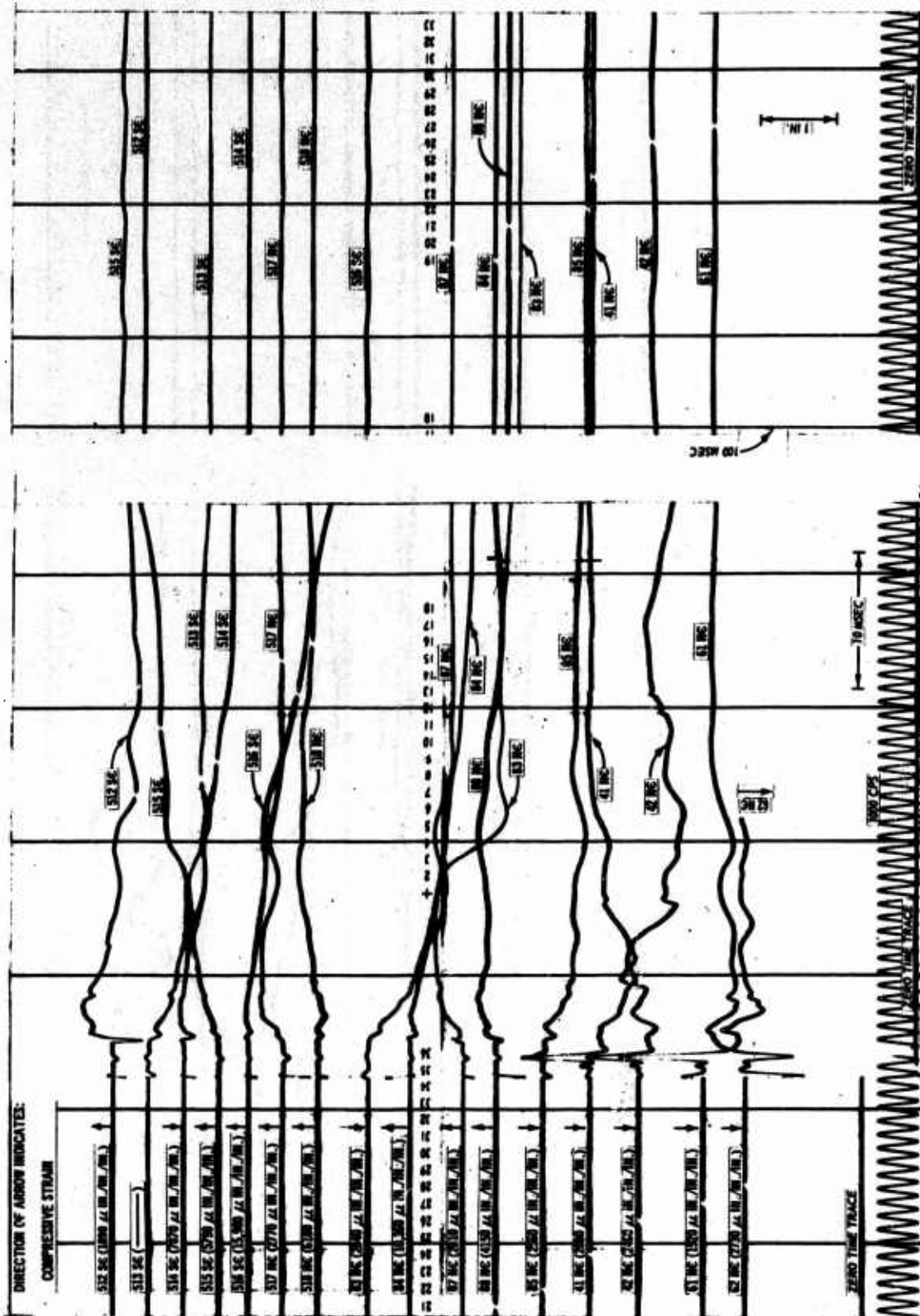


Figure B.18 Shot 4, oscillograph record from Recorder 2.

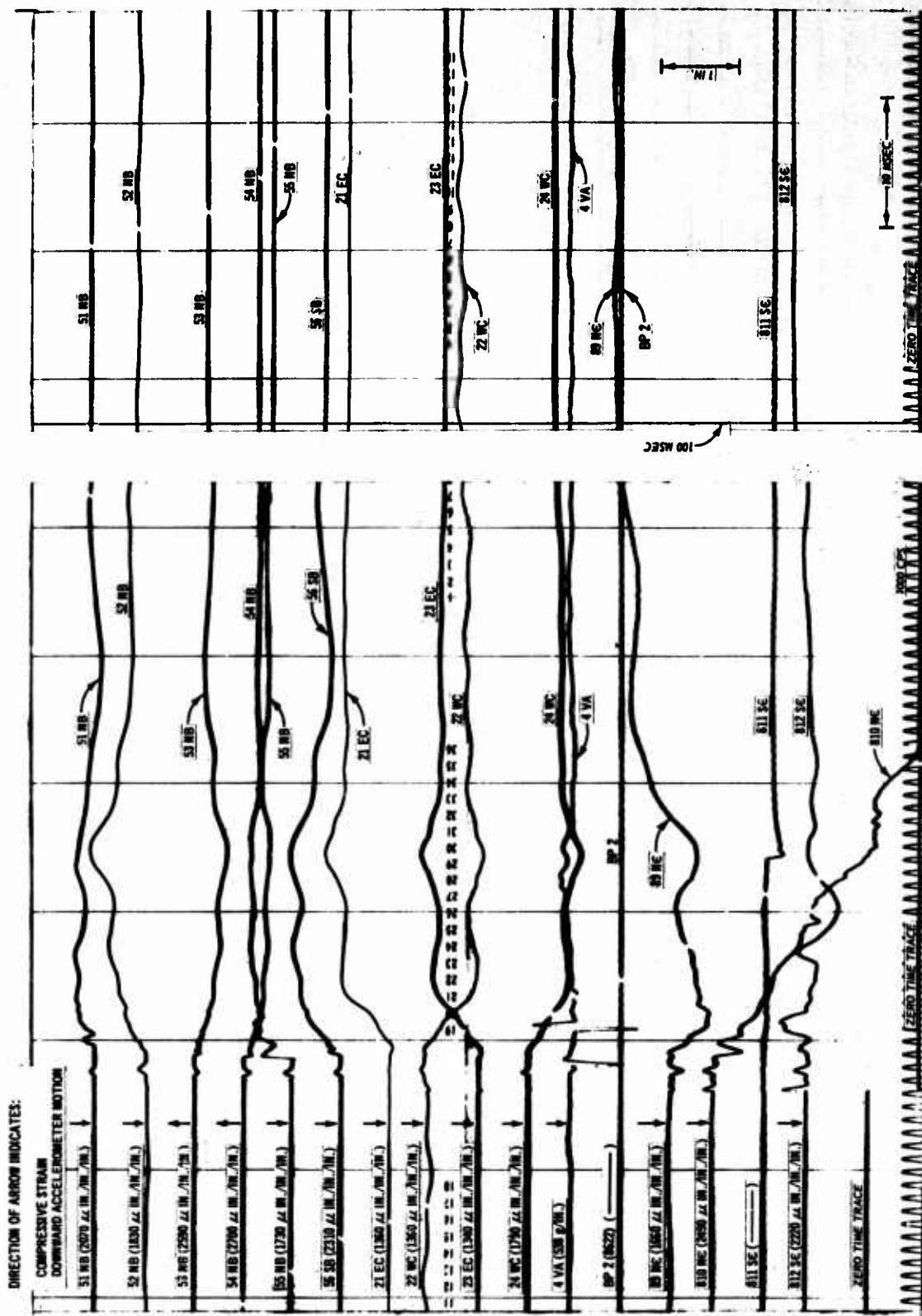


Figure B.19 Shot 4, oscillograph record from Recorder 3.

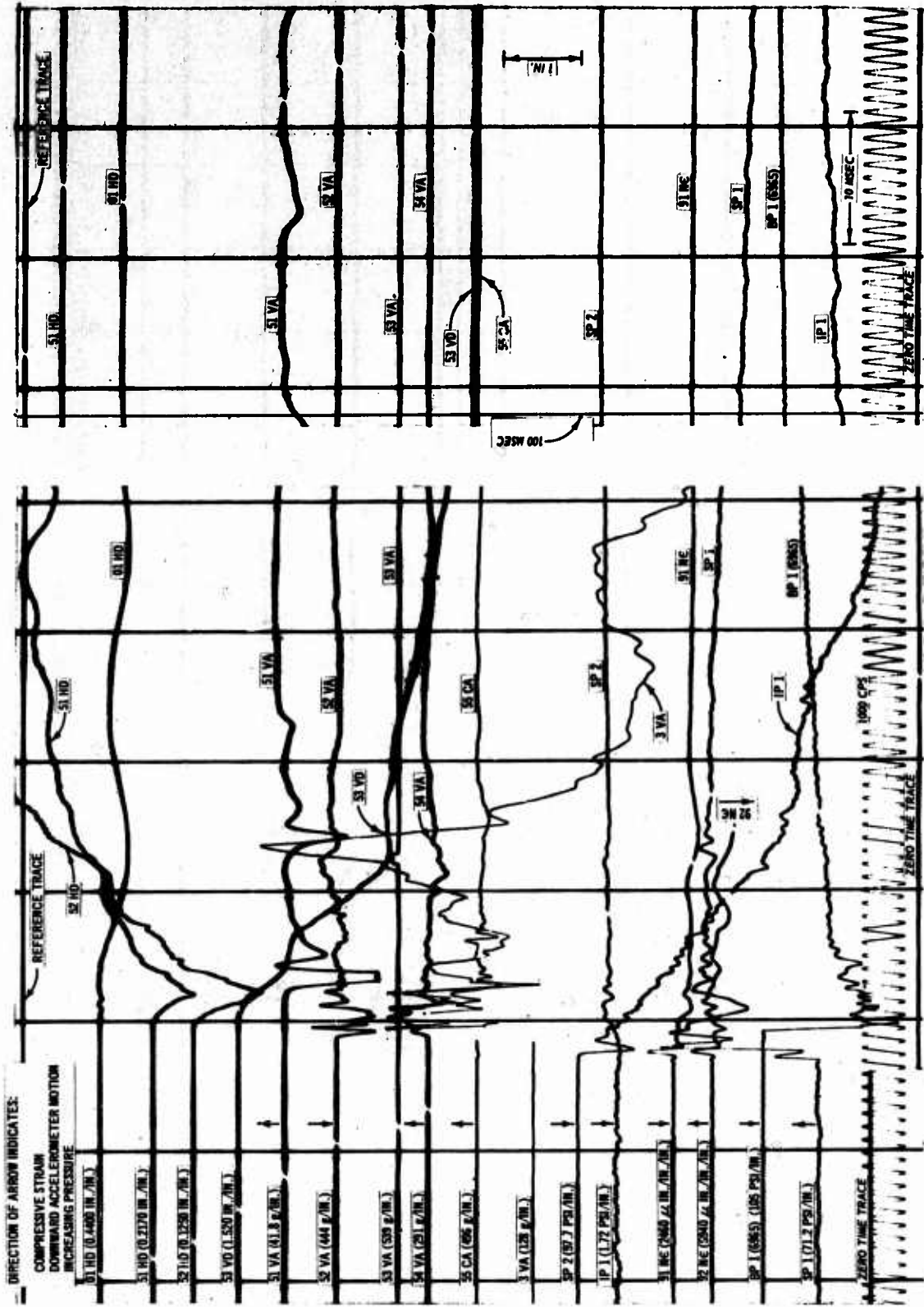


Figure B.20 Shot 4, oscillograph record from Recorder 4.

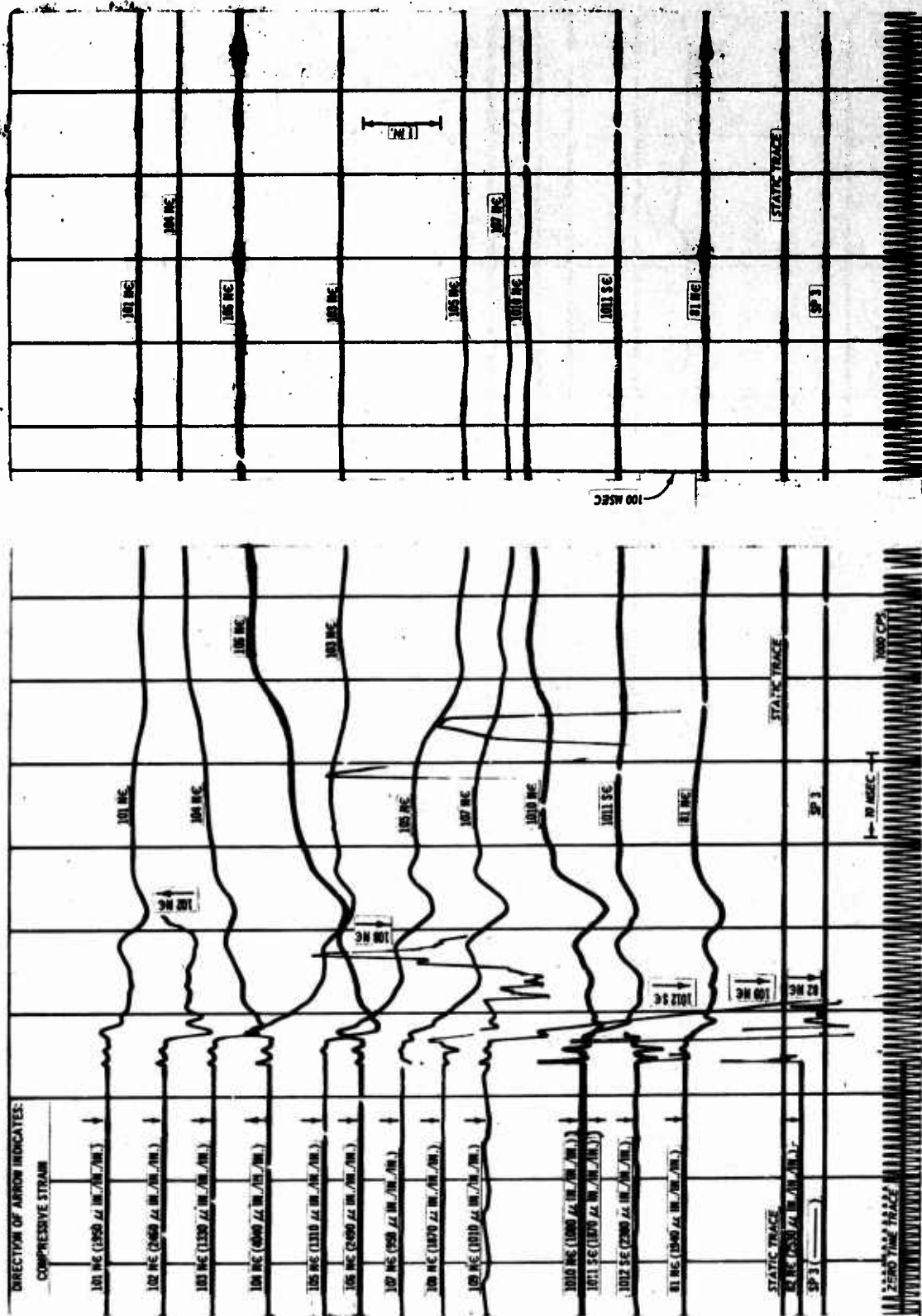


Figure B.21 Shot 4, oscillograph record from Recorder 5.

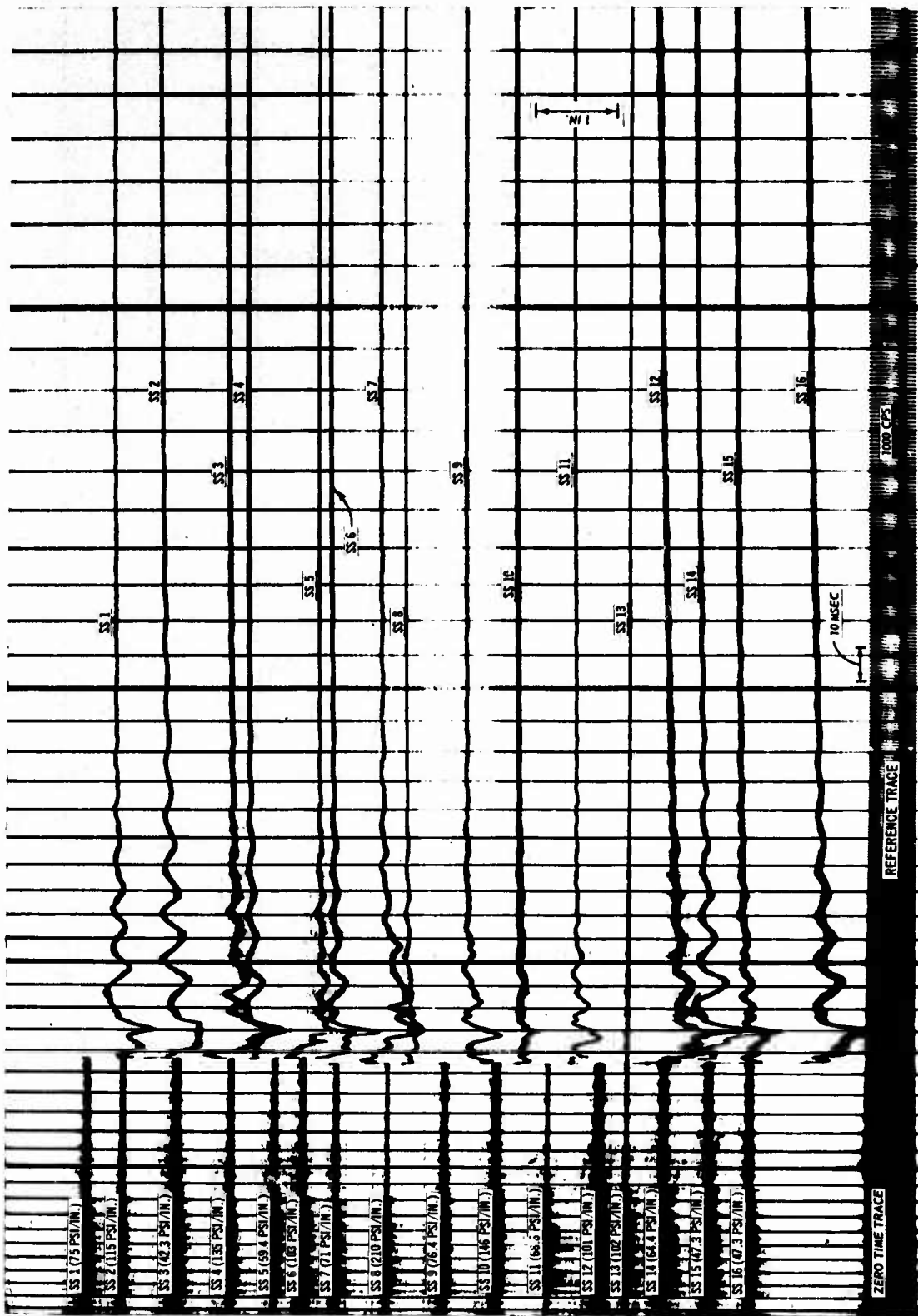


Figure B.22 Shot 4, oscillograph record from Recorder 6.

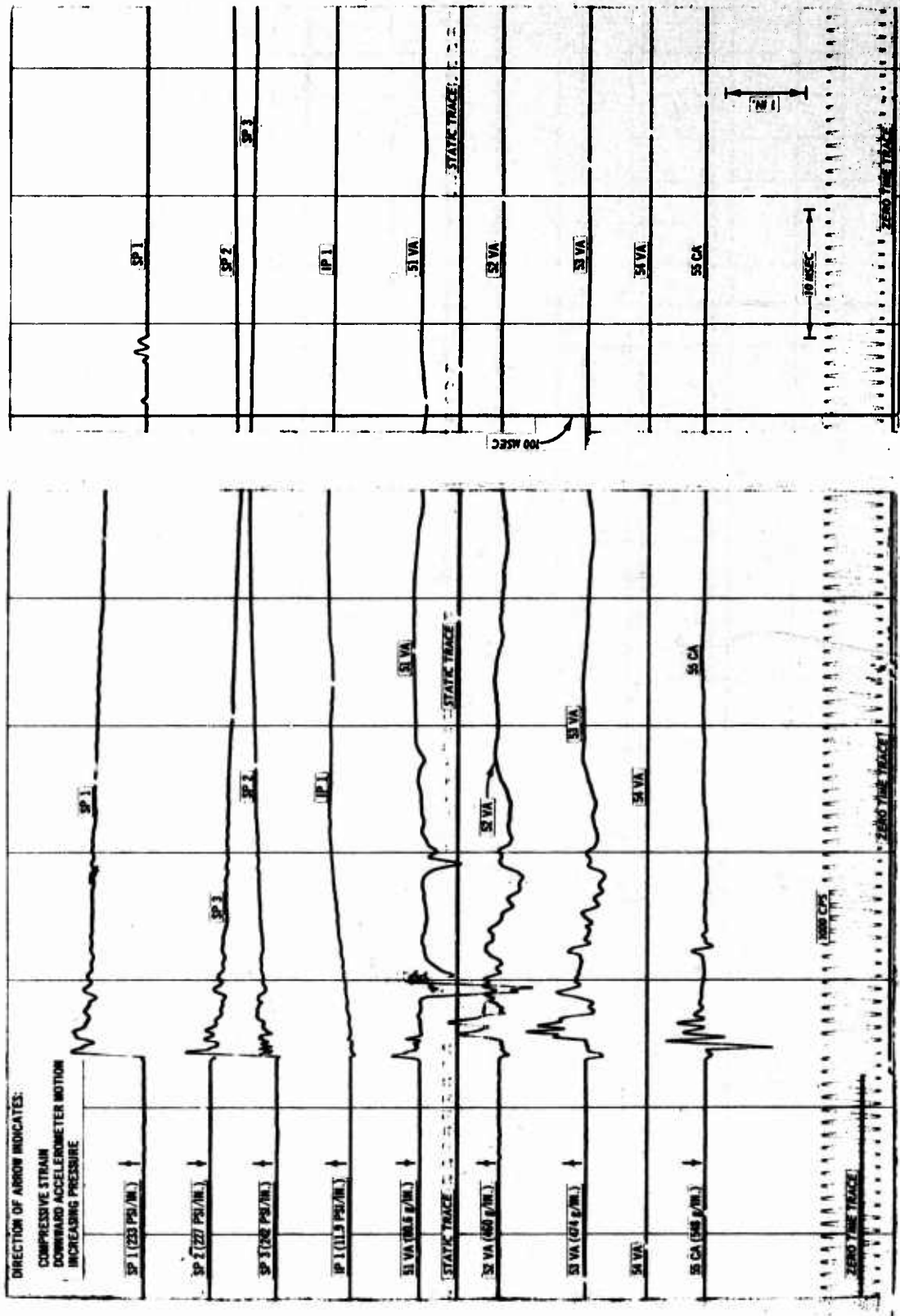


Figure B.23 Shot 5, oscillograph record from Recorder 1.

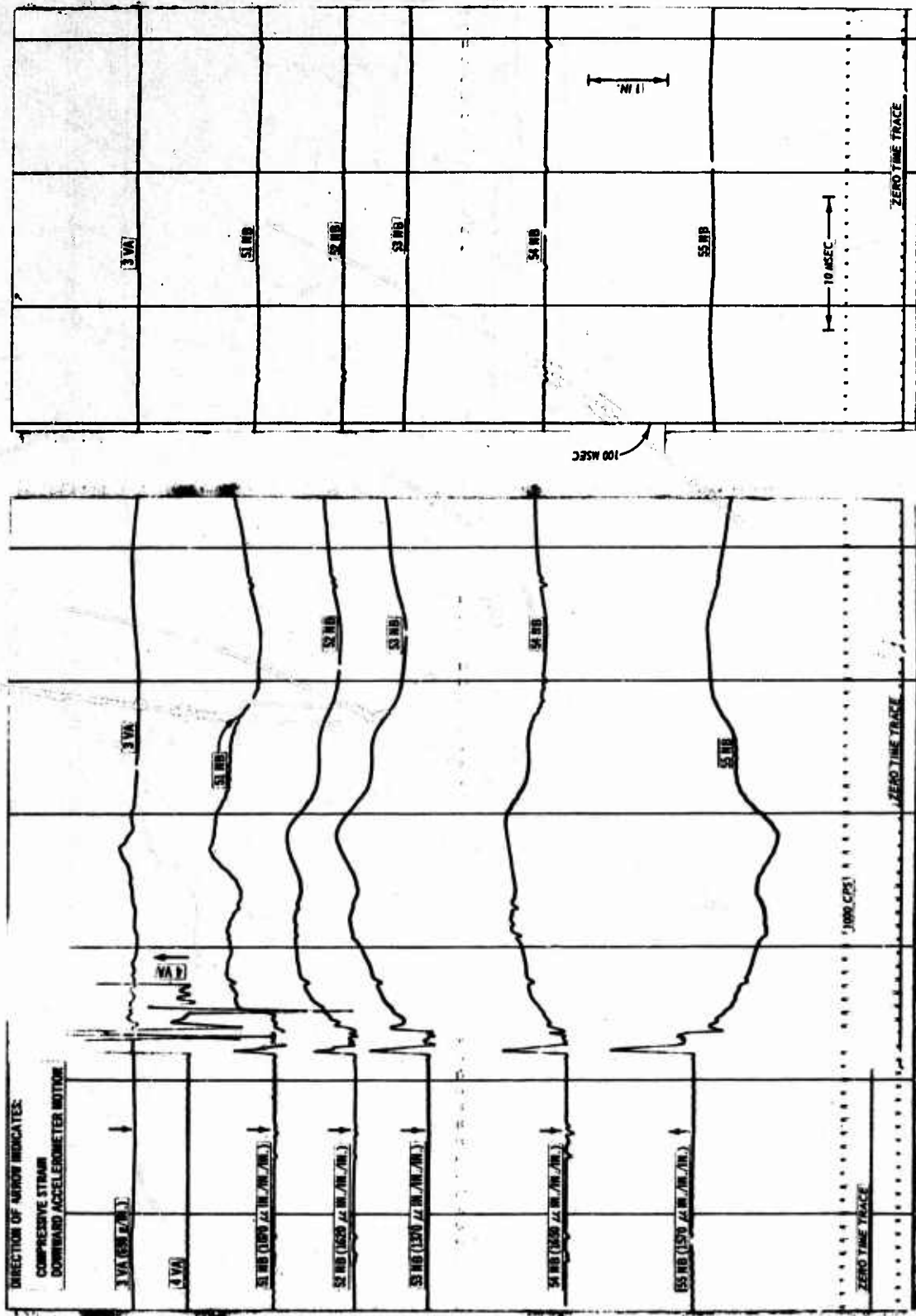


Figure B.24 Shot 5, oscillograph record from Recorder 2.

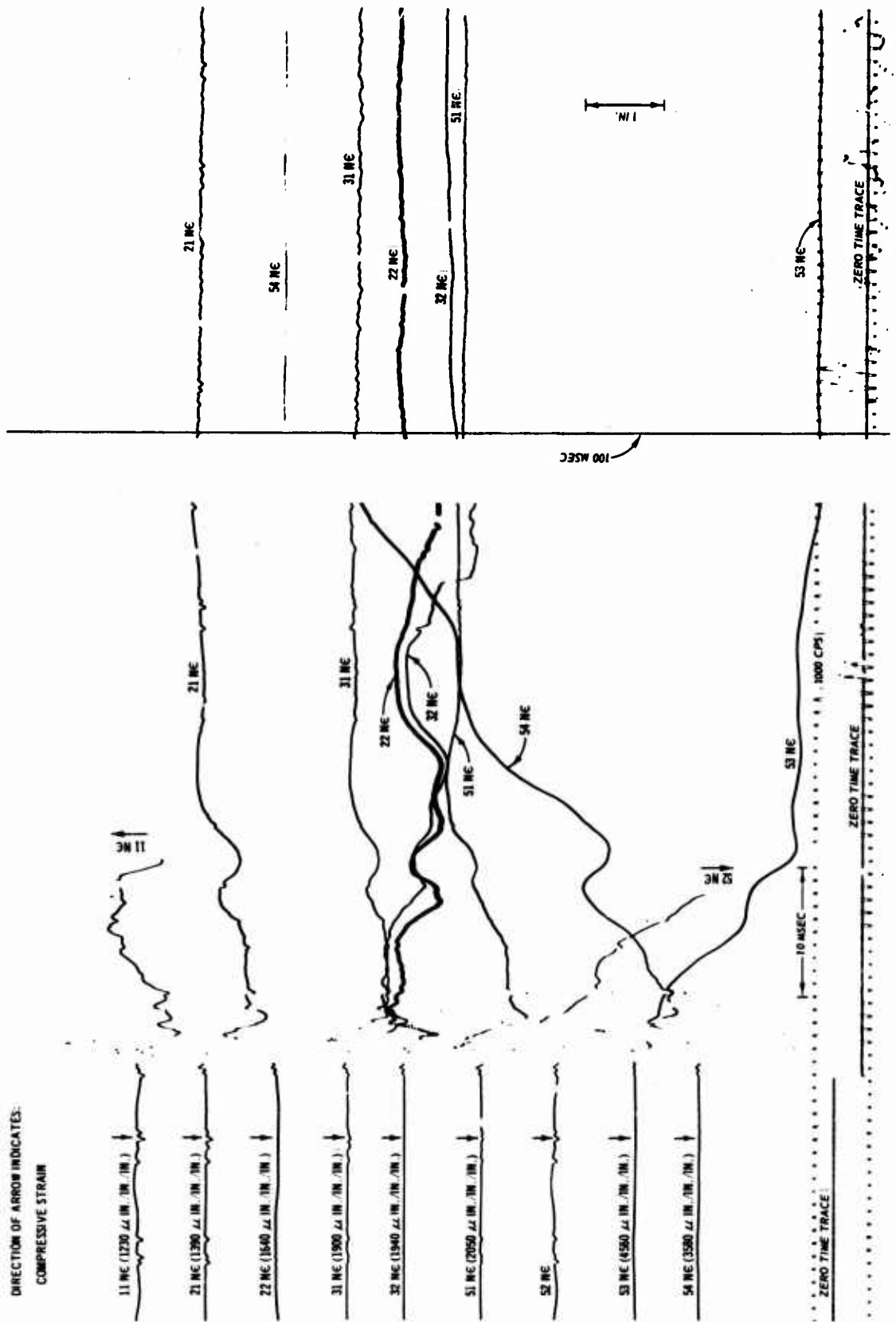


Figure B.25 Shot 5, oscillograph record from Recorder 3.

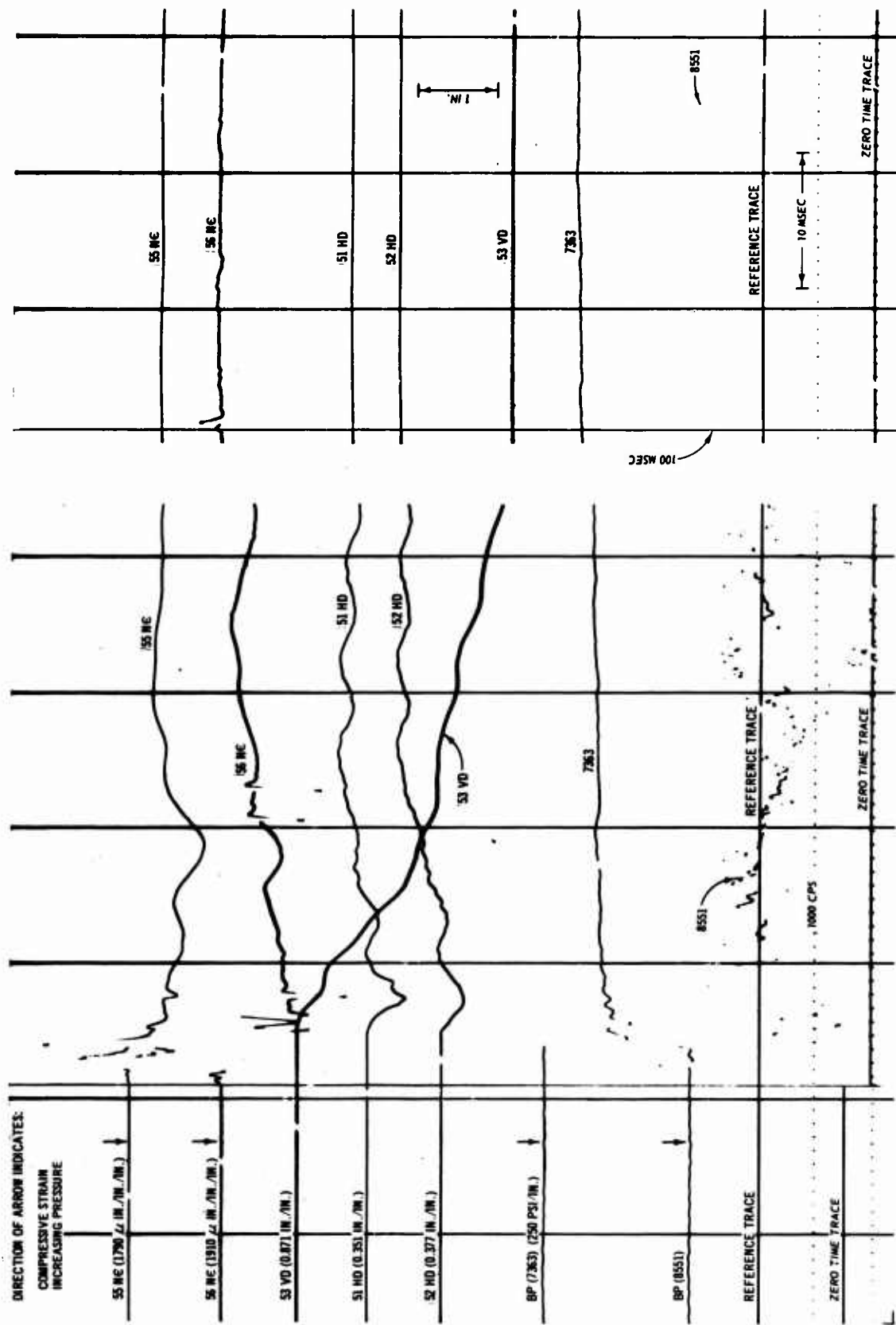


Figure B.26 Shot 5, oscillograph record from Recorder 4.



APPENDIX C  
COMPUTED DATA

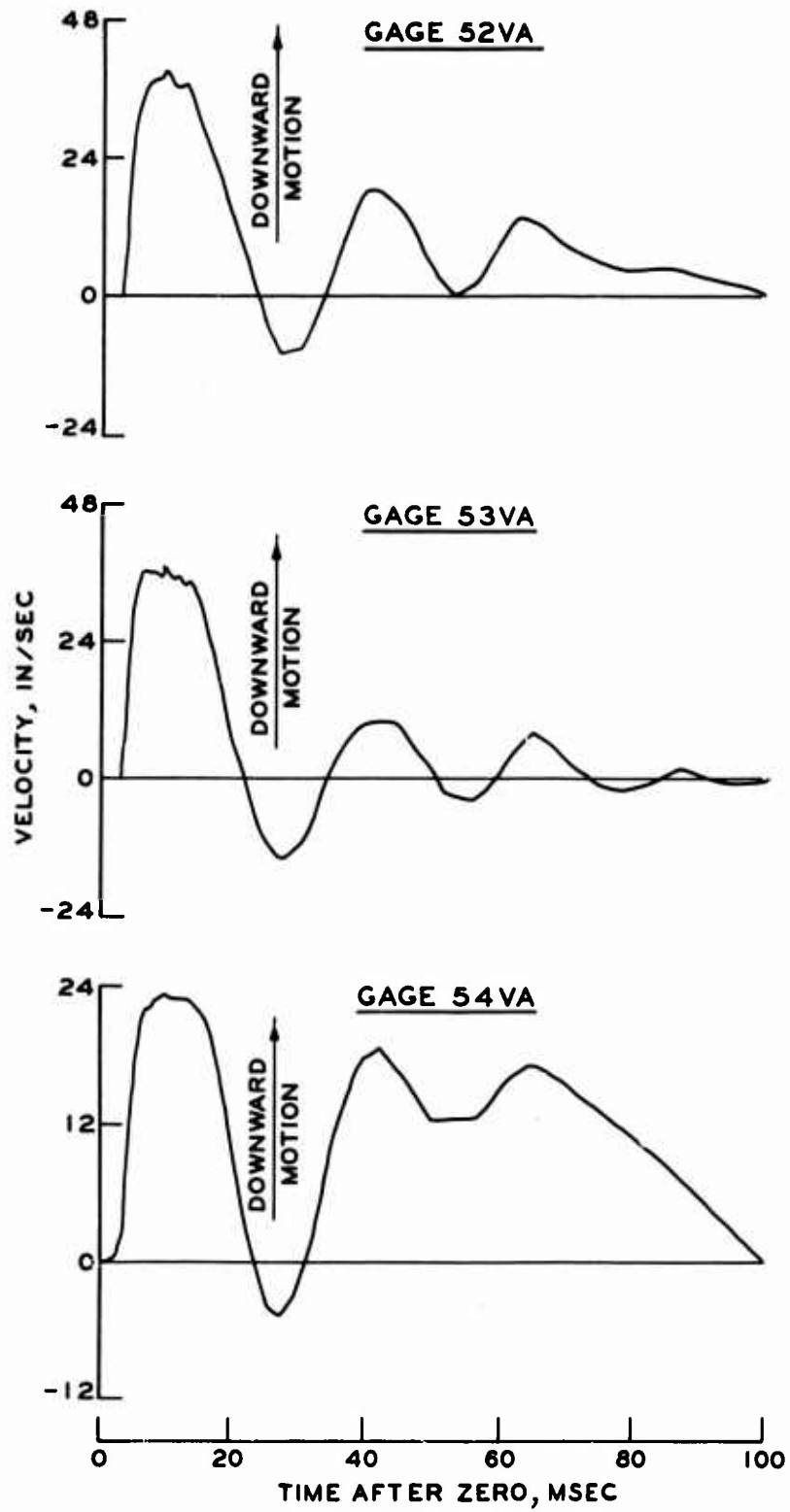


Figure C.1 Velocity data, Shot 1.

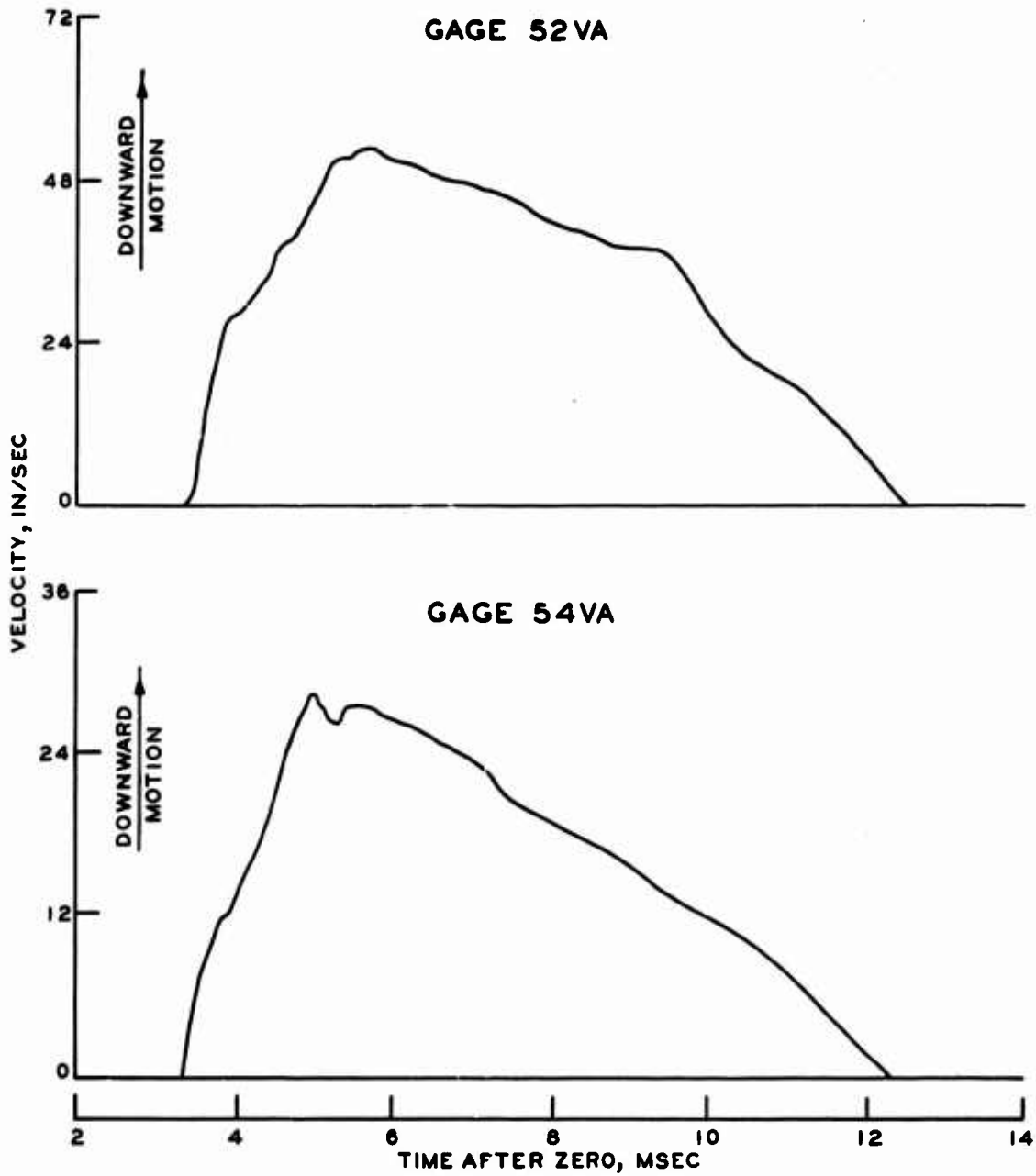


Figure C.2 Velocity data, Shot 2.

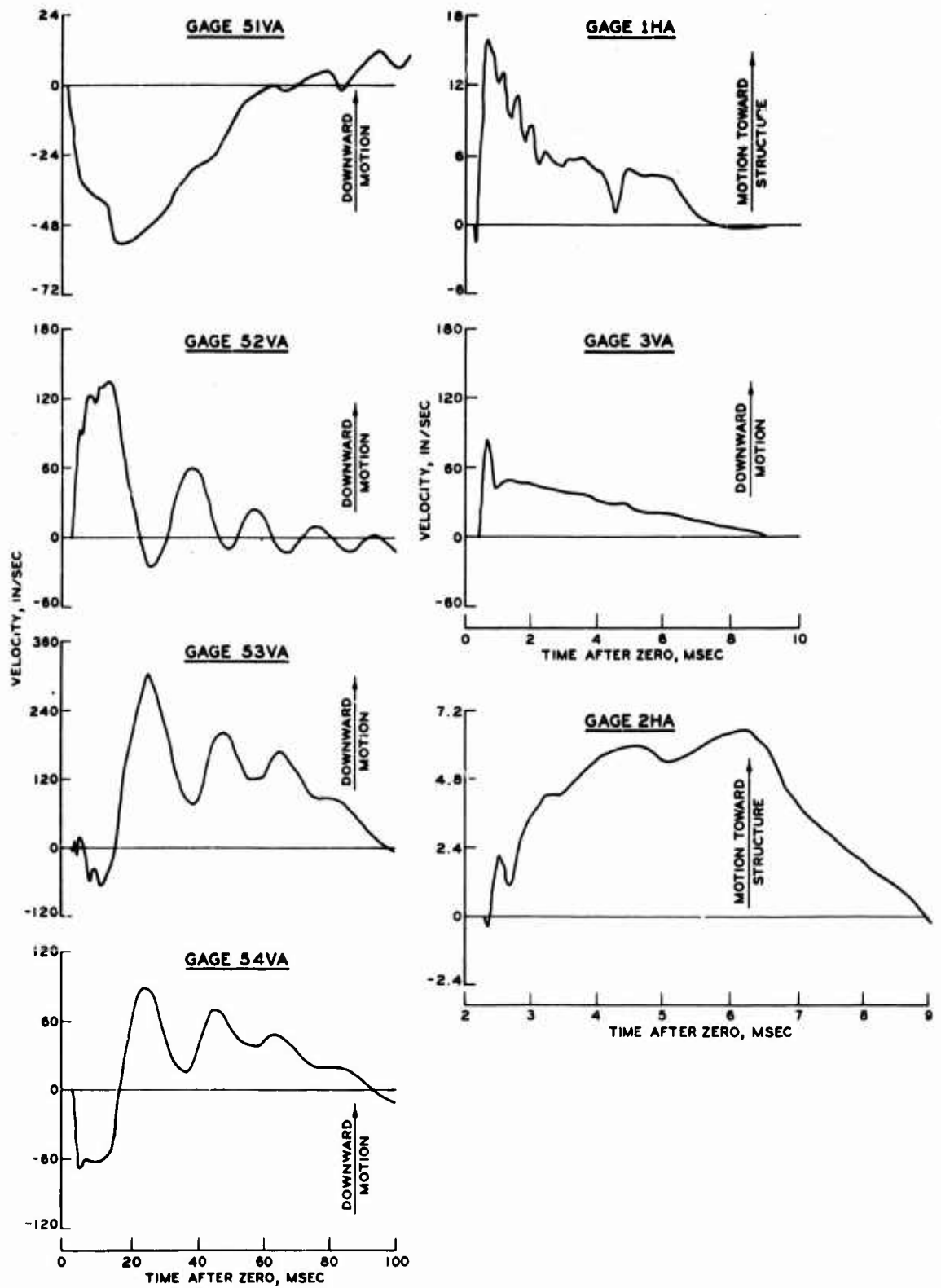


Figure C.3 Velocity data, Shot 3.

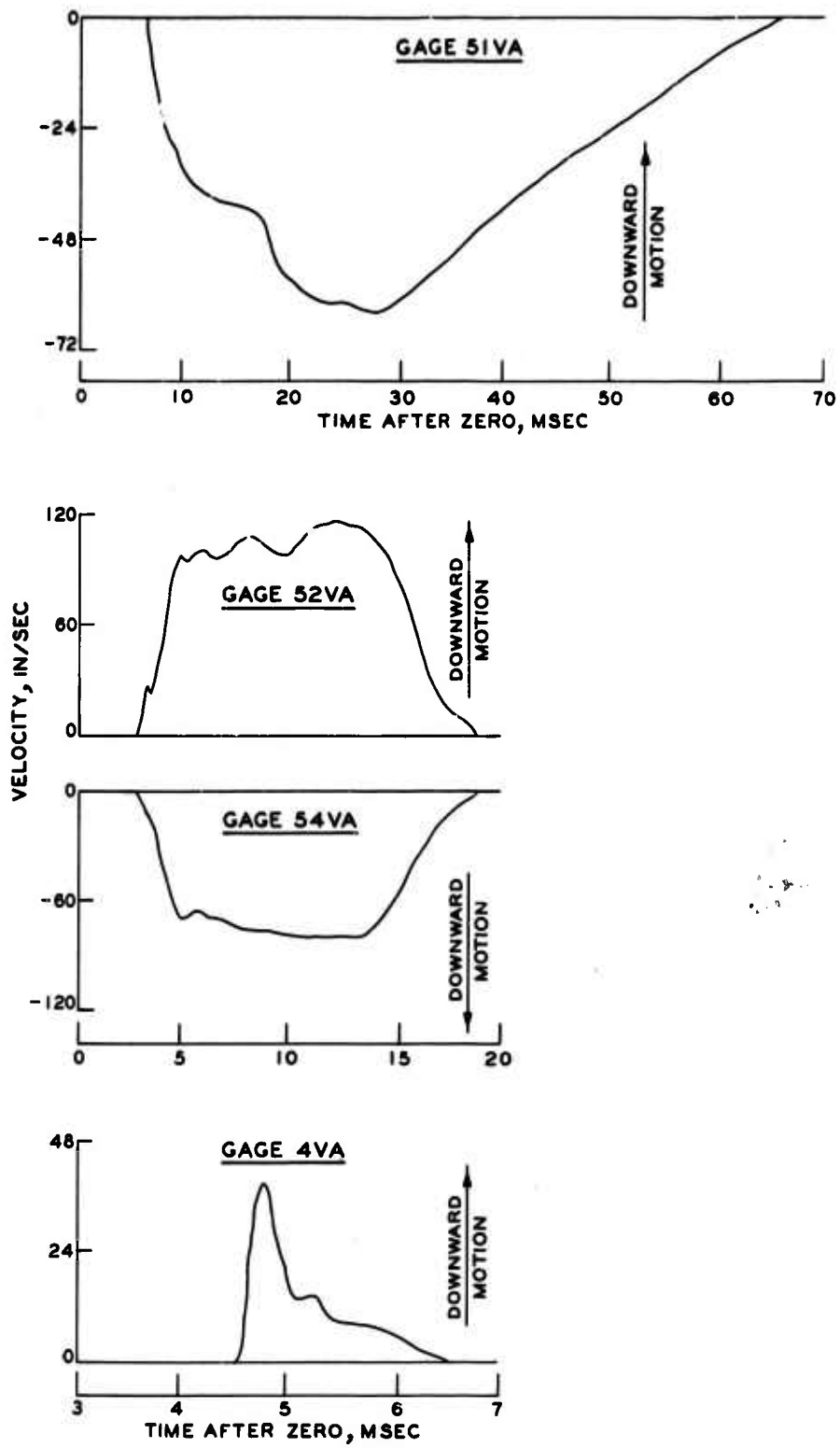


Figure C.4 Velocity data, Shot 4.

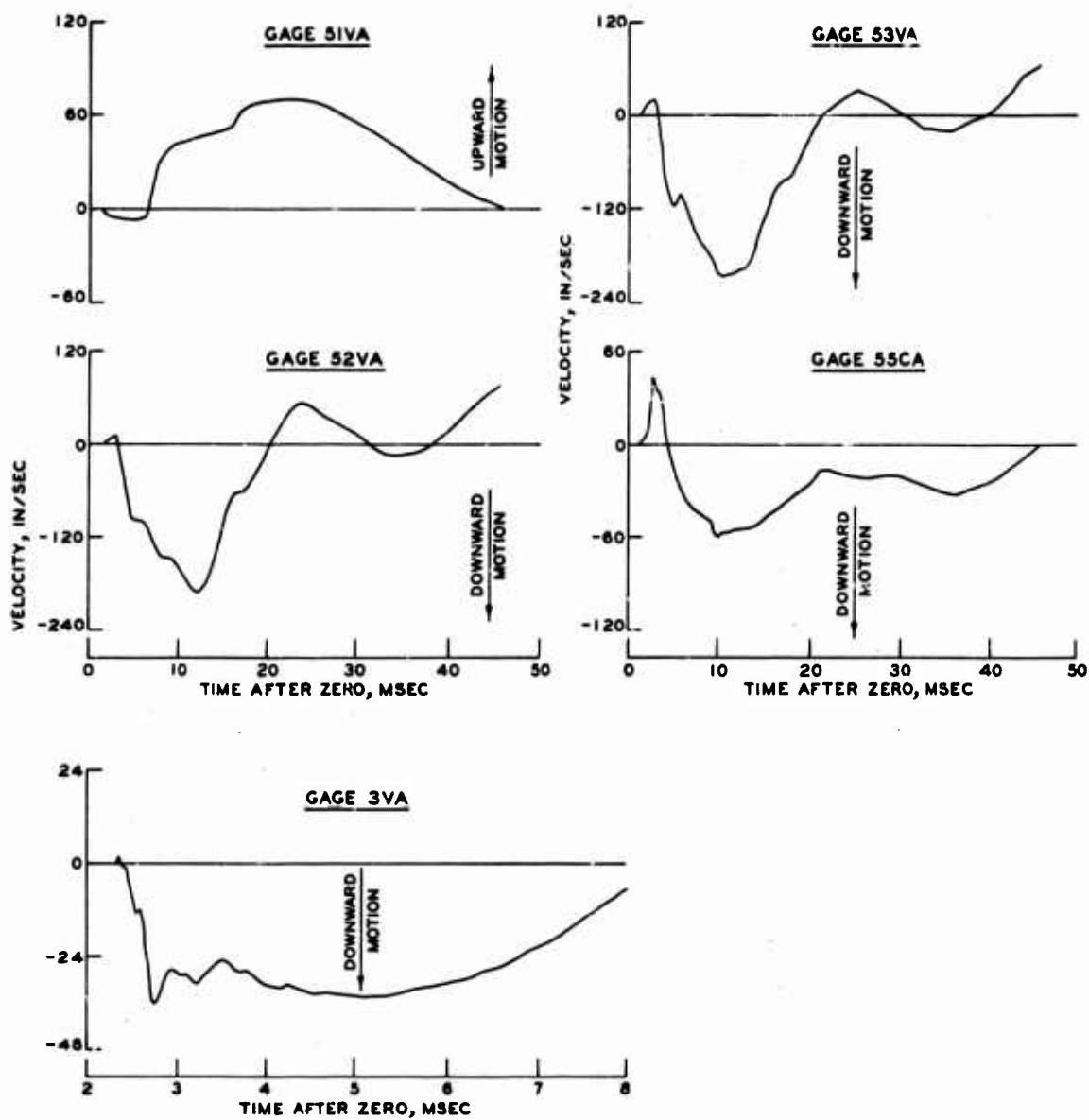


Figure C.5 Velocity data, Shot 5.

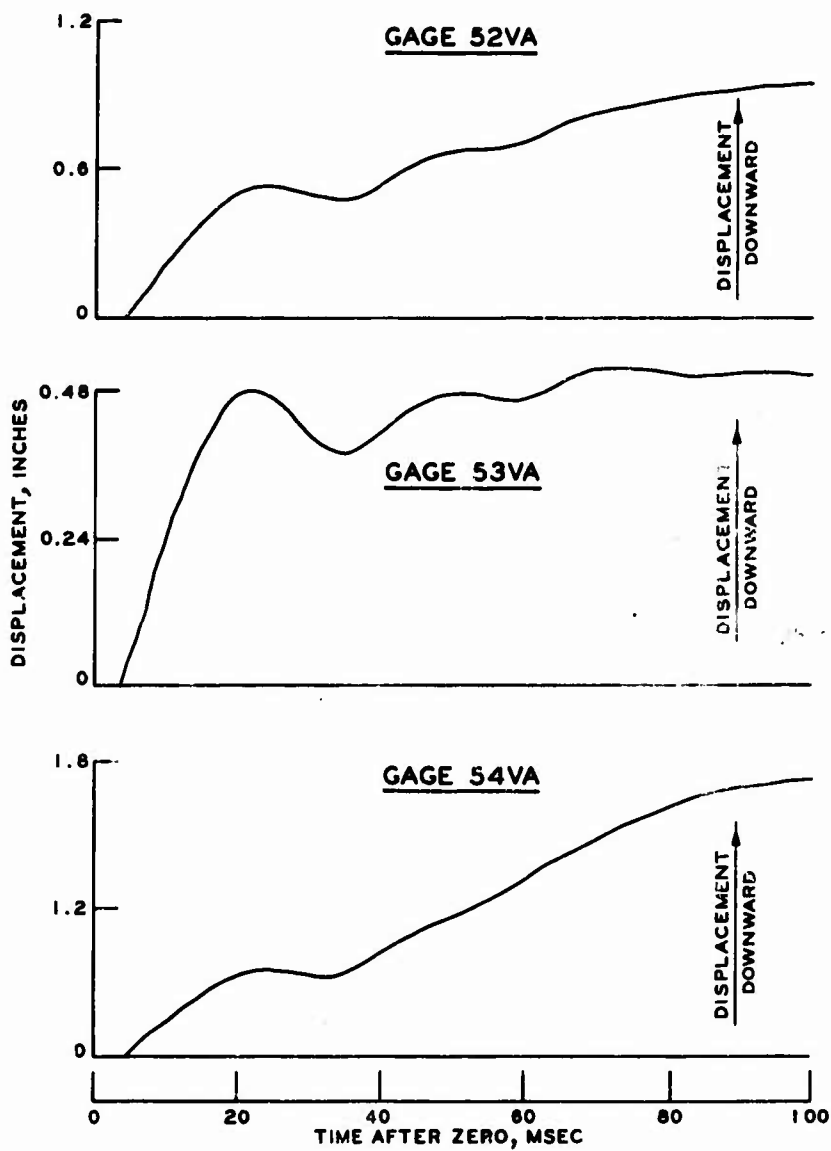


Figure C.6 Displacement data, Shot 1.

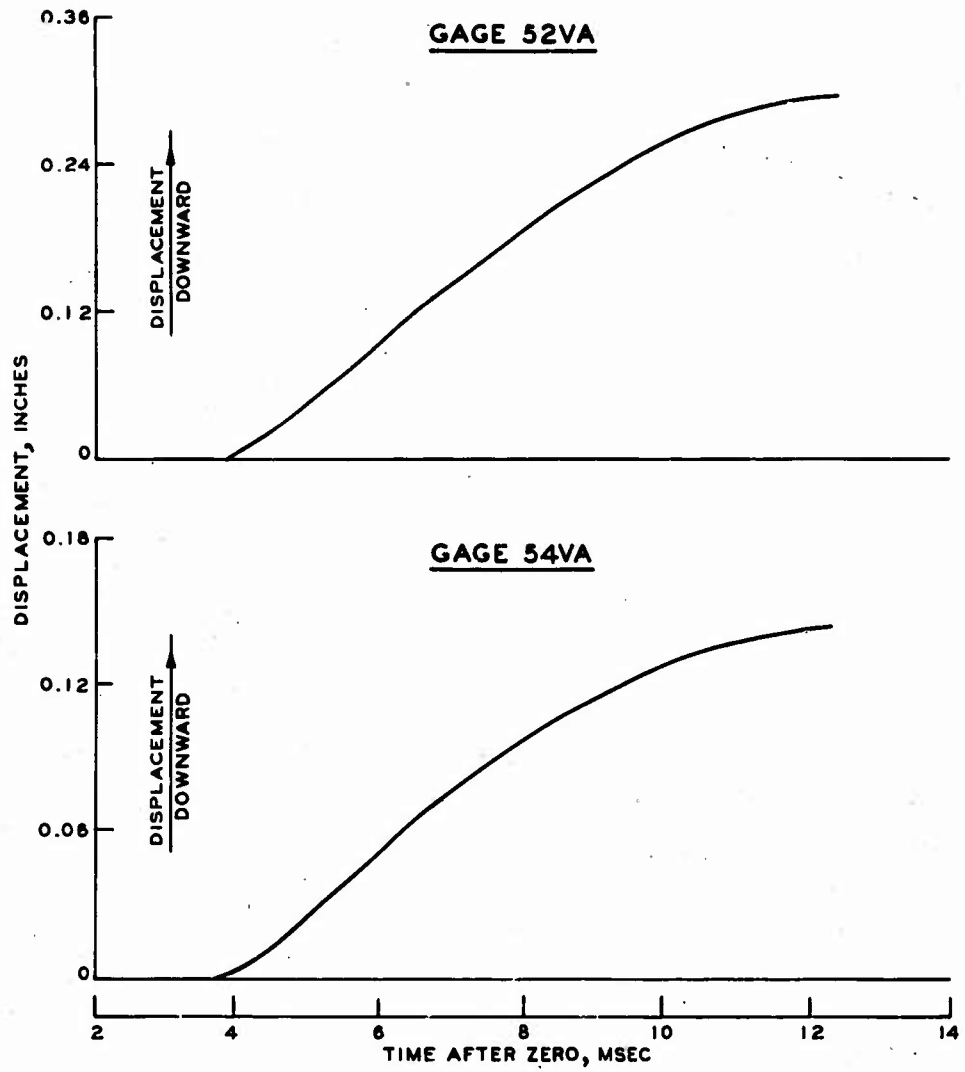


Figure C.7 Displacement data, Shot 2.

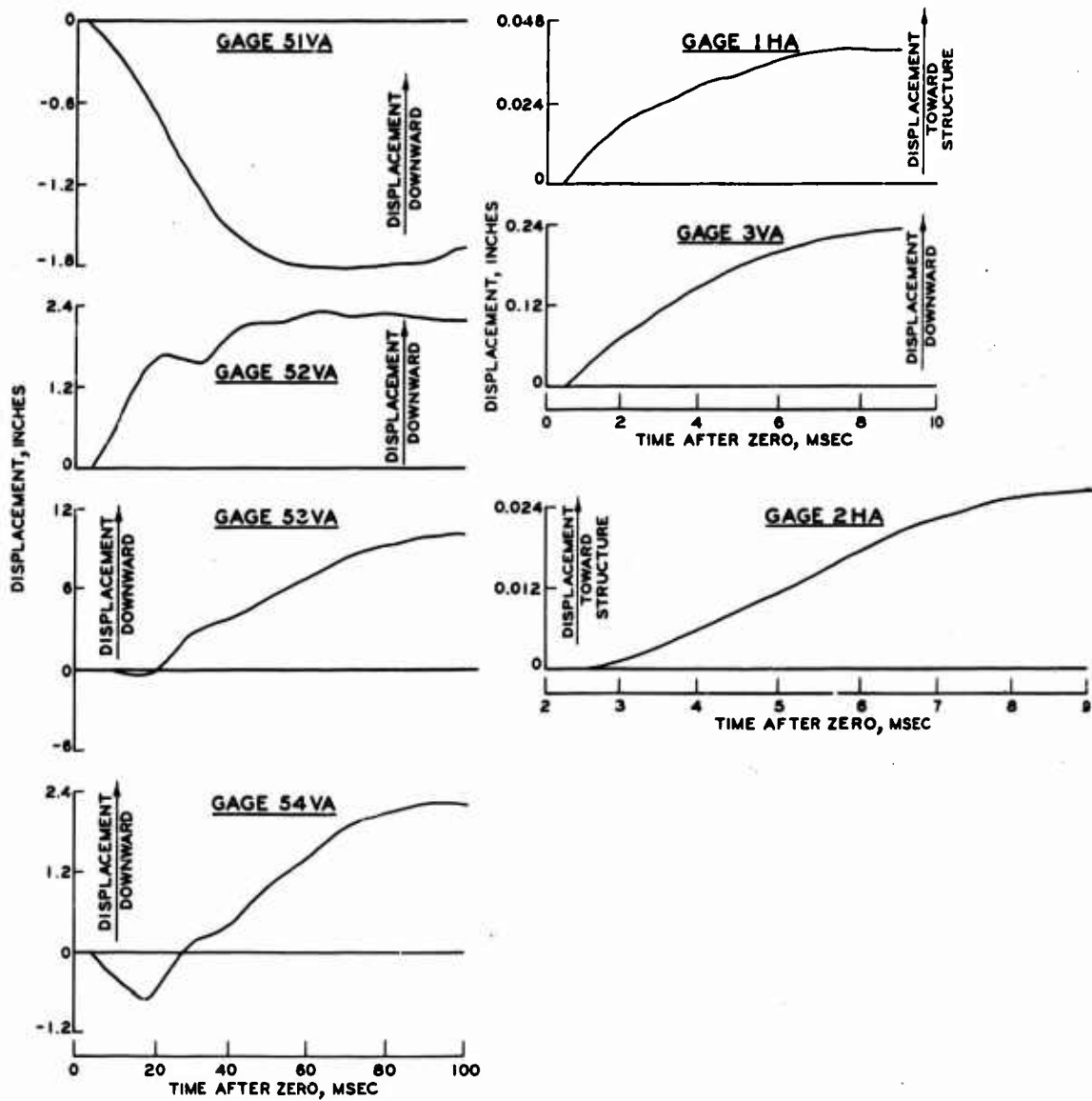


Figure C.8 Displacement data, Shot 3.

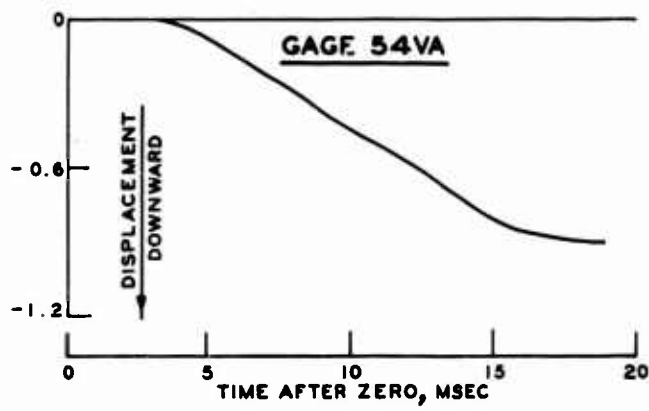
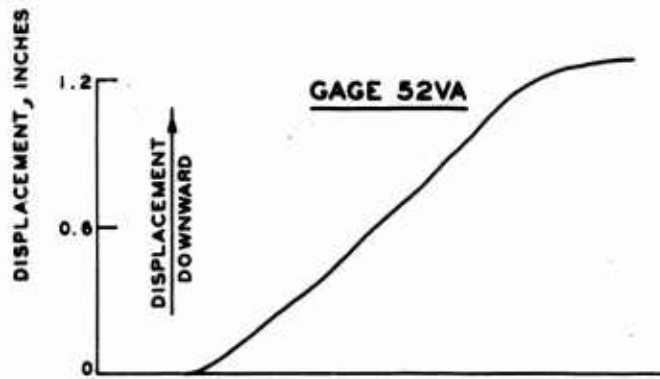
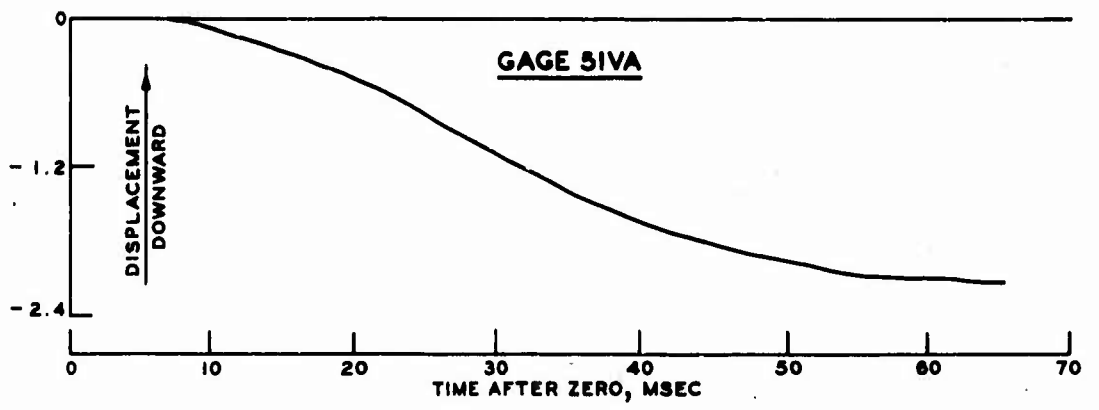


Figure C.9 Displacement data, Shot 4.

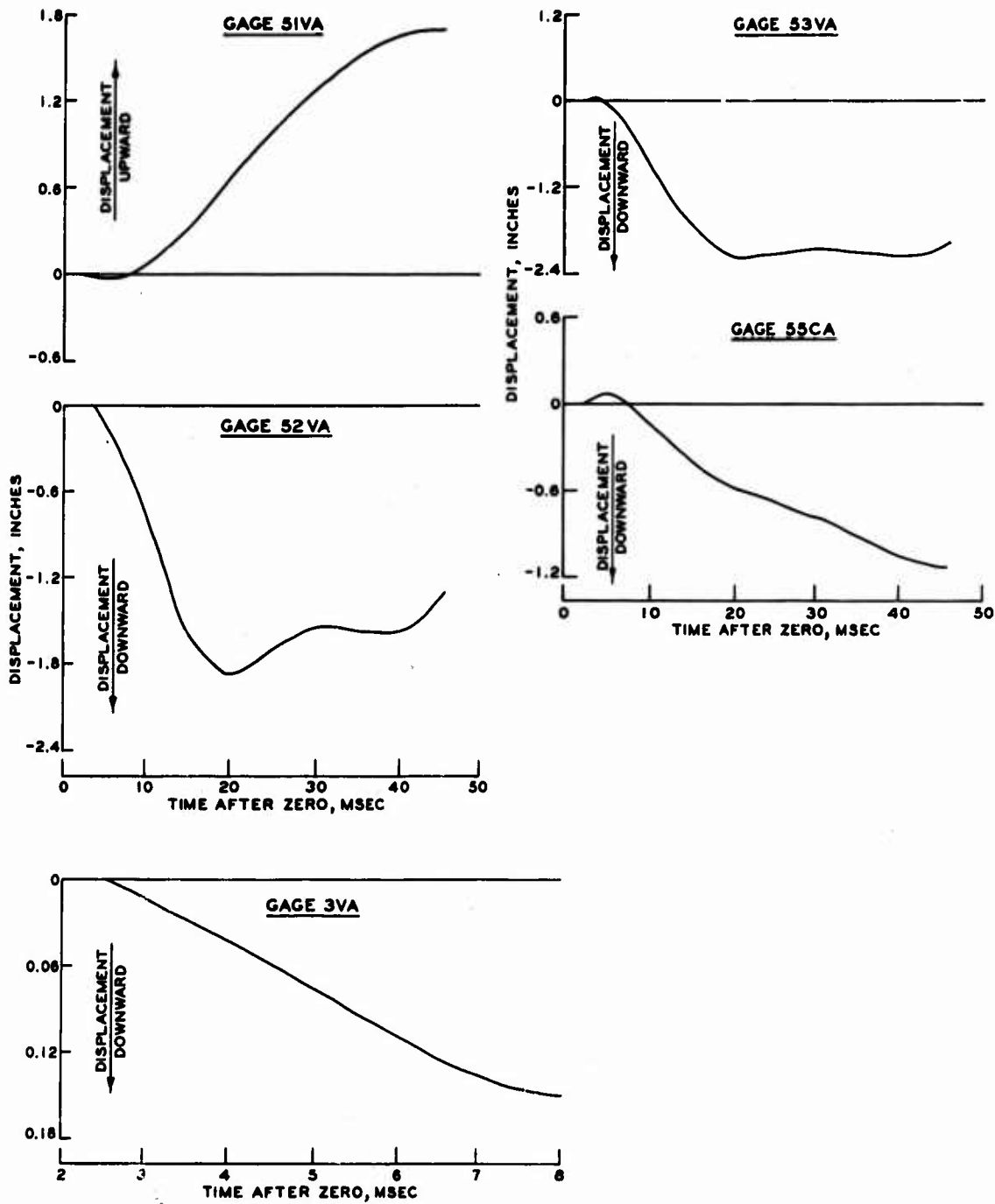


Figure C.10 Displacement data, Shot 5.

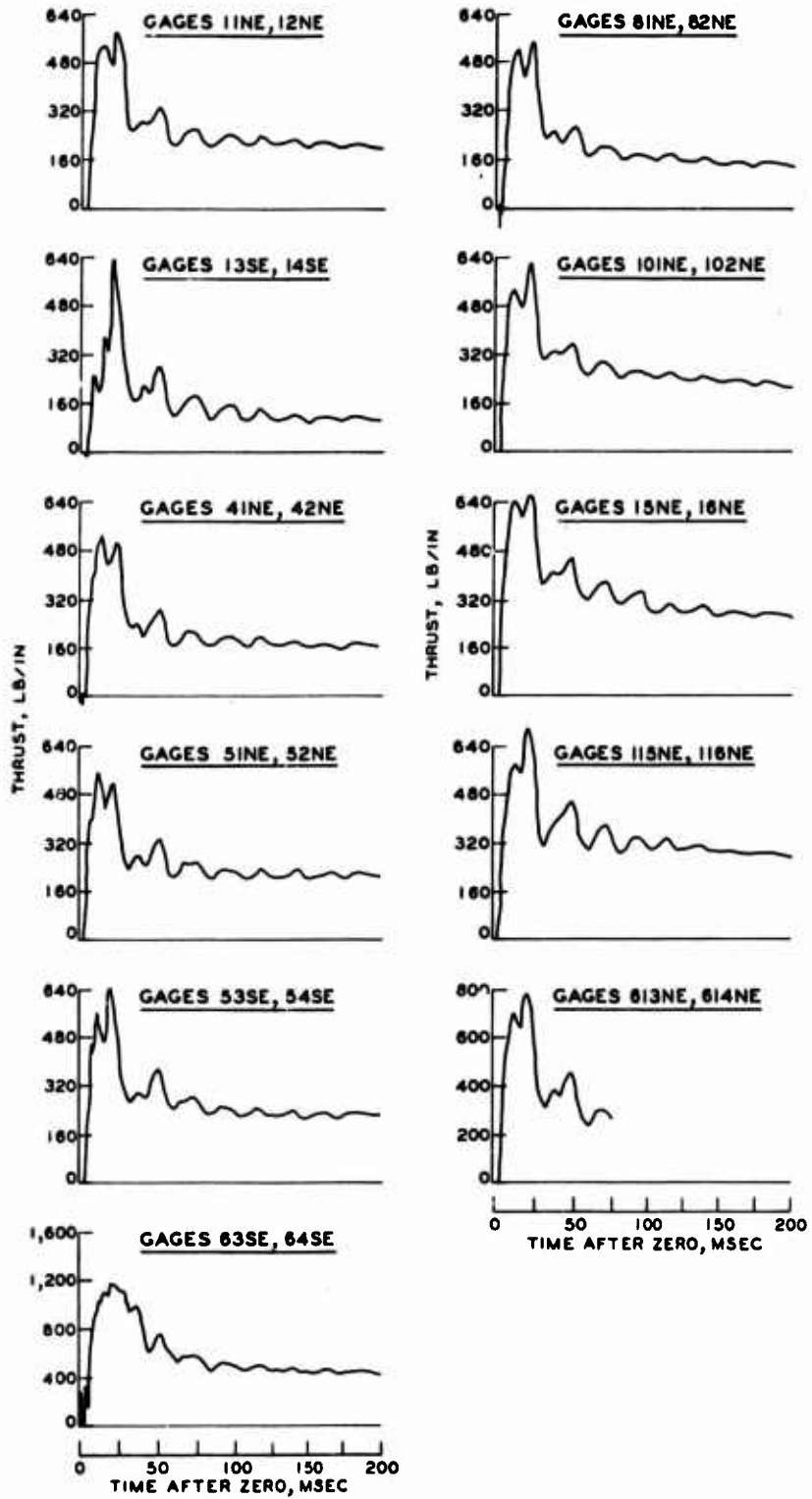


Figure C.11 Thrust data, Shot 1.

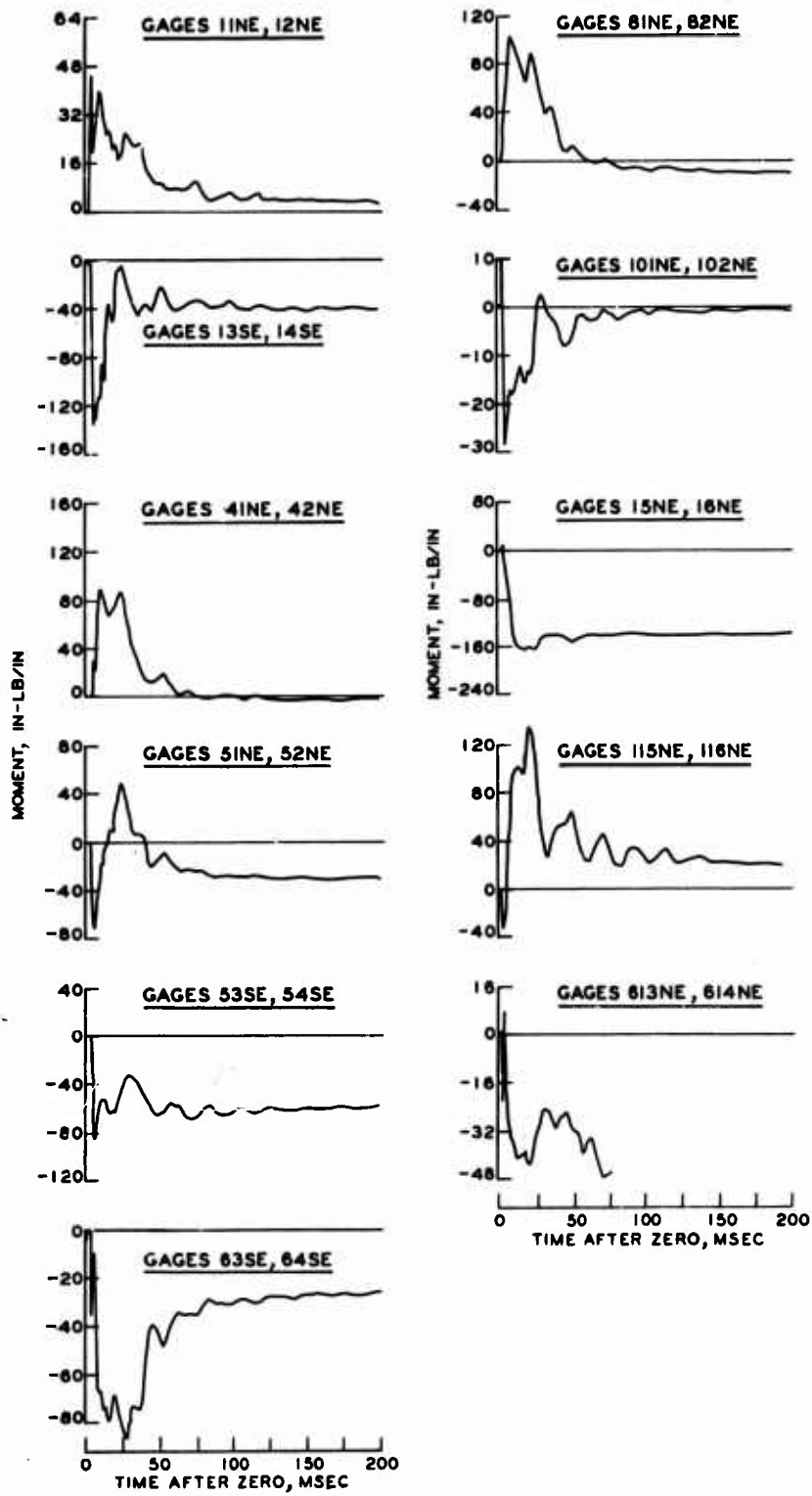


Figure C.12 Moment data, Shot 1.

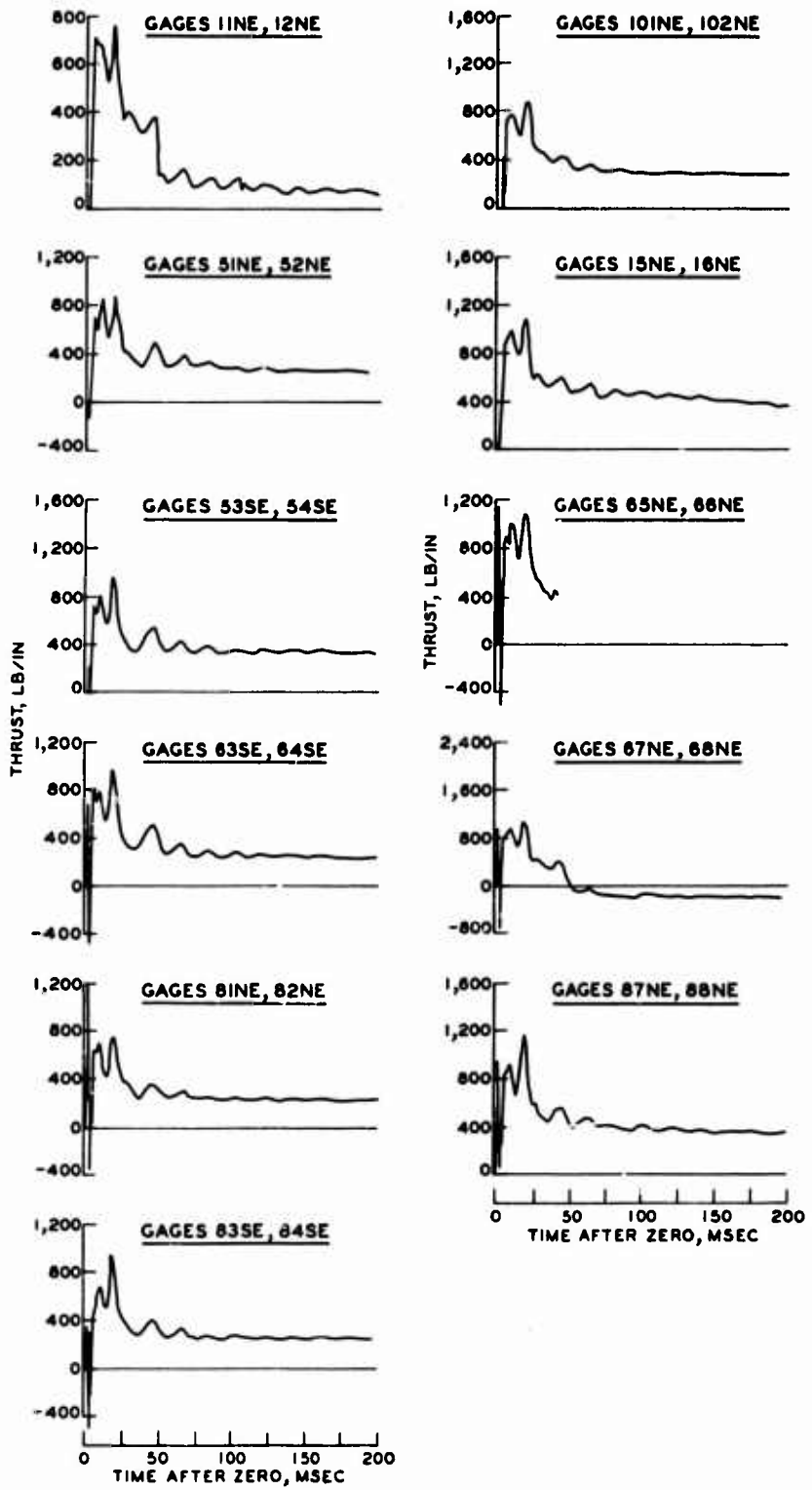


Figure C.13 Thrust data, Shot 2.

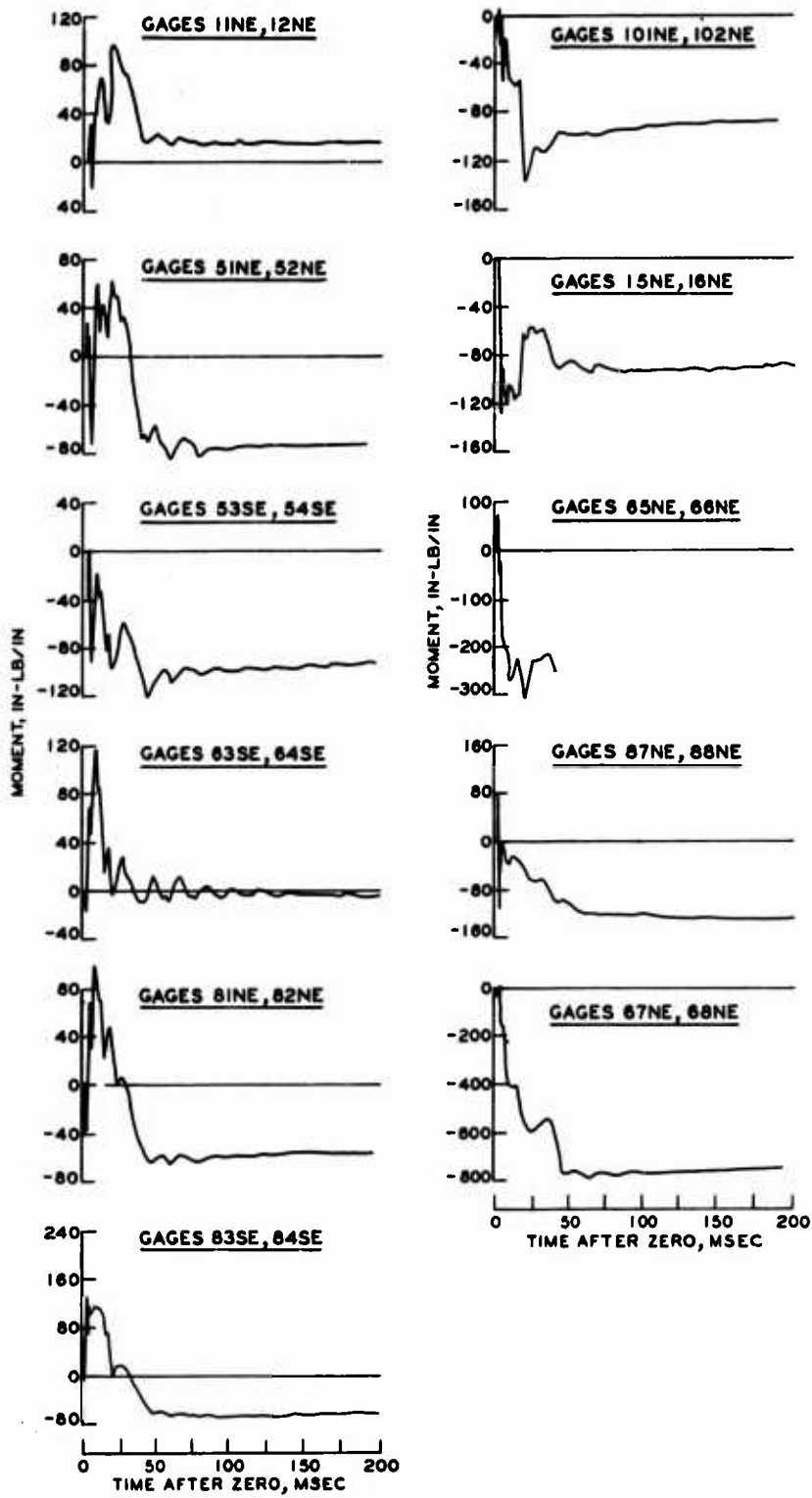


Figure C.14 Moment data, Shot 2.

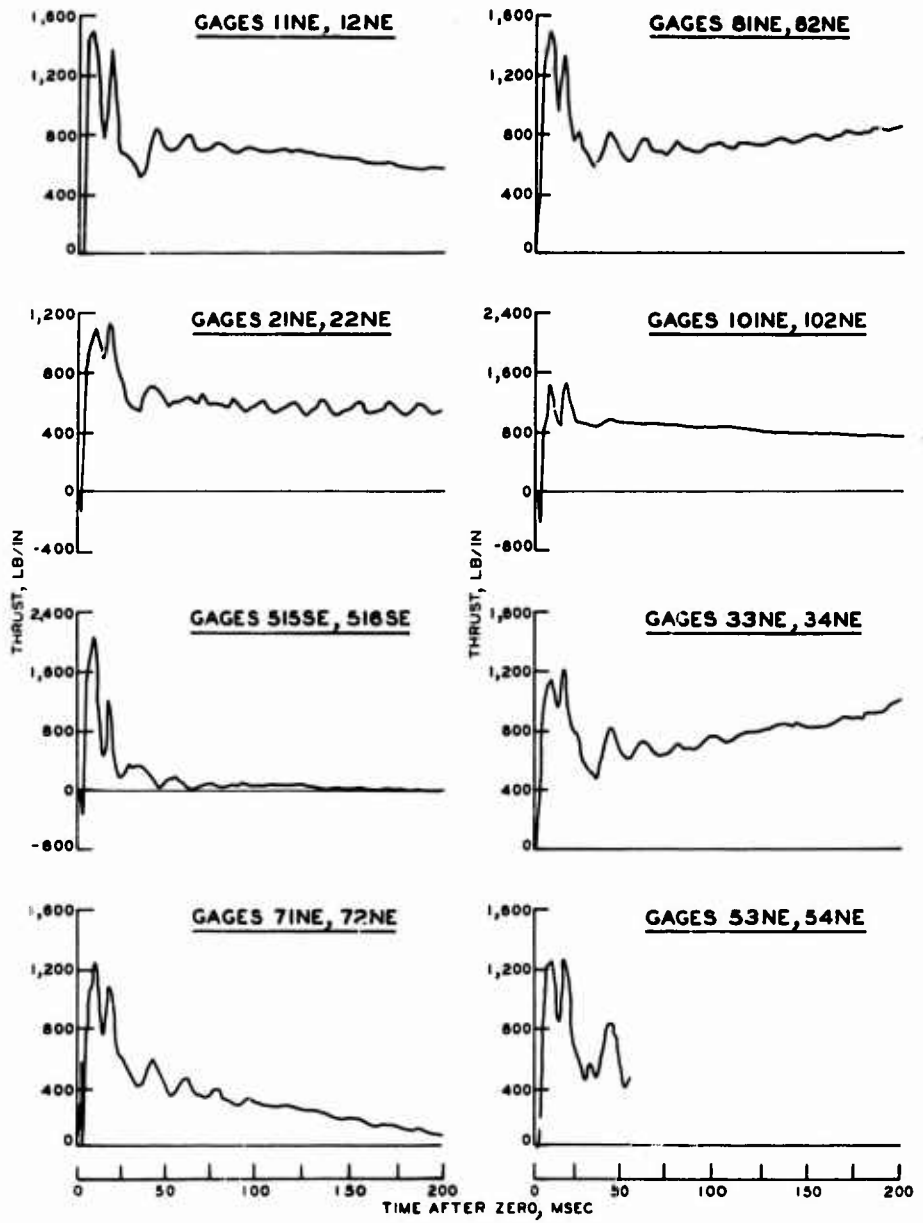


Figure C.15 Thrust data, Shot 3 (Sheet 1 of 2).

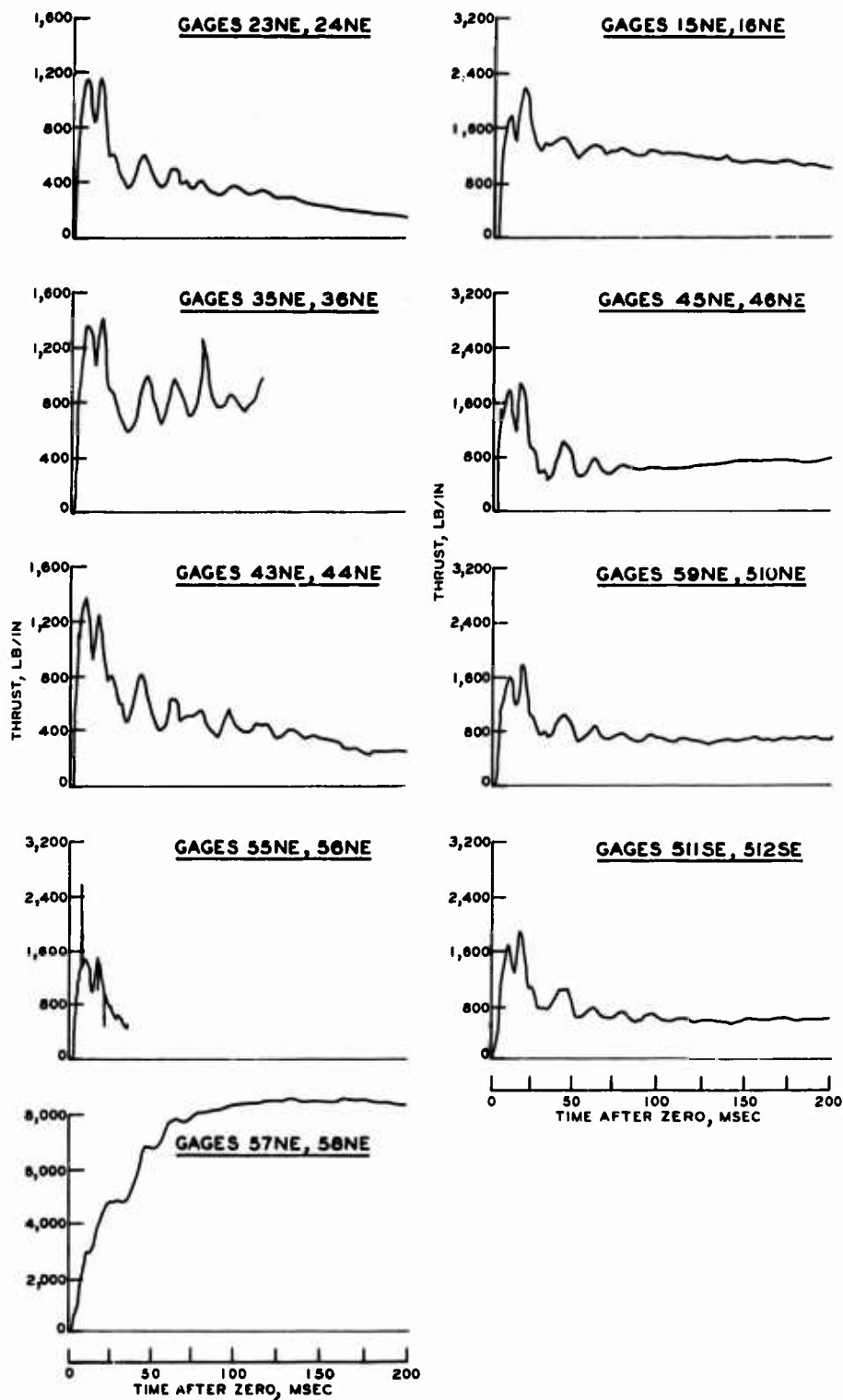


Figure C.15 (Sheet 2 of 2).

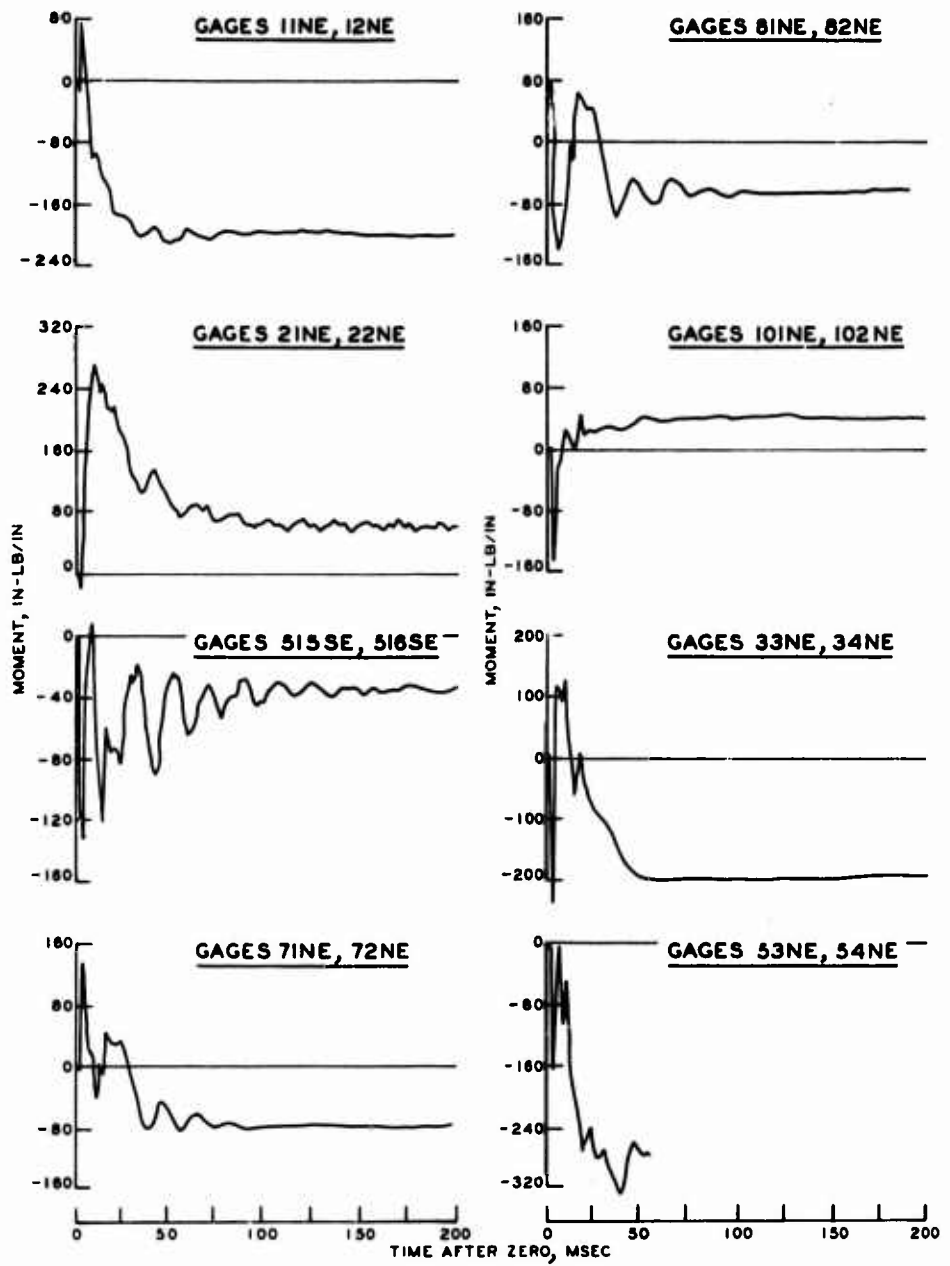


Figure C.16 Moment data, Shot 3 (Sheet 1 of 2).

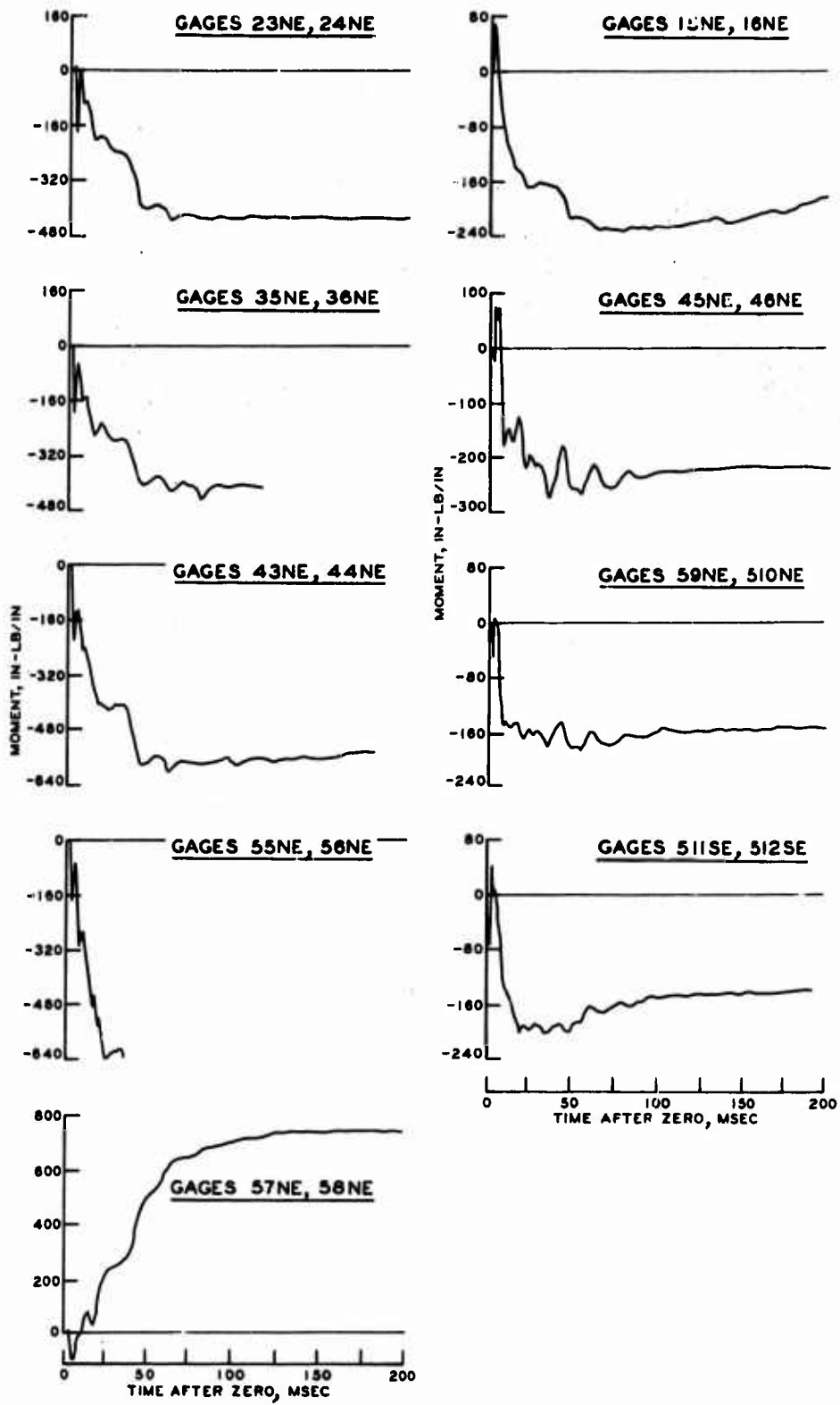


Figure C.16 (Sheet 2 of 2).

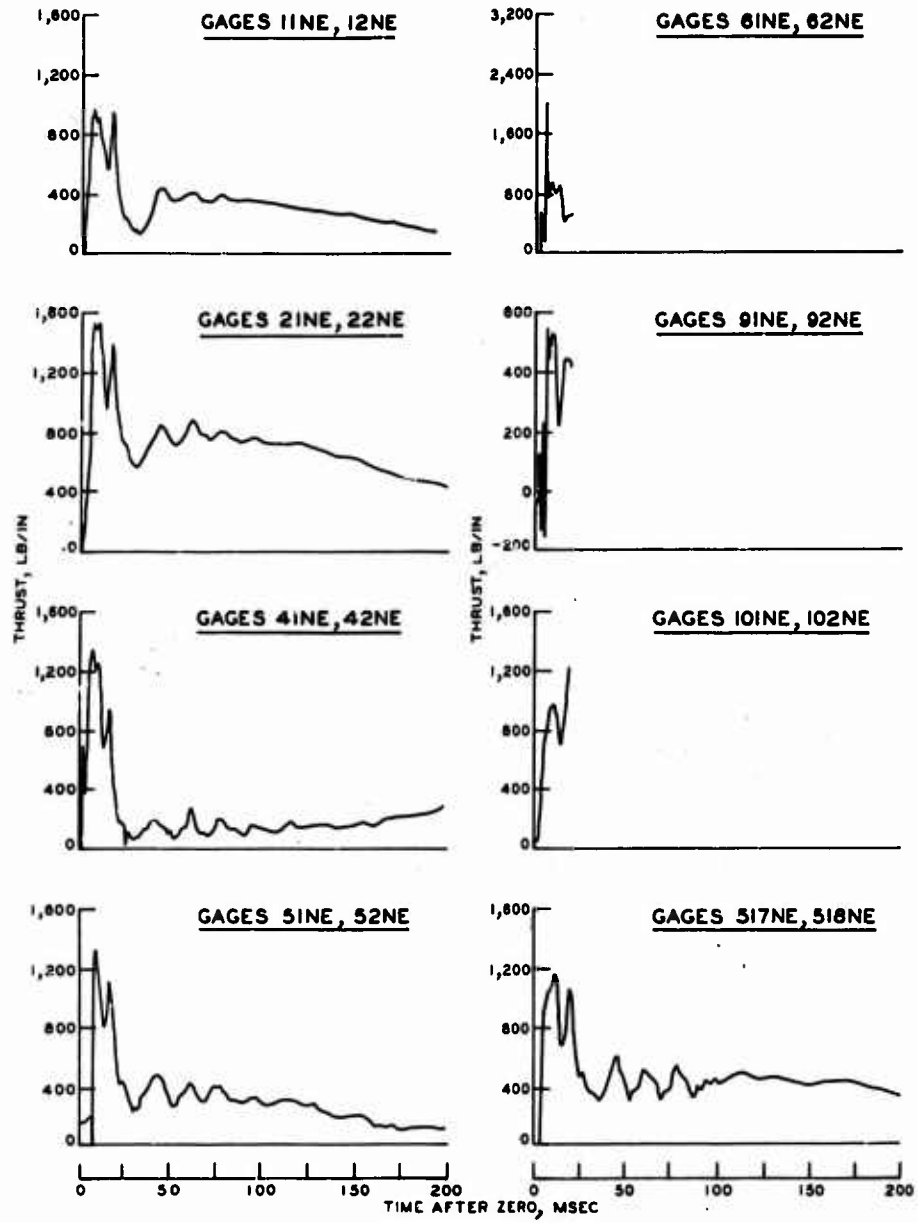


Figure C.17 Thrust data, Shot 4 (Sheet 1 of 2).

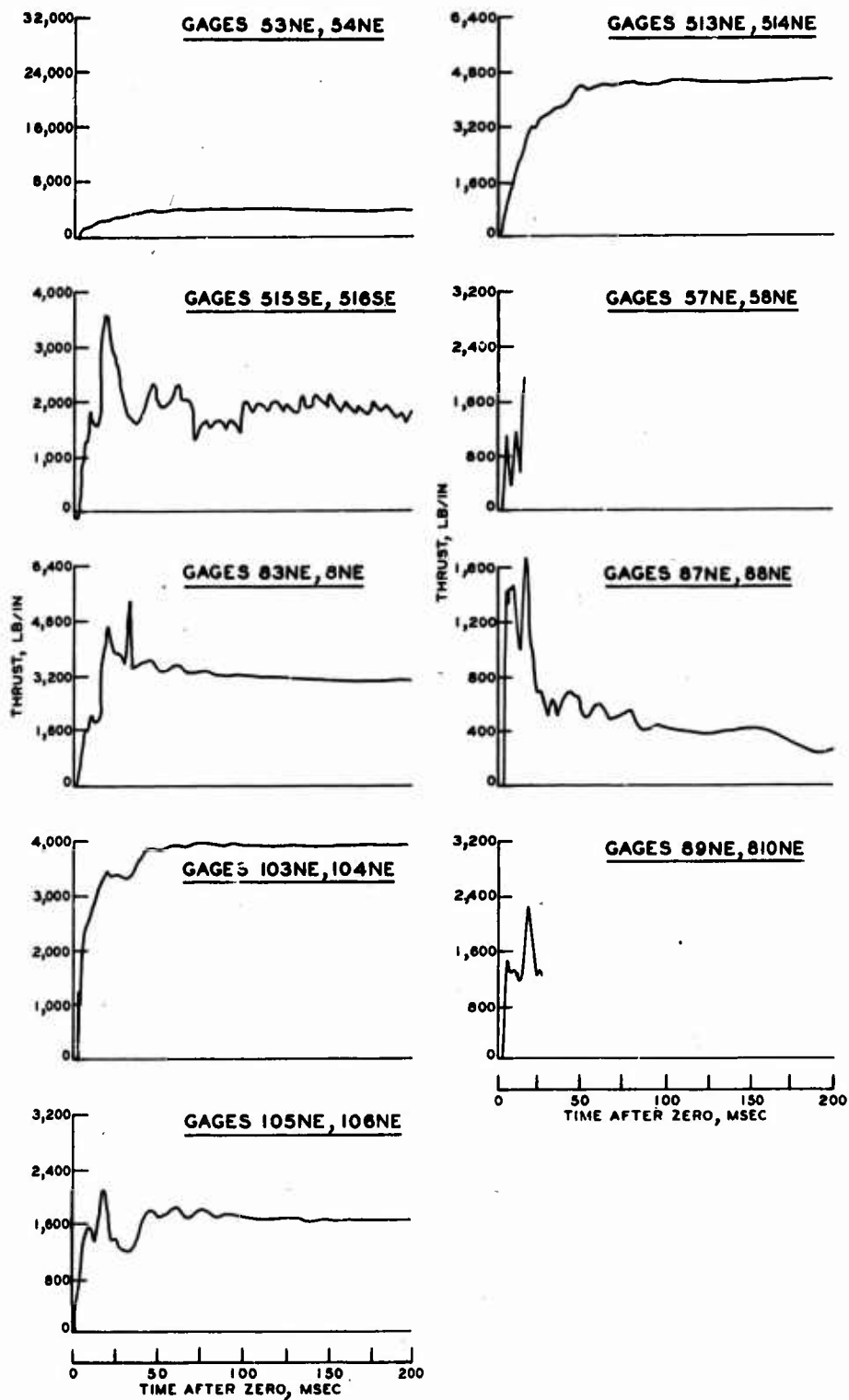


Figure C.17 (Sheet 2 of 2).

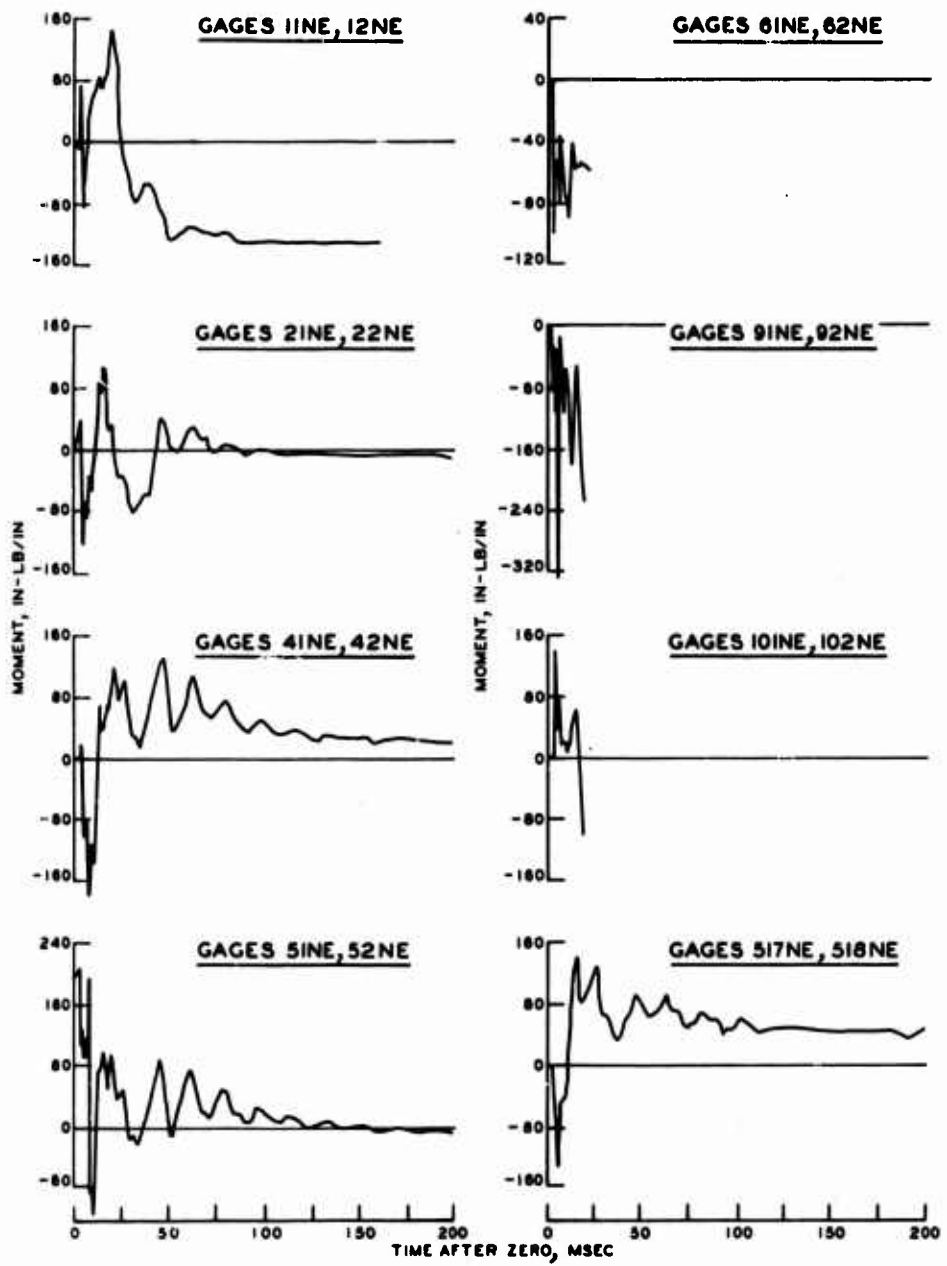


Figure C.18 Moment data, Shot 4 (Sheet 1 of 2).

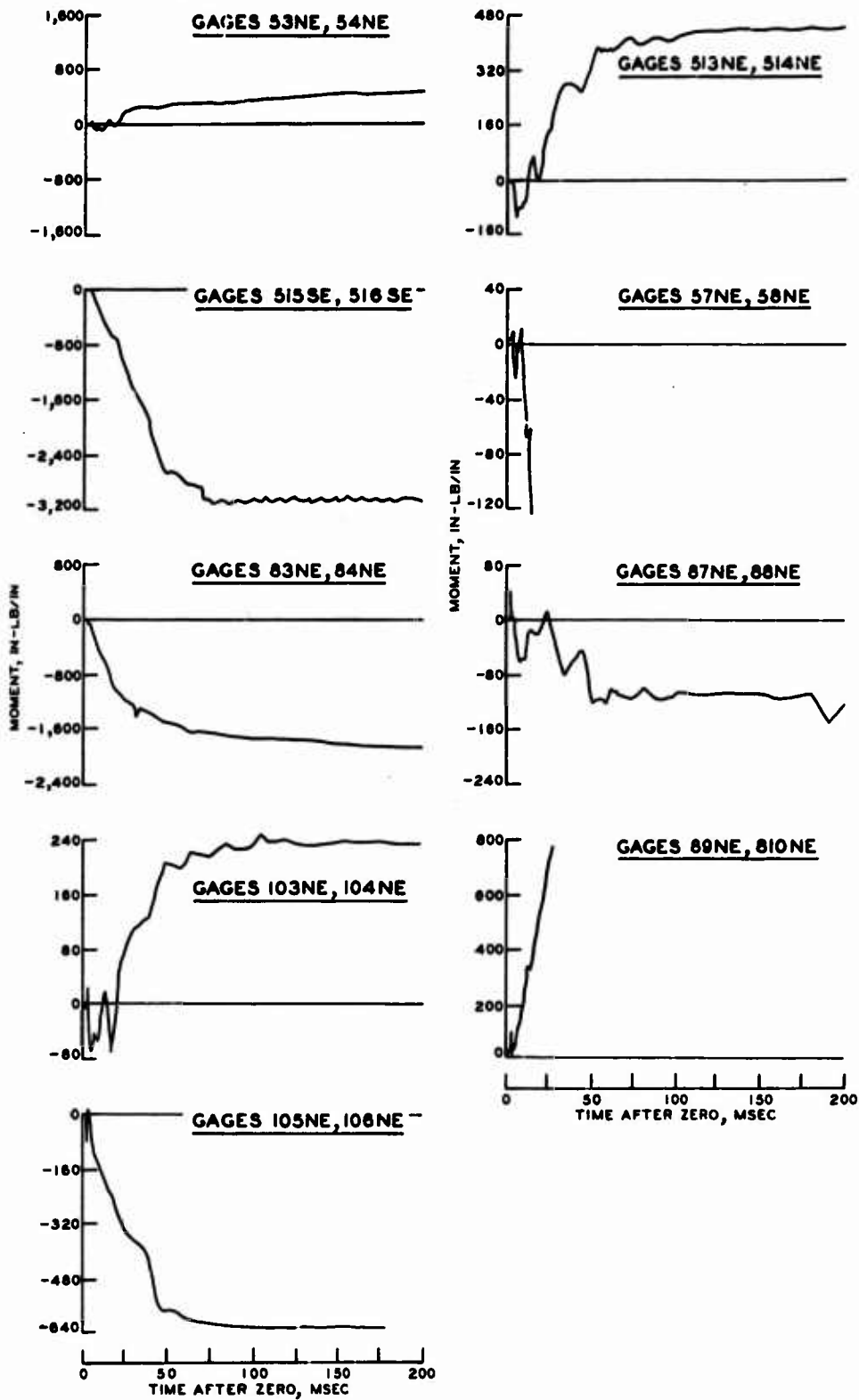


Figure C.18 (Sheet 2 of 2).

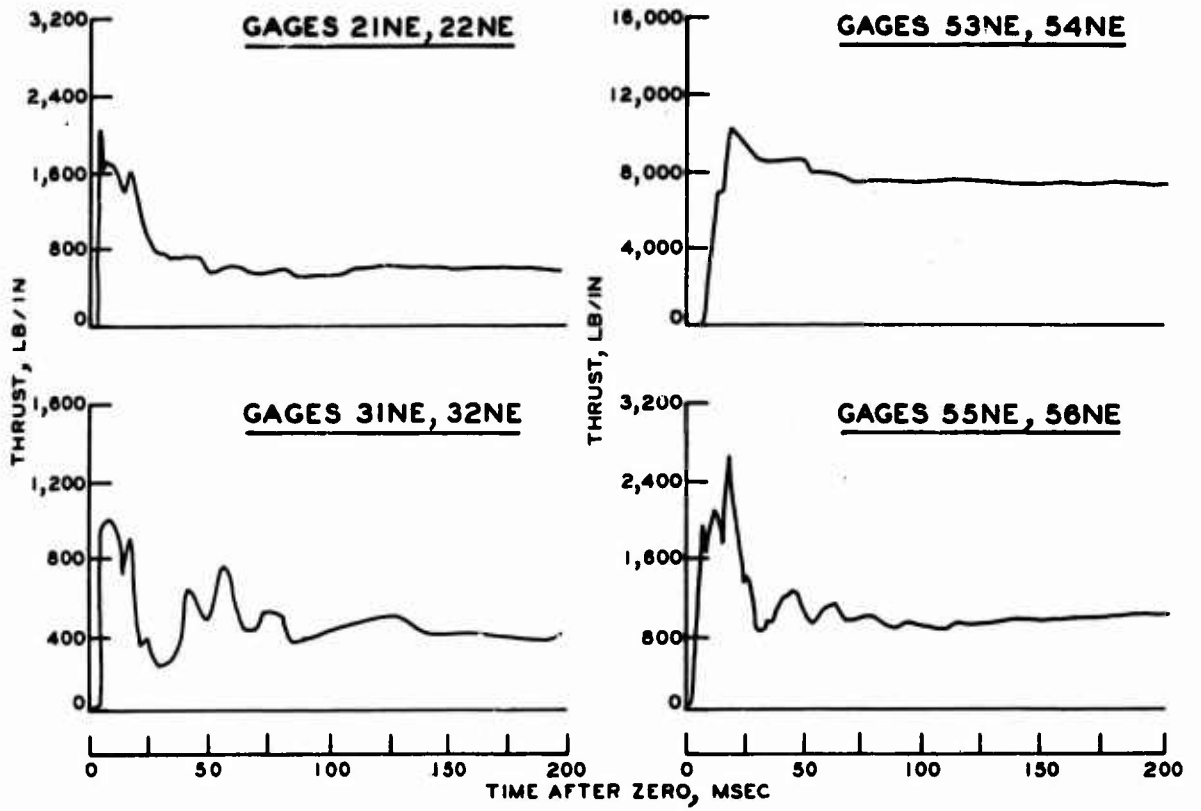


Figure C.19 Thrust data, Shot 5.

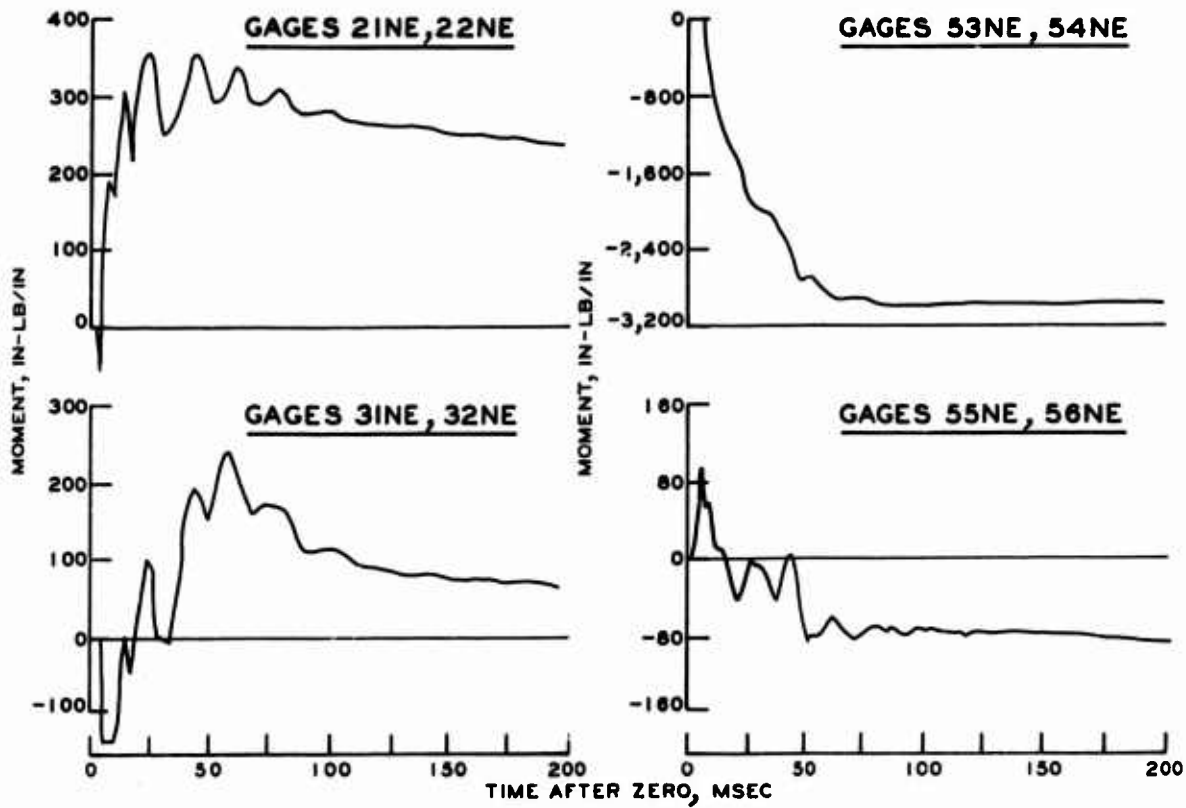


Figure C.20 Moment data, Shot 5.

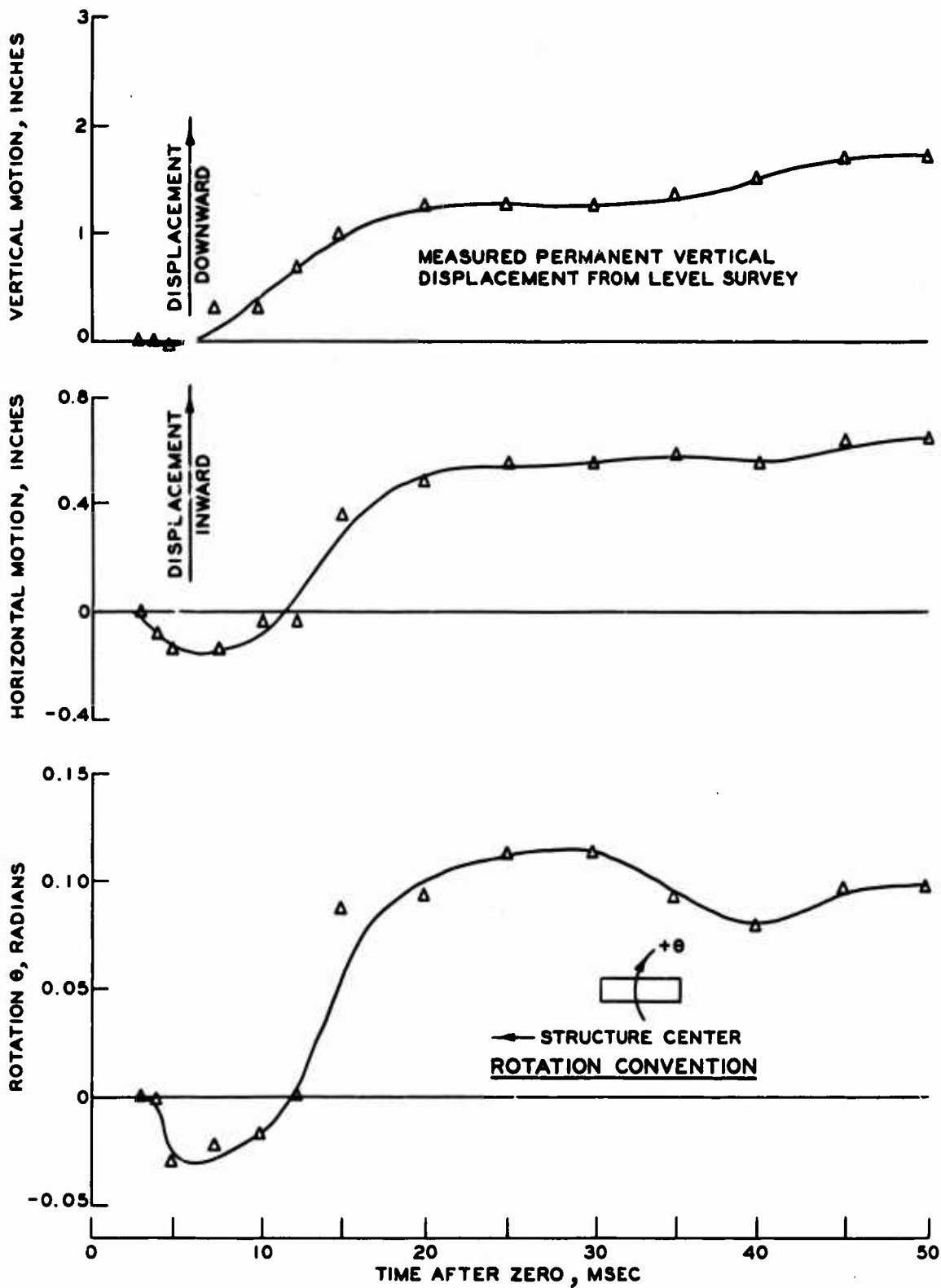


Figure C.21 Footing motion components, Shot 3.

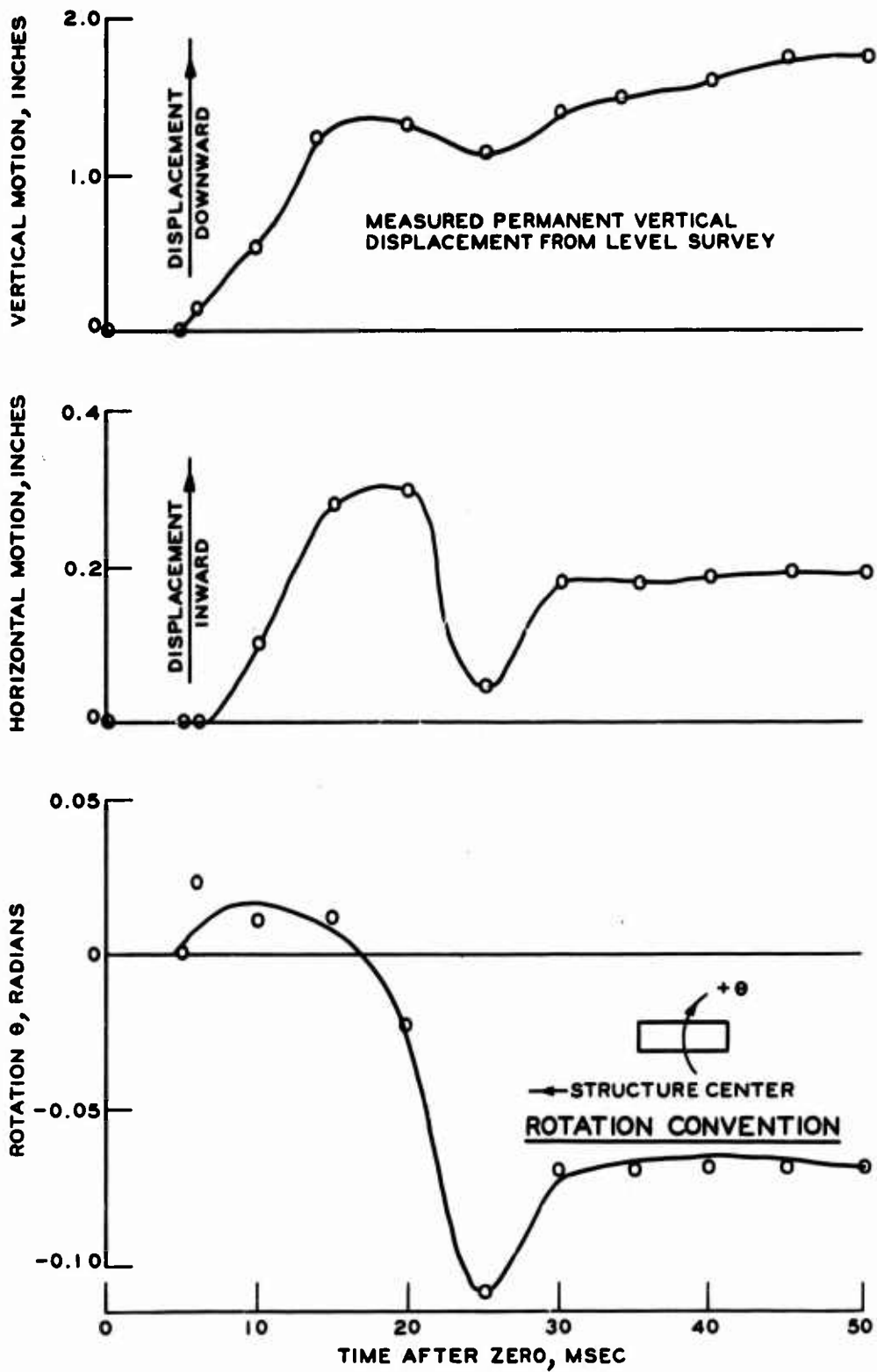


Figure C.22 Footing motion components, Shot 4.

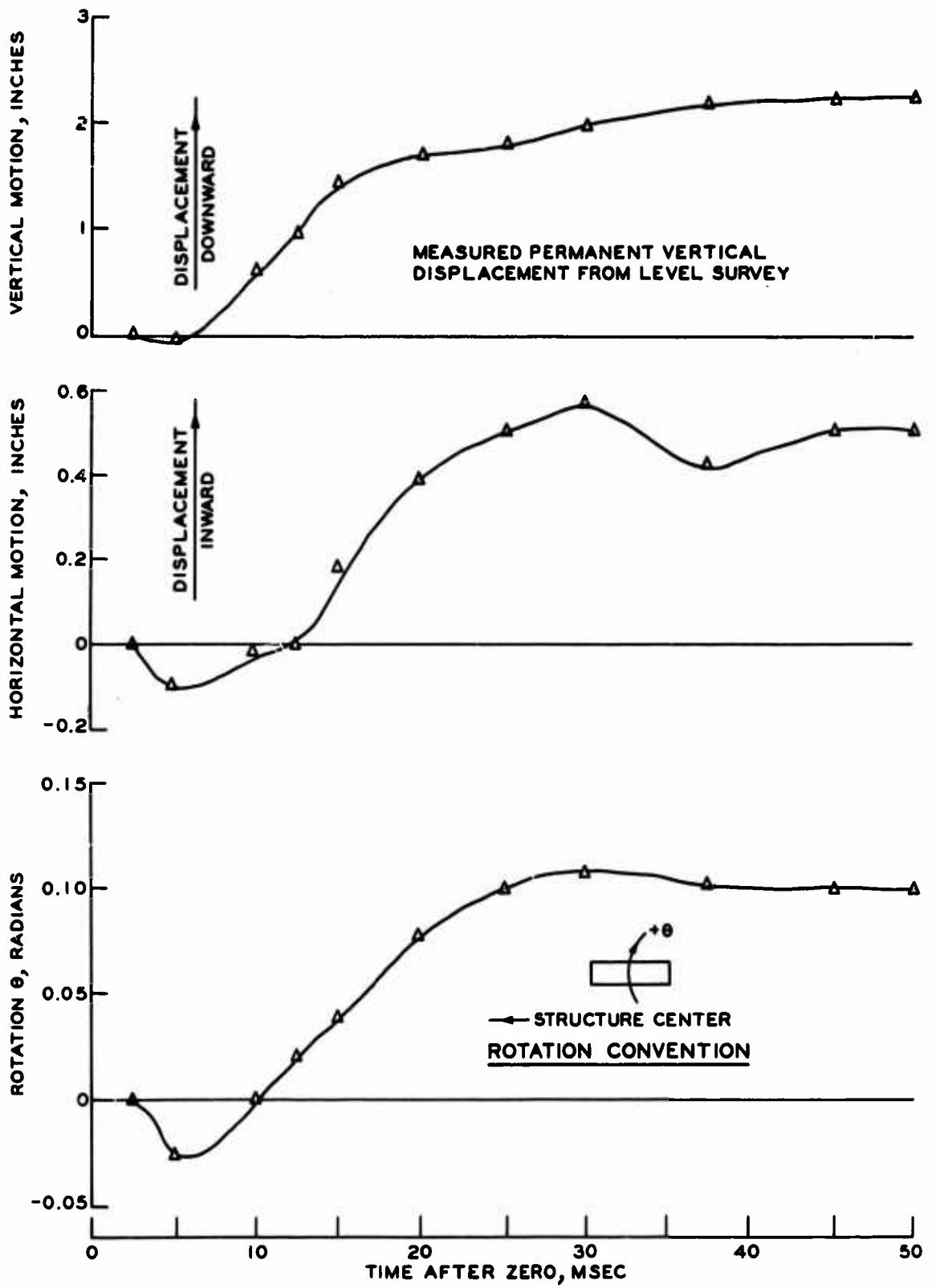


Figure C.23 Footing motion components, Shot 5.

APPENDIX D  
BULKHEAD-TRUSS CONNECTOR REDESIGN

As discussed in Section 3.2.2, difficulties were encountered at the connection between the bulkhead columns and the end truss. These problems arose because of the rotation of the end truss about the connecting bolts which was caused by the gross motion of the structure. To alleviate this problem it was necessary to redesign the connectors to allow for this rotation. This redesign was done between Shots 2 and 3 and was in use during Shot 3. The new connection was designed as a pinned joint. This appendix details the redesign procedures and the redesign, and uses all of the original assumptions made in Reference 1.

It is assumed that the horizontal loading is 0.5 times the vertical load. Based on this assumption the loads carried by the prototype truss and by the structure truss are as shown in Figure D.1 for an overpressure of 150 psi (an overpressure of 150 rather than 100 psi as used in Reference 1, because indications at the time were that the other component parts of the structure would withstand this higher overpressure). The maximum loads that must therefore be carried by the prototype and the structure connector are 150 and 7.4 kips, respectively. It is further assumed that the ultimate shear strength and the ultimate tensile strength of the steel are 40 kips/in<sup>2</sup> and 50 kips/in<sup>2</sup>, respectively.

The design modification made to the structure is as shown in Figure D.2 and was chosen because of the ease with which the changes could be effected in the existing connectors. Dimensions were chosen as follows. The pin is in double shear and thus

$$\begin{aligned} 2(40 \text{ kips}) \text{ Area} &= 7.4 \text{ kips} \\ \text{Pin Area} &= 0.093 \text{ in}^2 \\ \text{Pin Diameter Required} &= 0.346 \text{ inch or about} \\ &\quad 3/8\text{-inch diameter} \end{aligned}$$

For the structure truss the required area is

$$\begin{aligned} (50 \text{ kips}) \text{ Area} &= 7.4 \text{ kips} \\ \text{Area} &= 0.148 \text{ in}^2 \end{aligned}$$

Using a 0.25-inch thickness, the resulting area is 0.155 in<sup>2</sup>, which was

used. In like manner, the required area of the column is  $0.148 \text{ in}^2$ , and by adding another  $1/8$ -inch-thick plate, this area was achieved.

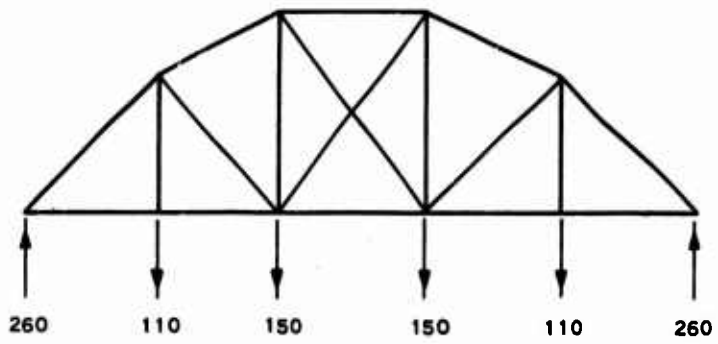
For the prototype, the procedure is the same with the exception that the load is 15 kips. Thus, the pin area is

$$\begin{aligned} 2(40 \text{ kips}) \text{ Area} &= 150 \text{ kips} \\ \text{Pin Area} &= 1.88 \text{ in}^2 \end{aligned}$$

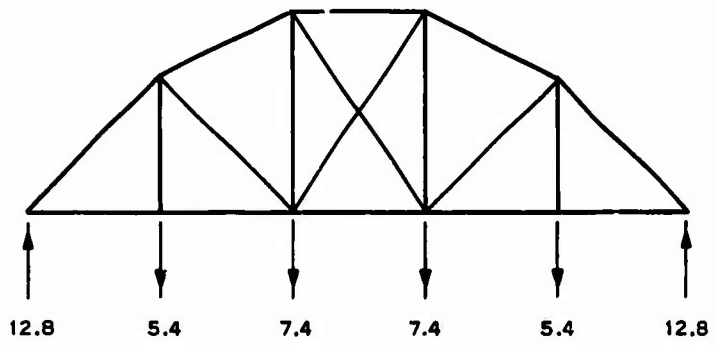
The nearest standard pin with a conservative area is a  $1-3/4$ -inch pin with an area of  $2.41 \text{ in}^2$ . The required truss area is

$$\begin{aligned} (50 \text{ kips}) \text{ Area} &= 150 \text{ kips} \\ \text{Area} &= 3 \text{ in}^2 \end{aligned}$$

Prototype truss design calls for 8.2-lb/ft, 6-inch channel to be used as this connector. This means that a reinforcing strip on either side can only be 4.5 inches wide and, thus, the thickness of this plate should be  $7/16$  inch. This yields an area of  $3.2 \text{ in}^2$ . These plates are to extend 5 inches past the outer edge of the truss as shown in Figure D.3. Column modifications are made as shown in Figures D.4 and D.5. Using the  $3/8$ -inch plate as shown and assuming that the resisting area extends above the pin a distance equal to the length below, then the resisting area is  $3.2 \text{ in}^2$ , which is sufficient.

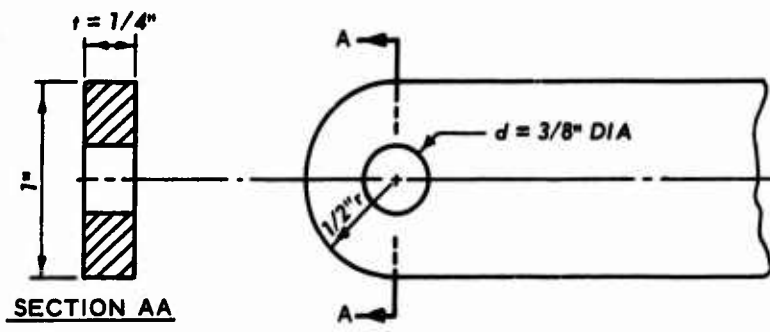


PROTOTYPE TRUSS LOADING

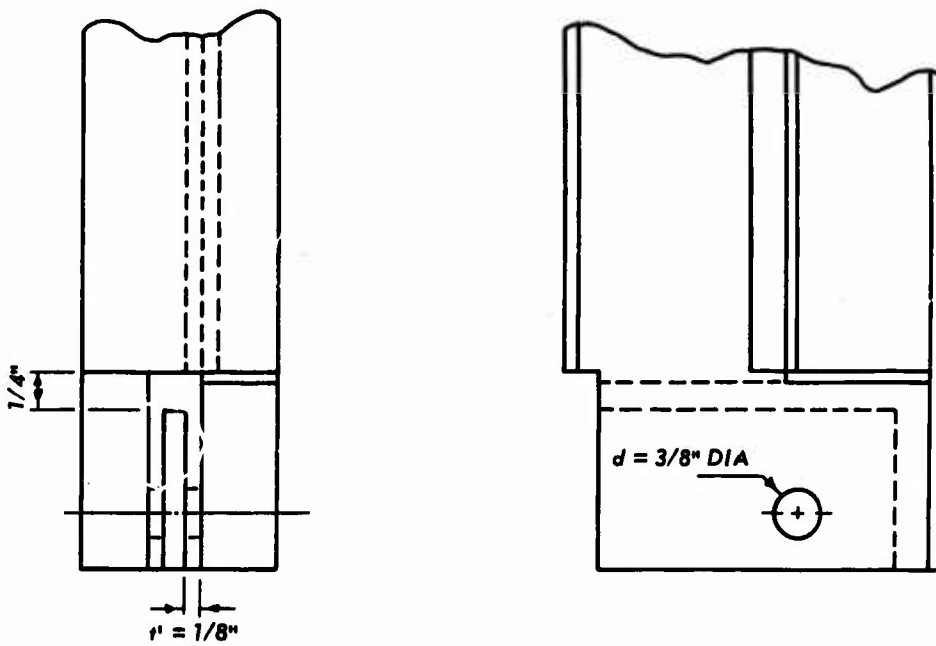


MODEL TRUSS LOADING

Figure D.1 Assumed loading on the prototype and on the model truss. Loads are in kips.

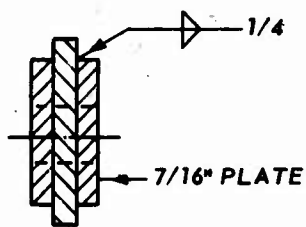
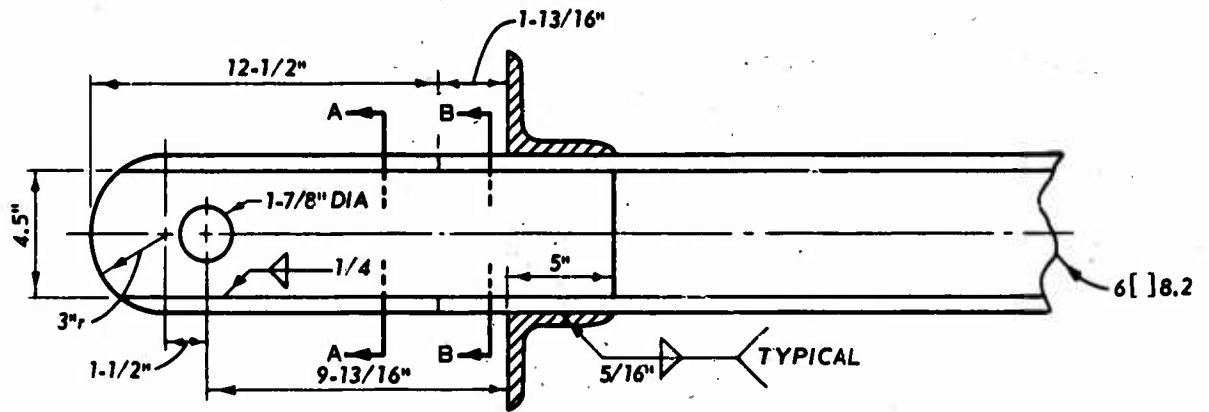


a. TRUSS MODIFICATION

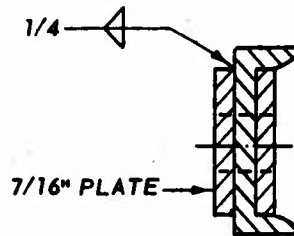


b. COLUMN MODIFICATION

Figure D.2 Detail of the modifications made to the structure column-truss connection.

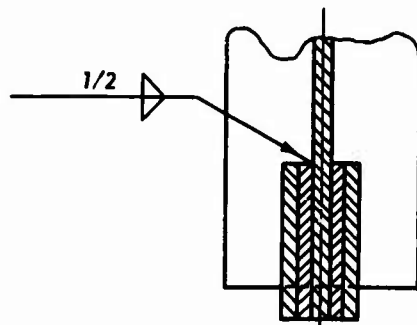
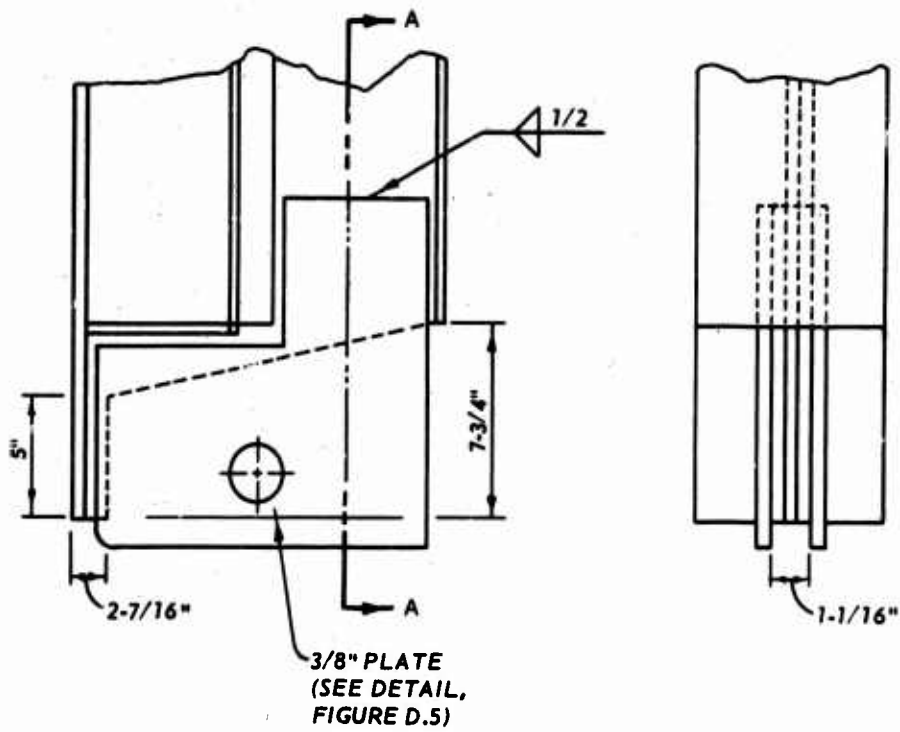


SECTION AA



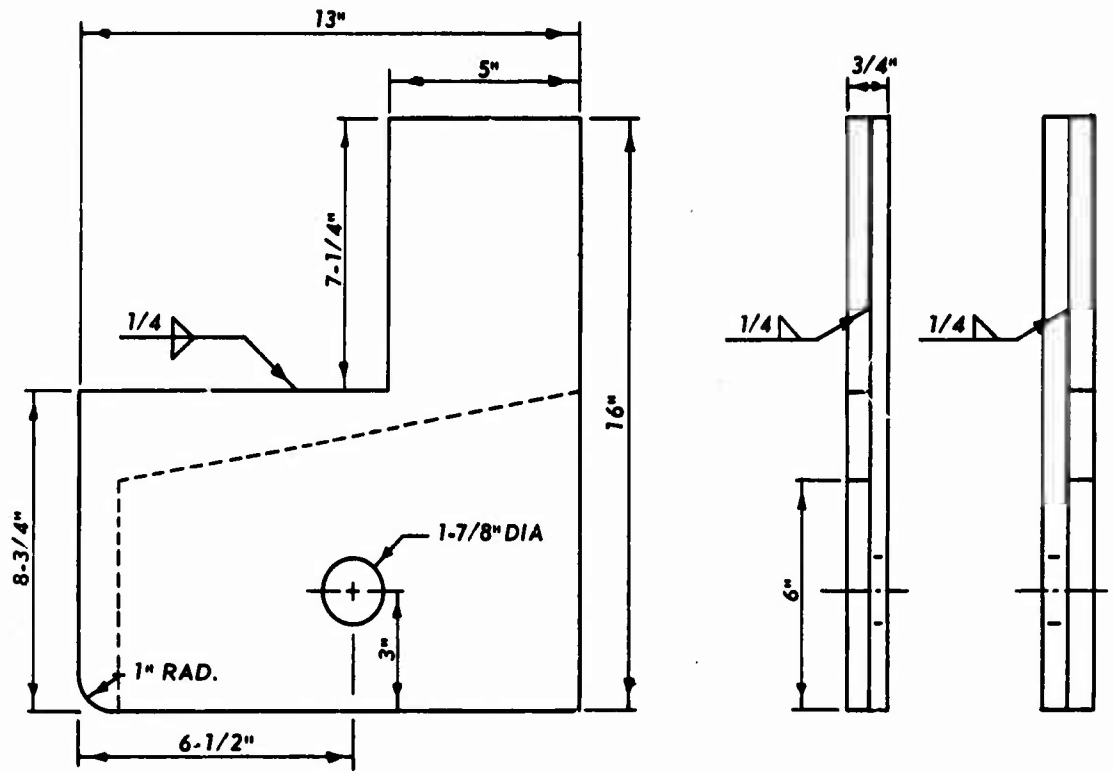
SECTION BB

Figure D.3 Detail of the modifications made in the prototype truss connector design.



SECTION AA

Figure D.4 Detail of the modifications made in the prototype column connector design.



NOTE: SPACERS WELDED ON NEAR SIDE AND ON FAR SIDE. A LEFT-HANDED PLATE AND A RIGHT-HANDED PLATE REQUIRED FOR EACH COLUMN. WELD FROM 3/8 INCH PLATE.

Figure D.5 Plate detail for prototype column connector modification.

## REFERENCES

1. N. M. Newmark, J. W. Briscoe, and J. L. Merritt; "Analysis and Design of Flexible Underground Structures"; Contract Report No. 2-41, Final Report, Phase I, October 1962; U. S. Army Engineer Waterways Experiment Station, CE, Vicksburg, Mississippi; Report prepared under Contract DA-22-079-eng-225; Unclassified.
2. N. M. Newmark and Associates; "Design of Model Test Program for a Buried Field Shelter"; Contract Report No. 1-110, Phase III, May 1965; U. S. Army Engineer Waterways Experiment Station, CE, Vicksburg, Mississippi; Report prepared under Contract DA-22-079-eng-225; Unclassified.
3. T. E. Kennedy and J. T. Ballard; "Dynamic Test of a Model Flexible-Arch-Type Protective Shelter; Pilot Test"; Technical Report No. 1-768, Report 1, April 1967; U. S. Army Engineer Waterways Experiment Station, CE, Vicksburg, Mississippi; Unclassified.
4. G. E. Albritton; "Description, Proof Test, and Evaluation of Blast Load Generator Facility"; Technical Report No. 1-707, December 1965; U. S. Army Engineer Waterways Experiment Station, CE, Vicksburg, Mississippi; Unclassified.
5. T. E. Kennedy, G. E. Albritton, and R. E. Walker; "Initial Evaluation of the Free-Field Response of the Large Blast Load Generator"; Technical Report No. 1-723, June 1966; U. S. Army Engineer Waterways Experiment Station, CE, Vicksburg, Mississippi; Unclassified.
6. R. V. Whitman, Z. Getzler, and K. Hoeg; "Tests Upon Thin Domes Buried in Sand"; Professional Paper P62-15, December 1962; Massachusetts Institute of Technology, Cambridge, Massachusetts; Unclassified.
7. W. L. Durbin; "Study of the Dynamic Stress-Strain and Wave-Propagation Characteristics of Soils; Measurements of Stress-Strain Peak Particle Velocity, and Wave-Propagation in Three Sands"; Contract Report No. 3-91, Report 3, February 1965; U. S. Army Engineer Waterways Experiment Station, CE, Vicksburg, Mississippi; Report prepared under Contract No. DA-22-079-eng-373; Unclassified.
8. J. K. Ingram; "The Development of a Free-Field Soil Stress Gage for Static and Dynamic Measurements"; 1965; Instruments and Apparatus for Soil and Rock Mechanics, ASTM STP 392, American Society for Testing and Materials, Philadelphia, Pennsylvania; Unclassified.
9. A. C. Whiffin and S. A. H. Morris; "Piezoelectric Gauge for Measuring Dynamic Stresses Under Roads"; The Engineer, April 1962, Vol. 213, No. 5544, Pages 741-746; London, England; Unclassified.